Thermodynamic study of complex systems containing gas, water, and electrolytes : application to underground gas storage

Salaheddine Chabab

PSL UNIVERSITÉ PARIS

THÈSE DE DOCTORAT
DE L'UNIVERSITÉ PSL

Préparée à MINES ParisTech

Étude thermodynamique de systèmes complexes contenant du gaz, de l'eau et des électrolytes : application au stockage souterrain de gaz

Soutenue par
Salaheddine CHABAB
Le 27 novembre 2020

Ecole doctorale n° 621
Ingénierie des systèmes, matériaux, mécanique, énergétique

Spécialité
Énergétique et génie des Procédés

Composition du jury :

Antonin CHAPOY Professeur, Heriot-Watt University	*Président*
Martin TRUSLER Professeur, Imperial College London	*Rapporteur*
Pascale BÉNÉZETH Directrice de recherche, CNRS	*Rapporteur*
Pierre CÉZAC Professeur, Université de Pau et des Pays de l'Adour	*Examinateur*
Simon JALLAIS Docteur, Air Liquide	*Examinateur*
André BURNOL Docteur, BRGM	*Examinateur*
Patrice PARICAUD Professeur, ENSTA Paris – IP Paris	Co-*Directeur de thèse*
Christophe COQUELET Professeur, Mines ParisTech – PSL	*Directeur de thèse*

MINES ParisTech | PSL

Remerciements

Ce projet doctoral de trois ans, démarré le 1er octobre 2017 et soutenu le 27 novembre 2020, a été codirigé par le Prof. Christophe Coquelet et le Prof. Patrice Paricaud et co-encadré par Dr. Céline Houriez et Dr. Elise El Ahmar. Les travaux ont été menés dans le cadre des projets "ANR FluidSTORY", "GÉODÉNERGIES Rostock H" et "Carnot M.I.N.E.S HyTrend". Ce travail n'aurait pas été possible sans le financement, le soutien, et l'environnement de travail idéal de la prestigieuse grande école française, l'École des Mines de Paris.

Je tiens avant tout à remercier les Profs. Christophe Coquelet et Patrice Paricaud de m'avoir donné l'opportunité et de m'avoir fourni tous les éléments nécessaires pour réaliser ce travail, de m'avoir guidé vers les objectifs soulignés, et de m'avoir laissé la possibilité d'explorer d'autres sujets d'intérêt qui n'étaient pas prévus au début de ce projet de thèse. Parallèlement à leur excellence scientifique et pédagogique, j'apprécie énormément leurs qualités humaines.

Je remercie également tous les membres du jury d'avoir accepté de juger ce travail, et je remercie sincèrement les Profs. J. P. Martin Trusler et Pascal Bénézeth pour leurs grands efforts dans la révision de mon manuscrit et pour leurs suggestions dans leurs rapports.

Je tiens à remercier Céline Houriez et Elise El Ahmar pour leurs conseils et leurs encouragements tout au long de la thèse. J'aimerais également remercier Jérôme Corvisier pour sa collaboration dans la plupart de nos articles et communications.

Un grand merci au comité de suivi, notamment les Profs. Pierre Cezac et Arnaud Delebarre pour l'évaluation de mon travail de thèse en première et deuxième année de doctorat, pour tous les encouragements, et pour les échanges que nous avons eus.

Je tiens également à remercier vivement Pascal Théveneau pour son grand soutien pendant mes travaux expérimentaux et je lui souhaite une très bonne retraite. Merci à Alain Valtz et au personnel technique du CTP (Eric, David, Snaide et Hervé) pour m'avoir aidé et avoir proposé des solutions à mes différents problèmes expérimentaux. Je voudrais également remercier Jocelyne et Marie-Claude pour avoir facilité nos recherches en s'occupant de toutes les tâches administratives.

Un grand merci au Prof. Antonin Chapoy pour m'avoir accueilli dans son équipe de recherche et avoir facilité mon séjour à l'université Heriot-Watt, et pour les discussions fructueuses avec lui et ses doctorants sur l'expérimentation et la modélisation, ainsi que Pezhman et Rod pour

leur grand soutien pendant que je faisais les mesures expérimentales. Je voudrais aussi remercier Abdullah, Valderio, et tous les collègues de leur groupe de recherche pour leur gentillesse et de m'avoir aidé à s'adapter rapidement à ce nouvel environnement de recherche. Je tiens également à remercier fortement la Fondation MINES ParisTech pour avoir financé ce séjour via le programme d'aide à la mobilité internationale des doctorants.

Un très grand merci à tous les collègues (ancien et actuel), Jamal, Chourouk, Marco, Paolo, Remi, Charlie, Mathieu, Thibault, Aurélien pour tous les moments qu'on a partagés ensemble. Je souhaite bon courage aux doctorants qui auront prochainement leurs soutenances Julien, Serena, Salem, Gabrielly, Driss, Nicolo, Mert, et je souhaite aux post-doctorants Dhia et Esther une belle carrière. Je n'oublie pas aussi tous mes amis, Mansour, Simo, Soufiane, Amine, Abdelkebir, Abdelwahed, Mehdi, Boubker, Yacoub, Momo et tous ceux que je n'ai pas pu citer.

Mes plus grands remerciements vont à mes parents Abdelkhalek et Ez-zohra pour leur amour inconditionnel, leur encouragement et leur soutien continus. Un très grand merci à eux d'avoir pris l'entière responsabilité de mon éducation et de mon orientation professionnelle. Je remercie très chaleureusement mes chères sœurs Soukaina et Asmae, qui continuent à rendre toute la famille fière de leur succès. Merci très sincèrement à mes grands-parents et aux familles Chabab et Raouf.

Je garde le mot de fin pour ma fiancée Halla qui est entrée dans ma vie au meilleur moment, et qui m'a énormément soutenue au cours de cette dernière année cruciale. Un énorme merci pour le bonheur que son amour, son affection et sa gentillesse m'apportent. Un très grand merci à mes beaux-parents Noureddine et Hanifa et à ma belle-sœur Lina.

French summary / Résumé

L'étude thermodynamique (expérimentation et modélisation) des systèmes Gaz+Eau+Sels est d'une grande importance, que ce soit dans un contexte environnemental comme le Captage et le Stockage du dioxyde de Carbone (CSC) ou dans un contexte économique comme la récupération assistée du pétrole par injection de CO_2, ou le Stockage Souterrain réversible massif de Gaz (SSG) à usage industriel (« Power-to-Gas » (PtG) et « Gas-to-Power » (GtP), industries chimiques, pétrochimiques et pharmaceutiques, etc.). Dans le cadre du SSG, l'industrie de l'énergie s'intéresse aux vecteurs énergétiques gazeux les plus demandés dans le secteur, tels que le méthane (ou le gaz naturel (GN)), le dioxyde de carbone (pur à destination des unités de méthanation ou mélangé avec le méthane pour le stockage du GN), l'oxygène (pour les unités d'oxycombustion) et l'hydrogène (utilisé directement ou pour alimenter les unités de méthanation). La conception et l'optimisation des installations de stockage, ainsi que la surveillance de la température, de la pression, de la quantité du gaz stocké dans les réservoirs géologiques (cavités salines, aquifères salins profonds et gisements de GN épuisés) et leurs pilotages selon différents scénarii (stockage journalier, hebdomadaire, mensuel ou annuel), nécessitent la connaissance des diagrammes de phases et plus spécifiquement la solubilité des gaz dans les saumures, les teneurs en eau et aussi les conditions de stabilité des hydrates de gaz dans le cadre de l'exploitation de gaz. Pour ce faire, il est essentiel de disposer d'un modèle thermodynamique qui repose sur des fondements théoriques et qui soit peu dépendant de l'acquisition de données expérimentales. L'objectif est de pouvoir extrapoler le modèle en dehors de la gamme d'ajustement des paramètres (température, pression et composition de la saumure) et également le transposer à d'autres applications. Pour pallier le manque de données expérimentales à haute pression de la solubilité des gaz (CO_2, O_2 et H_2) dans la saumure, un dispositif expérimental basé sur la méthode "statique-analytique" a été adapté et utilisé pour mesurer la solubilité des gaz dans l'eau pure et la saumure. Pour comparer/valider les nouvelles mesures, un deuxième dispositif basé sur une technique dite "volumétrique" a également été utilisé. Une équation d'état pour les électrolytes (e-PR-CPA) a été développée en prenant en compte toutes les interactions entre espèces chimiques (molécules et ions). Les résultats de ce modèle ont été comparés avec des modèles existants tels que ceux utilisés par les géochimistes et en génie des procédés. Pour une meilleure évaluation des performances de notre modèle, les paramètres des modèles précédemment cités ont été réoptimisés en incluant les nouvelles données acquises.

Abstract

The thermodynamic study (experimental and modeling) of Gas+Water+Salt systems is of great importance, whether in an environmental context such as Carbon Dioxide Capture and Storage (CCS) or in an economic context such as Enhanced Oil Recovery (EOR) by CO2 injection, or massive reversible Underground Gas Storage (UGS) for industrial use ("Power-to-Gas" (PtG) and "Gas-to-Power" (GtP), chemical, petrochemical and pharmaceutical industries, etc.). In the context of UGS, the energy industry is interested in the gaseous energy carriers that are most in demand in the sector, such as methane (or natural gas (NG)), carbon dioxide (pure for methanation units or mixed with methane for NG storage), oxygen (for Oxy-fuel combustion units) and hydrogen (used directly or to feed methanation units). The design and optimization of storage facilities, as well as the monitoring of the temperature, pressure and quantity of gas stored in geological reservoirs (salt caverns, deep saline aquifers and depleted NG fields) and their control according to different scenarios (daily, weekly, monthly or annual storage), require knowledge of phase diagrams and more specifically gas solubility in brine, water content and also gas hydrate stability conditions during gas exploitation. For this purpose, it is essential to develop a thermodynamic model based on theoretical foundations and with a low dependence on experimental data. The objective is to be able to extrapolate the model outside the adjustment range of the parameters (temperature, pressure and brine composition) and also to transpose it to other applications. To overcome the lack of experimental data of high pressure gas (CO_2, O_2 and H_2) solubility in brine, an experimental apparatus based on the "static-analytic" method has been adapted and used to measure gas solubility in pure water and brine. To compare/validate the new measurements, a second apparatus based on a "volumetric" technique was also used. An electrolyte equation of state (e-PR-CPA) was developed taking into account all interactions between chemical species (molecules and ions). The results of this model were compared with existing models such as those used by geochemists and in process engineering. For a better evaluation of the performance of our model, the parameters of the previously mentioned models were re-optimized by including the newly acquired data.

Table of Contents

Abstract 2

Introduction 16

Chapter 1: Underground Gas Storage (UGS) 20

1.1 Introduction 20

1.2 Carbon dioxide Capture and Storage (CCS) 22

1.3 Massive gas and energy storage 25

1.3.1 Compressed Air Energy Storage (CAES) 25

1.3.2 Underground Hydrogen Storage (UHS) 26

1.3.3 From Power-to-Gas (PtG) to massive underground energy carriers storage 29

1.4 Issues: Phase equilibria involving gas, water and electrolytes 32

1.4.1 Gas solubility 32

1.4.2 Water content (or moisture content) in gas-rich phase 36

1.4.3 Gas Hydrates 38

References 39

Chapter 2: Phase equilibria: Measurements and modeling 45

2.1 Introduction 45

2.2 Gas solubility measurements 46

2.2.1 Experimental equipment 47

2.2.2 Review of available experimental data 54

2.3 Modeling phase equilibria 66

2.3.1 Fluid phase equilibria calculation approaches 66

2.3.2 Model presentation 70

2.3.3 Gas hydrates and fluid phase equilibria 78

References 78

Chapter 3: Article 1: Thermodynamic study of the CO_2 – H_2O – NaCl system: Measurements of CO_2 solubility and modeling of phase equilibria using Soreide and Whitson, electrolyte CPA and SIT models 90

Abstract 92

3.1 Introduction 93

3.2 Experimental 95

3.2.1 Materials 95

3.2.2 Apparatus description 96

3.2.3 Calibrations 97

3.2.4 Experimental procedure and results 97

3.3 Thermodynamic modeling 101

3.3.1 Soreide and Whitson EoS 101

3.3.2 e-PR-CPA EoS 103

3.3.3 Geochemical model 108

3.4 Results and discussions 110

3.4.1 H_2O + CO_2 binary system 110

3.4.2 Prediction of the phase equilibria of the CO_2-H_2O system at very high pressure and temperature. 113

3.4.3 H_2O + CO_2 + NaCl system 113

3.5 Conclusions 120

Nomenclature 121

References 123

Chapter 4: Article 2: Measurements and modeling of high-pressure O_2 and CO_2 solubility in brine (H_2O+NaCl) between 303 and 373 K and pressures up to 36 MPa 130

Abstract 133

4.1 Introduction 134

4.2 Experimental 137

4.2.1 Literature and measured solubility data of CO_2 and O_2 in water and brine 137

4.2.2 Materials 138
4.2.3 Apparatus and method 139
4.2.4 Experimental results 140
4.3 Thermodynamic modeling 144
4.4 Results and discussions 145
4.4.1 CO_2 + H_2O + NaCl system 145
4.4.2 O_2 + H_2O + NaCl system 146
4.5 Conclusions 159
References 161
Chapter 5: Article 3: Measurements and predictive models of high-pressure H_2 solubility in brine (H_2O+NaCl) for Underground Hydrogen Storage application 165
Abstract 168
5.1 Introduction 169
5.2 Experimental 173
5.2.1 Literature and measured (this work) solubility data of H_2 in water and brine 173
5.2.2 Materials 174
5.2.3 Apparatus and method 175
5.2.4 Experimental results 177
5.3 Thermodynamic modeling 180
5.3.1 Approaches and models 180
5.3.2 H_2+H_2O system: H_2 solubility and water content 183
5.3.3 H_2+H_2O+NaCl system: H_2 solubility 190
5.4 Conclusions 197
References 198
Chapter 6: Article 4: Hydrate Stability of carbon dioxide + oxygen binary mixture (CO_2 + O_2) in pure water: Measurements and modeling 203
Abstract 205
6.1 Introduction 206

6.2 Experimental 208
6.2.1 Materials 208
6.2.2 Apparatus and method 209
6.2.3 Experimental results 211
6.3 Thermodynamic modeling 214
6.3.1 Model presentation: procedure description and parameter estimation 214
6.3.2 Hydrate stability of the O_2+H_2O and CO_2+H_2O+(NaCl) mixtures 224
6.3.3 Hydrate stability of the CO_2+O_2+H_2O mixture 227
6.3.4 Hydrate stability of the CO_2+O_2+H_2O+NaCl mixture 228
6.4 Conclusions 230
References 231
Chapter 7: Major findings and perspectives 238
Appendix A: PT-Flash calculation 245
Appendix B: ThermoReservoir® software 248
Appendix C: List of publications 250
Appendix D: Article 5: Experimental Density Data of Three Carbon Dioxide and Oxygen Binary Mixtures at Temperatures from 276 to 416 K and at Pressures up to 20 MPa 254

List of figures

Figure 1.1: Principal types of underground gas storage [1. 6]. 21

Figure 1.2: Different CO_2 storage options in deep underground geological formations [1. 12]. 23

Figure 1.3: CO_2 trapping mechanisms [1. 10]. 24

Figure 1.4: Overview of the different types of energy storage according to their discharge times and storage capacities ([1. 13]). 25

Figure 1.5: Principle of a CAES process [1. 14]. 26

Figure 1.6: Hydrogen Production, Storage and Use (modified after EARTO 2014 [1. 17]) 27

Figure 1.7: Comparison of different options for high-pressure hydrogen storage [1. 22]. 28

Figure 1.8: Power-to-Gas concept [1. 23]. 29

Figure 1.9: EMO unit concept (FLUIDSTORY project). 30

Figure 1.10: Schematic of underground bio-methanation concept [1. 21]. 31

Figure 1.11: (a): Example of the effect of moisture (in terms of relative humidity) on the corrosion rate of X70 steel used in pipelines transporting a CO_2-rich gas stream in the context of CCS [1. 43]; (b): saturated water content tables of CO_2/CH_4 mixtures [1. 44]. 37

Figure 1.12: Molecular structure of CO_2 hydrates. 38

Figure 1.13: (a): in situ methane hydrate [1. 46]; (b): Gas hydrate plug in a pipeline [1. 47]. 38

Figure 1.14: CH_4 and CO_2 hydrate stability curves [1. 51]. 39

Figure 2.1: From methodologies (experimentation and modeling) to applications. 45

Figure 2.2: Classification of high-pressure phase equilibria measurement techniques [2. 3]. 47

Figure 2.3.C: Simplified schematic representation of the "static-analytic" apparatus for phase equilibria measurement. 49

Figure 2.4.C: Schematic representation of the rocking cell apparatus used to measure the solubility of gases in NaCl brine [2. 6]. PI01: gasometer pressure indicator; PIC01: equilibrium cell pressure indicator/logger; PC01: computer controller/logger; TI01: gasometer temperature indicator; TIC01: equilibrium cell temperature indicator controller; V01: gas cylinder control valve; V02: equilibrium cell injection valve; V03: equilibrium cell drain valve; V04: equilibrium cell drain valve (backup); V05: gasometer inlet valve; VI01: gasometer volume indicator. 53

Figure 2.5: CO_2-H_2O system: data distribution of mutual solubilities of CO_2 and H_2O available in the literature (Table 2.2). The red dashed rectangle delimits the estimated CCS operating conditions. 56

Figure 2.6: O_2-H_2O system: data distribution of mutual solubilities of O_2 and H_2O available in the literature (Table 2.3). The red dashed rectangle delimits the estimated CAES operating conditions. 58

Figure 2.7: H_2-H_2O system: data distribution of mutual solubilities of H_2 and H_2O available in the literature (Table 2.4). The red dashed rectangle delimits the estimated UHS operating conditions. 60

Figure 2.8: CO_2-H_2O-NaCl system: distribution of CO_2 solubility data available in the literature (Table 2.5). 62

Figure 2.9: O_2-H_2O-NaCl system: distribution of O_2 solubility data available in the literature (Table 2.6).....64

Figure 2.10: H_2-H_2O-NaCl system: distribution of O_2 solubility data available in the literature (Table 2.7). 65

Figure 2.11: Intermolecular and electrolyte interactions considered in the e-PR-CPA model. ed: electron donor association site, ea: electron acceptor association site. 73

Figure 3.1 : Schematic representation of the apparatus for measuring the solubility of CO2 in NaCl brine. DAS: data acquisition system, EC: equilibrium cell, GC: gas chromatography, HPT: high pressure transducer, LPT: low pressure transducer, LS: liquid ROLSI® Sampler-Injector, MPT: medium pressure transducer, O: oven, PP: platinum resistance thermometer probe, PT: pressure transducer, IV: homemade shut off valve, SM: samplers monitoring, SW: sapphire window, TP: thermal press, TR: temperature regulator, Vi: valve i, VP: vacuum pump, VS: vapor ROLSI® Sampler-Injector, VSS: variable speed stirrer and VVC: Variable Volume Cell. 95

Figure 3.2 : Comparison of the e-PR-CPA model (with the three parameter sets in Table 3.4) with the NIST model. a) Water vapor pressure, b) Water density at saturation. 105

Figure 3.3 : Saturation vapor pressure of water + NaCl at low temperature and at different NaCl molalities. Comparison of the e-PR-CPA model with the experimental data of Hubert et al. [3. 39]. 106

Figure 3.4: Saturation vapor pressure of water + NaCl at high temperature and at 0.5 and 6 moles/kgw of NaCl. Comparison of the e-PR-CPA model with the data correlated by Hass [3. 40]. 106

Figure 3.5: Osmotic coefficient of water + NaCl versus NaCl molality at 298.15 K (a) and 323.15 K (b). Comparison of the results of the e-PR-CPA model with the experimental data from [3. 41, 42, 43, 44, 45, 46].....107

Figure 3.6 : Molecular representations of water and carbon dioxide in terms of electron donor/acceptor sites. ed: electron donor site, ea: electron acceptor site.....110

Figure 3.7 : Influence of temperature on $kH2O - CO2$ (×) and on $\beta H2O - CO2$ (o) for the H_2O-CO_2 system. Symbols represent optimized parameter values; solid lines represent correlations (Equations 3.11-3.12). 111

Figure 3.8 : CO_2-H_2O binary system: Calculation of CO_2 solubility in water (a and c) and water content (b and d) at 298, 323, 373 and 423 K by e-PR-CPA (solid line), m-SW (dashed line) and geochemical (dotted line) models. The symbols are literature data: (a): [3. 6, 7, 58, 59, 60, 61, 62],

(b): [3. 59, 61, 63, 64, 65, 66], (c): [3. 59, 67, 68, 69, 70, 71], and (d): [3. 59, 67, 68, 69, 70, 72]. 112

Figure 3.9 : CO_2-H_2O system: Prediction of liquid-vapor equilibria at very high temperature and pressure by the e-PR-CPA model. The symbols are literature data: [3. 5, 6]. 113

Figure 3.10 : CO_2-H_2O-NaCl system: Calculation of CO_2 solubility in high molality NaCl brine at 313 K and at 433 K by the Soreide and Whitson (SW) model using the original kij (dashed line) and the kij proposed in this work (solid line). Literature data from Rumpf et al. [3. 74]. 114

Figure 3.11 : Influence of molality on $kCO2 - ions$ for the H_2O-CO_2-NaCl system. 115

Figure 3.12 : CO_2-H_2O-NaCl system: Calculation of CO_2 solubility by e-PR-CPA (solid line), m-SW (dashed line) and geochemical (dotted line) models. The black symbols (a, b, c and d) are the literature data [3. 4, 7, 11, 12], and the red symbols (a and b) are the measured data (Table 3.2). 116

Figure 3.13 : CO_2-H_2O-NaCl system: Calculation of CO_2 solubility at different temperatures and pressures by e-PR-CPA (solid line), m-SW (dashed line) and geochemical (dotted line) models. The symbols are the literature data from Guo et al. [3. 11]. 118

Figure 4.1 : Distribution of literature (×) and new measured (◊) solubility data. (a): CO_2+H_2O system (solubility and water content); (b): O_2+H_2O system (solubility and water content); (c): CO_2 solubility in NaCl brine; (d): O_2 solubility in NaCl brine. 136

Figure 4.2 : Simplified schematic representation of the "static-analytic" apparatus for phase equilibria measurement. 137

Figure 4.3 : Simplified schematic representation of the "Rocking cell" apparatus for solubility measurement.....138

Figure 4.4 : CO_2+H_2O+NaCl system : Experimental CO_2 solubility in 6m NaCl-brine at 323 K and 373 K. The black symbols are the literature data [4. 13, 17], and the red symbols with dotted lines (to guide the eye) are the measured data. 141

Figure 4.5 : O_2+H_2O+NaCl system : Validation of measured O_2 solubility data in 1m and 4m NaCl-brine at 323 K. The blue and red symbols represent data measured by the Technique 1 and 2 respectively. The solid lines represent a trend line to guide the eye. 142

Figure 4.6 : CO_2+H_2O+NaCl system : Prediction of CO_2 solubility by e-PR-CPA (solid line), SW (dashed line) and geochemical (dotted line) models. The black symbols are the literature data [4. 13, 14, 25, 26, 27, 28, 29, 30, 31], and the red symbols are the measured data (Table 4.2). 146

Figure 4.7 : Solubility of O_2 in H_2O + NaCl. The black symbols are the literature data [4. 34], the red symbols are the measured data (Table 4.3), and the solid lines are the prediction by e-PR-CPA model. 147

Figure 4.8 : O_2+H_2O+NaCl system : Prediction of O_2 solubility by e-PR-CPA (solid line), SW (dashed line) and geochemical (dotted line) models. The black symbols are the literature data ((a) : [4. 34], (b) : [4. 35]), and the red symbols are the measured data (Table 4.3). 148

Figure 4.9 : O_2+H_2O+NaCl system : Calculation of O_2 solubility by the Zheng and Mao (ZM) model using original (dotted line) and reoptimized (dashed line) parameters (Table 4.4). The black symbols are the literature data [4. 34], and the red symbols are the measured data (Table 4.3). 153

Figure 4.10 : Geng and Duan [4. 7] model predictions of O_2 solubility compared with data measured at 333 K (2m). 154

Figure 4.11 : Prediction of the water content in O_2 as a function of pressure at different temperatures by e-PR-CPA (solid line), SW (dashed line) and geochemical (dotted line) models. The data (symbols) are from Wylie and Fisher [4. 42]. 155

Figure 5.1 : Distribution of literature solubility data (×) and this work (◊). (a): H_2-H_2O system (solubility and water content); (b): H_2 solubility in NaCl brine. 172

Figure 5.2 : Schematic representation of the static-analytic apparatus [5. 17] used to measure the solubility of gas (H_2) in NaCl brine. DAS: data acquisition system, EC: equilibrium cell, GC: gas chromatography, HPT: high pressure transducer, LPT: low pressure transducer, LS: liquid ROLSI® capillary Sampler-Injector, MPT: medium pressure transducer, O: oven, PP: platinum resistance thermometer probe, PT: pressure transducer, IV: homemade shut off valve, SM: samplers monitoring, SW: sapphire window, TP: thermal press, TR: temperature regulator, Vi: valve i, VP: vacuum pump, VS: vapor ROLSI® capillary Sampler-Injector, VSS: variable speed stirrer and VVC: Variable Volume Cell. 175

Figure 5.3: Solubility of H_2 in H_2O + NaCl. Literature data [5. 20, 49, 52] are represented by black symbols (△: 323 K – pure water; ◊: 373K – pure water) and measured ones (Table 5.4) are represented by colored symbols (▲: 323 K – pure water; □: 323 K – 1m; +: 323 K – 3m; ×: 323 K – 5m; ●: 348 K – 1m; ◆: 373K – pure water; ■: 373 K – 1m; ✱: 373 K – 3m). The solid lines represent the predictions of the e-PR-CPA model. 178

Figure 5.4 : Solubility of H_2 in H_2O at 323 K (a) and 373 K (b). Literature data [5. 20, 49, 52] are represented by black symbols (◆) and measured ones (Table 5.4) are represented by red symbols (◆). The solid, dotted and dashed lines represent the H_2 solubilities calculated by the e-PR-CPA, SW, and geochemical models, respectively. 185

Figure 5.5 : Isobars of solubility of H_2 in H_2O showing solubility minimum temperatures at 50, 100, 150 and 200 atm. Comparison of data smoothed by IUPAC [5. 20] represented by black symbols, with predictions by e-PR-CPA, SW, and geochemical models represented by solid, dotted, and dashed lines, respectively. 186

Figure 5.6 : Water content in H_2-rich phase at (a): 311 K; (b): 366, 422, and 478 K. Comparison of literature data [5. 48] represented by black symbols, with predictions with the e-PR-CPA, SW, and geochemical models represented by solid, dotted, and dashed lines, respectively. 189

Figure 5.7 : Solubility of H_2 in H_2O + NaCl at 323 K (a) and 373 K (b) and different NaCl molalities. Literature data [5. 20, 49, 52] are represented by black symbols and measured ones (Table 5.4) are represented by red symbols. The solid, dotted and dashed lines represent the H_2 solubilities calculated by the e-PR-CPA, SW, and geochemical models, respectively. 192

Figure 5.8 : Effect of temperature, pressure and NaCl concentration (molality) on H_2 solubility. Comparison of literature [5. 20, 49, 52] and some measured (Table 5.4) data with e-PR-CPA (solid lines) model predictions. 193

Figure 5.9: Calculated Solubility (solid lines) of H_2 in H_2O + NaCl using correlation (Equations 5.12 and 5.13). (a): measured vs calculated $xH2$; (b): Isobars of H_2 solubility in pure water; (c) and (d): Isotherms of solubility of H_2 in water and brine at different molalities. Literature data [5. 20, 49, 52] are represented by black symbols and measured ones (Table 5.4) are represented by red symbols.....196

Figure 6.1: Schematic representation of the used apparatus. DW: degassed water; DAU: data acquisition unit; EC: equilibrium cell; GC: Gas cylinder; LPT: low pressure transducer; HPT: high pressure transducer; LB: liquid bath; PP: platinum probe; SD: stirring de-vice; TR: temperature regulator; VP: vacuum pump; VVC: variable volume cell; PF: pressurizing fluid; DT: displacement transducer. 209

Figure 6.2: Measurement principle of gas hydrate dissociation points by isochoric pressure search method.....210

Figure 6.3: Hydrate dissociation points of the CO_2+O_2 gas mixture: measured data (a) and consistency tests (b, c and d). The red symbols (graph c) represent measurements where the gas mixture was in liquid-vapor equilibrium (see Figure 6.9b).....213

Figure 6.4: Schematic diagram of the approach used to calculate gas hydrate equilibria with the e-PR-CPA model combined with the Van der Waals and Platteeuw model.....214

Figure 6.5: Saturation vapor pressure (a) and osmotic coefficient (b) of H_2O + NaCl system. Comparison of literature data (symbols) [6. 32, 33, 34, 35, 36, 37, 38] with predictions (solid lines) by e-PR-CPA EoS. 220

Figure 6.6: Comparison of experimental data (symbols) [6. 6, 39, 40, 41, 42, 43, 44, 45, 46, 47] with predicted CO_2 (a) and O_2 (b) solubilities in NaCl-brine at 323 K for different salt molalities using the e-PR-CPA EoS (solid lines).....222

Figure 6.7: Water content in CO_2+H_2O and O_2+H_2O systems (a) and VLE of the CO_2+O_2 mixture (b) at different temperatures: Comparison of experimental data (symbols, (a): [6. 45, 46, 48, 49, 50, 51, 52]; (b): [6. 29]) with predictions (solid lines) using e-PR-CPA model (a) and PR EoS (b). 223

Figure 6.8: Hydrate dissociation conditions of the O_2+H_2O (a) and CO_2+H_2O+(NaCl) (b) mixtures: Comparison of literature experimental data with predictions using the (e-PR-CPA + vdWP) model. 225

Figure 6.9: Hydrate dissociation conditions of the CO_2+O_2+H_2O ternary system at different O_2 "water-free" mole fractions 32% (a), 11% (b), 50% (c) and 5% (d): Comparison of measured (a, b and c, see Table 6.3) and literature [6. 11] (d) experimental data with predictions using the (e-PR-CPA + vdWP) model (solid lines). The bubble and dew lines of the different gas mixtures are determined by the PR EoS. 226

Figure 6.10: Hydrate dissociation conditions of the CO_2+O_2+H_2O ternary system from pure O_2 hydrate to pure CO_2 hydrate. Comparison of literature and measured data with predictions using the (e-PR-CPA + vdWP) model (solid lines). 228

Figure 6.11: Hydrate dissociation conditions of the CO_2+O_2+H_2O+(NaCl) quaternary system: Prediction of the effect of NaCl concentration (from salt-free to 4m) on the mixed-gas hydrate system (32% O_2 , at fixed aqueous fraction AqFr=0.7) using the (e-PR-CPA + vdWP) model. The bubble and dew lines are determined by the PR EoS. 229

Figure 7.1: Gas (H_2, O_2, CH_4, and N_2) solubility in water and brine at 323 K: Comparison of literature and measured data (symbols) with predictions (solid lines) by e-PR-CPA EoS. 240

Figure 7.2: (a): Lines of equal solubilities in different salts of CO_2 with respect to NaCl (as salt reference), taken from Ratnakar et al. 2020. (b): Equivalent NaCl salinity of different salts, taken from Schlumberger (Log Interpretation Charts, 2009). 242

List of tables

Table 1.1: Operational H_2 storage caverns around the world [1. 19]. 27

Table 2.1: Chemicals used in this work: purities and suppliers 48

Table 2.2: Literature experimental data for CO_2 solubility in pure water 56

Table 2.3: Literature experimental data for O_2 solubility in pure water 58

Table 2.4: Literature experimental data for H_2 solubility in pure water. 61

Table 2.5: Literature experimental data for CO_2 solubility in NaCl-brine 63

Table 2.6: Literature experimental data for O_2 solubility in NaCl-brine 64

Table 2.7: Literature experimental data for H_2 solubility in NaCl-brine 65

Table 3.1 : Purities and suppliers of the chemicals used in this work 96

Table 3.2 : Experimental and calculated solubilities of carbon dioxide in the CO_2 + H_2O + NaCl system, expressed as "salt-free" mole fractions. 99

Table 3.3 : Coefficients of the $kCO2, wAQNew$ correlation (Equation 3.6) 102

Table 3.4 : Pure water parameters (e-PR-CPA model), comparison with parameters from Hajiw et al. [3. 23] and parameters from Wang et al. [3. 24]. 104

Table 3.5 : The parameters of the Na^+ and Cl^- ions (e-PR-CPA model). 105

Table 3.6 : AAD (%) of the vapor pressure and osmotic coefficient calculated with the e-PR-CPA model. 108

Table 3.7 : Solubility of CO_2 in the CO_2-H_2O-NaCl system. AAD between experimental literature data and model predictions at different temperature and pressure ranges. 117

Table 4.1 : Chemical samples used for experimental work (CAS Registry Number, mole fraction purity and suppliers of chemicals). 138

Table 4.2 : Measured solubility of CO_2 in the H_2O + NaCl at 6m NaCl by the rocking cell setup, expressed as "salt-free" mole fractions. $uT = 0.17\ K$ and $uP = 0.068\ MPa$. 141

Table 4.3 : Measured solubility of O_2 in the H_2O + NaCl, expressed as "salt-free" mole fractions. For Technique 1: $uT = 0.02\ K$ and $uP = 0.005\ MPa$; For Technique 2: $uT = 0.17\ K$ and $uP = 0.068\ MPa$. 142

Table 4.4 : Coefficients of the binary interaction parameter $kO2, H2OAQSW$ of the SW model (Equation 4.4) 150

Table 4.5 : Zheng and Mao model interaction parameters for the O_2 solubility in NaCl brine 153

Table 4.6 : Calculated solubility (in terms of salt-free mole fraction) of CO_2 in water + NaCl by the e-PR-CPA model. 156

Table 4.7 : Calculated solubility (in terms of salt-free mole fraction) of O_2 in water + NaCl by the e-PR-CPA model. 157

Table 5.1 : Literature experimental data for H_2 solubility in pure water 173

Table 5.2 : Literature experimental data for H_2 solubility in saline water 174

Table 5.3 : Chemicals used in this work: purities and suppliers 174

Table 5.4: Measured solubility of H_2 in the H_2O + NaCl solutions, expressed as "salt-free" mole fractions (Equation 5.1). $uT = 0.02\ K$ and $uP = 5\ kPa$. 179

Table 5.5: Optimized coefficients of the binary interaction parameters in aqueous $kH2 - H2OAQ$ and non-aqueous $kH2 - H2ONA$ phases (Equation 5.7). 182

Table 5.6 : H_2+H_2O binary system: Predicted water content $yH2O$ in H_2-rich phase by the e-PR-CPA model. 187

Table 5.7: Coefficients for Equations 5.12 and 5.13. 191

Table 5.8 : Calculated solubility (in terms of salt-free mole fraction) of H_2 in water + NaCl by the e-PR-CPA model. 194

Table 6.1: Chemical samples used for experimental work (CAS Registry Number, mole fraction purity and suppliers of chemicals). 208

Table 6.2: Compositions of the studied CO_2+O_2 mixtures: Expected composition and real composition mole fractions 209

Table 6.3: Measured data of hydrate dissociation conditions of the CO_2+O_2 gas mixture and expanded uncertainties (k=2): $0.1 \leq U(T) \leq 0.6$ MPa and $0.04 \leq U(p) \leq 0.25$ MPa. 211

Table 6.4: e-PR-CPA EoS configuration: model parameters and properties used in the fitting. . 221

French summary / Introduction en Français

Les électrolytes aqueux sont très courants dans l'industrie et sont présents dans de nombreux applications. La compréhension thermodynamique du comportement des phases des systèmes Gaz+Eau+Sels est d'une grande importance pour des applications d'ingénieries comme le Captage et le Stockage du dioxyde de Carbone (CSC), le Stockage Souterrain réversible massif de Gaz (SSG) et l'inhibition de la formation d'hydrates durant la production et le transport de gaz. Dans le cadre du SSG, l'industrie de l'énergie s'intéresse aux vecteurs énergétiques gazeux les plus demandés dans le secteur, tels que l'hydrogène, l'oxygène, l'air comprimé, le méthane et le dioxyde de carbone. La conception, l'optimisation et la surveillance des installations de stockage, ainsi que leurs pilotages selon différents scénarii (stockage journalier, hebdomadaire, mensuel ou annuel) et l'évaluation des différents risques (mobilité du gaz dans le réservoir géologique, interaction avec la roche, production d'H_2S...) nécessitent la connaissance des diagrammes de phases et plus spécifiquement de la solubilité des gaz dans les saumures, les teneurs en eau et aussi les conditions de stabilité des hydrates de gaz dans le cadre de l'exploitation du gaz. Pour ce faire, il est primordial de disposer d'un modèle thermodynamique suffisamment précis dans les conditions opératoires du stockage et du transport, et le développement du modèle nécessite de disposer d'un minimum de données expérimentales fiables. Dans ce travail, l'effet "salting-out" sur les gaz est étudié par l'expérimentation et la modélisation. Cela concerne les mesures de solubilité des gaz dans la saumure en utilisant deux techniques expérimentales différentes, et la modélisation de la solubilité des gaz et teneur en eau des systèmes d'intérêt par des équations d'état développées et optimisées. L'étude est également étendue à la prédiction des courbes de stabilité des hydrates de gaz (purs ou mélangés) en présence ou sans sels.

Introduction

Aqueous electrolytes are very common in industry and are present in many contexts (salting-out of gases, gas hydrate inhibition, purification of proteins by ATPS technique, water desalination, corrosion and scale formation, etc.). The thermodynamic study of aqueous systems in the presence of electrolyte is crucial for the understanding of the various phenomena involved at the molecular scale, and for the determination of the thermophysical properties that are necessary for the design, optimization and control of processes. To do this, it is essential to develop a thermodynamic model based on theoretical foundations and with a low dependence on experimental data in order to be able to extrapolate it outside the adjustment range and possibly transpose it to other applications.

Understanding the phase behavior of Gas-Water-Salt systems is of great importance, whether in an environmental context such as Carbon dioxide Capture and Storage (CCS) or in an economic context such as enhanced oil recovery by CO_2 injection, or massive reversible Underground Gas Storage (UGS) for industrial use (Power-to-Gas (PtG), chemical, petrochemical and pharmaceutical industries, etc.). In the context of Underground Gas Storage, the gas industry is interested in the compounds that are most in demand in the sector, such as methane (or Natural Gas (NG) storage), carbon dioxide (pure for methanation units or mixed with methane for NG storage), oxygen (for oxycombustion units) and hydrogen (Underground Hydrogen Storage (UHS)), etc. The design and optimization of storage facilities, as well as the monitoring of temperature, pressure and quantity of gas in geological reservoirs (salt caverns and deep saline aquifers), require knowledge of phase diagrams (solubility, water content and hydrate stability conditions). The development of thermodynamic models for such systems (gas/water/salt) requires the availability of reliable experimental data. Na^+ and Cl^- are the main species found in the salts of most geological formations. Sodium chloride (NaCl) can therefore be considered a representative model of salt.

The main objective of this work is to study the thermodynamic equilibria of Gas+H_2O+NaCl systems and more precisely to highlight the "salting-out" effect which is materialized by the decrease of the solubility of gases in saline water compared to pure water because of the presence of salt ions which reduce the free volume and compete with the gas by interacting with the solvent (in particular the solvation of ions by water molecules). The thermodynamic study of the salting-out effect in Gas+H_2O+NaCl systems is carried out in two parts: Experimental and modeling. A

first step consists in performing the necessary experimental measurements to fill the lack of high-pressure experimental data of gas solubility in brine which will then be used to parameterize the thermodynamic models developed in order to describe qualitatively and quantitatively the phase equilibria for the mixtures of interest.

This manuscript is an article-based thesis based on the results obtained and published in four papers that report on experimental and modeling studies of the phase behavior of gas/water and gas/brine systems. The author's contribution in the various publications is presented in Appendix C. After an introduction to the context and challenges of underground gas storage in **Chapter 1**, a discussion on the study of phase equilibria, in particular gas solubility, through experimentation and modeling is provided in **Chapter 2**. In this chapter, the experimental apparatus and the developed models used in the published articles are presented. For gas solubility measurements, two different analytical techniques were used: The first one is based on the "static-analytic" method (phase sampling and Gas Chromatography (GC) analysis) and the second one is a rocking cell setup (liquid phase sampling, gas/brine separation, brine gravimetric analysis and gas volumetric analysis with gasometer). For the different applications (CCS, PtG-UGS and UHS) in the context of underground gas storage, the systems of interest considered in this study are: CO_2+H_2O+NaCl (**Chapter 3 and 4**), O_2+H_2O+NaCl (**Chapter 4**) and H_2+H_2O+NaCl (**Chapter 5**).

A new electrolyte thermodynamic model (e-PR-CPA), which takes into account all molecular and electrolyte interactions, has been developed. The model developed by Soreide and Whitson (SW) is widely used to study gas solubility in water + NaCl. During this work, the SW model with new proposed parameters (from this work) and the e-PR-CPA model were used to model the literature and measured solubility data and literature water content data. These models using the symmetrical (phi-phi) approach are also compared with a geochemical model using the asymmetrical (gamma-phi) approach. The excellent results obtained with the e-PR-CPA model motivated us to apply it to the prediction of hydrate stability conditions of single-gas and mixed gas systems in the presence or absence of salt (**Chapter 6**).

Finally, a user-friendly graphical interface (Appendix B) for the calculation of thermophysical properties of complex systems (electrolytes, gas hydrates, etc.) has been developed. The models used and developed in this work (SW and e-PR-CPA) as well as other equations of state (PR, SRK,

GERG) have been implemented in the interface. This software package (ThermoReservoir®) is intended for industrial and academic research labs.

This work is carried out as part of the “ANR FluidSTORY” project to store fluid energy carriers (O_2, CO_2, CH_4) in salt caverns, and also as part of the “GIS Géodénergies Rostock H” and “Carnot M.I.N.E.S HyTrend” projects, which aim to improve knowledge of the phenomena involved in underground hydrogen storage.

French summary / Chapitre 1 - Stockage Souterrain de Gaz (SSG)

Le stockage souterrain dans des réservoirs géologiques (naturels ou construits) est une technologie mature et une excellente solution pour le stockage à grande échelle de différents types de produits : liquides (hydrocarbures liquides et liquéfiés, éthylène, propylène...) ou gazeux (gaz naturel, hydrogène, air comprimé...). Etant une étape nécessaire pour assurer l'équilibre entre la production, l'offre et l'utilisation des produits, le stockage souterrain permet aussi de disposer d'une réserve "stratégique" afin de garantir la sécurité de l'approvisionnement en cas de perturbation. Le Stockage Souterrain de Gaz (SSG) est la principale solution pour le stockage massif de gaz et d'énergie, qu'il s'agisse d'un stockage réversible pour des raisons économiques (combustibles gazeux ou gaz à usage industriel) ou d'un stockage permanent pour des raisons environnementales (séquestration du dioxyde de carbone). À partir du début du XXe siècle, cette technologie a commencé à être de plus en plus utilisée, principalement pour le stockage du gaz naturel, du gaz de ville et de l'hydrogène. Par rapport aux installations de stockage en surface (réservoirs de gaz), les installations de stockage géologique sont moins coûteuses et sont protégées par une roche de couverture très épaisse. Ces installations peuvent supporter des pressions de stockage élevées, ce qui augmente la quantité de gaz stocké, mais également une très forte densité énergétique dans le cas du stockage d'énergie (air comprimé, gaz naturel et hydrogène), tout en maintenant des normes de sécurité plus élevées. Outre les volumes importants réalisables dans les stockages souterrains, ils permettent également des installations centralisées et très discrètes, sachant que seuls la salle de contrôle, les compresseurs, les colonnes de déshydratation et de désulfuration apparaissent en surface. Selon le type de stockage (réversible ou permanent), la nature du composé stocké (propriétés thermophysiques, taille, réactivité et mobilité...) ainsi que les conditions opératoires telles que la température, la pression et le scénario de stockage (injection/soutirage rapide ou lent), il existe différentes options de stockage de gaz dans des réservoirs géologiques : les gisements de pétrole et de gaz épuisés, les cavités salines ou minières, et les aquifères salins profonds.

Chapter 1: Underground Gas Storage (UGS)

1.1 Introduction

Following fluctuations in demand for any given product, storage is a necessary step to balance production, supply and use in order to avoid any under- or over-capacity, and also to have a "strategic" reserve to ensure security of supply in case of disruption. Underground storage in geological reservoirs (natural or constructed) is a mature technology and an excellent solution for the large-scale storage of different types of products: liquid (liquid and liquefied hydrocarbons, ethylene, propylene, etc.), gaseous (natural gas, hydrogen, compressed air, etc.) [1. 1].

Underground Gas Storage is the main solution for the massive storage of gas and energy, whether it is reversible storage for economic reasons (gaseous fuels or gas for industrial use) or permanent storage for environmental reasons (carbon sequestration). From the beginning of the 20th century, this technology started to be used more and more, mainly for the storage of natural gas and hydrogen. Compared to above-ground storage facilities (gas tanks), geological storage facilities are less costly [1. 2, 3, 4] and are protected by a cover rock several hundred meters thick that can withstand high storage pressures [1. 5], which increases the amount of gas stored, and hence a very high energy density in the case of energy storage (compressed air and hydrogen), while maintaining higher safety standards. In addition to the large volumes achievable in underground storage facilities, they also allow centralized and very discreet installations, knowing that only control room, compressors, dehydration and desulphurization columns appear on the surface.

Depending on the type of storage (reversible or permanent), the nature of the stored compound (thermophysical properties, size, reactivity, and mobility, etc.) as well as storage conditions such as temperature, pressure, and cycling time (rapid or slow injection/withdrawal), there are different storage options (geological reservoirs). Three main categories of geological reservoirs exist for underground gas storage (Figure 1.1): depleted oil and gas field, salt or mined caverns, and deep saline aquifers.

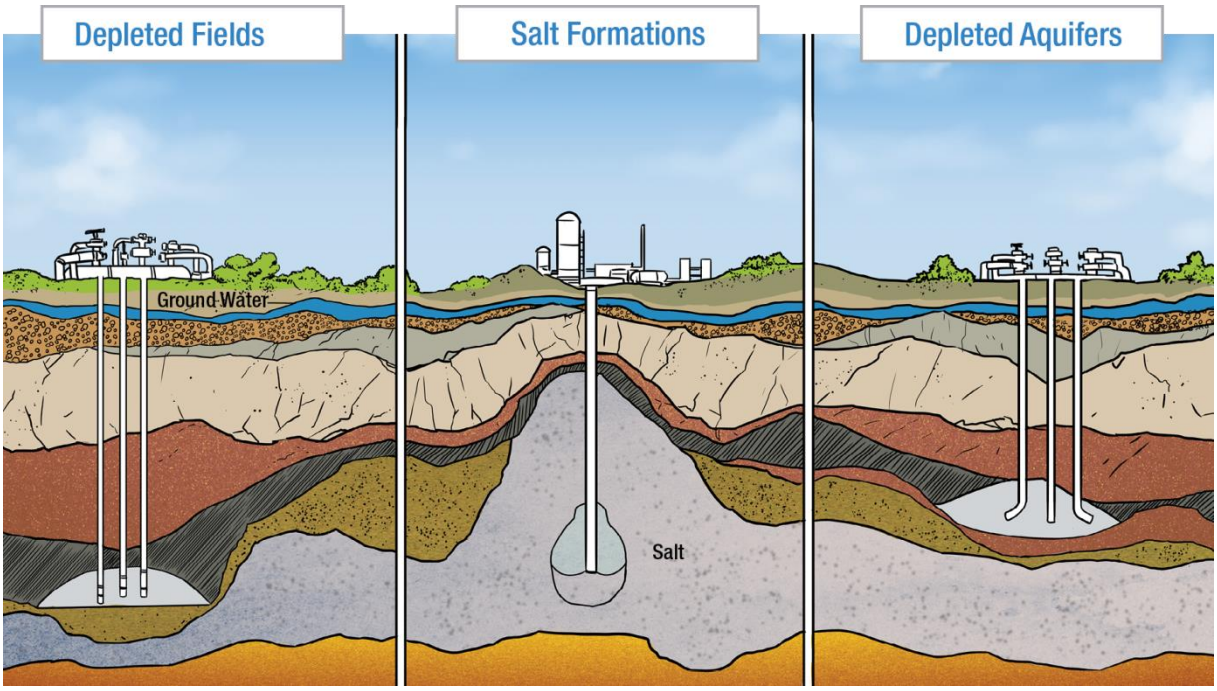

Figure 1.1: Principal types of underground gas storage [1. 6].

- Storage in depleted fields

The natural location of hydrocarbons can be used for gas storage. These large-volume fields are protected by impermeable geological rocks and are used to store gaseous hydrocarbons, particularly Natural Gas (NG), of which approximately 76% of NG storage worldwide [1. 1] and 68% of storage in Europe [1. 5] are of this type. However, this type of storage with high inertia [1. 7] (interesting for seasonal storage) is not suitable for rapid injection/withdrawal cycles. Moreover the gas fields are not completely depleted, approximately 50% of the gas remains in the reservoir (cushion gas) [1. 8], that's why this storage is well suited for NG but not for other gases like pure hydrogen or compressed air.

- Storage in salt or mined caverns

Salt caverns are man-made reservoirs constructed by dissolution in a massive layer of salt (bedded or domal salt), especially halite (NaCl) [1. 1], which can be used to store any type of fluid (liquid or gaseous). These cavities are characterized by their high volume (up to more than 1 million m^3 [1. 5]), excellent salt tightness, safe storage and resistance to high pressures (up to more than 200 bar). In contrast to depleted fields and aquifers, salt caverns are distinguished by their reactivity and flexibility of use [1. 7], knowing that several cycles (up to 10 times compared to natural porous

reservoirs) can be reached, and the relative volume of cushion gas (compared to recoverable gas) in this type of storage is much less (20 to 30%) [1. 5, 8]. This type of reservoir is well suited for highly mobile and reactive compounds such as hydrogen and compressed air. In addition, the percentage of storage in salt caverns is constantly increasing (e.g. in the USA: 11% in 1998, 16% in 2005, and 25% (projected) in 2008 [1. 9]) due to their technical advantages and economic benefits with a very low cost compared to other forms of storage.

The mined caverns are in the form of tunnels built by mechanical excavation of the rock at medium depths (less than 200 meters) which increases the risk of accidents when compared with salt caverns which are created only by dissolution. Mined caverns can also be used to store liquid or gaseous products, however their volumes are smaller in comparison with other forms of storage and have a higher CAPEX than salt caverns [1. 7].

- Storage in deep saline aquifers

Deep saline aquifers are rock formations containing non-potable water (brine with a high salt concentration called formation water), located at a depth of more than 1000 meters, and covered by an impermeable sedimentary layer called “caprock”. These huge natural reservoirs are distinguished by their large volumes (several billion m^3) and by long-standing experience (since 1953) [1. 7], however, they are much less flexible than salt caverns and require risk assessment related to the reactivity of the stored compounds with the rock entrained by significant microbial activity existing in the aquifers. With a very high percentage of the cushion gas (50 to 80%) [1. 8], storage in deep aquifers is less and less considered for reversible storage especially after the increase in NG prices, and even less recommended for pure hydrogen (requires very large volumes), however, it is still the predominant form of storage in the world as the majority of storage facilities were developed when NG was not so expensive, and it is considered the ideal solution for permanent storage, such as carbon dioxide sequestration [1. 10].

1.2 Carbon dioxide Capture and Storage (CCS)

Carbon dioxide (CO_2) emissions, which is the main greenhouse gas (in terms of quantity) produced by human activity, are constantly increasing, mainly due to the exploitation and use of fossil fuels. One of the possible solutions, that is of great interest to industrial actors in the gas sector, is to capture, transport and store CO_2 in deep geological formations. The latter solution can be combined

with Enhanced Oil Recovery by CO_2 injection (CO_2-EOR). This is part of another variety of CCS which is the CCUS (Carbon dioxide Capture, Utilization and Storage) whose principle is to valorize CO_2 to make the technology profitable or at least compensate the high cost of the capture part which is mainly done by absorption using amine based solvents (very expensive process from an energy point of view). A second Utilization/Storage option is CO_2 Enhanced Coal Bed Methane recovery (CO_2-ECBM), which consists of extracting adsorbed methane from unminable coal beds by replacing it with CO_2 (sorption trapping), which has a higher heat of adsorption [1. 11]. These different storage options are illustrated in Figure 1.2.

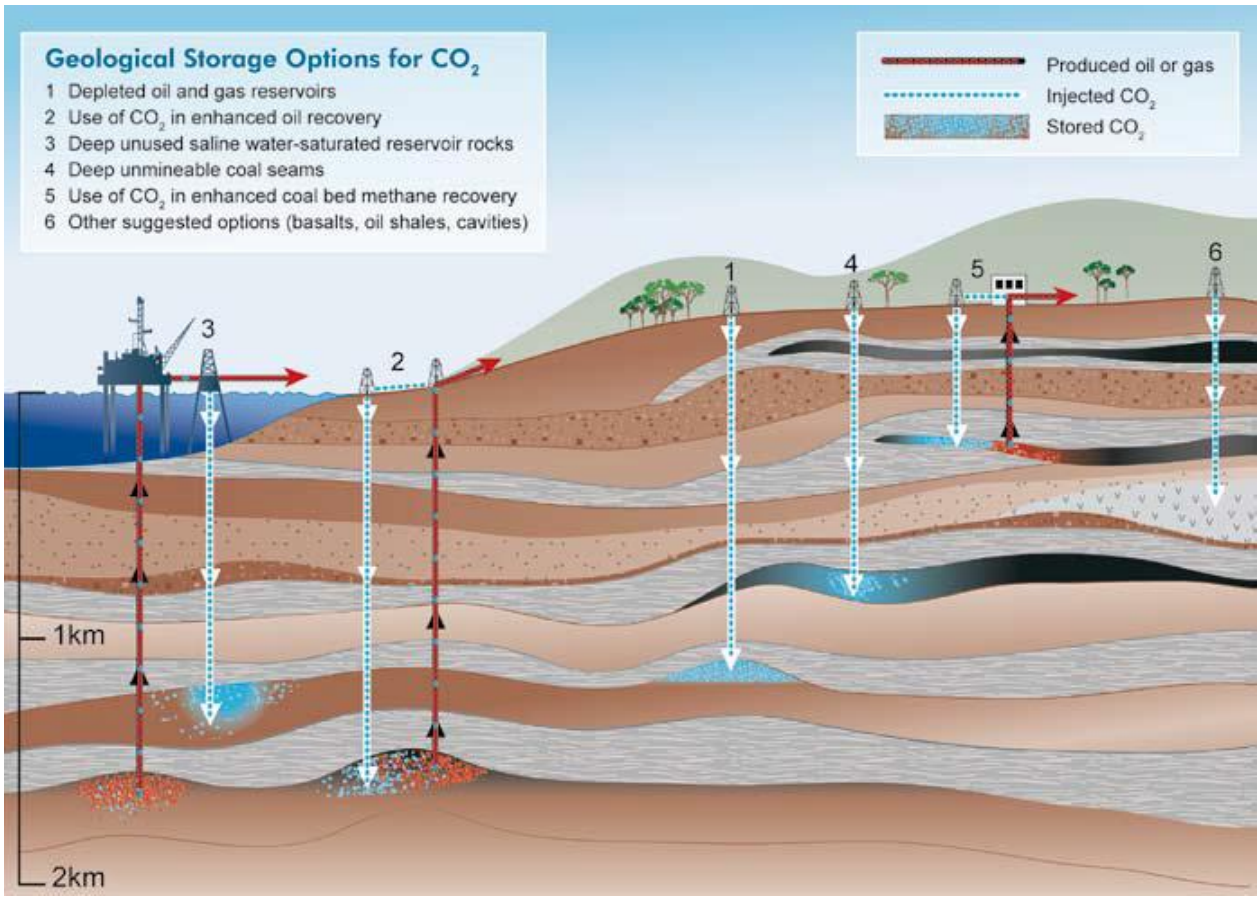

Figure 1.2: Different CO_2 storage options in deep underground geological formations [1. 12].

Moreover, for an economic purpose, the reversible storage of carbon dioxide (especially in salt caverns) is an interesting solution to meet the high demand for this gas in several chemical (urea, methanol, and polyurethanes production [1. 11], etc.) and biochemical applications (fermentation, water treatment, carbonation of drinks, etc.) and in applications within the Power-To-Gas concept

(see session 1.3.3) by combining it with hydrogen (through methanation) produced from renewable electricity by water electrolysis. To date, CO_2 storage in deep porous media (saline aquifers and oil and gas fields) is a mature technology, and has been deployed in several countries around the world through several industrial-scale projects (Sleipner in Norway, Weyburn in Canada, In Salah in Algeria, Salt Creek in USA, etc.) [1. 12]. Permanent storage (sequestration) of CO_2 in deep saline aquifers is considered the best option given the huge storage volumes [1. 10] as well as the fact that it is more widespread around the world.

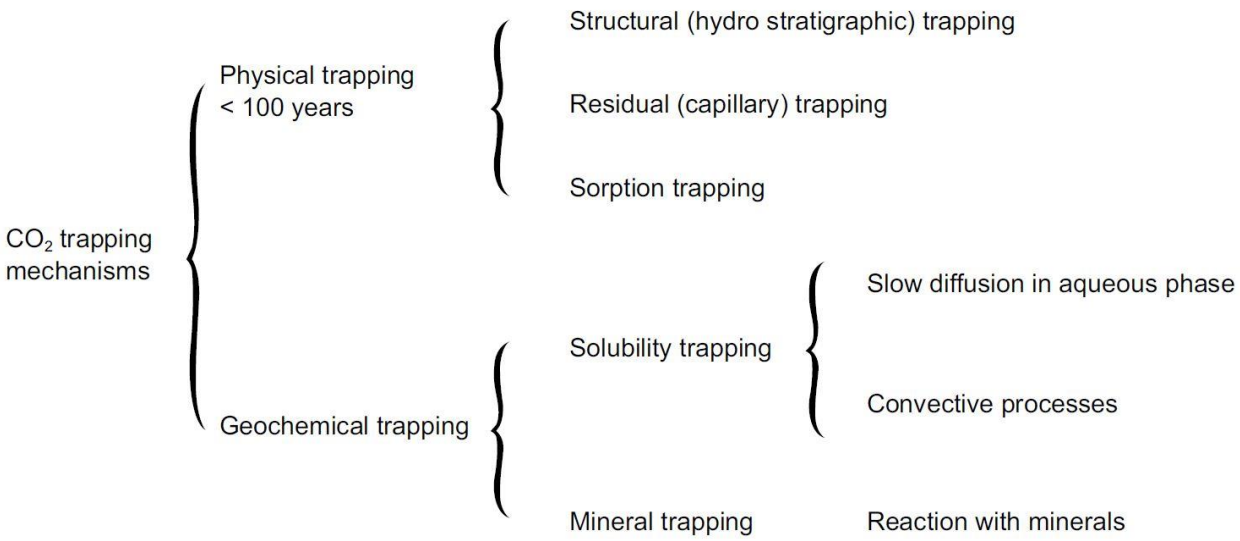

Figure 1.3: CO_2 trapping mechanisms [1. 10].

For CO_2 sequestration in deep saline aquifers, four mechanisms (structural, residual, solubility, and mineral trapping, see Figure 1.3) occur and are classified into two categories (physical and geochemical). First, by being denser than the formation water, the injected CO_2 will float to the caprock to stagnate in a structural trap under this impermeable rock (hydrodynamic, structural, or stratigraphic trapping). Then the formation water invades the CO_2 plume by saturating and isolating some of the CO_2 (residual trapping). Depending on the hydrodynamic activity of the aquifer, CO_2 dissolves (solubility trapping) in the brine over time until the saturation of the brine is reached, and this is the major trapping mechanism (active in an order of magnitude of time from 1 to 1000 years [1. 11]). The solubility of CO_2 in brine depends on the thermodynamic conditions of the geological environment, which are: the temperature and pressure in the reservoir, and the composition (brine salinity and impurity fractions) of the fluids involved (gas and brine). Eventually, the dissolved

CO_2 reacts with the reservoir minerals to form carbonate species (mineral trapping), which transforms the CO_2 into its most stable form for millions of years [1. 12].

1.3 Massive gas and energy storage

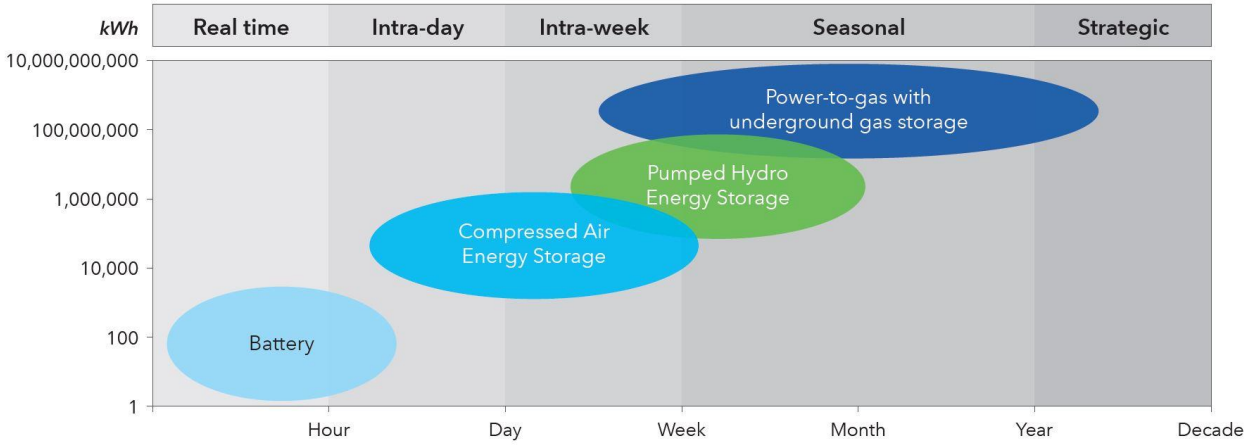

Figure 1.4: Overview of the different types of energy storage according to their discharge times and storage capacities ([1. 13]).

The storage of excess electrical energy in batteries is not suitable for storing large amounts of electricity. However, large-scale solutions exist in the form of mechanical storage (Compressed Air Energy Storage and Pumped Hydro Energy Storage) and chemical storage (Power-to-Gas: hydrogen and/or synthetic natural gas) in underground geological reservoirs. This is illustrated in Figure 1.4 which shows the different forms of energy storage according to their discharge times and storage capacity. Solutions involving underground gas storage are discussed below.

1.3.1 Compressed Air Energy Storage (CAES)

Compressed Air Energy Storage (CAES, Figure 1.5) is an important solution for storing surplus electricity by using it to compress air at high pressure and store it in an underground reservoir (mainly salt or mined caverns). Later, when the demand for electricity is high, the compressed air is recovered from the cavern, and burned and expanded in a gas turbine with fuel.

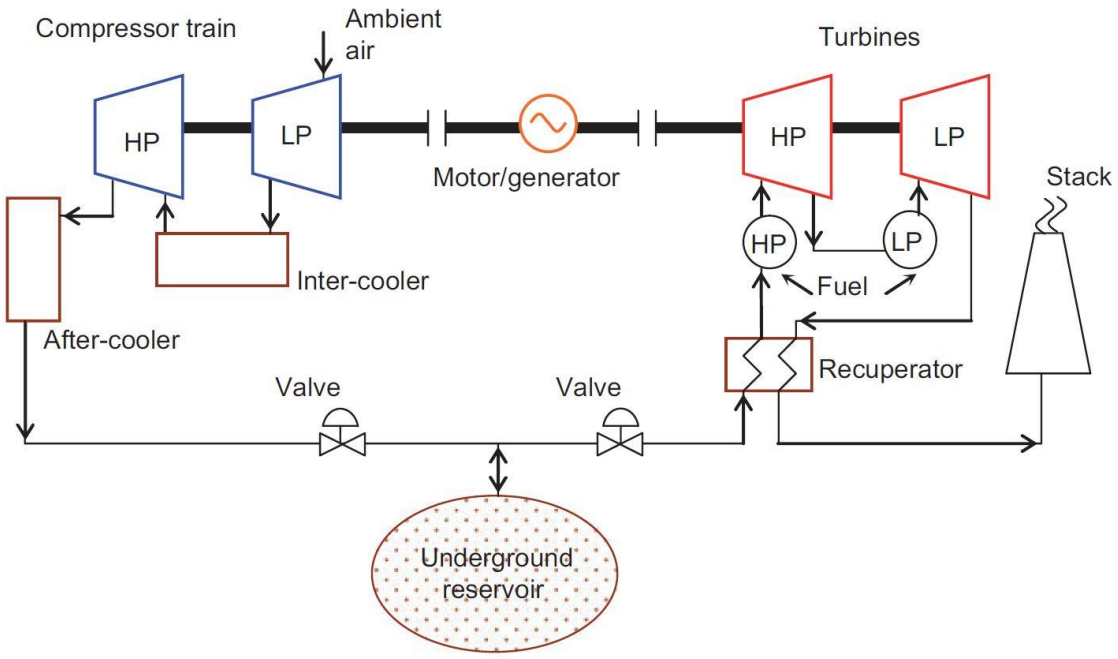

Figure 1.5: Principle of a CAES process [1. 14].

The CAES technology is a mature process and currently there are two operational storage sites (in salt caverns) around the world: Huntorf in Germany (since 1979) with a capacity of 290 MW, and McIntosh in the USA (since 1991) with a capacity of 110 MW [1. 1].

1.3.2 Underground Hydrogen Storage (UHS)

Hydrogen (H_2) is considered to be a renewable energy carrier with promising prospects for energy transition (Figure 1.6). It can be used directly in fuel cells for transport and mobility applications, or as a complement to existing energy resources such as the production of synthetic methane by combining it with CO_2 through methanation, and the injection into existing Natural Gas (NG) networks with the aim of reducing consumption (in the short term) and stopping the use (in the long term) of fossil fuels. To manage the intermittent nature of renewable energy sources such as wind and solar power, surplus electricity can be stored in chemical form by producing H_2 through water electrolysis (Power-to-Gas concept, see section 1.3.3). In order to balance the temporal differences between production and demand, storage of pure or blended (e.g. with NG [1. 15, 16]) hydrogen is necessary.

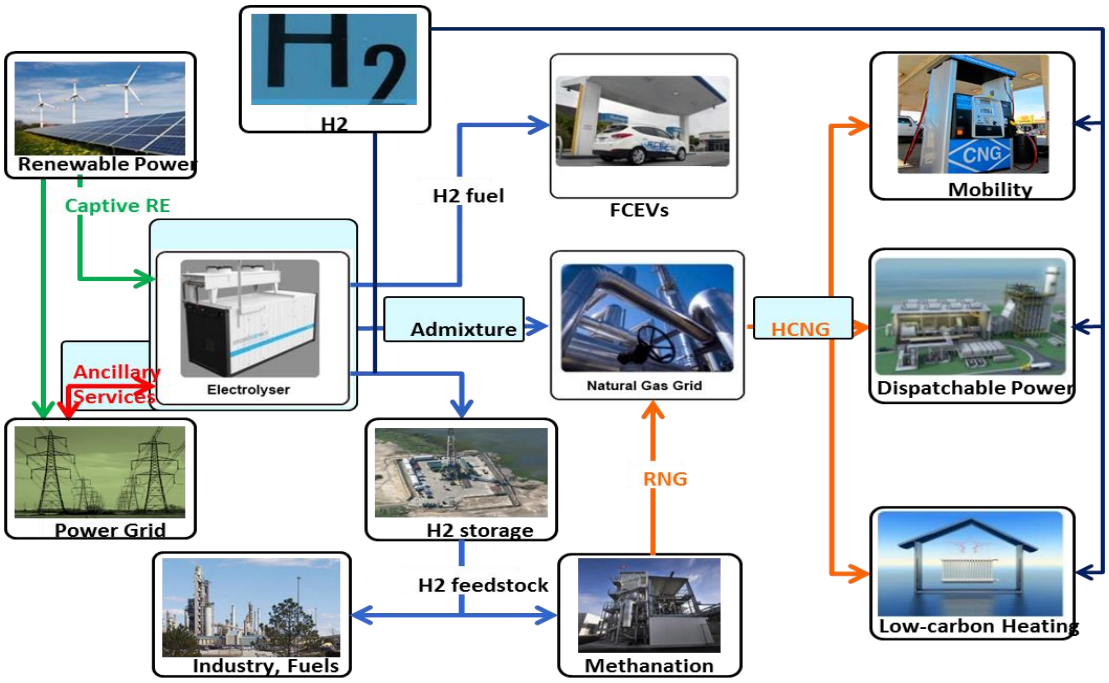

Figure 1.6: Hydrogen Production, Storage and Use (modified after EARTO 2014 [1. 17])

Hydrogen can be stored in gaseous form in gas cylinders, in liquid form in cryogenic tanks, or in solid form by adsorption, absorption or by reacting with some chemical compounds [1. 18]. However, the most studied and used technology for hydrogen large-scale storage is underground storage in geological formations such as salt caverns, deep aquifers, and depleted gas fields.

Table 1.1: Operational H_2 storage caverns around the world [1. 19].

	Clemens Dome (USA)	Moss Bluff (USA)	Spindletop (USA)	Teesside (United Kingdom)
Geology	Salt dome	Salt dome	Salt dome	Bedded salt
Operator	ConocoPhillips	Praxair	Air Liquide	Sabic
Implementing	1983	2007	2014	1972
Geom. Volume [m^3]	580 000	566 000	906 000	3 * 70 000
Mean cavern depth [m]	1 000	1 200	1 340	365
Pressure range [bar]	70-137	55-152	68-202	45
H_2-capacity [GWh]	81	123	274	27
Amount of H_2 [t]	2 400	3 690	8 230	810
Net volume [Sm^3]	27.3E06	41.5E06	92.6E06	9.12E06

Hydrogen storage in salt caverns has been done successfully for decades. However, none of this storage has been done for energetic purposes, since the stored hydrogen was mainly dedicated to

the chemical and petrochemical industry. Large quantities of hydrogen are used [1. 20] in refineries (50%) to remove/recover sulfur from fuels using hydrotreating (hydrogenation process), and in the Haber process (32%) for ammonia (NH_3) synthesis by combining nitrogen (N_2) and hydrogen (H_2). Currently, four sites for hydrogen storage in salt caverns are operational worldwide (Table 1.1): three in the USA (Clemens Dome, Moss Bluff, Spindletop) and one in the UK (Teesside). Several projects are in progress or have just been completed studying for energy purposes the storage of pure hydrogen in salt caverns (H2STORE, HyUnder, HyStock, Rostock H, STOPIL H2, etc.) and in gas fields (SunStorage and HyChico projects) or possibly mixed with CO_2 in deep saline aquifers (Underground bio-methanation concept [1. 21]) or with CH_4 (SunStorage and HyChico projects).

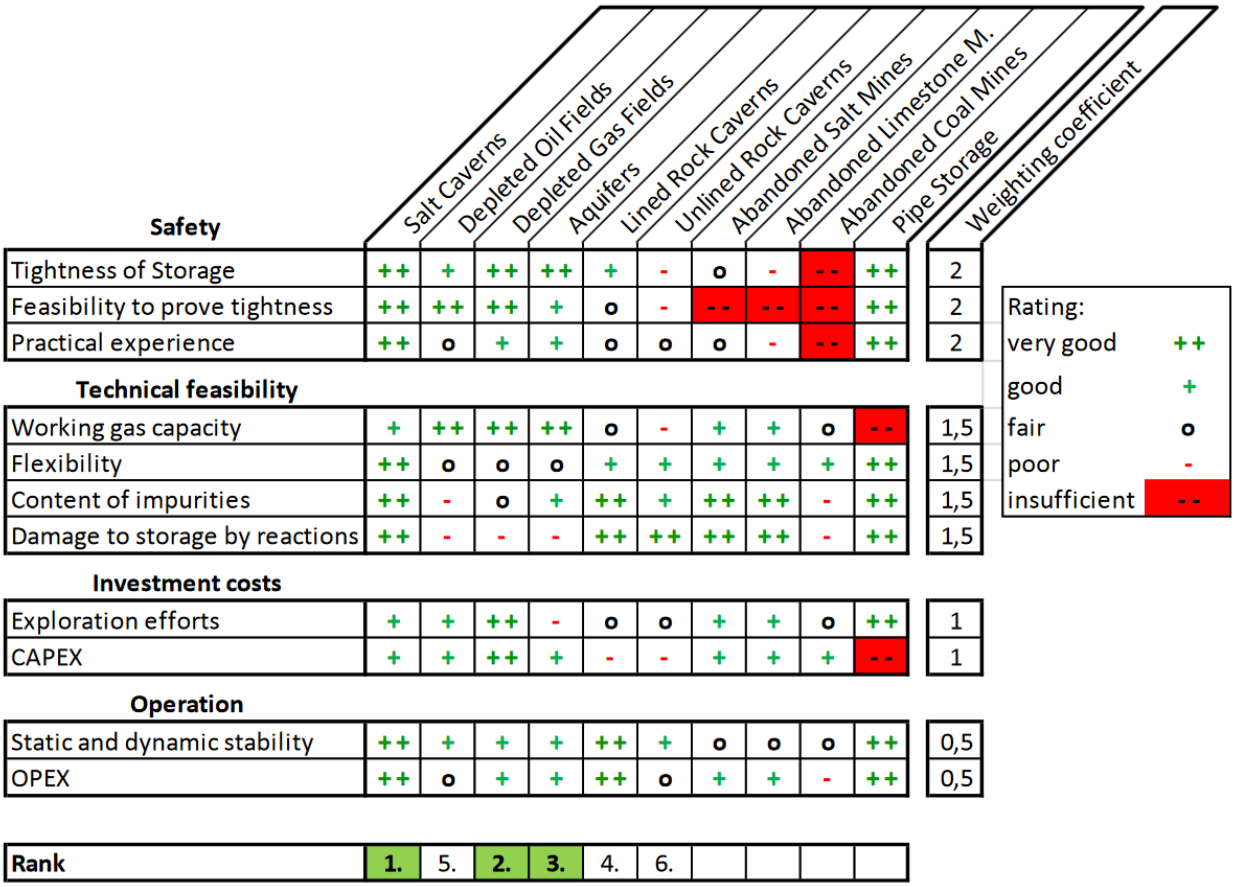

Figure 1.7: Comparison of different options for high-pressure hydrogen storage [1. 22].

A benchmarking study of the different options for high-pressure hydrogen storage was carried out as part of the European project HyUnder [1. 22]. The results of this comparative study are illustrated in Figure 1.7, and show that, according to the different techno-economic and safety

factors, storage in salt caverns is first in the ranking, followed by storage in depleted gas fields and storage in deep saline aquifers. Finally, hydrogen (especially pure) storage in salt caverns is preferred for several reasons [1. 19]: the least expensive of all forms of storage, less cushion gas than storage in porous media, the possibility of several injection/withdrawal cycles, and a positive experience feedback.

1.3.3 From Power-to-Gas (PtG) to massive underground energy carriers storage

The growing integration of renewable energies, mainly intermittent (with issues of overcapacity and redundancy) in the short term (energy transition) and the total replacement of fossil fuel use in the long term, requires a flexible solution for large-scale energy storage.

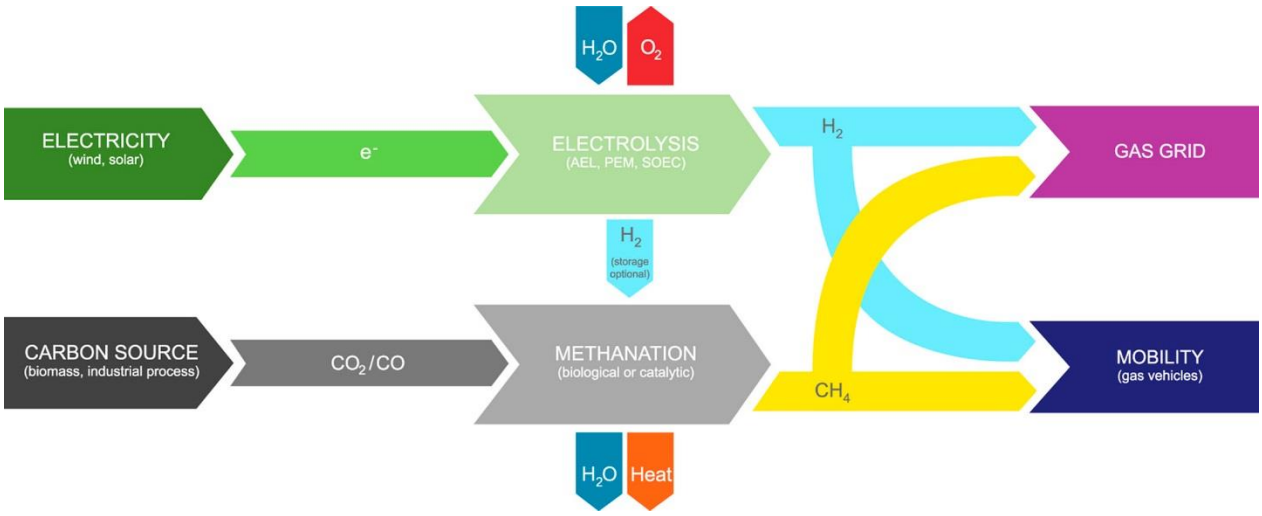

Figure 1.8: Power-to-Gas concept [1. 23].

The conversion of electricity surplus into H_2 by electrolysis of H_2O is one of the best solutions for the storage of intermittent renewable energies (wind and solar). Methanation (Sabatier process) is a catalytic (or biological) reaction to produce CH_4 from a mixture of CO_2 and H_2, and energy supply. This technology known as Power-to-Gas (PtG) is illustrated in Figure 1.8.

The reactions involved in PtG process chain are as follows:

Electrolysis: $2\,H_2O \rightarrow 2\,H_2 + O_2$ **1.1**

Methanation: $CO_2 + 4\,H_2 \rightarrow CH_4 + 2\,H_2O$ **1.2**

Large quantities of CO_2 and energy carriers (H_2 and CH_4) involved in the PtG process need to be stored to control the whole process and the time interval between production, transport, and use of these gases. Being a mature technology, underground gas storage is the best (and only) solution for the massive storage of these large quantities of gas (see Figure 1.4). Several underground storage options can be used to store these energy carriers as well as different process configurations are possible such as the combination of Electrolysis, Methanation and Oxycombustion (EMO).

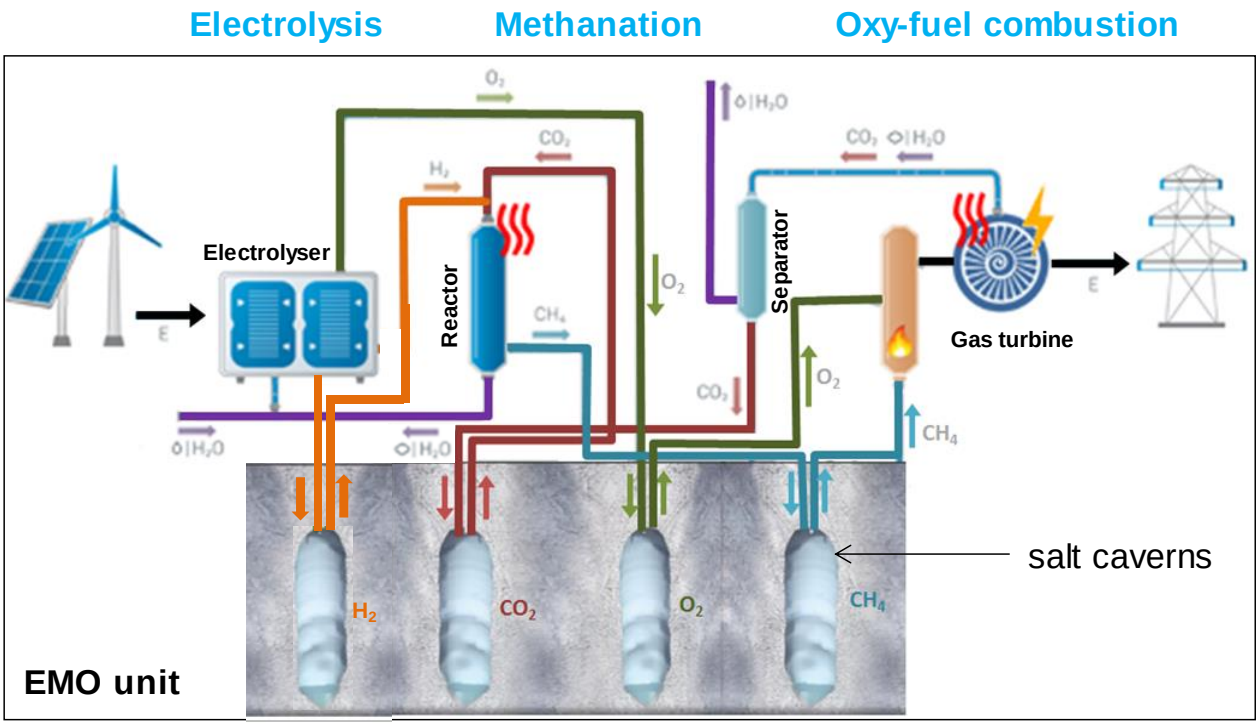

Figure 1.9: EMO unit concept (FLUIDSTORY project).

The oxycombustion process uses oxygen as an oxidant instead of air for energy production while avoiding NOx emissions and facilitating the recovery of CO_2 from the flue gases since they are mostly enriched by the latter. This technology needs large quantities of oxygen and requires the centralization of oxygen production and storage. In the framework of the ANR FLUIDSTORY project, an innovative concept (Electrolysis-Methanation-Oxycombustion (EMO) unit) [1. 24] for energy storage (Figure 1.9) concerns the supply of oxycombustion with oxygen from water electrolysis using renewable electricity, and with methane produced by methanation using

hydrogen from electrolysis as well and CO_2 recovered from oxycombustion flue gases. To manage the time laps between the production and use of these energy carriers (H_2, O_2, CH_4, and CO_2), the underground storage in salt caverns is suggested since it is considered to be the most flexible (high rates of injection/withdrawal cycles) solution for large-scale gas storage.

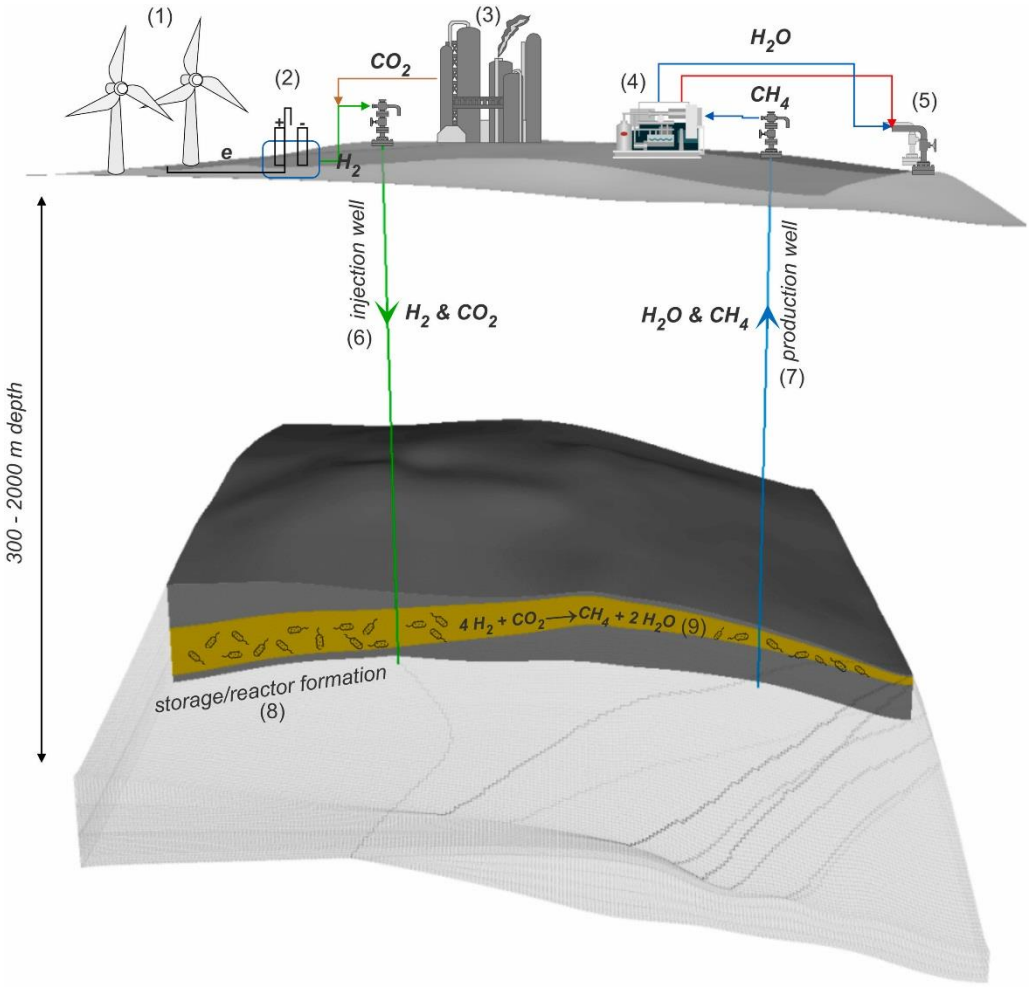

Figure 1.10: Schematic of underground bio-methanation concept [1. 21].

Other prospects exist for PtG, such as the mixed storage of H_2 and CO_2 in porous media (depleted oil and/or gas reservoirs or deep saline aquifers). The idea is to carry out the methanation reaction using the biological activity (methanogenic archaea) existing in this type of geological formation (see Figure 1.10), and which catalyzes the reaction. These natural reactors, also known as Underground Methanation Reactors (UMR), increase the stored energy by transforming hydrogen into methane, which has greater energy potential [1. 25]. It should be noted that there is good feedback concerning the storage of hydrogen mixed with carbon dioxide, methane, and other

impurities. In the middle of the 20th century (1940-1970), the storage of "town gas" which was industrially produced from coal gasification and mainly composed of H_2, CH_4, N_2, and $CO+CO_2$ was carried out in depleted oil and/or gas fields and saline aquifers in several countries (Germany, France, Poland, Czech Republic, and USA, etc.) to control seasonal fluctuations in gas demand [1. 21]. In most reservoirs, significant changes in the stored gas have been observed, such as its quantity (gas dissolution, its reaction with rock minerals, and precipitation), composition (gases consumption and production as a result of various geochemical reactions) and temperature (heating value due to methanation), the appearance of significant quantities of H_2S (hydrolysis of carbonyl sulfide or reduction of sulfate by bacteria [1. 19]), acidification (carbonic acid (H_2CO_3) production), and increased corrosion in reservoir facilities. This was explained by the fact that the biological activity is generally very favorable in this type of geological environment.

Finally, past and current experience with the storage of hydrogen mixtures (town gas) in porous media and pure hydrogen in salt caverns prove the possibility and reliability of underground storage of this precious energy carrier. However, several practical problems have been encountered, and require in-depth study for the total control of massive underground storage of gas and energy.

1.4 Issues: Phase equilibria involving gas, water and electrolytes

The presence of brine in salt caverns and porous media completely changes the thermodynamic behavior of the stored gas (salting-out effect and geochemical reactions) due to the existence of electrolytes (NaCl, KCl, $MgCl_2$, etc.) [1. 26] dissolved in the residual water of the cavern or deep aquifer, so studying these systems becomes very complicated. Na+ and Cl- are the main species found in the salts of most geological formations. The sodium chloride solution is therefore considered to be a representative model of brine [1. 27]. Therefore, thermophysical study of gas-water-NaCl systems is of great industrial interest. The solubility and water content of stored gases as well as the hydrate formation conditions of systems containing gas, water and salt are extremely important information to be known for the monitoring and control of the storage facilities as well as for the assessment of the various possible risks.

1.4.1 Gas solubility

The solubility of gases in brine is a very important property for the estimation of storage capacities, the study of dissolved gas mobility, and the calculation of chemical speciation including gases,

rock minerals and other species existing in the reservoir. Depending on the type and conditions of the geological storage environment (temperature, pressure, salinity, pH-value, presence of oxygen, etc.), several reactions can be initiated and accelerated by the existing biological activity, and this also depends on the reactivity of the stored gas. Below, some details are given on the importance of solubility specifically for each (reactive) gas of interest, which has a direct effect on the degree of reactivity since the majority (if not all) of geochemical reactions take place in the aqueous phase.

- **Carbon dioxide (CO_2)**

The solubility of CO_2 in brine plays a crucial role in several chemical and geochemical/petrochemical applications such as: formation/dissociation of gas hydrates for inhibition or separation purposes, seawater desalination, CO_2-EOR, CO_2 sequestration in deep saline aquifers or CO_2 injection into deep seabed. As indicated earlier, solubility trapping in porous media is the most important storage mechanism (up to 90% [1. 28, 29]) in the medium term, which is one more reason for the need for accurate quantification of the maximum amount (solubility) of dissolved CO_2 in the aqueous phase. Dissolution of CO_2 decreases the pH of the medium and creates geochemical disequilibria [1. 30], causing fluid/fluid and fluid/rock reactions (dissolution-precipitation process). CO_2 dissolved in the aqueous phase forms carbonic acid (H_2CO_3) which decomposes into cations (H^+) and anions (HCO_3^- and/or CO_3^{2-}) [1. 10] as follows:

$$\mathrm{CO_{2(aq)} + H_2O \leftrightarrow H_2CO_3 \leftrightarrow H^+ + HCO_3^- \leftrightarrow CO_3^{2-} + 2H^+} \qquad \textbf{1.3}$$

Some minerals (originally stable in solid state) such as calcium, sodium, magnesium, potassium basic silicate, etc. can be destabilized, released in the brine from the rock and react with other ions to form insoluble species as shown by the following reactions [1. 10]:

$$Ca^{2+} + CO_{2(aq)} + H_2O \leftrightarrow H^+ + CaHCO_{3(aq)}^+ \quad \textbf{1.4}$$

$$Na^+ + CO_{2(aq)} + H_2O \leftrightarrow H^+ + NaHCO_{3(aq)} \quad \textbf{1.5}$$

$$Mg^{2+} + 2CO_{2(aq)} + 2H_2O \leftrightarrow 2H^+ + Mg(HCO_3)_{2(aq)} \quad \textbf{1.6}$$

$$Ca^{2+} + CO_{2(aq)} + H_2O \leftrightarrow 2H^+ + \text{Calcite} \quad \textbf{1.7}$$

$$3\ \text{K-feldspar} + 2CO_{2(aq)} + 2H_2O \leftrightarrow \text{Muscovite} + 6\ \text{Quartz} + 2K^+ + 2HCO_3^- \quad \textbf{1.8}$$

To account for these potential reactions, the solubility of CO_2 in the aqueous phase under the different geological conditions of storage (temperature, pressure, and salinity) must be known.

- **Oxygen (O_2)**

The study of the solubility of oxygen in natural water, which is generally saline, is important for several scientific and engineering fields such as hydrometallurgy [1. 31], bioprocess engineering [1. 32], oceanography and geochemistry [1. 33], etc. Underground gas and energy storage is one of the geochemical applications that require the knowledge of the phase equilibrium of the O_2 + water + salt mixture, since oxygen is generally always present in gas streams, whether as impurity as in the case of flue gases storage in the context of Carbon Capture and Storage (CCS), or in large quantities as in the case of Compressed Air Energy Storage (CAES). Due to its very high reactivity in the aqueous phase, oxygen can lead to some corrosion mechanisms [1. 34], participate in geochemical reactions such as the oxidation of pyrite possibly present in the geological formation or can be used by micro-organisms leading to the contamination of the stored products [1. 35]. The injection of oxygen into porous formations leads to the reduction of its concentration mainly by the presence of sulfide minerals in the reservoir [1. 34]. Pyrite (FeS_2) is considered to be the major reactant, and its oxidation (Equation 1.9) results in the production of ferric ions (Fe^{3+}) which hydrolyze (Equation 1.10) to form the precipitate (insoluble) ferric hydroxide ($Fe(OH)_3$) as follows:

$$FeS_2 + {}^{15}/_4\, O_{2(aq)} + {}^{1}/_2\, H_2O \leftrightarrow Fe^{3+} + 2SO_4^{2-} + H^+ \quad \textbf{1.9}$$

$$Fe^{3+} + 3H_2O \leftrightarrow Fe(OH)_3 + 3H^+ \quad \textbf{1.10}$$

Depending on the conditions of storage formation (temperature and pH), the ferric hydroxide ($Fe(OH)_3$) can be transformed to other minerals such as goethite, ferryhydrite, hematite and

jarosite, etc. [1. 34, 36]. These different oxidation reactions can lead to the reduction of permeability for storage in porous media [1. 34].

In the case of CAES, the consumption of oxygen in the various geochemical reactions can lead to a significant decrease in the composition of oxygen in the stored air and can become lower than the minimum oxygen concentration (MOC) necessary for flame propagation for combustion in gas turbines, especially for long residence time storage [1. 36]. For this reason, as well as those discussed earlier, accurate determination of oxygen solubility in the aqueous phase (residual brine in salt caverns or formation water of porous media) under the thermodynamic conditions of storage (temperature, pressure, and salinity) is therefore necessary for the quantification of oxygen losses and the assessment of different risks related to oxidation and corrosion.

- **Hydrogen (H_2)**

Underground Hydrogen Storage (UHS) is much less studied than underground natural gas storage, therefore in most existing hydrogen storage sites, the pressure does not exceed more or less than 150 bar (and more recently up to 200 bars in the USA by Air Liquide, see Table 1.1). This is explained by its high mobility due to its small size [1. 37], as well as its high reactivity (redox reactions) by possibly participating in certain biochemical reactions, especially in the case of storage in porous formation, due to the microbial metabolism [1. 38, 39]. Below the reactions that may occur (depending on the presence of carbon dioxide and the geological formation conditions) are presented:

Methanogenesis: $CO_2 + 4H_2 \rightarrow CH_4 + 2H_2O$ **1.11**

Acetogenesis: $2CO_2 + 4H_2 \rightarrow CH_3COOH + 2H_2O$ **1.12**

Sulfate-reduction: $SO_4^{2-} + 5H_2 \rightarrow H_2S + 4H_2O$ **1.13**

Iron-reduction: $3Fe_2^{III}O_3 + H_2 \rightarrow 2Fe_3^{II}O_4 + H_2O$ **1.14**

Most of these types of reactions can take place in the aqueous medium, i.e. in the residual brine after the solution mining of salt caverns or in the formation water of porous formation. The study of the mobility and reactivity of hydrogen is therefore necessary for the total control of the storage of this molecule (quality and quantity control), as well as for the reduction of the safety factors used (just by experience feedback), and consequently a more efficient and economical storage. In

order to be able to perform chemical speciation calculations and study its mobility, it is therefore necessary to determine precisely the solubility of hydrogen in the aqueous phase under the thermodynamic storage conditions taking into account temperature, pressure and salinity. Finally, the simulation and control of storage facilities, as well as the monitoring of hydrogen (temperature, pressure and quantity) in the reservoir (salt cavern, depleted gas fields or aquifer), requires knowledge of phase diagrams (solubility and water content of hydrogen) [1. 40].

1.4.2 Water content (or moisture content) in gas-rich phase

In reversible underground storage of gas and energy, it is necessary to control the quality of the gas after withdrawal before it is delivered to end users. One of the crucial properties to be checked is the water content (moisture content) in the gas stream. The presence of a non-negligible amount of water vapor in the gas stream can cause several problems, e.g. equipment damage and flow insurance issues. Corrosion and ice and/or hydrate formation (see Section 1.4.3) in surface facilities are the major problems resulting from the presence of water vapor in the gas which can condense [1. 41] by cooling (and/or compressing) during gas transmission (the operating temperature at the surface is generally lower than the storage temperature in the reservoir). The lifetime of surface installations (compressors, valves, process units, and pipelines) depends on the corrosion rate, which is proportional to the amount of water in the gas stream. In addition, the presence of even small amounts of oxygen makes localized corrosion more severe [1. 42].

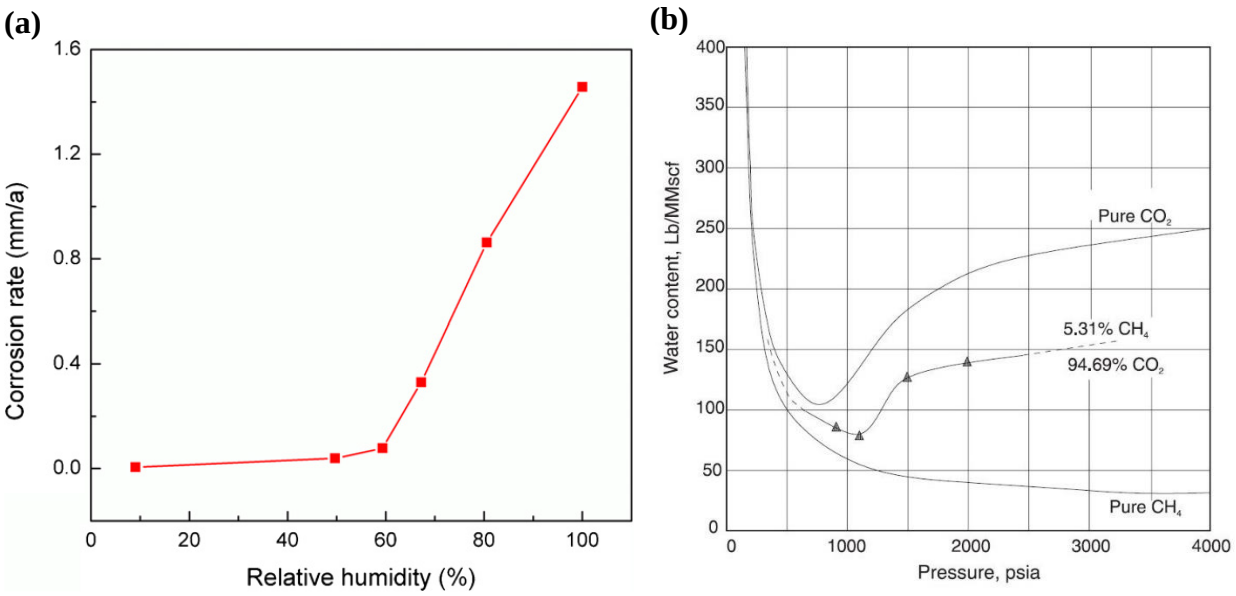

Figure 1.11: (a): Example of the effect of moisture (in terms of relative humidity) on the corrosion rate of X70 steel used in pipelines transporting a CO_2-rich gas stream in the context of CCS [1. 43]; (b): saturated water content tables of CO_2/CH_4 mixtures [1. 44].

CO_2 causes significant economic losses due to its high corrosion potential, accounting for about 55% of the damage suffered by the oil and gas industries [1. 45]. For example, in the case of CO_2 transport, once dissolved in condensed water, the CO_2 is hydrated to form carbonic acid (H_2CO_3) which dissociates to form the various ions (HCO_3^-, CO_3^{2-} and H^+, see Equation 1.3) that are mainly involved in the corrosion process in the presence of this acid gas. In Figure 1.11, an example of the effect of moisture (relative to water saturation of the gas) on the corrosion rate of X70 steel used in pipelines transporting a CO_2-rich gas stream in the context of CCS [1. 43] is illustrated (a), and an example of gas (CO_2/CH_4 mixtures) water content tables under operating conditions used in gas industry [1. 44] is given (b).

Gases extracted from geological reservoirs are mainly saturated with water vapor (liquid-vapor equilibrium) due to the contact (mass transfer) of the gas with formation water in porous media or with residual brine in salt caverns. An obligatory dehydration stage is carried out after the gas is withdrawn from the underground storage [1. 44]. The knowledge of the saturated water content of the gas under storage conditions is necessary e.g. for the study of the risk of corrosion and hydrate formation (see session 1.4.3) and for the calculation (material and energy balance) and design of the dehydration process to meet certain water content specification.

1.4.3 Gas Hydrates

Hydrates consist of small molecules in liquid or vapor state called "guest molecules" surrounded by a solid network (in the form of cages) of water molecules considered as "host molecules" by means of Van der Waals forces and hydrogen bonding forming an “ice-like” solid but with different properties and structures than ice. Gases such as NG, CH_4, CO_2, O_2, etc. in the presence of water can form gas hydrates (e.g. CO_2 hydrates, see Figure 1.12) even at temperatures above the melting temperature of the ice.

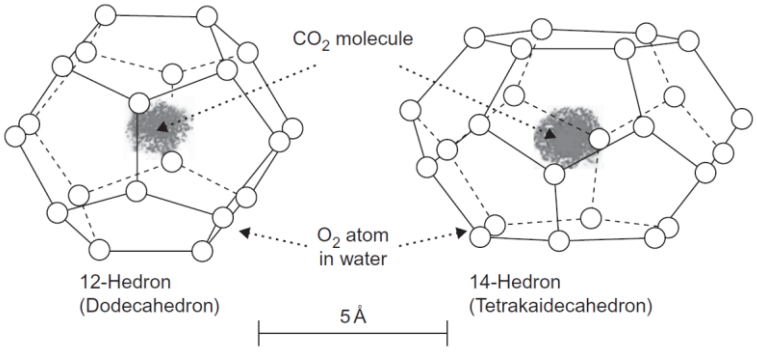

Figure 1.12: Molecular structure of CO_2 hydrates.

Hydrates exist in nature in the form of massive amounts of methane (CH_4) trapped in clathrate hydrates in permafrost and on the ocean floor (Figure 1.13-a). Despite the difficulty of extracting the sequestered methane, several studies and tests have been done or are in progress (e.g. in Japan) to extract it at a lower cost and possibly replace CH_4 by CO_2 that can be sequestered in these clathrates on the seabed within the framework of the CCUS technology.

(a) **(b)**

Figure 1.13: (a): in situ methane hydrate [1. 46]; (b): Gas hydrate plug in a pipeline [1. 47].

A very common problem in the gas industry is the clogging of pipelines and equipment by the formation of gas hydrates, which causes a flow assurance issue by limiting or even interrupting the flow (Figure 1.13-b). In the context of underground gas storage especially in salt caverns, rapid decompression and therefore significant drop in temperature (including Joule-Thomson effect [1. 48]) during withdrawal of water-saturated gas can lead to temperature and pressure conditions favorable for hydrate formation at the top of the wellbore [1. 49, 50]. In order to avoid production stoppage, which is very expensive in time and cost, it is necessary to know precisely the domain of stability of these hydrates (see Figure 1.14) which depend on the gas composition in order to set a limit to the operating conditions (pressure and temperature) and to know if it is necessary to add thermodynamic or kinetic inhibitors to the system to move away from the hydrate formation conditions.

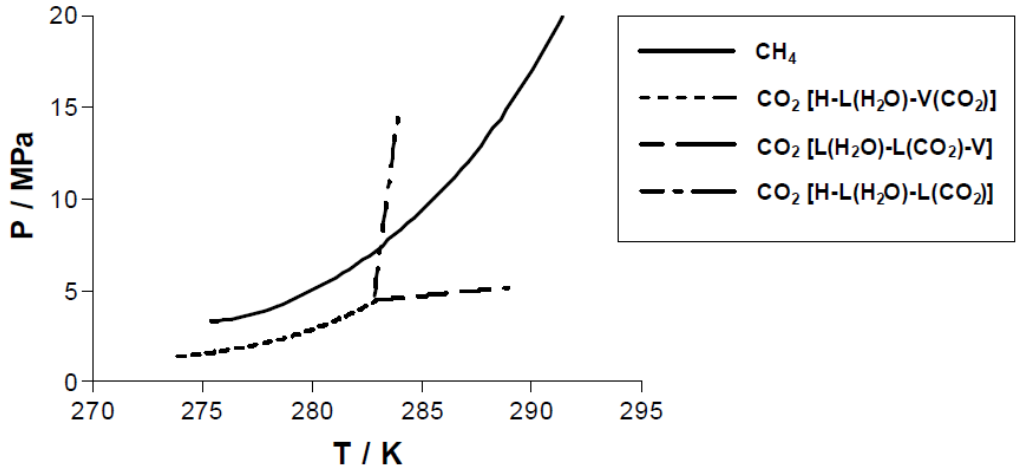

Figure 1.14: CH_4 and CO_2 hydrate stability curves [1. 51].

Finally, solubility is also a key factor in modeling gas hydrate stability conditions. Given the lack of high-pressure solubility data for some gases in water and brine, the experimental apparatus used in this work as well as the required information for the modeling of phase equilibria (gas solubility, water content and gas hydrate stability conditions) are presented in the following chapter.

References

[1. 1] M. Ghoreychi, P. Gombert, F. Lahaie, R. Cointe, C. Boudet, Underground storage within the context of energy transition, (2016).
[1. 2] P. Berest, Stockage souterrain des gaz et hydrocarbures : des perspectives pour la transition énergétique, Encyclopédie de l'Environnement [en ligne ISSN 2555-0950], (2019).

[1. 3] A. Ozarslan, Large-scale hydrogen energy storage in salt caverns, International Journal of Hydrogen Energy, 37 (2012) 14265-14277.
[1. 4] R. Tarkowski, Underground hydrogen storage: Characteristics and prospects, Renewable and Sustainable Energy Reviews, 105 (2019) 86-94.
[1. 5] O. Kruck, F. Crotogino, R. Prelicz, T. Rudolph, Assessment of the potential, the actors and relevant business cases for large scale and seasonal storage of renewable electricity by hydrogen underground storage in Europe, HyUnder Deliverable, (2013).
[1. 6] J.I.T. Force, Underground natural gas storage: Integrity and safe operations, 83 p.: July 2016, Report available at http://www.energyinfrastructure.org/energy-101/natural-gas-storage, (2016).
[1. 7] F. LAHAIE, P. GOMBERT, C. BOUDET, "Le stockage souterrain dans le contexte de la transition énergétique" Maîtrise des risques et impacts, (2016).
[1. 8] F.E.R. Commission, Current state of and issues concerning underground natural gas storage, Energy, Washington DC Retrieved from www. ferc. gov/eventcalendar/files/20041020081349-final-gsreport. pdf, (2004).
[1. 9] J. Tobin, Underground natural gas storage, developments: 1998-2005, US Energy Information Administration, Office of Oil and Gas, DOE/EIA-0131, (2006) 1-16.
[1. 10] T. Ajayi, J.S. Gomes, A. Bera, A review of CO 2 storage in geological formations emphasizing modeling, monitoring and capacity estimation approaches, Petroleum Science, (2019) 1-36.
[1. 11] S.A. Rackley, Carbon capture and storage, Butterworth-Heinemann, 2017.
[1. 12] B. Metz, O. Davidson, H. De Coninck, Carbon dioxide capture and storage: special report of the intergovernmental panel on climate change, Cambridge University Press, 2005.
[1. 13] P. Schulze, J. Holstein, A. van den Noort, J. Knijp, Power-to-gas in a decarbonized european energy system based on renewable energy sources, DNV GL, (2017).
[1. 14] R. Kushnir, A. Ullmann, A. Dayan, Thermodynamic and hydrodynamic response of compressed air energy storage reservoirs: a review, Reviews in Chemical Engineering, 28 (2012) 123-148.
[1. 15] M.W. Melaina, O. Antonia, M. Penev, Blending hydrogen into natural gas pipeline networks. a review of key issues, in, National Renewable Energy Laboratory, 2013.
[1. 16] Z. Shi, K. Jessen, T.T. Tsotsis, Impacts of the subsurface storage of natural gas and hydrogen mixtures, International Journal of Hydrogen Energy, 45 (2020) 8757-8773.
[1. 17] M. Honselaar, E. Weidner, M. Steen, Workshop report: summary & outcomes "Putting Science into Standards Power-to-Hydrogen and HCNG", in, 2014.
[1. 18] A. Züttel, Hydrogen storage methods, Naturwissenschaften, 91 (2004) 157-172.
[1. 19] F. Crotogino, Larger scale hydrogen storage, in: Storing energy, Elsevier, 2016, pp. 411-429.
[1. 20] N. Bader, R. Bleischwitz, A.N. Madsen, P.D. Andersen, EU policies and cluster development of hydrogen communities, Bruges European Economic Research papers, (2008).
[1. 21] G. Strobel, B. Hagemann, T.M. Huppertz, L. Ganzer, Underground bio-methanation: Concept and potential, Renewable and Sustainable Energy Reviews, 123 (2020) 109747.
[1. 22] O. Kruck, F. Crotogino, Benchmarking of selected storage options, Hannover, Germany, (2013).
[1. 23] M. Götz, J. Lefebvre, F. Mörs, A.M. Koch, F. Graf, S. Bajohr, R. Reimert, T. Kolb, Renewable Power-to-Gas: A technological and economic review, Renewable energy, 85 (2016) 1371-1390.

[1. 24] N. Kezibri, C. Bouallou, Conceptual design and modelling of an industrial scale power to gas-oxy-combustion power plant, International Journal of Hydrogen Energy, 42 (2017) 19411-19419.
[1. 25] M. Panfilov, V. Reitenbach, L. Ganzer, Self-organization and shock waves in underground methanation reactors and hydrogen storages, Environmental Earth Sciences, 75 (2016) 313.
[1. 26] I. Søreide, C.H. Whitson, Peng-Robinson predictions for hydrocarbons, CO2, N2, and H2S with pure water and NaCl brine, Fluid Phase Equilibria, 77 (1992) 217-240.
[1. 27] D. Koschel, J.-Y. Coxam, L. Rodier, V. Majer, Enthalpy and solubility data of CO 2 in water and NaCl (aq) at conditions of interest for geological sequestration, Fluid phase equilibria, 247 (2006) 107-120.
[1. 28] S.M. Gilfillan, B.S. Lollar, G. Holland, D. Blagburn, S. Stevens, M. Schoell, M. Cassidy, Z. Ding, Z. Zhou, G. Lacrampe-Couloume, Solubility trapping in formation water as dominant CO 2 sink in natural gas fields, Nature, 458 (2009) 614-618.
[1. 29] D. Tong, J.M. Trusler, D. Vega-Maza, Solubility of CO2 in aqueous solutions of CaCl2 or MgCl2 and in a synthetic formation brine at temperatures up to 423 K and pressures up to 40 MPa, Journal of Chemical & Engineering Data, 58 (2013) 2116-2124.
[1. 30] S.J. Baines, R.H. Worden, Geological storage of carbon dioxide, Geological Society, London, Special Publications, 233 (2004) 1-6.
[1. 31] D. Tromans, Oxygen solubility modeling in inorganic solutions: concentration, temperature and pressure effects, Hydrometallurgy, 50 (1998) 279-296.
[1. 32] M. Jamnongwong, K. Loubiere, N. Dietrich, G. Hébrard, Experimental study of oxygen diffusion coefficients in clean water containing salt, glucose or surfactant: consequences on the liquid-side mass transfer coefficients, Chemical engineering journal, 165 (2010) 758-768.
[1. 33] G. Ming, D. Zhenhao, Prediction of oxygen solubility in pure water and brines up to high temperatures and pressures, Geochimica et Cosmochimica Acta, 74 (2010) 5631-5640.
[1. 34] S. Succar, R.H. Williams, Compressed air energy storage: theory, resources, and applications for wind power, Princeton environmental institute report, 8 (2008) 81.
[1. 35] R. Roffey, Microbial problems during long-term storage of petroleum products underground in rock caverns, International biodeterioration, 25 (1989) 219-236.
[1. 36] B. Wang, S. Bauer, Induced geochemical reactions by compressed air energy storage in a porous formation in the North German Basin, Applied Geochemistry, 102 (2019) 171-185.
[1. 37] M. Bai, K. Song, Y. Sun, M. He, Y. Li, J. Sun, An overview of hydrogen underground storage technology and prospects in China, Journal of Petroleum Science and Engineering, 124 (2014) 132-136.
[1. 38] V. Reitenbach, L. Ganzer, D. Albrecht, B. Hagemann, Influence of added hydrogen on underground gas storage: a review of key issues, Environmental Earth Sciences, 73 (2015) 6927-6937.
[1. 39] B. Hagemann, M. Rasoulzadeh, M. Panfilov, L. Ganzer, V. Reitenbach, Hydrogenization of underground storage of natural gas, Computational Geosciences, 20 (2016) 595-606.
[1. 40] C. Lopez-Lazaro, P. Bachaud, I. Moretti, N. Ferrando, Predicting the phase behavior of hydrogen in NaCl brines by molecular simulation for geological applicationsPrédiction par simulation moléculaire des équilibres de phase de l'hydrogène dans des saumures de NaCl pour des applications géologiques, Bulletin de la Société Géologique de France, 190 (2019).
[1. 41] R. Kolass, C. Parker, Moisture measurement in natural gas, Michell Instruments Ltd. Technical article, (2011).

[1. 42] Y. Hua, R. Barker, A. Neville, The effect of O2 content on the corrosion behaviour of X65 and 5Cr in water-containing supercritical CO2 environments, Applied Surface Science, 356 (2015) 499-511.
[1. 43] Y. Xiang, Z. Wang, X. Yang, Z. Li, W. Ni, The upper limit of moisture content for supercritical CO2 pipeline transport, The Journal of Supercritical Fluids, 67 (2012) 14-21.
[1. 44] G. Processors, Suppliers Association Engineering Data Book, Tulsa, Oklahoma, USA, (2004).
[1. 45] M.H. Nazari, S. Allahkaram, M. Kermani, The effects of temperature and pH on the characteristics of corrosion product in CO2 corrosion of grade X70 steel, Materials & Design, 31 (2010) 3559-3563.
[1. 46] Ifremer, Les hydrates - Hydrates in situ (©Ifremer), in, 2017.
[1. 47] J. Lee, J.W. Kenney III, Clathrate Hydrates, Solidification, (2018) 129.
[1. 48] B. Yadali Jamaloei, K. Asghari, The Joule-Thomson Effect in Petroleum Fields: I. Well Testing, Multilateral/Slanted Wells, Hydrate Formation, and Drilling/Completion/Production Operations, Energy Sources, Part A: Recovery, Utilization, and Environmental Effects, 37 (2015) 217-224.
[1. 49] P. Bérest, Heat transfer in salt caverns, International Journal of Rock Mechanics and Mining Sciences, 120 (2019) 82-95.
[1. 50] B. Sedaee, M. Mohammadi, L. Esfahanizadeh, Y. Fathi, Comprehensive modeling and developing a software for salt cavern underground gas storage, Journal of Energy Storage, 25 (2019) 100876.
[1. 51] I. GHG, Issues underlying the feasibility of storing CO2 as hydrate deposits, IEA Greenhouse Gas R&D Programme Report PH3/25, (2000).

French summary / Chapitre 2 - Équilibres de phases : Mesures et modélisation

Dans un système fermé, la matière peut exister dans un état monophasique ou multiphasique, et la thermodynamique des équilibres entre phases vise à comprendre et à quantifier la répartition des différentes espèces dans les différentes phases en équilibre dans le cas d'une séparation de phases. Les équilibres de phase ont plusieurs applications : 1) dans l'industrie chimique, en particulier dans les procédés de séparation et de purification tels que la chromatographie pour de petites quantités de matière ou la distillation, l'extraction et l'absorption... pour des opérations à grande échelle ; 2) dans l'industrie pétrolière et gazière dans des domaines tels que l'ingénierie des réservoirs, le transport et le stockage des hydrocarbures et le traitement du pétrole et du gaz. Comme dans la plupart des domaines scientifiques, la thermodynamique, et plus précisément l'étude des équilibres entre phases, fait appel à deux méthodologies différentes : l'expérimentation et la modélisation. Ces deux méthodologies très complémentaires permettent de comprendre et de simuler les phénomènes thermodynamiques d'un point de vue microscopique (par exemple les forces intermoléculaires) et macroscopique (par exemple le changement de phase et l'évolution thermique d'un système…). Avec l'évolution des moyens de calcul numérique, de grands progrès ont été réalisés dans le développement de modèles thermodynamiques relativement fiables qui permettent de résoudre un grand nombre de problèmes tout en réduisant le nombre d'expériences nécessaires, parfois très coûteuses et compliquées pour des raisons techniques et de sécurité. Pour différents contextes, l'une des propriétés essentielles d'équilibre de phase à déterminer (voir le Chapitre 1) est la solubilité des gaz dans l'eau saline. Dans ce chapitre, nous présentons : un état des lieux sur les données expérimentales disponibles de solubilité des gaz dans l'eau et la saumure, les méthodes de mesure des équilibres de phases utilisées dans ce travail, en particulier les mesures de la solubilité des gaz dans les systèmes gaz/eau/sel ainsi que la modélisation des équilibres de phases (solubilité des gaz et teneur en eau). Le sel considéré dans cette étude est le NaCl, puisque le Na+ et le Cl- sont les principales espèces présentes dans l'eau naturel (l'eau de formation dans les milieux poreux ou la saumure résiduelle dans les cavités salines).

Chapter 2: Phase equilibria: Measurements and modeling

2.1 Introduction

A phase is a medium characterized by the uniformity of its thermophysical properties such as composition, density, viscosity (if fluid), and thermal conductivity, etc. Depending on the conditions of temperature, pressure and composition (type and quantity of species in the system), a substance is stable in a certain state (or phase) which may be fluid (liquid or vapor) or solid or possibly stable in several states simultaneously (several phases in equilibrium). In a closed system, matter can exist in a single-phase or multiphase state, and the thermodynamics of phase equilibria aims at understanding and quantifying the distribution of different species in different phases in equilibrium in the case of phase-split. Phase equilibria have several applications: 1) in the chemical industry, particularly in Separation and Purification Processes (SPP) such as chromatography for small amounts of material or distillation, extraction and absorption, etc. for large-scale operations; 2) in the oil and gas industry in areas such as reservoir engineering, hydrocarbon transport and storage, and oil and gas processing.

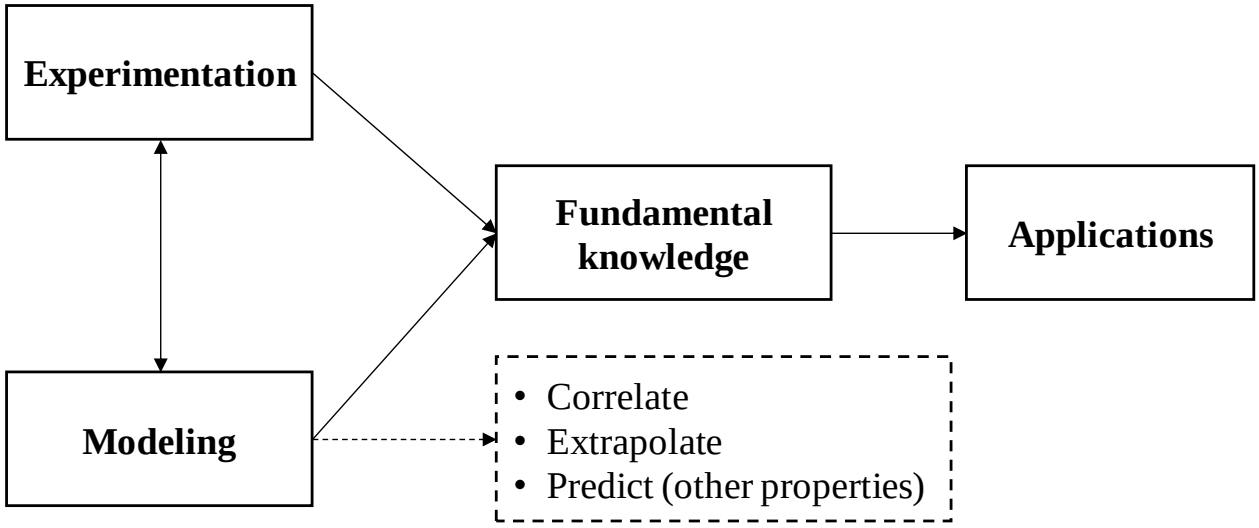

Figure 2.1: From methodologies (experimentation and modeling) to applications.

As in most scientific fields, thermodynamics, and more precisely studying phase equilibria, involves two different methodologies: experimentation and modeling (see Figure 2.1). These two highly complementary methodologies allow the understanding and simulation of thermodynamic phenomena from a microscopic (e.g. intermolecular forces) and macroscopic (e.g. phase change, thermal evolution of a system, etc.) point of view. With the evolution of numerical computation means, great progress has been made with the development of relatively

reliable thermodynamic models that make it possible to solve a large number of problems while reducing the number of experiments required, which are sometimes very costly and complicated for technical and safety reasons.

For different contexts, one of the essential phase equilibrium properties to be determined (see the previous chapter) is gas solubility in saline water. In this chapter, we present: a review of available experimental solubility data, the phase equilibria measurement methods used in this work, in particular the measurement of gas solubility in gas/water/salt systems as well as phase equilibria modeling (gas solubility and water content). The salt considered in this study is NaCl since Na+ and Cl- are the main species found in formation water (reservoir water) [2. 1].

2.2 Gas solubility measurements

Measuring high-pressure gas solubility in aqueous systems is not an easy task from a technical and safety point of view. For an accurate quantification of the different constituents using the different analytical methods, phase sampling is necessary. However, during sampling, disturbance of the thermodynamic equilibrium must be avoided, which is not easy due to the high pressure. Several techniques exist to minimize the disturbance of equilibrium during sampling or even circumvent this problem by using synthetic methods. A classification of high pressure phase equilibria measurement methods is given by Dohrn and coworkers [2. 2, 3]. They classified the different measurement methods into two categories (Figure 2.2):

- Analytical methods: As indicated by its designation, these methods consist of the determination of phase equilibria with or without sampling, using analytical techniques such as chromatography, titration, volumetric and gravimetric methods, or Raman spectroscopy.
- Synthetic methods: These methods consist of the determination of phase equilibria by material balance without phase change, or by visual or non-visual detection of phase change starting with a single-phase system.

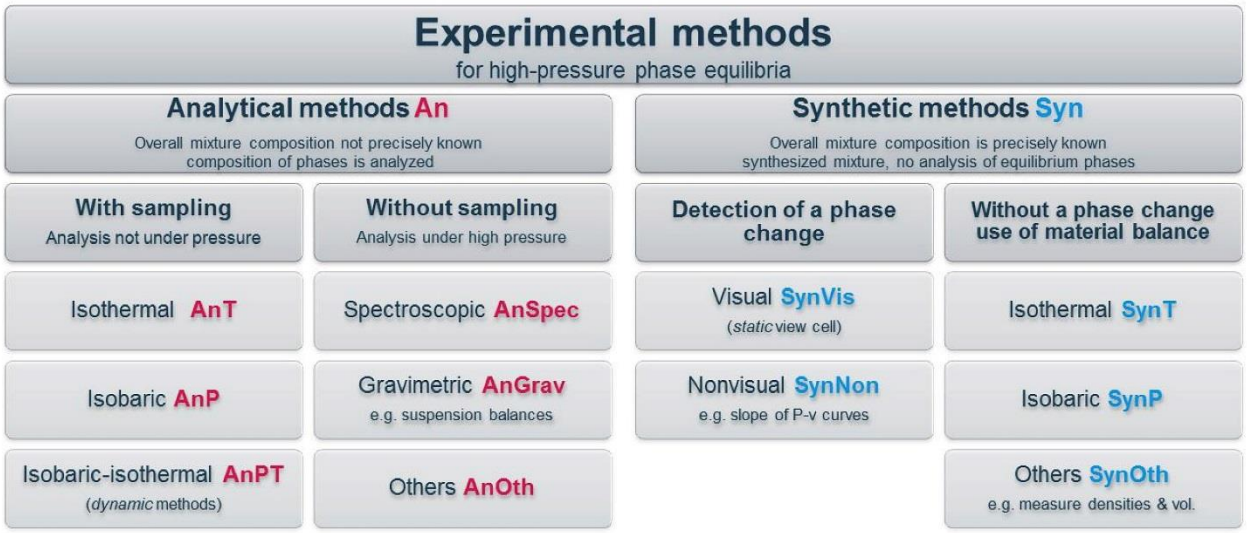

Figure 2.2: Classification of high-pressure phase equilibria measurement techniques [2. 3].

Detailed descriptions of each method can be found in Dohrn and coworkers [2. 2, 3] publications. In addition, Lara Cruz [2. 4] presented in his PhD thesis a comprehensive review of different analytical and synthetic techniques for measuring high-pressure gas solubility.

2.2.1 Experimental equipment

In this section, two different analytical techniques used in this work for gas solubility measurements are presented. The first one is based on the static-analytic method (phase sampling and Gas Chromatography (GC) analysis) and the second one is a rocking cell setup [2. 5, 6, 7] (liquid phase sampling, gas/brine separation, brine gravimetric analysis and gas volumetric analysis with gasometer). Within the different contexts discussed earlier in Chapter 1, the systems of interest considered in this study are: CO_2+H_2O+NaCl, O_2+H_2O+NaCl and H_2+H_2O+NaCl. In Table 2.1, the suppliers of Carbon dioxide (CO_2, CAS Number: 124-38-9), Oxygen (O_2, CAS Number: 7782-44-7), Hydrogen (H_2, CAS Number: 1333-74-0) and Sodium Chloride (NaCl, CAS Number: 7647-14-5) and the given purities are listed. CO_2 and O_2 solubility measurements were performed in two different laboratories (1- CTP, Mines ParisTech; 2- HFAPE, Institute of GeoEnergy Engineering, Heriot-Watt University), therefore in Table 2.1 two suppliers are listed for these two gases. H_2 solubility measurements were performed at CTP, Mines ParisTech. Water was deionized and degassed before the preparation of the brine (water + NaCl).

Table 2.1: Chemicals used in this work: purities and suppliers

Chemicals	Purity	Analytical Method	Supplier
CO_2	99.995 vol%	GC: Gas Chromatography	BOC / MESSER
O_2	99.995 vol%	GC	BOC / Air Liquide
H_2 (Hydrogen 5.0)	99.999 vol%	GC	Messer
NaCl	99.6%	None	Fisher Chemical

2.2.1.1 **Static-analytic setup**

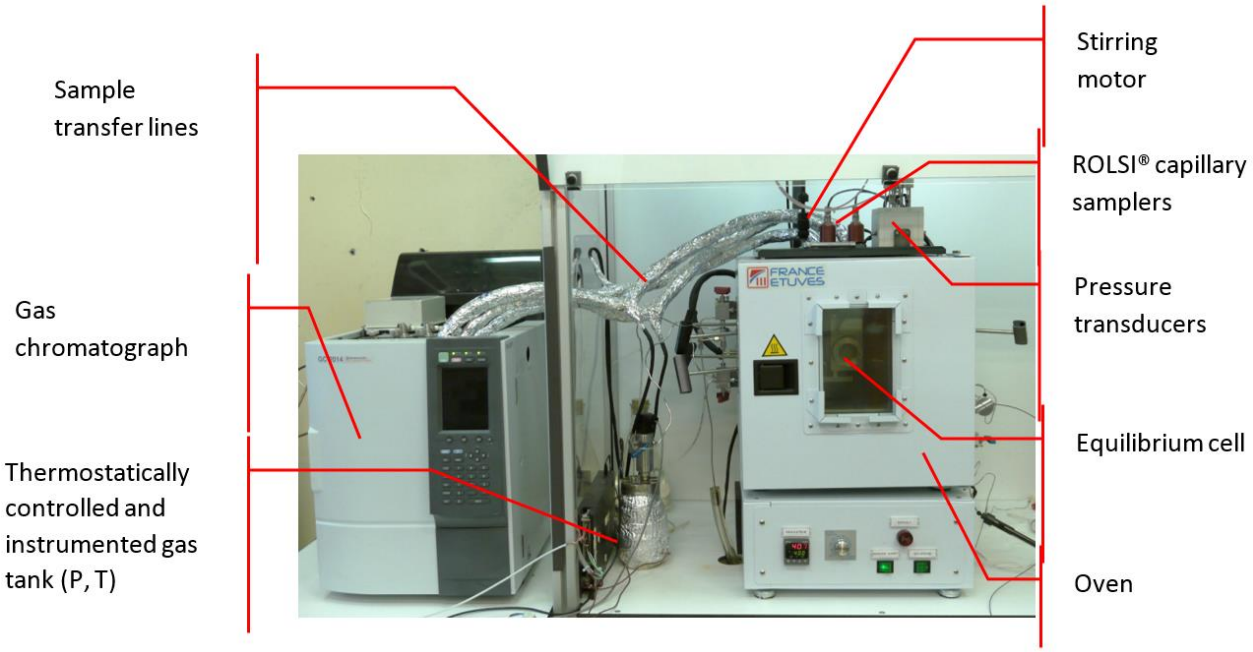

Figure 2.3.A: Presentation of the "static-analytic" apparatus for phase equilibria measurement.

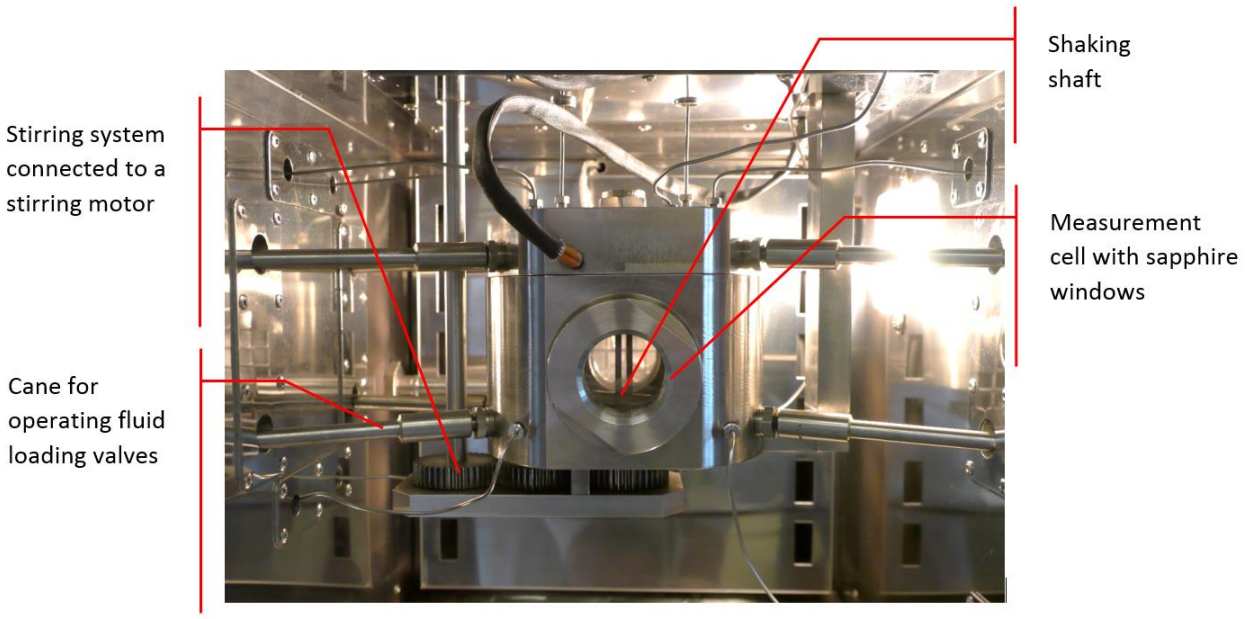

Figure 2.3.B: View of the equilibrium cell inside the oven.

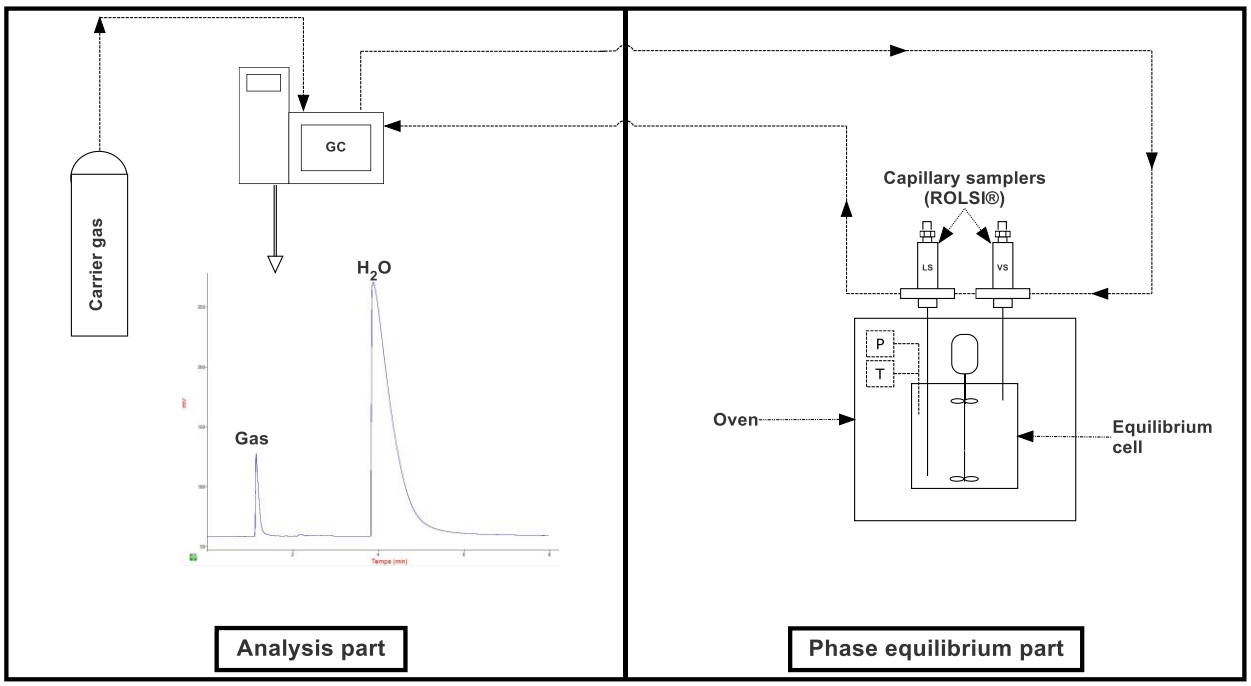

Figure 2.3.C: Simplified schematic representation of the "static-analytic" apparatus for phase equilibria measurement.

The first setup used in this work is based on the “static-analytic” method. This apparatus developed within the framework of the ANR SIGARRR project (ANR-13-SEED-006) and improved in this work (especially on the analytical part: boosted TCD detector, addition of a pre-column to block salt deposition in tubing) is described in detail in our recent work (Chabab

et al. [2. 8]) presented in Chapter 3. However, a brief description is given below. Figure 2.3 (A-C) shows a real picture of the "static-analytic" apparatus as well as a simplified description of this technique. It consists of an equilibrium cell positioned in an oven for temperature control, and equipped with pressure transducers, temperature probes and two ROLSI® (Rapid On-Line Sampler-Injector, French patent number 0304073) capillary samplers for each phase (liquid and vapor). After setting the temperature and charging the cell with the saline solution and the gas up to the desired pressure, the thermodynamic equilibrium is reached in some dozens of minutes after continuous agitation, assuming that the equilibrium is verified by the stabilization of the temperature and pressure in the cell. Several samples (for repeatability check) are then taken by the liquid ROLSI® and sent through a transfer line to GC to determine the mole fraction of gas and water. This last step depends on GC detector calibration, which is carried out under the same measurement conditions, to convert the areas obtained by integration of the chromatogram peaks into numbers of moles. Using the mole number of gas (n_{gas}) and H_2O (n_{H_2O}), the gas solubility in the saline solution in terms of "salt-free" mole fraction x_{gas} is determined:

$$x_{gas} = \frac{n_{gas}}{n_{gas} + n_{H_2O}} \tag{2.1}$$

The solubility in terms of "salt-free" mole fraction x_{gas} can be converted in terms of molality m_{gas} (in mol/kgw) easily by the following relationship:

$$m_{gas} = \frac{1000\, x_{gas}}{M_{H_2O}(1 - x_{gas})} \tag{2.2}$$

or in terms of "true" mole fraction by

$$x_{gas}^{true} = \frac{n_{gas}}{n_{gas} + n_{H_2O} + n_s} = \frac{n_{gas}}{n_{gas} + n_{H_2O} + m_s n_{H_2O} M_{H_2O}} = \frac{x_{gas}}{x_{gas} + (1 - x_{gas})(1 + m_s M_{H_2O})} \tag{2.3}$$

where n_s and m_s are respectively the mole number and molality (in mol/kgw) of the salt (NaCl), and M_{H_2O} is the molecular weight of water (in g/mol).

Another equilibrium point is measured by adding more gas and so on until the desired maximum pressure is reached. Before starting a new isotherm or introducing a solution with a different

molality than the one before, the equilibrium cell is cleaned and evacuated. The specificity of this technique is that the samples taken by the ROLSI® samplers are very small and do not disturb the thermodynamic equilibrium, which is checked continuously through the pressure and temperature in the cell which must remain constant during the manipulation. Moreover, even if some of the water is evaporated (the water content in the gas-rich phase is very low, especially at high pressure), there is no significant increase in the concentration of the salt (NaCl) in the solution, so the molality of the solution has been considered constant.

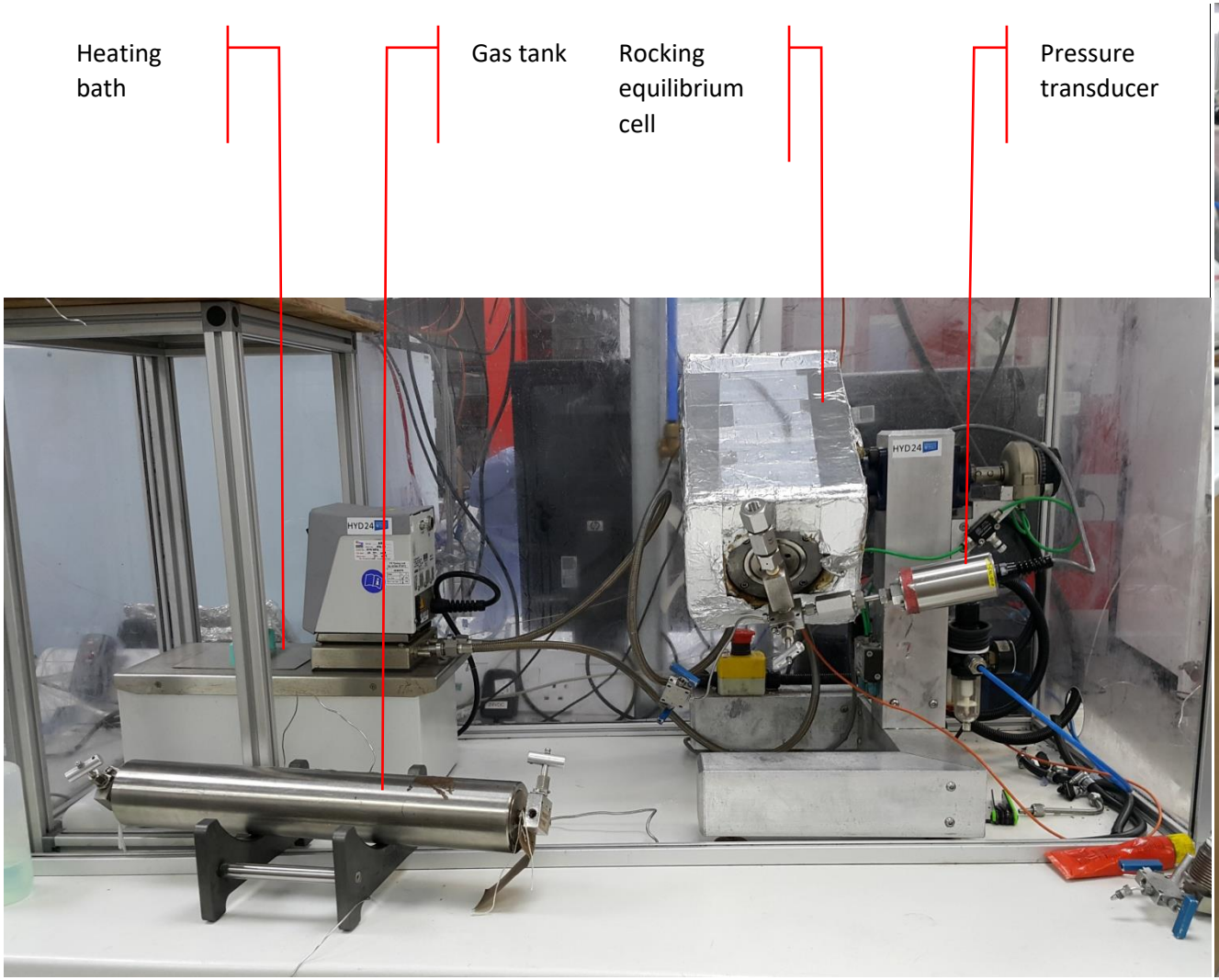

Figure 2.4.A: Presentation of the rocking cell apparatus

Figure 2.4.B: Gasometer

2.2.1.2 **Rocking cell setup**

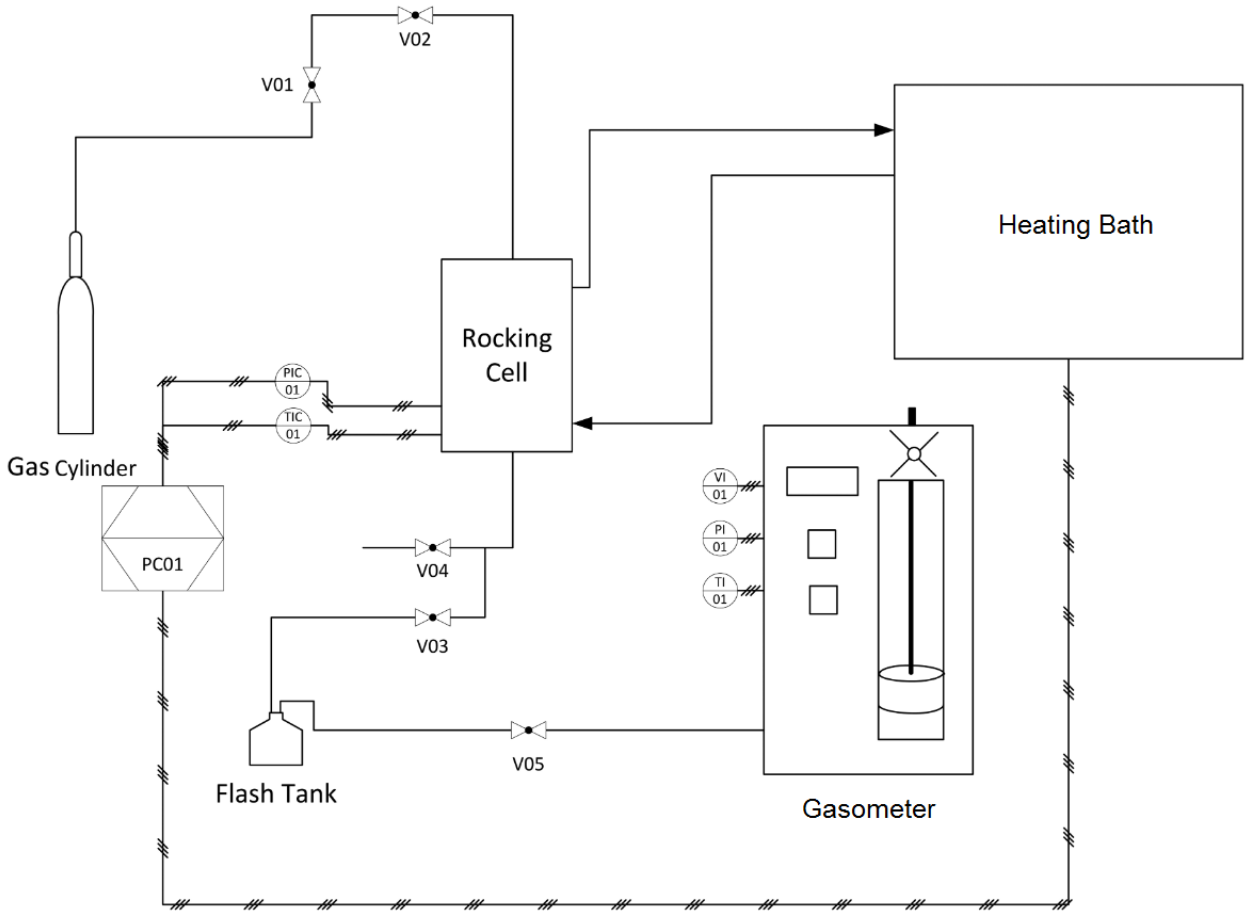

Figure 2.4.C: Schematic representation of the rocking cell apparatus used to measure the solubility of gases in NaCl brine [2. 6]. PI01: gasometer pressure indicator; PIC01: equilibrium cell pressure indicator/logger; PC01: computer controller/logger; TI01: gasometer temperature indicator; TIC01: equilibrium cell temperature indicator controller; V01: gas cylinder control valve; V02: equilibrium cell injection valve; V03: equilibrium cell drain valve; V04: equilibrium cell drain valve (backup); V05: gasometer inlet valve; VI01: gasometer volume indicator.

Based on a volumetric technique, the "rocking cell" setup illustrated in Figure 2.4 (A-C) is the same as that presented by Chapoy et al. [2. 5] and recently used by Burgass et al. [2. 6] and Ahmadi and Chapoy [2. 7]. It consists of a rocking equilibrium cell with a volume of 350 cm^3 mounted on an adjustable rotary axis of the pneumatic rocking system and surrounded by a heating jacket connected to a thermostat bath to maintain a constant temperature. The cell is equipped with a

Quartzdyne pressure transducer and a platinum resistance thermometer placed in the heating jacket of the cell. Since the temperature probe is not placed inside the cell, the real temperature in the cell is determined by calibration with respect to the jacket temperature.

For each measured point, the following procedure was followed: setting the target temperature, introducing 300 cm^3 of the saline solution and evacuating the equilibrium cell to remove the air. Then, the gas is introduced from V01 and V02 until the desired pressure is reached. The gas injection line is disconnected from V02 to allow the shaking of the system by the rocking system. Once the pressure and temperature are stabilized, the rocking is stopped and the cell is locked in a vertical position to take a sample of the aqueous phase. The gas injection line is reconnected to the cell using V02, the flash tank is connected to the bottom of the cell using V03 to collect the sample, and the gasometer (VINCI TECHNOLOGIES) is connected to the flash tank using V05. During sampling, the gas is injected continuously to maintain a constant pressure. The gas is separated from the liquid at the flash tank and transferred to the gasometer. The volume difference at constant pressure and temperature is then determined using the gasometer and knowing the density of the pure gas, the mass of the gas is deduced. The mass of the brine is determined gravimetrically using a balance. Finally, by knowing the quantities of gas and brine in the sample, the solubility of the gas is obtained. The quantity of gas remaining (dissolved) in the brine under laboratory atmospheric conditions is also taken into account in the solubility calculation and is determined using a precise thermodynamic model whose parameters are previously optimized on experimental data at atmospheric pressure and temperature. The calculation procedure is described in detail by Ahmadi and Chapoy [2. 7]. More gas is added to increase the pressure, and the procedure is repeated to measure another equilibrium point.

2.2.2 Review of available experimental data

In this section, experimental data of liquid-vapor equilibria existing in the literature and more specifically of gas solubility in water and brine are presented for the systems of interest in a wide range of temperature, pressure and salinity covering the geological underground gas storage conditions. The inventory of available experimental data was carried out on the basis of the various reviews, articles, and PhD Theses found in the literature. The operating conditions for the geological storage of CO_2, O_2 and H_2 in different contexts (CCS, CCUS, PtG-UGS, CAES and UHS, see Chapter 1) were considered based on information from literature [2. 9, 10]. The maximum

gas pressure (Pmax in bar) allowed in the storage to minimize the risk of rock fractures, cracking and capillary leakage through the caprock depends on the depth (H in meters (m)) of the reservoir [2. 11]: for salt caverns Pmax=0.18×H; for saline aquifers: Pmax=0.14×H. For example, a salt cavern built at a depth of 1500m can "safely" withstand pressures up to 270 bar, and a deep saline aquifer at a depth of 2500m can "safely" withstand pressures up to 350 bar.

2.2.2.1 **Gas / Water systems**

Gas solubility in pure water is generally well-studied over wide temperature and pressure ranges for different scientific and engineering contexts. CO_2, O_2 and H_2 are the gases considered in this work for experimental and modelling study. The collected data on the solubility of these gases in pure water are listed chronologically in Tables 2.2, 2.3 and 2.4, and presented in Figures 2.5, 2.6 and 2.7 as a function of temperature and pressure, respectively. As shown in these Figures, gas solubility data in pure water are sufficiently available under the different geological storage conditions for the different contexts (CCS, CAES, or UHS). However, some areas need to be completed for the case of O_2 and H_2, and this can simply be done by appropriate thermodynamic models (see section 2.3).

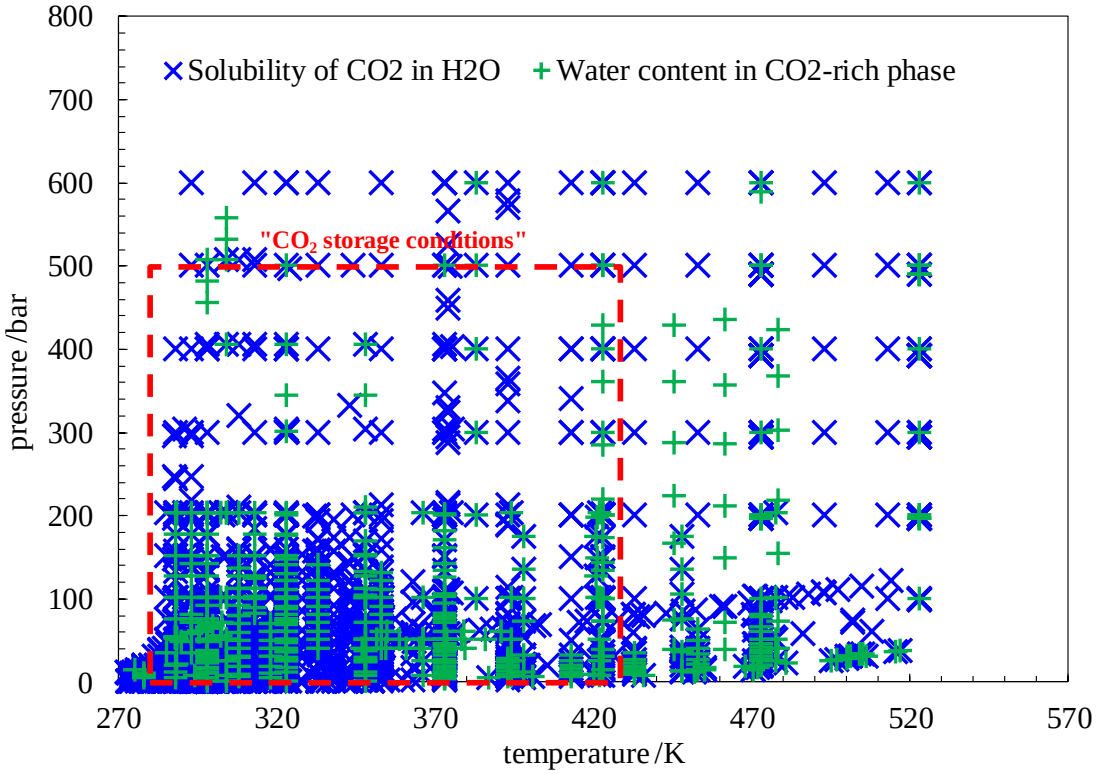

Figure 2.5: CO_2-H_2O system: data distribution of mutual solubilities of CO_2 and H_2O available in the literature (Table 2.2). The red dashed rectangle delimits the estimated CCS operating conditions.

Table 2.2: Literature experimental data for CO_2 solubility in pure water

Reference	Year	Tmin/K	Tmax/K	Pmin/bar	Pmax/bar
Zel'venskii [2. 12]	1937	273.15	373.15	10.80	94.40
Wiebe & Gaddy [2. 13]	1939	323.15	373.15	25.30	709.30
Wiebe & Gaddy [2. 14]	1940	291.15	313.15	25.30	506.60
Prutton & Savage [2. 15]	1945	348.15	393.15	21.20	717.40
Bartholome & Friz [2. 16]	1956	283.15	303.15	1.03	20.31
Dodds et al. [2. 17]	1956	278.00	298.00	1.00	50.70
Ellis [2. 18]	1959	387.00	592.00	5.07	164.05
Tödheide & Franck [2. 19]	1963	323.15	623.15	200.00	3500.00
Takenouchi & Kennedy [2. 20]	1964	383.15	623.15	100.00	1500.00
Vilcu & Gainar [2. 21]	1967	293.16	308.16	25.33	75.99
Matous et al. [2. 22]	1969	303.15	353.15	9.90	38.90
King & Coan [2. 23]	1971	298.15	373.15	1.01	51.67
Shagiakhmetov & Tarzimanov [2. 24]	1981	323.15	423.15	100.00	600.00

Zawisza & Malesinska [2. 25]	1981	323.15	473.15	2.54	53.89
Cramer [2. 26]	1982	306.15	486.25	8.00	58.00
Gillespie [2. 27]	1982	288.00	366.00	7.00	203.00
Briones et al. [2. 28]	1987	323.15	323.15	68.20	176.80
Nakayama et al. [2. 29]	1987	298.20	298.20	36.30	109.90
Song & Kobayashi [2. 30]	1987	244.82	298.15	6.90	137.90
d'Souza et al. [2. 31]	1988	323.00	348.00	101.00	152.00
Müller et al. [2. 32]	1988	373.15	473.15	3.25	81.10
Sako et al. [2. 33]	1991	348.20	421.40	101.80	209.40
King et al. [2. 34]	1992	288.15	298.15	60.80	243.20
Dohrn et al. [2. 35]	1993	323.15	323.15	101.00	301.00
Rumpf et al. [2. 36]	1994	323.15	323.15	10.59	57.98
Jackson et al. [2. 37]	1995	313.15	383.15	10.00	344.80
Malegaonkar et al. [2. 38]	1997	274.00	278.00	8.90	20.90
Dhima et al. [2. 39]	1999	344.25	344.25	100.00	1000.00
Bamberger et al. [2. 40]	2000	323.20	353.10	40.50	141.10
Yang et al. [2. 41]	2000	298.00	298.00	21.00	77.00
Rosenbauer et al. [2. 42]	2001	294.00	294.00	100.00	600.00
Kiepe et al. [2. 43]	2002	313.20	393.17	0.95	92.58
Anderson [2. 44]	2002	274.00	288.00	1.00	22.00
Bando et al. [2. 45]	2003	303.15	333.15	100.00	200.00
Chapoy et al. [2. 46]	2004	274.14	351.31	1.90	93.33
Valtz et al. [2. 47]	2004	278.22	318.23	4.65	79.63
Koschel et al. [2. 48]	2006	323.10	373.10	20.60	194.70
Qin et al. [2. 49]	2008	323.60	375.80	106.00	499.00
Han et al. [2. 50]	2009	313.20	343.20	43.30	183.40
Ferrentino et al. [2. 51]	2010	313.00	313.00	75.00	150.00
Liu et al. [2. 52]	2011	308.15	328.15	20.80	159.90
Yan et al. [2. 53]	2011	323.20	413.20	50.00	400.00
Hou et al. [2. 54]	2013	298.15	448.15	10.89	175.51
Langlais [2. 55]	2013	298.15	423.15	6.70	201.70
Al Ghafri et al.	2014	323.15	323.15	20.66	186.83
Guo et al. [2. 56]	2014	273.15	573.15	100.00	1200.00
Carvalho et al. [2. 57]	2015	283.00	363.00	3.10	120.80
Mohammadian et al. [2. 58]	2015	333.15	353.15	1.00	213.00
Zhao et al. [2. 59]	2015	323.15	423.15	150.00	150.00
Caumon et al. [2. 60]	2016	338.15	338.15	3.00	194.80
Gilbert et al. [2. 61]	2016	308.15	413.15	104.00	347.00
Jacob & Saylor [2. 62]	2016	297.00	297.00	13.80	124.10
Messabeb et al. [2. 63]	2016	323.15	323.15	50.10	200.00
Liborio [2. 64]	2017	323.10	323.10	23.00	162.00

Messabeb et al. [2. 65]	2017	373.15	423.15	50.50	199.50
Deng et al. [2. 66]	2018	303.15	363.15	50.00	250.00
Ahmadi and Chapoy [2. 7]	2018	300.95	423.48	12.92	420.77
Wang et al. [2. 67]	2019	303.15	353.15	30.00	300.00
Cruz et al. [2. 68]	2019	333.15	333.15	60.70	400.8

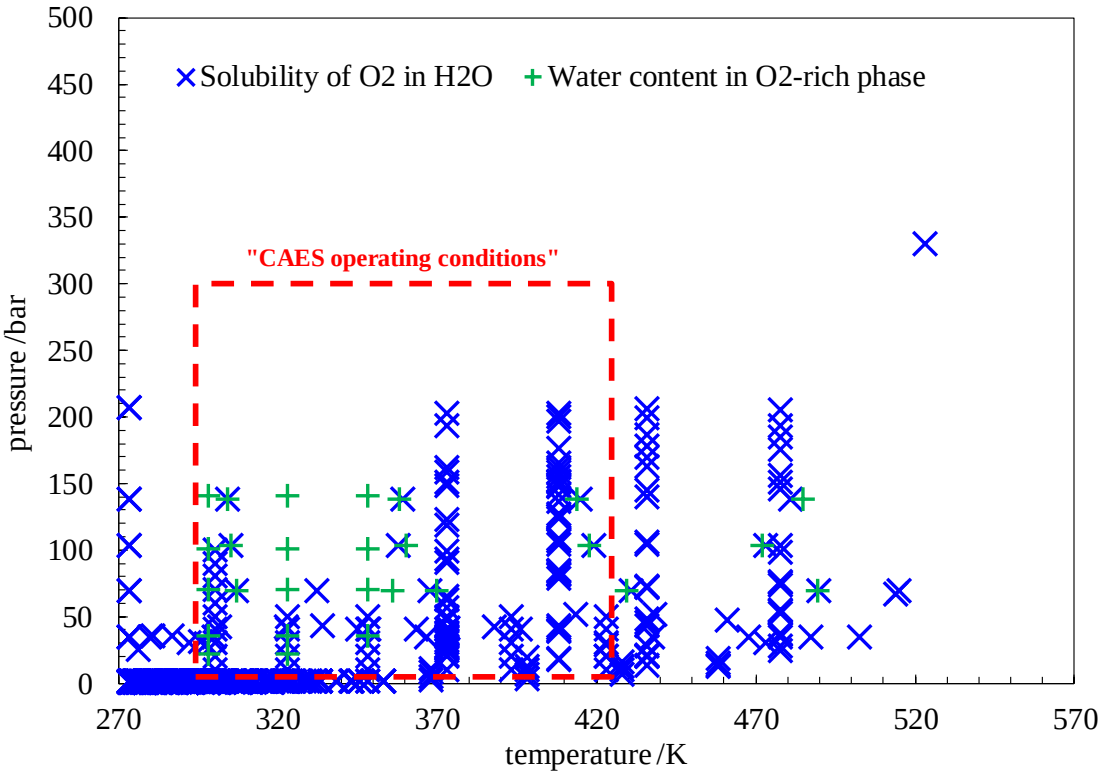

Figure 2.6: O_2-H_2O system: data distribution of mutual solubilities of O_2 and H_2O available in the literature (Table 2.3). The red dashed rectangle delimits the estimated CAES operating conditions.

Table 2.3: Literature experimental data for O_2 solubility in pure water

Reference	Year	Tmin/K	Tmax/K	Pmin/bar	Pmax/bar
Bunsen [2. 69]	1855	279.15	295.95	1.02	1.04
Timofejew [2. 70]	1890	279.55	285.72	1.02	1.03
Bohr & Bock [2. 71]	1891	280.45	333.21	1.02	1.21
Winkler [2. 72]	1891	293.50	353.20	1.04	1.49
Geffcken [2. 73]	1904	288.15	298.15	1.03	1.05
Fox [2. 74]	1909	273.76	323.44	1.02	1.14
Bohr [2. 75]	1910	294.15	294.15	1.04	1.04

Muller [2. 76]	1913	288.45	289.35	1.03	1.03
MacArthur [2. 77]	1916	298.15	298.15	0.21	0.21
Adeney & Becker [2. 78]	1920	275.65	308.25	1.02	1.07
Livingston et al. [2. 79]	1930	288.35	298.15	0.26	1.23
Orcutt & Seevers [2. 80]	1937	298.15	298.15	1.05	1.05
Eucken & Hertzberg [2. 81]	1950	273.15	298.15	1.02	1.05
Morrison & Billett [2. 82]	1952	285.85	348.05	1.03	1.40
Pray et al. [2. 83]	1952	435.93	616.48	13.55	173.93
Zoss [2. 84]	1952	273.15	604.82	34.50	138.00
Mc Kee [2. 85]	1953	273.15	273.15	34.50	207.00
Stephan et al. [2. 86]	1956	373.15	533.15	17.22	205.64
Clever et al. [2. 87]	1957	298.15	298.15	1.05	1.05
Steen [2. 88]	1958	279.15	297.15	1.02	1.04
Elmore & Hayes [2. 89]	1960	274.96	302.45	1.02	1.05
Mishnina et al. [2. 90]	1961	273.15	303.15	1.02	1.06
Anderson et al. [2. 91]	1962	373.15	473.15	19.32	30.02
Douglas [2. 92]	1964	281.15	302.30	1.02	1.05
Montgomery et al. [2. 93]	1964	273.53	310.15	1.02	1.08
Green [2. 94]	1965	273.74	307.96	1.02	1.07
Carpenter [2. 95]	1966	273.63	307.97	0.21	0.21
Power [2. 96]	1968	310.15	310.15	1.08	1.08
Shchukarev & Tolmacheva [2. 97]	1968	277.15	323.15	1.02	1.14
Murray et al. [2. 98]	1969	286.75	301.46	1.03	1.05
Murray & Riley [2. 99]	1969	273.89	307.95	0.21	0.21
Shoor et al. [2. 100]	1969	298.15	353.15	1.05	1.49
Wise & Houghton [2. 101]	1969	283.15	333.15	1.03	1.21
Power & Stegall [2. 102]	1970	310.15	310.15	1.08	1.08
Novak & Conway [2. 103]	1974	298.15	298.15	1.05	1.05
Wilcock & Battino [2. 104]	1974	298.15	298.15	1.05	1.05
Tokunaga [2. 105]	1975	273.15	313.15	1.02	1.09
Benson & Krause [2. 106]	1976	273.63	308.10	1.02	1.07
Cargill [2. 107]	1976	277.00	348.00	1.02	1.40
Yasunishi [2. 108]	1977	288.15	308.15	1.03	1.07
Broden & Simenson [2. 109]	1978	323.15	423.15	10.00	50.00
Matheson & King [2. 110]	1978	298.15	298.15	1.05	1.05
Benson et al. [2. 111]	1979	273.20	333.15	0.81	1.21
Da Silva et al. [2. 112]	1980	297.20	297.20	1.04	1.04
Cosgrove & Walkley [2. 113]	1981	278.15	313.15	1.02	1.09
Cramer [2. 26]	1982	276.15	561.15	1.00	123.00
Japas & Franck [2. 114]	1985	472.00	662.00	195.00	2798.00

Kimweri [2. 115]	1990	323.00	458.00	1.12	18.32
Sherwood et al. [2. 116]	1991	273.15	308.55	0.21	0.21
Rettich et al. [2. 117]	2000	274.15	328.14	0.72	1.20
Tan et al. [2. 118]	2001	300.15	300.15	10.00	100.00
Millero et al. [2. 119]	2002a	278.27	318.26	0.22	0.31
Millero et al. [2. 120]	2002b	273.72	318.06	0.22	0.31
Kaskiala & Salminen [2. 121]	2003	293.15	323.15	1.01	1.01
Millero & Huang [2. 122]	2003	278.16	318.15	0.22	0.31
Cuvelier et al. [2. 123]	2017	278.15	323.15	0.212	0.212

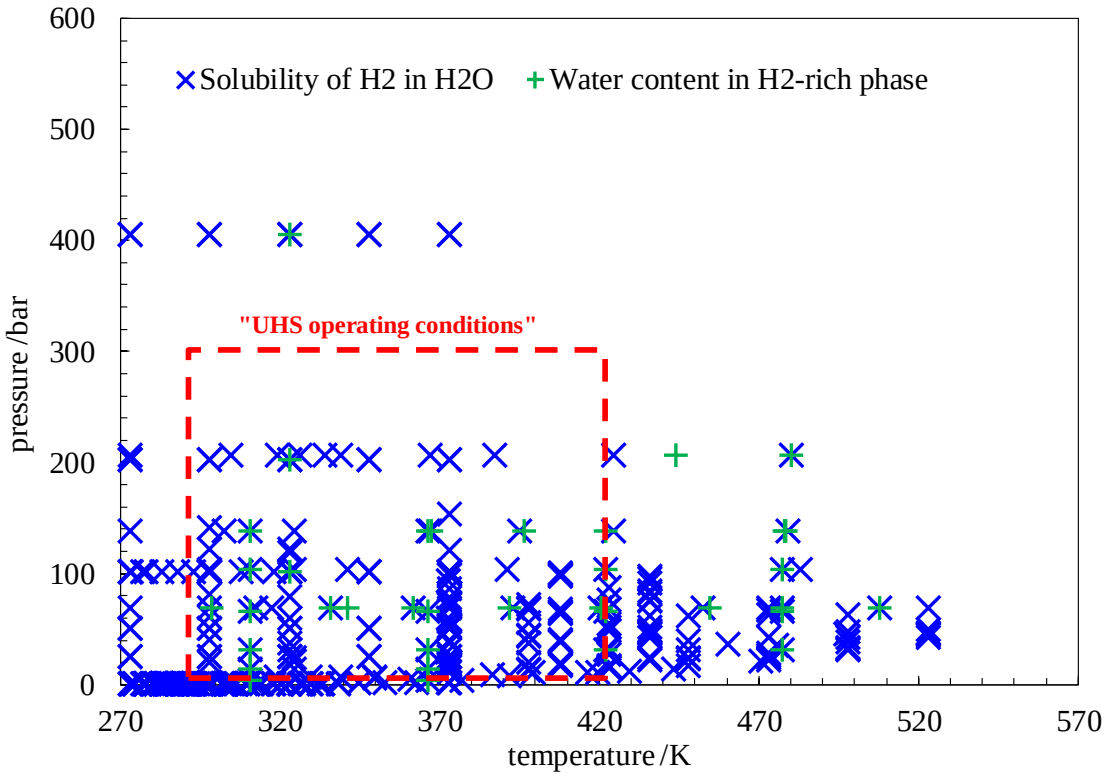

Figure 2.7: H_2-H_2O system: data distribution of mutual solubilities of H_2 and H_2O available in the literature (Table 2.4). The red dashed rectangle delimits the estimated UHS operating conditions.

Table 2.4: Literature experimental data for H_2 solubility in pure water.

Reference	Year	Tmin/K	Tmax/K	Pmin/bar	Pmax/bar
Bunsen [2. 69]	1855	277.15	296.75	1.021	1.042
Timofejew [2. 70]	1890	274.55	298.85	1.020	1.046
Bohr and Bock [2. 71]	1891	273.20	373.15	1.019	2.030
Winkler [2. 124]	1891	273.65	323.25	1.020	1.138
Steiner [2. 125]	1894	288.20	288.20	1.030	1.030
Braun [2. 126]	1900	278.15	298.15	1.022	1.045
Geffcken [2. 73]	1904	288.15	298.15	1.030	1.045
Knopp [2. 127]	1904	293.15	293.15	1.037	1.037
Hufner [2. 128]	1907	293.15	293.34	1.037	1.037
Findlay and Shen [2. 129]	1912	298.15	298.15	1.009	1.840
Muller [2. 76]	1913	289.35	290.35	1.032	1.033
Ipatiew et al. [2. 130]	1932	273.65	318.15	20.265	141.855
Wiebe and Gaddy [2. 131]	1934	273.15	373.15	25.331	1013.250
Morrison and Billett [2. 82]	1952	285.65	345.65	1.028	1.350
Pray et al. [2. 132]	1952	324.82	588.71	6.900	24.150
Zoss [2. 84]	1952	273.15	606.48	34.500	207.000
Pray and Stephan [2. 133]	1953	373.15	435.93	14.133	100.308
Wet [2. 134]	1964	291.65	304.55	1.035	1.059
Ruetschi and Amlie [2. 135]	1966	303.15	303.15	1.056	1.056
Shoor et al. [2. 100]	1969	298.15	333.15	1.045	1.213
Longo et al. [2. 136]	1970	310.15	310.15	1.076	1.076
Power and Stegall [2. 102]	1970	310.15	310.15	1.076	1.076
Gerecke and Bittrich [2. 137]	1971	298.15	298.15	1.045	1.045
Jung et al. [2. 138]	1971	373.15	423.15	9.962	85.844
Schroder [2. 139]	1973	298.15	373.15	101.300	101.300
Crozier and Yamamoto [2. 140]	1974	274.60	302.47	1.013	1.013
Gordon et al. [2. 141]	1977	273.29	302.40	1.013	1.013
Cargill [2. 142]	1978	277.70	344.83	1.022	1.350
Gillespie and Wilson [2. 143]	1980	310.93	588.71	3.450	138.000
Choudhary et al. [2. 144]	1982	323.15	373.15	25.331	101.325
Dohrn and Brunner [2. 145]	1986	473.15	623.15	100.000	300.000
Alvarez et al. [2. 146]	1988	318.90	497.50	4.360	45.940
Kling and Maurer [2. 147]	1991	323.15	423.15	31.800	153.700
Jauregui-Haza et al. [2. 148]	2004	353.00	373.00	1.486	2.025

2.2.2.2 **Gas / Brine systems**

Gas solubility in saline water is less studied than in pure water, especially at high pressure. However, the solubility of CO_2 at high pressure and temperature in saline solutions is extensively studied, given the growing interest in the topic of Carbon dioxide Capture and Storage (CCS) as the best option today for reducing CO_2 emissions, especially during the energy transition period in the short and medium term. The collected data on the solubility of CO_2, O_2 and H_2 in brine (H_2O+NaCl) are listed chronologically in Tables 2.5, 2.6 and 2.7, and presented in Figures 2.8, 2.9 and 2.10 as a function of temperature, pressure and salinity (in terms of NaCl molality m in mol/kgw), respectively.

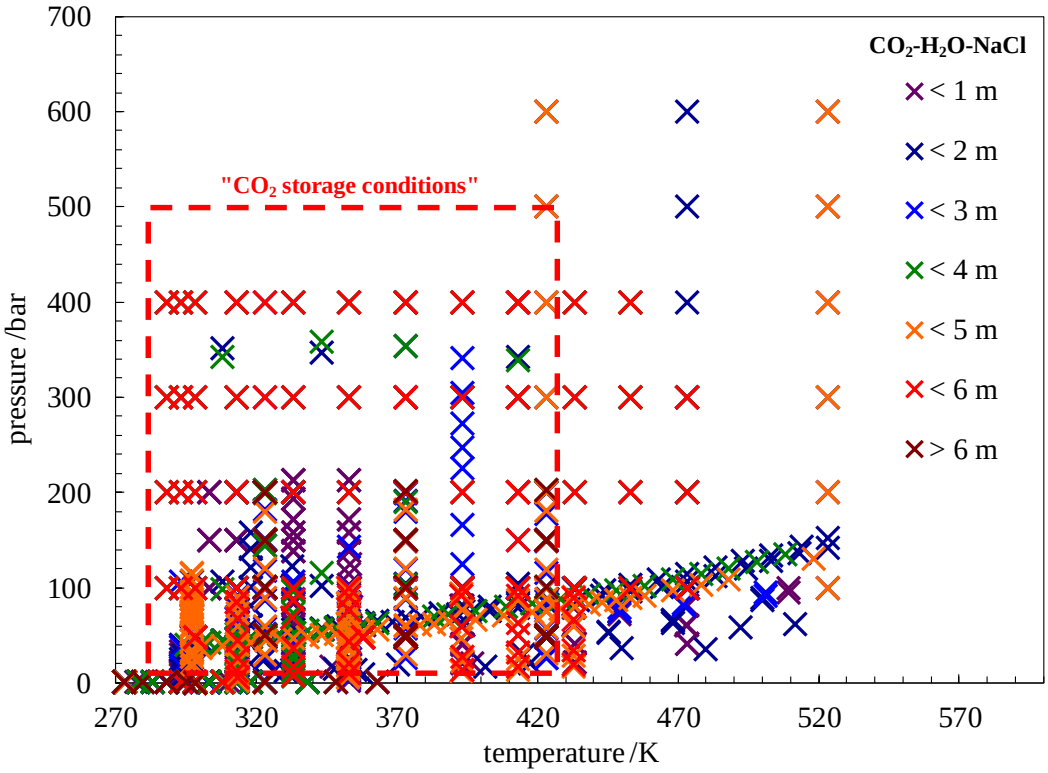

Figure 2.8: CO_2-H_2O-NaCl system: distribution of CO_2 solubility data available in the literature (Table 2.5).

Table 2.5: Literature experimental data for CO_2 solubility in NaCl-brine

Reference	Year	Max Molality	Tmin/K	Tmax/K	Pmin/bar	Pmax/bar
Ellis & Golding [2. 149]	1963	2.80 m	445	607	25.22	213.37
Takenouchi & Kennedy [2. 150]	1965	4.28 m	423.15	723.15	100.00	1400.00
Drummond [2. 151]	1981	6.48 m	293.65	673.15	34.48	292.78
Cramer [2. 26]	1982	1.95 m	296.75	511.75	8.00	62.00
Gehrig et al. [2. 152]	1986	4.28 m	415	783	30.00	2717.00
Rumpf et al. [2. 36]	1994	6.00 m	313.14	433.12	1.51	96.37
Gu [2. 153]	1998	2.00 m	303.15	323.15	17.73	58.96
Kiepe et al. [2. 43]	2002	4.34 m	313.38	353.07	0.98	101.00
Koschel et al. [2. 48]	2006	3.00 m	323.1	373.1	50.00	202.40
Liu et al. [2. 52]	2011	1.90 m	318.15	318.15	21.00	158.30
Yan et al. [2. 53]	2011	5.00 m	323.2	413.2	50.00	400.00
Rosenqvist et al. [2. 154]	2012	1.00 m	294.00	294.00	3.00	38.000
Savary et al. [2. 155]	2012	2.00 m	393.15	393.15	125.00	341.00
Hou et al. [2. 156]	2013	4.00 m	323.15	423.15	26.13	182.11
Langlais [2. 55]	2013	1.00 m	323.15	423.15	25.00	200.70
Carvalho et al. [2. 57]	2015	2.00 m	293.08	353.23	10.20	142.90
Zhao et al. [2. 59]	2015	6.00 m	323.15	423.15	150.00	150.00
Gilbert et al. [2. 61]	2016	3.40 m	308.15	413.15	98.90	358.00
Guo et al. [2. 157]	2016	5.00 m	273.15	473.15	100.00	400.00
Jacob & Saylor [2. 62]	2016	4.00 m	297.00	297.00	17.20	115.80
Messabeb et al. [2. 63]	2016	6.00 m	323.15	423.15	49.90	202.30
Liborio [2. 64]	2017	2.00 m	323.10	323.10	49.00	99.00
Wang et al. [2. 67]	2019	3.00 m	303.15	353.15	30.00	300.00
Cruz et al. [2. 68]	2019	1.20 m	323.15	333.15	50.70	400.40

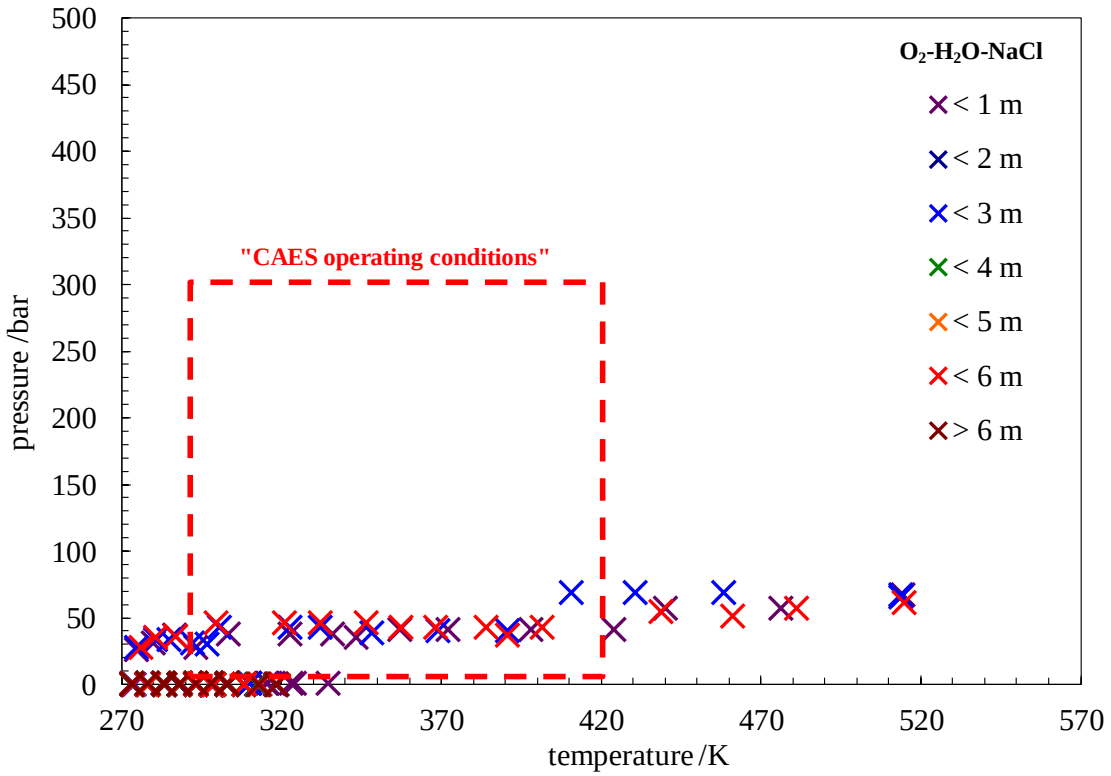

Figure 2.9: O_2-H_2O-NaCl system: distribution of O_2 solubility data available in the literature (Table 2.6).

Table 2.6: Literature experimental data for O_2 solubility in NaCl-brine

Reference	Year	Max Molality	Tmin/K	Tmax/K	Pmin/bar	Pmax/bar
Geffcken [2. 73]	1904	2.0 m	288.15	298.15	1.030	1.045
MacArthur [2. 77]	1916	4.4 m	298.15	298.15	0.212	0.212
Eucken & Hertzberg [2. 81]	1950	2.5 m	273.15	298.15	1.019	1.045
Mishnina et al. [2. 90]	1961	6.1 m	273.15	303.15	1.019	1.056
Cramer [2. 158]	1980	5.7 m	274.65	569.35	43.00	52.00
Armenante & Karlsson [2. 159]	1982	5.4 m	293.15	293.15	0.213	0.213
Elliott et al. [2. 160]	1990	5.6 m	298.15	298.15	1.045	1.045
Iwai et al. [2. 161]	1993	2.1 m	303.15	310.15	1.056	1.076
Millero et al. [2. 119]	2002a	5.9 m	298.15	298.15	0.245	0.245
Millero et al. [2. 120]	2002b	6.2 m	273.19	318.54	0.218	0.310

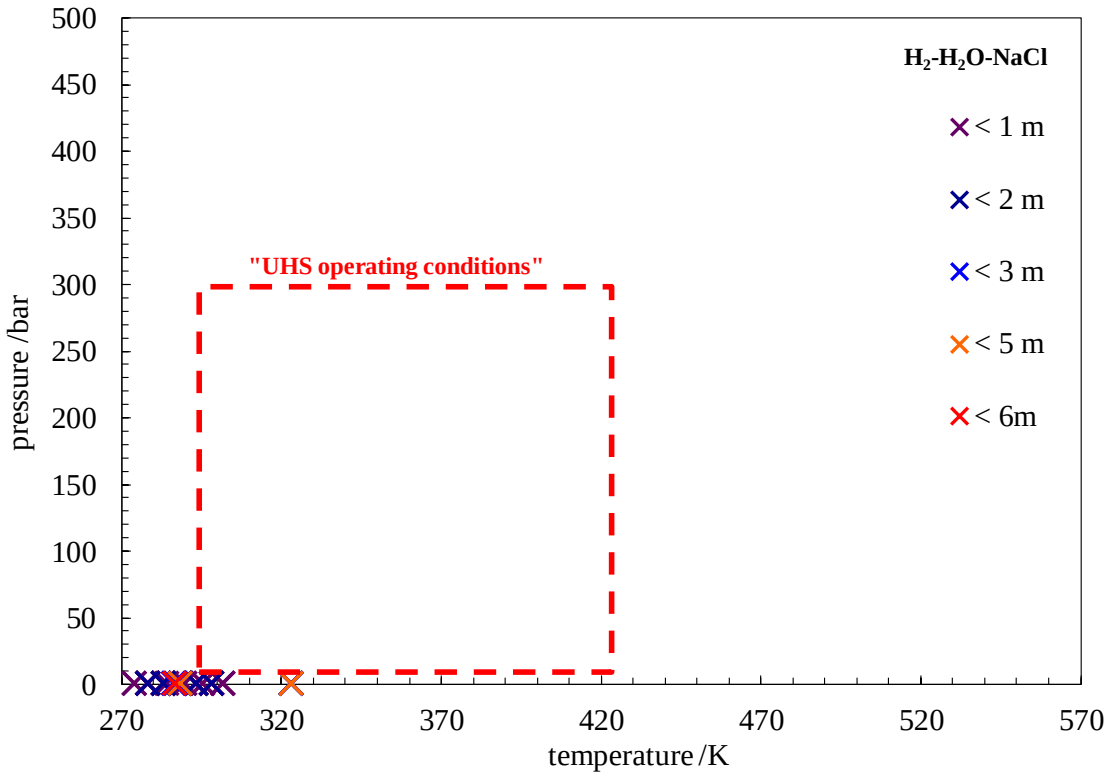

Figure 2.10: H_2-H_2O-NaCl system: distribution of O_2 solubility data available in the literature (Table 2.7).

Table 2.7: Literature experimental data for H_2 solubility in NaCl-brine

Reference	Year	Max Molality	Tmin/K	Tmax/K	Pmin/bar	Pmax/bar
Steiner [2. 125]	1894	5.3 m	286.32	286.95	1.028	1.029
Braun [2. 126]	1900	1.1 m	278.15	298.15	1.022	1.045
Gerecke & Bittrich [2. 137]	1971	4.3 m	288.15	298.15	1.030	1.045
Crozier & Yamamoto [2. 140]	1974	0.5 m	274.03	301.51	1.013	1.013

As shown in Figure 2.8 and Table 2.5, there is sufficient data on CO_2 solubility in NaCl-brine under geological storage conditions. However, this is not the case for O_2 and H_2 (see Figures 2.9 and 2.10 and Tables 2.6 and 2.7), as there is a significant lack of high-pressure solubility data. Only Cramer (1980) [2. 158] reported solubility data for O_2 at medium pressure (in the vicinity of 50 bar) expressed in terms of Henry's law constant and not in terms of pressure. However, to date there are no high-pressure H_2 solubility data in brine.

2.3 Modeling phase equilibria

The study of complex systems generally involving several phases in which gases (natural gas, CO_2, H_2, O_2, etc.) are in equilibrium with water, which often contains electrolytes, requires the understanding of these phase equilibria. In this part, the objective is to introduce the thermodynamic laws and functions involved in the calculation of phase equilibria.

2.3.1 Fluid phase equilibria calculation approaches

To determine and calculate the state of a non-reactive system at thermodynamic equilibrium in general or to act on the conditions of a particular process, it is important to know the number of independent intensive variables that can be freely specified. This number called degree of freedom (F) is obtained according to the Gibbs phase rule (Equation 2.4) by relating the number of compounds (N) and the number of coexisting phases (π) in the system.

$$F = N - \pi + 2 \quad \textbf{(2.4)}$$

By specifying F independent intensive variables, the others will be constrained to a single solutions (values). To clarify this, let us give an example. For a binary system: in the two-phase region, F=2 we can for example specify the temperature and pressure to obtain unique solutions for the compositions in the liquid phase x_i and vapor phase y_i. However, in the single-phase region, F=3, the composition can also be specified.

During the years 1875 to 1878, Gibbs' work [2. 162] solved the problem of phase equilibria by introducing the chemical potential, which is a thermodynamic function having as variables the pressure P, the temperature T and the number of moles n_i (or the molar fraction x_i). The condition of equilibrium (system stability) is to be at the minimum of the free enthalpy of the system ($G = G(T, P, n_i)$), at fixed temperature and pressure. Therefore, the derivative of G with respect to the number of mole (n_i) becomes zero:

$$\left(\frac{dG}{dn_i}\right)_{T,P,n_j} = 0 \quad \textbf{(2.5)}$$

For a multiconstituent system, the free enthalpy in differential form is given as follows:

$$dG = VdP - SdT + \sum_i \mu_i dn_i \quad \textbf{(2.6)}$$

where μ_i is the chemical potential of constituent i, n_i is the number of moles of constituent i. S is the entropy of the system, and V is the volume.

At constant temperature and pressure, and by combining the Equations (2.5) and (2.6), we obtain:

$$\sum_i \mu_i dn_i = 0 \quad \textbf{(2.7)}$$

For a two-phase system, we have a transfer of the quantity dn_i between the two phases α and β which can be translated as:

$$dG = \left(\mu_i^{\beta} - \mu_i^{\alpha}\right) dn_i \quad \textbf{(2.8)}$$

By combining Equations (2.5) and (2.8), the following equilibrium condition is obtained:

$$\mu_i^{\alpha}(T, P, n_i^{\alpha}) = \mu_i^{\beta}(T, P, n_i^{\beta}) \quad \textbf{(2.9)}$$

In other words, phase equilibrium involves the uniformity of temperature, pressure and chemical potential in the different phases.

To facilitate the resolution of equilibrium relations, in 1901, Lewis [2. 163] introduced the notion of fugacity (f), which is an "equivalent" of pressure and represents the deviation from ideality. The relationship between chemical potential and fugacity is:

$$\mu_i^{\alpha}(T, P, n^{\alpha}) = \mu_i^{(std)}(T) + RT\, Ln\left(\frac{f_i^{\alpha}(T, P, n_i^{\alpha})}{f_i^{(std)}(T)}\right) \quad \textbf{(2.10)}$$

Equilibrium can therefore be written in terms of fugacity. Equation (2.9) is then substituted by:

$$f_i^{\alpha}(T, P, n_i^{\alpha}) = f_i^{\beta}(T, P, n_i^{\beta}) \quad \textbf{(2.11)}$$

It is therefore necessary to determine the fugacity of each constituent in each phase (Equation 2.11) in order to calculate the phase equilibria. To do this, two approaches exist:

A) Symmetric (phi-phi) approach

In the symmetric approach, the fluid phases in equilibrium are represented by the same model (Equation of State (EoS), e.g. cubic: PR, SRK, non-cubic: CPA, SAFT, GERG-2008, etc.). The fugacity f_i^π of the compound i in the π (=liquid or vapor) phase (Equation 2.12) is determined by multiplying its mole fraction x_i^π with its fugacity coefficient (phi) $\emptyset_i^\pi$ in this phase and the total pressure of the system P.

$$f_i^\pi(T,P,x_i^\pi) = x_i^\pi \times \emptyset_i^\pi(T,P,x_i^\pi) \times P \quad \textbf{(2.12)}$$

B) Asymmetric (gamma-phi) approach

In the asymmetric approach, the non-ideality of the vapor phase is taken into account by considering fugacity coefficients in the vapor phase, which are obtained by using an EoS as in the symmetric approach (Equation 2.12). However, the non-ideality of the liquid phase is considered with a G-excess model (e-NRTL, Pitzer, COSMO-type, UNIQUAC, etc.) through the activity coefficients γ_i^L. The fugacity f_i^L of the compound i in the liquid phase L (Equation 2.13) is determined by multiplying its mole fraction x_i^L with its activity coefficient γ_i^L in this phase and the standard fugacity f_i^0.

$$f_i^L(T,P,x_i^L) = x_i^L \times \gamma_i^L(T,x_i^L) \times f_i^0(T,P) \quad \textbf{(2.13)}$$

The fugacity of the pure liquid $f_i^{pure,L} = \emptyset_i^L(T,P_i^{sat}) \times P_i^{sat}$ is generally considered as a reference for the standard fugacity f_i^0 (Equation 2.14), however in the case of solubility calculation, the gases are mainly in the supercritical state, therefore it is no longer possible to use this reference state. However, the fugacity of the pure liquid is replaced by the Henry's law constant K_i^g (Equation 2.15) for this type of calculation.

$$f_i^0(T,P) = f_i^{pure,L} \times Poy = f_i^{pure,L}(T,P_i^{sat})\exp\left(v_i^L \frac{P-P_i^{sat}}{RT}\right) \quad \textbf{(2.14)}$$

$$f_{i=solute}^0(T,P) = \mathrm{K}_{i=gas}^g \times Poy = \mathrm{K}_{i=gas}^g(T,P_i^{sat,solvent})\exp\left(v_i^\infty \frac{P-P_i^{sat,solvent}}{RT}\right) \quad \textbf{(2.15)}$$

where P_i^{sat} is the vapor pressure, R the ideal gas constant, v_i^L and v_i^∞ the molar liquid volume and the molar volume of the dissolved solutes (gas) at infinite dilution, respectively. The term Poy called the Poynting correction factor is used to adjust the pure liquid vapor pressure P_i^{sat} or the solvent vapor pressure $P_i^{sat,solvent}$ to the system pressure P.

Being simple (no liquid volume resolution and less complicated than EoS) and fast, the gamma-phi approach is the most used approach by geochemists for correlating gas solubility data in water and brine. Moreover, this approach is still more used for systems with polar compounds (water, alcohols, amines, etc.) because the activity coefficients are more adapted to quantify the non-ideality of these types of compounds in solution. However, unlike the phi-phi approach, the gamma-phi approach cannot be used to predict the critical region (in particular the critical points of mixtures) since two different methodologies are used for the representation of the liquid and vapor phases (hence the nomination: asymmetric approach). Another advantage of using equations of state over activity models is the ability to compute other properties (densities and properties derived from Helmholtz free energy, e.g. enthalpy, entropy, heat capacity, etc.) than phase equilibria. The expression of the residual Helmholtz free energy A^r is the key function in thermodynamics [9], because other thermodynamic properties are calculable simply by partial derivatives of A^r with respect to temperature T, volume V, and the mole number n. Among the main thermodynamic properties that can be determined using Helmholtz free energy are:

- Pressure (P)

$$P = -RT\left(\frac{\partial F}{\partial V}\right)_{T,n} + \frac{nRT}{V} \quad \textbf{(2.16)}$$

$$F = \frac{A^r(T,V,n)}{RT} \quad \textbf{(2.17)}$$

- Fugacity coefficient (φ_i)

$$\ln(\varphi_i) = \left(\frac{\partial F}{\partial n_i}\right)_{T,V} - \ln(Z) \quad \textbf{(2.18)}$$

$$Z = \frac{PV}{nRT} \quad \textbf{(2.19)}$$

- Chemical potential (μ_i)

$$\frac{\mu_i}{\mathrm{RT}} = \left(\frac{\partial F}{\partial n_i}\right)_{T,V} \quad \textbf{(2.20)}$$

- Residual entropy (S^r) and enthalpy (H^r)

$$\frac{S^r(T,V,n)}{R} = -T\left(\frac{\partial F}{\partial T}\right)_{V,n} - F \quad \textbf{(2.21)}$$

$$H^r(T,P,n) = A^r(T,V,n) + TS^r(T,V,n) + PV - nRT \quad \textbf{(2.22)}$$

All other properties derivable from Helmholtz free energy can be found in the book by Michelsen and Mollerup [2. 164].

2.3.2 Model presentation

As previously seen, fugacity coefficients and activity coefficients are indispensable for the calculation of phase equilibria. Both properties can be obtained under any specification (for instance: temperature, pressure and/or salinity) using thermodynamic models. There are two categories of thermodynamic model: 1) **G-excess models** (used in the gamma-phi approach) which express the deviation from the ideal solution using the activity coefficient; 2) **Equations of State** that relate volume, temperature and mole number to express the deviation from ideal gas. This allows to determine the residual Helmholtz free energy expression, which can then be derived to obtain fugacity coefficients and other properties. Despite the wide variety of existing models, one model may be chosen over another depending on the type of the studied system, including the types of the components (polar, associative, electrolyte, etc.) and the operating conditions, and also on the computational complexity and speed of the model. The main existing models have been discussed in our recent work Chabab et al. (a) [2. 165] and (b) [2. 166]. In addition, a very detailed guide on the selection of thermodynamic models is given in the book by De Hemptinne and Ledanois [2. 167].

As part of the study of the salting-out effect applied to gas storage, using the phi-phi approach, two equations of state (1: Soreide and Whitson; 2: e-PR-CPA) were used in this work. These two EoS are presented in the following sections. To compare the different approaches, a geochemical model using the gamma-phi approach was tested. This model is presented in the first three articles of this manuscript (Chapters 3, 4 and 5).

2.3.2.1 Soreide and Whitson EoS

The first model is the cubic EoS proposed by Soreide and Whitson (SW) [2. 168], which is a revised form of the well-known Peng-Robinson EoS (PR EoS, Equation 2.23) [2. 169]. The Soreide-

Whitson model is widely used in the oil and gas field especially for systems in the presence of water or brine, and is implemented in several modeling software like reservoir simulators such as Eclipse 300 (by Schlumberger), IHRRS (by Total), TOUGH (by LBNL) and IPM (by Petex), and thermophysical properties calculators like Simulis Thermodynamics (by Prosim), etc.

$$P(T,v) = \frac{RT}{v-b} - \frac{a(T)}{v(v+b)+b(v-b)} \quad \textbf{(2.23)}$$

where P is the pressure, T the temperature, R the ideal gas constant, v the molar volume. The energy parameter a and the molar co-volume b for a pure compound i are given by

$$a_i(T) = 0.457235529\frac{R^2T_{c,i}^2}{P_{c,i}} \times \alpha(T) \quad \textbf{(2.24)}$$

$$\alpha(T) = \left[1 + (0.37464 + 1.54226\omega_i - 0.26992{\omega_i}^2)\left(1 - \sqrt{\frac{T}{T_{c,i}}}\right)\right]^2 \quad \textbf{(2.25)}$$

$$b_i = 0.0777960739\frac{RT_{c,i}}{P_{c,i}} \quad \textbf{(2.26)}$$

In Equations 2.24 to 2.26, $P_{c,i}$, $T_{c,i}$ and ω_i are respectively the critical pressure, the critical temperature and the acentric factor of compound i.

In the SW EoS, the salt (NaCl) is not considered as a compound, but the salting-out effect is accounted for by adding salinity (NaCl molality) dependencies to some model parameters. To improve the vapor pressure of water and brine, a specific alpha function $\alpha_w(T, m_s)$ depending on the reduced temperature and NaCl molality m_s was proposed (Equation 2.27). However, the generalized alpha function proposed by Soave [2. 170] and used in the original PR EoS has been retained for gases (Equation 2.25).

$$\alpha_w(T,m_s) = \left[1 + 0.4530\left[1 - \frac{T}{T_{c,w}}(1 - 0.0103\ \mathrm{m_s}^{1.1})\right] + 0.0034\left(\left(\frac{T}{T_{c,w}}\right)^{-3} - 1\right)\right]^2 \quad \textbf{(2.27)}$$

The second modification in the SW EoS concerns the binary interaction parameters (k_{ij}) used in the mixing rules to calculate the energy parameter of the mixture (a_m). The classical mixing rules (Equations 2.28 and 2.31) have been used with two different binary interaction parameters. The

first one (k_{ij}^{AQ}) is for the aqueous phase and the second one (k_{ij}^{NA}) is for the non-aqueous (gas-rich) phase which can be in vapor or liquid state. Nevertheless, the calculation of the co-volume of the mixture b_m has not been modified (Equation 2.31).

$$a_m(T) = \sum_{i=1}^{n_c}\sum_{i=1}^{n_c} x_i x_j \sqrt{a_i(T)a_j(T)}\left(1 - k_{ij}\right) \quad \textbf{(2.28)}$$

$$a_m^{AQ}(T) = \sum_{i=1}^{n_c}\sum_{i=1}^{n_c} x_i x_j \sqrt{a_i(T)a_j(T)}\left(1 - k_{ij}^{AQ}\right) \quad \textbf{(2.29)}$$

$$a_m^{NA}(T) = \sum_{i=1}^{n_c}\sum_{i=1}^{n_c} y_i y_j \sqrt{a_i(T)a_j(T)}(1 - k_{ij}^{NA}) \quad \textbf{(2.30)}$$

$$b_m = \sum_i x_i b_i \quad \textbf{(2.31)}$$

The two parameters k_{ij}^{AQ} and k_{ij}^{NA} are respectively adjusted on gas solubility data and water content data of gas-water-NaCl systems. The k_{ij}^{NA} is generally constant (N_2, O_2, H_2, C_1-C_4, etc.) or slightly dependent on temperature (H_2S and CO_2), however, the k_{ij}^{AQ} depends on temperature and molality. The use of two different binary interaction parameters for the aqueous and non-aqueous phases makes the model inconsistent (equivalent to an asymmetric gamma-phi approach) and very empirical (to be used just within the adjustment range of the parameters). This limitation is discussed in detail in Chapter 3.

2.3.2.2 **e-PR-CPA EoS**

The second equation of state is the e-PR-CPA model (the extension of the PR-CPA model to electrolytes) that was developed in this work. Unlike the SW EoS, the e-PR-CPA (electrolyte Peng-Robinson Cubic Plus Association) EoS takes into account the presence of salt theoretically. The choice of CPA-type model for the non-electrolyte part is justified by its adaptation to systems in the presence of associative molecules (water in our case). The e-PR-CPA EoS considers molecular interactions (attraction, dispersion, and association by hydrogen bonding) by the PR (Peng-Robinson) cubic term [2. 171] and the Wertheim's association theory [2. 172], and ionic interactions ion/ion (electrostatic forces) by the MSA (Mean Spherical Approximation) theory [2.

173] and ion/solvent (solvation phenomenon) by the Born term [2. 174]. In Figure 2.11, the types of chemical species (molecules and ions) that can be found are classified more or less in order of bond energy, showing the evolution of the types of interaction starting from simple fluids, associating fluids to molecules and ions interacting with chemical bonds. The representation of electrostatic forces (long range interactions) can be done by one of the two theories: the complete Debye-Huckel theory (DH) used by the Sadowski [2. 175], Kontogeorgis [2. 176] research groups, etc. and which treats ions as point charges; the MSA theory which is used by various research groups (Jackson [2. 177], De Hemptinne [2. 178], Fürst [2. 179], etc.) and which considers ions as charged hard spheres. A very good comparison of the two theories was made by Maribo-Mogensen et al. [2. 180] shows that numerically the two theories behave in a very similar way. They also showed that only MSA correctly predicts the increase in screening length by increasing the ion diameter, since in DH the screening length is independent of the diameter.

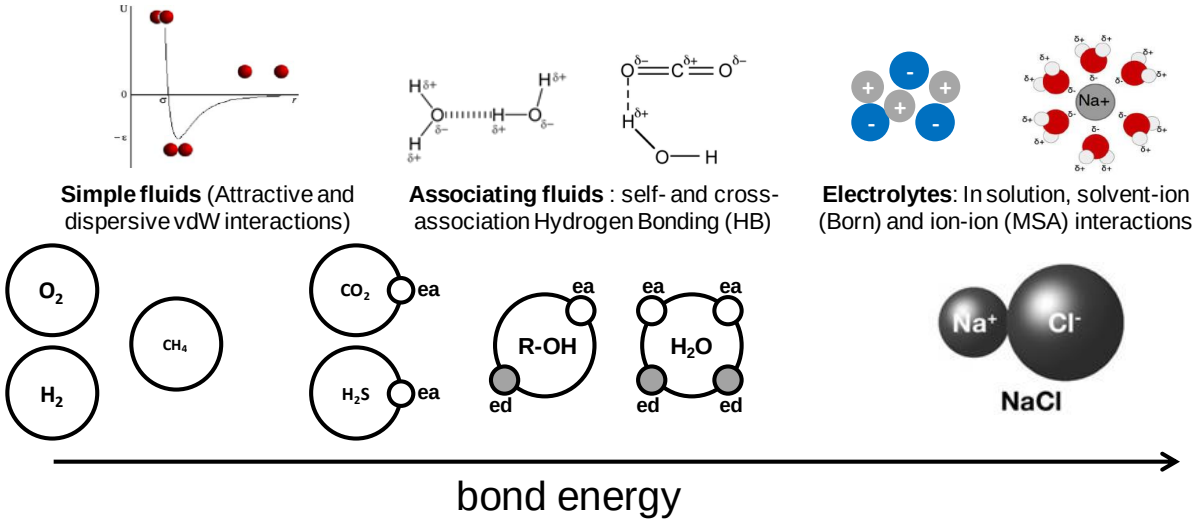

Figure 2.11: Intermolecular and electrolyte interactions considered in the e-PR-CPA model. ed: electron donor association site, ea: electron acceptor association site.

The expression of the reduced residual Helmholtz free energy $\frac{A^{res}}{RT}$ of the e-PR-CPA EoS is as follows:

$$\frac{A^{res}_{e-PR-CPA}}{RT} = \frac{A^{PR}}{RT} + \frac{A^{Association}}{RT} + \frac{A^{MSA}}{RT} + \frac{A^{Born}}{RT} \quad \textbf{(2.32)}$$

The non-electrolyte part of this model consists of two terms. Repulsive and attractive interactions are taken into account with the term $\frac{A^{PR}}{RT}$ of the PR EoS (Equation 2.33). The association phenomenon (self-association and cross-association) are represented by the term $\frac{A^{Association}}{RT}$ from Wertheim's theory (Equation 2.37).

$$\frac{A^{PR}}{RT} = -\ln\left(1-\frac{b}{v}\right) - \frac{a(T)}{2\sqrt{2}RTb}\ln\left(\frac{1+\left(1+\sqrt{2}\right)\frac{b}{v}}{1+\left(1-\sqrt{2}\right)\frac{b}{v}}\right) \quad \textbf{(2.33)}$$

The energy parameter $a(T)$ for the pure (non-ionic) associative compound i is obtained by the following equation:

$$a_i = a_{0,i} \times \left[1 + m_i\left(1-\sqrt{\frac{T}{T_{c,i}}}\right)\right]^2 \quad \textbf{(2.34)}$$

For non-associative pure compounds (gases in our case), Equations 2.24 to 2.26 are used to determine a_i and b_i. For associative compounds such as water, the parameters $a_{0,i}$, m_i and the co-volume b_i are adjusted to pure component experimental data.

Critical temperatures of ionic compounds are unknown. Courtial et al. [2. 181] proposed to replace the critical temperature in Equation 2.34 by the reference temperature 298.15 K for ions, since the majority of the available data are at this temperature. For ionic species the Equation 2.34 becomes

$$a_{ion} = a_{0,ion} \times \left[1 + m_{ion}\left(1-\sqrt{\frac{T}{298.15}}\right)\right]^2 \quad \textbf{(2.35)}$$

The co-volume b of an ion is related to its diameter σ_{ion} (adjustable parameter) with the relationship proposed by Fürst and Renon [2. 182]:

$$b_{ion} = \frac{N_{Av}\pi(\sigma_{ion})^3}{6} \quad \textbf{(2.36)}$$

where N_{Av} is the Avogadro number. The adjustable parameters for each ion are $a_{0,ion}$, m_{ion} and σ_{ion}.

For mixtures a and b are determined by the van der Waals classical mixing rules (Equations 2.28 and 2.31).

$$\frac{A^{Association}}{RT} = \sum_i n_i \sum_{A^i} \left(\ln\left(X_{A_i}\right) + \frac{1 - X_{A_i}}{2}\right) \quad \textbf{(2.37)}$$

In Equation 2.37, n_i stands for the number of mole of component i; X_{A_i} is the fraction of sites of type *A* in molecule *i* that are non-bonded, and is obtained by solving the following equations:

$$X_{A_i} = \frac{1}{1 + \rho \sum_j x_j \sum_{B_j} X_{B_j} \Delta^{A_i B_j}} \quad \textbf{(2.38)}$$

where $\rho = \frac{1}{v}$ stands for the molar density. $\Delta^{A_i B_j}$ is the association strength between sites A_i and B_j of molecules i and j, and is determined by the following equation.

$$\Delta^{A_i B_j} = g(\rho)\left[\exp\left(\frac{\varepsilon^{A_i B_j}}{RT}\right)\right] b_{ij}\, \beta^{A_i B_j} \quad \textbf{(2.39)}$$

where:

$$b_{ij} = \frac{b_i + b_j}{2} \quad \textbf{(2.40)}$$

$g(\rho)$ is the radial distribution function [2. 183] at contact, which is given by:

$$g(\rho) = \frac{1}{1 - 1.9\,\eta} \quad \textbf{(2.41)}$$

with $\eta = \frac{1}{4} b\rho$

The association energy $\varepsilon^{A_i B_j}$ and the bonding volume $\beta^{A_i B_j}$ are two adjustable parameters for pure self-associating compounds. For mixtures, some combining rules are used to the cross association

parameters. Generally, the CR1 [2. 184] combining rules are used in the case of a mixture with two self-associating fluids:

$$\varepsilon^{A_iB_j} = \frac{\varepsilon^{A_iB_i} + \varepsilon^{A_jB_j}}{2} \quad \textbf{(2.42)}$$

$$\beta^{A_iB_j} = \sqrt{\beta^{A_iB_i}\beta^{A_jB_j}} \quad \textbf{(2.43)}$$

In the case of solvation of a non-self-associating fluid by a self-associating fluid (water, alcohol, etc.), the modified combining rules (m-CR1) proposed by Folas et al. [2. 185] can be used:

$$\varepsilon^{A_iB_j} = \frac{\varepsilon_{associating}}{2} \quad \textbf{(2.44)}$$

while the parameter $\beta^{A_iB_j}$ is adjusted to mixture experimental data.

Long-range electrostatic forces (Coulomb interaction) are described by the MSA term $\left(\frac{A^{MSA}}{RT}\right)$. In this work we use the form proposed by Ball et al. [2. 186] (Equation 2.45), which is a simplified version of the non-restricted primitive MSA (nRP-MSA) developed by Blum [2. 173]. The nRP-MSA model treats ions as charged hard spheres of different diameters and considers the solvent as a dielectric continuum through its dielectric constant D.

$$\frac{A^{MSA}}{RT} = -\frac{\alpha_{MSA}^2}{4\pi}\sum_i \frac{n_i Z_i^2 \Gamma}{1+\Gamma\sigma_i} + \frac{V\Gamma^3}{3\pi N_{Av}} \quad \textbf{(2.45)}$$

where:

$$\alpha_{MSA}^2 = \frac{N_{Av}e^2}{D_0 DRT} \quad \textbf{(2.46)}$$

where e is the elementary charge, n_i is the number of moles of the ion i, D_0 is the vacuum permittivity and Z_i is the electric charge of species i.

The screening length Γ is determined from the iterative resolution of the following equation.

$$4\Gamma^2 = \alpha_{MSA}^2 N_{Av}\sum_i \frac{n_i}{V}\left(\frac{Z_i}{1+\Gamma\sigma_i}\right)^2 \quad \textbf{(2.47)}$$

The Born's term $\frac{A^{Born}}{RT}$ (Equation 2.48) [2. 187] describes the short-range interactions (ion solvation). This contribution quantifies the energy of solvation by calculating the energy required to transfer an ion from the vacuum to a solvent of dielectric constant D [2. 184]. It is given by

$$\frac{A^{Born}}{RT} = -\frac{N_{Av}e^2}{4\pi D_0 RT}\left(1-\frac{1}{D}\right)\sum_i \frac{n_i Z_i^2}{\sigma_i} \qquad \textbf{(2.48)}$$

In both electrolyte terms (Born and MSA), the dielectric constant D must be determined. Inchekel et al. [2. 179] showed that the Born term has an effect of the activity coefficients of the species as long as the dielectric constant depends on the concentration of salts. In this word, we use Simonin's model [2. 188] to compute the dielectric constant D of the electrolyte solution:

$$D = \frac{D_s}{1+\alpha\sum_i^{ions} x_i} \qquad \textbf{(2.49)}$$

where α is salt dependent adjustable parameter. The value of 5.08 proposed by Inchekel et al. [2. 179] for the H_2O+NaCl system is used in this work. D_s is the dielectric constant of the pure solvent (water in our case). The correlation proposed by Uematsu and Franck [2. 189] was used to determine D_s:

$$\begin{aligned} D_s = 1 &+ \left(\frac{7.62571}{T^*}\right)\rho^* + \left(\frac{244.003}{T^*} - 140.569 + 27.7841T^*\right)\rho^{*2} \\ &+ \left(\frac{-96.2805}{T^*} + 41.7909T^* - 10.2099T^{*2}\right)\rho^{*3} \\ &+ \left(\frac{-45.2059}{T^{*2}} + \frac{84.6395}{T^*} - 35.8644\right)\rho^{*4} \end{aligned} \qquad \textbf{(2.50)}$$

where $T^* = \frac{T}{T_0}$ and $\rho^* = \frac{\rho_w}{\rho_0}$ with $T_0 = 298.15\ K$ and $\rho_0 = 1000\ kg/m^3$. T is the temperature (in K), ρ_w is the density of pure water (in kg/m^3).

As suggested by Myers et al. [2. 187], the water density used in Equation 2.50 is calculated from the number of moles of water in the solution n_w and the volume of the solution V, as

$$\rho_w = \frac{n_w M_{H_2O}}{V} \qquad \textbf{(2.51)}$$

where M_{H_2O} is the molar mass of water in kg/mol.

To reduce the number of parameters, the diameters σ_i of ions i used in the Born term and in the MSA term are the same as the ones used to calculate the co-volume of the ions b_{ion}. The determination of the pure species (water and ions) parameters is presented in detail in Chapter 3.

A salt-free fluid phase equilibrium calculation was used with the two equations of state (e-PR-CPA and SW) considering only the compositions of the molecular (non-ionic) species in the different types of Flash calculations (isobaric-isothermal, bubble point and dew point). In Appendix A, the procedure of the PT-Flash calculation is detailed.

2.3.3 Gas hydrates and fluid phase equilibria

Hydrate dissociation thermodynamic modeling is generally done by combining the well-established van der Waals and Platteeuw theory (vdWP) [2. 190] for hydrate phase calculation with an Equation of State (EoS) for fluid phases (liquid and vapor) calculation and possibly with a G-excess model for water activity coefficient estimation. The hydrate dissociation curve represents the equilibrium of the hydrate phase with the aqueous phase and the gas-rich phase (which can be liquid and/or vapor), and this more or less limits the hydrate stability domain at thermodynamic equilibrium. Given its very good performance (see next Chapters), the e-PR-CPA EoS was extended to study gas hydrate stability by combining it with vdWP model. The resulting model (e-PR-CPA + vdWP) and the procedure for calculating the equilibria between the hydrate and fluid phases are described in Chapter 6.

References

[2. 1] C.H. Whitson, M.R. Brulé, Phase behavior, Henry L. Doherty Memorial Fund of AIME, Society of Petroleum Engineers, 2000.
[2. 2] R. Dohrn, S. Peper, J.M. Fonseca, High-pressure fluid-phase equilibria: experimental methods and systems investigated (2000–2004), Fluid Phase Equilibria, 288 (2010) 1-54.
[2. 3] S. Peper, J.M. Fonseca, R. Dohrn, High-pressure fluid-phase equilibria: Trends, recent developments, and systems investigated (2009–2012), Fluid Phase Equilibria, 484 (2019) 126-224.
[2. 4] J.L. Lara Cruz, Caractérisation thermodynamique des ELV HPHT dans les saumures, in, Pau, 2019.
[2. 5] A. Chapoy, M. Nazeri, M. Kapateh, R. Burgass, C. Coquelet, B. Tohidi, Effect of impurities on thermophysical properties and phase behaviour of a CO2-rich system in CCS, International Journal of Greenhouse Gas Control, 19 (2013) 92-100.
[2. 6] R. Burgass, A. Reid, A. Chapoy, B. Tohidi, Glycols Partitioning At High Pressures In Gas Processing Systems, in: GPA Midstream Convention 2017, 2017.

[2. 7] P. Ahmadi, A. Chapoy, CO2 solubility in formation water under sequestration conditions, Fluid Phase Equilibria, 463 (2018) 80-90.
[2. 8] S. Chabab, P. Théveneau, J. Corvisier, C. Coquelet, P. Paricaud, C. Houriez, E. El Ahmar, Thermodynamic study of the CO2–H2O–NaCl system: Measurements of CO2 solubility and modeling of phase equilibria using Soreide and Whitson, electrolyte CPA and SIT models, International Journal of Greenhouse Gas Control, 91 (2019) 102825.
[2. 9] H. Li, J.P. Jakobsen, Ø. Wilhelmsen, J. Yan, PVTxy properties of CO2 mixtures relevant for CO2 capture, transport and storage: Review of available experimental data and theoretical models, Applied Energy, 88 (2011) 3567-3579.
[2. 10] P. Perazzelli, G. Anagnostou, Design issues for compressed air energy storage in sealed underground cavities, Journal of Rock Mechanics and Geotechnical Engineering, 8 (2016) 314-328.
[2. 11] F. Lahaie, P. Gombert, C. Boudet, "Le stockage souterrain dans le contexte de la transition énergétique" Maîtrise des risques et impacts, (2016).
[2. 12] Y.D. Zel'venskii, The solubility of carbon dioxide in water under pressure, Zh. Khim. Promsti, 14 (1937) 1250-1257.
[2. 13] R. Wiebe, V. Gaddy, The solubility in water of carbon dioxide at 50, 75 and 100, at pressures to 700 atmospheres, Journal of the American Chemical Society, 61 (1939) 315-318.
[2. 14] R. Wiebe, V. Gaddy, The solubility of carbon dioxide in water at various temperatures from 12 to 40 and at pressures to 500 atmospheres. Critical phenomena, Journal of the American Chemical Society, 62 (1940) 815-817.
[2. 15] C. Prutton, R. Savage, The solubility of carbon dioxide in calcium chloride-water solutions at 75, 100, 120 and high pressures1, Journal of the American Chemical Society, 67 (1945) 1550-1554.
[2. 16] E. Bartholomé, H. Friz, Solubility of CO2 in water, Chem. Ing. Tech, 28 (1956) 706-708.
[2. 17] W. Dodds, L. Stutzman, B. Sollami, Carbon dioxide solubility in water, Industrial & Engineering Chemistry Chemical & Engineering Data Series, 1 (1956) 92-95.
[2. 18] A. Ellis, The solubility of carbon dioxide in water at high temperatures, American Journal of Science, 257 (1959) 217-234.
[2. 19] K. Tödheide, E. Franck, Das Zweiphasengebiet und die kritische Kurve im System Kohlendioxid–Wasser bis zu Drucken von 3500 bar, Zeitschrift für Physikalische Chemie, 37 (1963) 387-401.
[2. 20] S. Takenouchi, G.C. Kennedy, The binary system H 2 O-CO 2 at high temperatures and pressures, American Journal of Science, 262 (1964) 1055-1074.
[2. 21] R. Vilcu, I. Gainar, Loslichkeit der gase unter druck in flussigkeiten. i. das system kohlendioxid-wasser, Revue Roumaine de Chimie, 12 (1967) 181-&.
[2. 22] J. Matouš, J. Šobr, J. Novak, J. Pick, Solubility of carbon dioxide in water at pressures up to 40 atm, Collection of Czechoslovak Chemical Communications, 34 (1969) 3982-3985.
[2. 23] A.D. King Jr, C. Coan, Solubility of water in compressed carbon dioxide, nitrous oxide, and ethane. Evidence for hydration of carbon dioxide and nitrous oxide in the gas phase, Journal of the American Chemical Society, 93 (1971) 1857-1862.
[2. 24] R. Shagiakhmetov, A. Tarzimanov, Measurements of CO2 solubility in water up to 60 MPa, Deposited Document SPSTL 200khp-D81-1982, (1981).
[2. 25] A. Zawisza, B. Malesinska, Solubility of carbon dioxide in liquid water and of water in gaseous carbon dioxide in the range 0.2-5 MPa and at temperatures up to 473 K, Journal of Chemical and Engineering Data, 26 (1981) 388-391.

[2. 26] S. Cramer, Solubility of methane, carbon dioxide, and oxygen in brines from 0/sup 0/to 300/sup 0/C, in, Bureau of Mines, Pittsburgh, PA, 1982.
[2. 27] P.C. Gillespie, Vapor-Liquid and Liquid-Liquid Equilibria: Water-Methane, Water-Carbon Dioxide, Water-Hydrogen Sulfide, Water-nPentane, Water-Methane-nPentane, Gas Processor's Association, Research Report, 48 (1982) 11.
[2. 28] J.A. Briones, J.C. Mullins, M.C. Thies, B.-U. Kim, Ternary phase equilibria for acetic acid-water mixtures with supercritical carbon dioxide, Fluid Phase Equilibria, 36 (1987) 235-246.
[2. 29] T. Nakayama, H. Sagara, K. Arai, S. Saito, High pressure liquid · liquid equilibria for the system of water, ethanol and 1, 1-difluoroethane at 323.2 K, Fluid Phase Equilibria, 38 (1987) 109-127.
[2. 30] K.Y. Song, R. Kobayashi, Water content of CO2 in equilibrium with liquid water and/or hydrates, SPE Formation Evaluation, 2 (1987) 500-508.
[2. 31] R. D'souza, J.R. Patrick, A.S. Teja, High pressure phase equilibria in the carbon dioxide-n-Hexadecane and carbon dioxide—water systems, The Canadian Journal of Chemical Engineering, 66 (1988) 319-323.
[2. 32] G. Muller, E. Bender, G. Maurer, Vapor-liquid-equilibrium in the ternary-system ammonia-carbon dioxide-water at high water contents in the range 373-K to 473-K, Berichte Der Bunsen-Gesellschaft-Physical Chemistry Chemical Physics, 92 (1988) 148-160.
[2. 33] T. Sako, T. Sugeta, N. Nakazawa, T. Okubo, M. Sato, T. Taguchi, T. Hiaki, Phase equilibrium study of extraction and concentration of furfural produced in reactor using supercritical carbon dioxide, Journal of chemical engineering of Japan, 24 (1991) 449-455.
[2. 34] M. King, A. Mubarak, J. Kim, T. Bott, The mutual solubilities of water with supercritical and liquid carbon dioxides, The Journal of Supercritical Fluids, 5 (1992) 296-302.
[2. 35] R. Dohrn, A. Bünz, F. Devlieghere, D. Thelen, Experimental measurements of phase equilibria for ternary and quaternary systems of glucose, water, CO2 and ethanol with a novel apparatus, Fluid Phase Equilibria, 83 (1993) 149-158.
[2. 36] B. Rumpf, H. Nicolaisen, C. Öcal, G. Maurer, Solubility of carbon dioxide in aqueous solutions of sodium chloride: experimental results and correlation, Journal of solution chemistry, 23 (1994) 431-448.
[2. 37] K. Jackson, L.E. Bowman, J.L. Fulton, Water solubility measurements in supercritical fluids and high-pressure liquids using near-infrared spectroscopy, Analytical Chemistry, 67 (1995) 2368-2372.
[2. 38] M.B. Malegaonkar, P.D. Dholabhai, P.R. Bishnoi, Kinetics of carbon dioxide and methane hydrate formation, The Canadian Journal of Chemical Engineering, 75 (1997) 1090-1099.
[2. 39] A. Dhima, J.-C. de Hemptinne, J. Jose, Solubility of hydrocarbons and CO2 mixtures in water under high pressure, Industrial & engineering chemistry research, 38 (1999) 3144-3161.
[2. 40] A. Bamberger, G. Sieder, G. Maurer, High-pressure (vapor+ liquid) equilibrium in binary mixtures of (carbon dioxide+ water or acetic acid) at temperatures from 313 to 353 K, The Journal of Supercritical Fluids, 17 (2000) 97-110.
[2. 41] S. Yang, I. Yang, Y. Kim, C. Lee, Measurement and prediction of phase equilibria for water+ CO2 in hydrate forming conditions, Fluid Phase Equilibria, 175 (2000) 75-89.
[2. 42] R. Rosenbauer, J. Bischoff, T. Koksalan, An experimental approach to CO 2 sequestration in saline aquifers: application to Paradox Valley, CO, AGUFM, 2001 (2001) V32B-0974.
[2. 43] J. Kiepe, S. Horstmann, K. Fischer, J. Gmehling, Experimental determination and prediction of gas solubility data for CO2+ H2O mixtures containing NaCl or KCl at temperatures between

313 and 393 K and pressures up to 10 MPa, Industrial & Engineering Chemistry Research, 41 (2002) 4393-4398.
[2. 44] G.K. Anderson, Solubility of carbon dioxide in water under incipient clathrate formation conditions, Journal of Chemical & Engineering Data, 47 (2002) 219-222.
[2. 45] S. Bando, F. Takemura, M. Nishio, E. Hihara, M. Akai, Solubility of CO2 in aqueous solutions of NaCl at (30 to 60) C and (10 to 20) MPa, Journal of Chemical & Engineering Data, 48 (2003) 576-579.
[2. 46] A. Chapoy, A. Mohammadi, A. Chareton, B. Tohidi, D. Richon, Measurement and modeling of gas solubility and literature review of the properties for the carbon dioxide− water system, Industrial & engineering chemistry research, 43 (2004) 1794-1802.
[2. 47] A. Valtz, A. Chapoy, C. Coquelet, P. Paricaud, D. Richon, Vapour–liquid equilibria in the carbon dioxide–water system, measurement and modelling from 278.2 to 318.2 K, Fluid phase equilibria, 226 (2004) 333-344.
[2. 48] D. Koschel, J.-Y. Coxam, L. Rodier, V. Majer, Enthalpy and solubility data of CO2 in water and NaCl (aq) at conditions of interest for geological sequestration, Fluid phase equilibria, 247 (2006) 107-120.
[2. 49] J. Qin, R.J. Rosenbauer, Z. Duan, Experimental measurements of vapor–liquid equilibria of the H2O+ CO2+ CH4 ternary system, Journal of Chemical & Engineering Data, 53 (2008) 1246-1249.
[2. 50] J.M. Han, H.Y. Shin, B.-M. Min, K.-H. Han, A. Cho, Measurement and correlation of high pressure phase behavior of carbon dioxide+ water system, Journal of Industrial and Engineering Chemistry, 15 (2009) 212-216.
[2. 51] G. Ferrentino, D. Barletta, F. Donsì, G. Ferrari, M. Poletto, Experimental measurements and thermodynamic modeling of CO2 solubility at high pressure in model apple juices, Industrial & Engineering Chemistry Research, 49 (2010) 2992-3000.
[2. 52] Y. Liu, M. Hou, G. Yang, B. Han, Solubility of CO2 in aqueous solutions of NaCl, KCl, CaCl2 and their mixed salts at different temperatures and pressures, The Journal of supercritical fluids, 56 (2011) 125-129.
[2. 53] W. Yan, S. Huang, E.H. Stenby, Measurement and modeling of CO2 solubility in NaCl brine and CO2–saturated NaCl brine density, International Journal of Greenhouse Gas Control, 5 (2011) 1460-1477.
[2. 54] S.-X. Hou, G.C. Maitland, J.M. Trusler, Measurement and modeling of the phase behavior of the (carbon dioxide+ water) mixture at temperatures from 298.15 K to 448.15 K, The Journal of Supercritical Fluids, 73 (2013) 87-96.
[2. 55] C. Langlais, Impacts géochimiques de la présence d'oxygène sur les saumures en conditions de stockage géologique de CO2 : caractérisation de solubilités, in, 2013.
[2. 56] H. Guo, Y. Chen, Q. Hu, W. Lu, W. Ou, L. Geng, Quantitative Raman spectroscopic investigation of geo-fluids high-pressure phase equilibria: Part I. Accurate calibration and determination of CO2 solubility in water from 273.15 to 573.15 K and from 10 to 120 MPa, Fluid Phase Equilibria, 382 (2014) 70-79.
[2. 57] P.J. Carvalho, L.M. Pereira, N.P. Gonçalves, A.J. Queimada, J.A. Coutinho, Carbon dioxide solubility in aqueous solutions of NaCl: Measurements and modeling with electrolyte equations of state, Fluid Phase Equilibria, 388 (2015) 100-106.
[2. 58] E. Mohammadian, H. Hamidi, M. Asadullah, A. Azdarpour, S. Motamedi, R. Junin, Measurement of CO2 solubility in NaCl brine solutions at different temperatures and pressures using the potentiometric titration method, Journal of Chemical & Engineering Data, 60 (2015) 2042-2049.

[2. 59] H. Zhao, M.V. Fedkin, R.M. Dilmore, S.N. Lvov, Carbon dioxide solubility in aqueous solutions of sodium chloride at geological conditions: Experimental results at 323.15, 373.15, and 423.15 K and 150 bar and modeling up to 573.15 K and 2000 bar, Geochimica et Cosmochimica Acta, 149 (2015) 165-189.
[2. 60] M.-C. Caumon, J. Sterpenich, A. Randi, J. Pironon, Measuring mutual solubility in the H2O–CO2 system up to 200 bar and 100 C by in situ Raman spectroscopy, International Journal of Greenhouse Gas Control, 47 (2016) 63-70.
[2. 61] K. Gilbert, P.C. Bennett, W. Wolfe, T. Zhang, K.D. Romanak, CO 2 solubility in aqueous solutions containing Na+, Ca 2+, Cl−, SO 4 2− and HCO 3-: The effects of electrostricted water and ion hydration thermodynamics, Applied Geochemistry, 67 (2016) 59-67.
[2. 62] R. Jacob, B.Z. Saylor, CO2 solubility in multi-component brines containing NaCl, KCl, CaCl2 and MgCl2 at 297 K and 1–14 MPa, Chemical Geology, 424 (2016) 86-95.
[2. 63] H. Messabeb, F. Contamine, P. Cézac, J.P. Serin, E.C. Gaucher, Experimental Measurement of CO2 Solubility in Aqueous NaCl Solution at Temperature from 323.15 to 423.15 K and Pressure of up to 20 MPa, Journal of Chemical & Engineering Data, 61 (2016) 3573-3584.
[2. 64] B. Liborio, Dissolution du dioxyde de carbone dans des solutions aqueuses d'électrolyte dans le contexte du stockage géologique: approche thermodynamique, in, 2017.
[2. 65] H. Messabeb, F. Contamine, P. Cézac, J.P. Serin, C.m. Pouget, E.C. Gaucher, Experimental measurement of CO2 solubility in aqueous CaCl2 solution at temperature from 323.15 to 423.15 K and pressure up to 20 MPa using the conductometric titration, Journal of Chemical & Engineering Data, 62 (2017) 4228-4234.
[2. 66] K. Deng, Y. Lin, H. Ning, W. Liu, A. Singh, G. Zhang, Influences of temperature and pressure on CO2 solubility in saline solutions in simulated oil and gas well environments, Applied Geochemistry, 99 (2018) 22-30.
[2. 67] J. Wang, B. He, L. Xie, K. Bei, G. Li, Z. Chen, I.-M. Chou, C. Lin, Z. Pan, Determination of CO2 Solubility in Water and NaCl Solutions under Geological Sequestration Conditions Using a Fused Silica Capillary Cell with in Situ Raman Spectroscopy, Journal of Chemical & Engineering Data, 64 (2019) 2484-2496.
[2. 68] J.L.L. Cruz, F. Contamine, P. Cézac, Experimental study of CO2 solubility on NaCl and CaCl2 solutions at 333.15 K and pressures up to 40.0 MPa, (2019).
[2. 69] R. Bunsen, Ueber das Gesetz der Gasabsorption, Justus Liebigs Annalen der Chemie, 93 (1855) 1-50.
[2. 70] W. Timofejew, Über die Absorption von Wasserstoff und Sauerstoff in Wasser und Alkohol, Zeitschrift für Physikalische Chemie, 6 (1890) 141-152.
[2. 71] C. Bohr, J. Bock, Bestimmung der Absorption einiger Gase in Wasser bei den Temperaturen zwischen 0 und 100°, Annalen der Physik, 280 (1891) 318-343.
[2. 72] L. Winkler, Die Löslichkeit der Gase in Wasser, Berichte der deutschen chemischen Gesellschaft, 24 (1891) 3602-3610.
[2. 73] G. Geffcken, Beiträge zur kenntnis der löslichkeitsbeeinflussung, Zeitschrift für Physikalische Chemie, 49 (1904) 257-302.
[2. 74] C.J. Fox, On the coefficients of absorption of nitrogen and oxygen in distilled water and sea-water, and of atmospheric carbonic acid in sea-water, Transactions of the Faraday Society, 5 (1909) 68-86.
[2. 75] C. Bohr, Über die Löslichkeit von Gasen in konzentrierter Schwefelsäure und in Mischungen von Schwefelsäure und Wasser, Zeitschrift für Physikalische Chemie, 71 (1910) 47-50.

[2. 76] C. Müller, Die Absorption von Sauerstoff, Stickstoff und Wasserstoff in wässerigen Lösungen von Nichtelektrolyten, Zeitschrift für Physikalische Chemie, 81 (1913) 483-503.
[2. 77] C. MacArthur, Solubility of oxygen in salt solutions and the hydrates of these salts, The Journal of Physical Chemistry, 20 (1916) 495-502.
[2. 78] W. Adeney, H. Becker, XXXVIII. The determination of the rate of solution of atmospheric nitrogen and oxygen by water.—Part II, The London, Edinburgh, and Dublin Philosophical Magazine and Journal of Science, 39 (1920) 385-404.
[2. 79] J. Livingston, R. Morgan, A. Richardson, Solubility of oxygen in water, J. Phys. Chem, 34 (1930) 2356-2366.
[2. 80] F. Orcutt, M. Seevers, A method for determining the solubility of gases in pure liquids or solutions by the Van Slyke-Neill manometric apparatus, Journal of Biological Chemistry, 117 (1937) 501-507.
[2. 81] A. Eucken, G. Hertzberg, Aussalzeffekt und ionenhydratation, Zeitschrift für Physikalische Chemie, 195 (1950) 1-23.
[2. 82] T. Morrison, F. Billett, 730. The salting-out of non-electrolytes. Part II. The effect of variation in non-electrolyte, Journal of the Chemical Society (Resumed), (1952) 3819-3822.
[2. 83] H.A. Pray, C. Schweickert, B.H. Minnich, Solubility of hydrogen, oxygen, nitrogen, and helium in water at elevated temperatures, Industrial & Engineering Chemistry, 44 (1952) 1146-1151.
[2. 84] L. Zoss, A Study of the Hydrogen and Water and Oxygen and Water Systems at Various Temperatures and Pressures, in, Ph. D. thesis, Purdue University, West Lafayette, IN, 1952.
[2. 85] O.G. Mckee, A Study of Solubilities of Several Gases in Water, (1953).
[2. 86] E.F. Stephan, N. Hatfield, R. Peoples, H. Pray, The solubility of gases in water and in aqueous uranyl salt solutions at elevated temperatures and pressures, in, Battelle Memorial Inst., Columbus, Ohio, 1956.
[2. 87] H.L. Clever, R. Battino, J. Saylor, P. Gross, The solubility of helium, neon, argon and krypton in some hydrocarbon solvents, The Journal of Physical Chemistry, 61 (1957) 1078-1082.
[2. 88] H. Steen, Determinations of the Solubility of Oxygen in Pure Water 1, Limnology and Oceanography, 3 (1958) 423-426.
[2. 89] H. Elmore, T. Hayes, Solubility of atmospheric oxygen in water, in: Proc. Am. Sot. Civil Engrs, 1960, pp. 41-53.
[2. 90] T. Mishinina, O. Avdeeva, T. Bozhovskaya, Solubility of gases in natural waters depending on temperature, pressure and salt composition, Materialy Vses. Nauchn. Issled. Geol. Inst, 46 (1961) 93-110.
[2. 91] C. Anderson, R. Keeler, S. Klach, Solubility of Krypton and Oxygen in Water and Aqueous Uranyl Sulphate Solutions at Elevated Temperatures, Journal of Chemical and Engineering Data, 7 (1962) 290-294.
[2. 92] E. Douglas, Solubilities of Oxygen, Argon, and Nitrogen in Distilled Water, The Journal of Physical Chemistry, 68 (1964) 169-174.
[2. 93] H. Montgomery, N. Thom, A. Cockburn, Determination of dissolved oxygen by the Winkler method and the solubility of oxygen in pure water and sea water, Journal of Applied Chemistry, 14 (1964) 280-296.
[2. 94] E.J. Green, A redetermination of the solubility of oxygen in sea water and some thermodynamic implications of the solubility relations, in, Massachusetts Institute of Technology, 1965.
[2. 95] J.H. Carpenter, New measurements of oxygen solubility in pure and natural water 1, Limnology and oceanography, 11 (1966) 264-277.

[2. 96] G. Power, Solubility of O2 and CO in blood and pulmonary and placental tissue, Journal of applied physiology, 24 (1968) 468-474.
[2. 97] S. Shchukarev, T. Tolmacheva, Translated from Zh, Strukt. Khim, 9 (1968) 21.
[2. 98] C. Murray, J. Riley, T. Wilson, The solubility of gases in distilled water and sea water—I. Nitrogen, in: Deep Sea Research and Oceanographic Abstracts, Elsevier, 1969, pp. 297-310.
[2. 99] C. Murray, J. Riley, The solubility of gases in distilled water and sea water—II. Oxygen, in: Deep Sea Research and Oceanographic Abstracts, Elsevier, 1969, pp. 311-320.
[2. 100] S. Shoor, R.D. Walker Jr, K. Gubbins, Salting out of nonpolar gases in aqueous potassium hydroxide solutions, The Journal of Physical Chemistry, 73 (1969) 312-317.
[2. 101] D. Wise, G. Houghton, Solubilities and diffusivities of oxygen in hemolyzed human blood solutions, Biophysical journal, 9 (1969) 36-53.
[2. 102] G.G. Power, H. Stegall, Solubility of gases in human red blood cell ghosts, Journal of Applied Physiology, 29 (1970) 145-149.
[2. 103] D.M. Novak*, B. Conway, Technique for repetitive gas solubility determinations at various pressures, (1974).
[2. 104] R.J. Wilcock, R. Battino, Solubility of oxygen–nitrogen mixture in water, Nature, 252 (1974) 614.
[2. 105] J. Tokunaga, Solubilities of oxygen, nitrogen, and carbon dioxide in aqueous alcohol solutions, Journal of Chemical & Engineering Data, 20 (1975) 41-46.
[2. 106] B.B. Benson, D. Krause Jr, Empirical laws for dilute aqueous solutions of nonpolar gases, The Journal of Chemical Physics, 64 (1976) 689-709.
[2. 107] R.W. Cargill, Solubility of oxygen in some water+ alcohol systems, Journal of the Chemical Society, Faraday Transactions 1: Physical Chemistry in Condensed Phases, 72 (1976) 2296-2300.
[2. 108] A. Yasunishi, Solubilities of sparingly soluble gases in aqueous sodium sulfate and sulfite solutions, Journal of Chemical Engineering of Japan, 10 (1977) 89-94.
[2. 109] A. Broden, R. Simonson, Solubility of oxygen, Svensk Papperstidning, 17 (1978) 541-544.
[2. 110] I. Matheson, A. King Jr, Solubility of gases in micellar solutions, Journal of Colloid and Interface Science, 66 (1978) 464-469.
[2. 111] B.B. Benson, D. Krause, M.A. Peterson, The solubility and isotopic fractionation of gases in dilute aqueous solution. I. Oxygen, Journal of Solution Chemistry, 8 (1979) 655-690.
[2. 112] A. Da Silva, S. Formosinho, C. Martins, Gas Chromatographic Determination of the Solubility of Gases in Liquids at Low Pressures, Journal of Chromatographic Science, 18 (1980) 180-182.
[2. 113] B.A. Cosgrove, J. Walkley, Solubilities of gases in H2O and 2H2O, Journal of Chromatography A, 216 (1981) 161-167.
[2. 114] M.L. Japas, E. Franck, High pressure phase equilibria and PVT-data of the water-oxygen system including water-air to 673 K and 250 MPa, Berichte der Bunsengesellschaft für physikalische Chemie, 89 (1985) 1268-1275.
[2. 115] H.T.H. Kimweri, Solubility of oxygen in aqueous sulphuric acid-metallic salt solutions under pressure leaching conditions, University of Ottawa (Canada), 1990.
[2. 116] J. Sherwood, F. Stagnitti, M. Kokkinn, W. Williams, Dissolved oxygen concentrations in hypersaline waters, Limnology and Oceanography, 36 (1991) 235-250.
[2. 117] T.R. Rettich, R. Battino, E. Wilhelm, Solubility of gases in liquids. 22. High-precision determination of Henry's law constants of oxygen in liquid water fromT= 274 K toT= 328 K, The Journal of Chemical Thermodynamics, 32 (2000) 1145-1156.

[2. 118] Z.-Q. Tan, G.-H. Gao, Y.-X. Yu, C. Gu, Solubility of oxygen in aqueous sodium carbonate solution at pressures up to 10 MPa, Fluid phase equilibria, 180 (2001) 375-382.
[2. 119] F.J. Millero, F. Huang, A.L. Laferiere, The solubility of oxygen in the major sea salts and their mixtures at 25 C, Geochimica et Cosmochimica Acta, 66 (2002) 2349-2359.
[2. 120] F. Millero, F. Huang, A. Laferriere, Solubility of oxygen in the major sea salts as a function of temperature and concentration, Mar. Chem, 78 (2002) 217-230.
[2. 121] T. Kaskiala, J. Salminen, Oxygen solubility in industrial process development, Industrial & engineering chemistry research, 42 (2003) 1827-1831.
[2. 122] F.J. Millero, F. Huang, Solubility of oxygen in aqueous solutions of KCl, K2SO4, and CaCl2 as a function of concentration and temperature, Journal of Chemical & Engineering Data, 48 (2003) 1050-1054.
[2. 123] M.-E. Cuvelier, P. Soto, F. Courtois, B. Broyart, C. Bonazzi, Oxygen solubility measured in aqueous or oily media by a method using a non-invasive sensor, Food control, 73 (2017) 1466-1473.
[2. 124] L. Winkler, The solubility of gases in water (first treatise), Ber. Dtsch. Chem. Ges, 24 (1891) 89-101.
[2. 125] P. Steiner, Ueber die Absorption des Wasserstoffs im Wasser und in wässerigen Lösungen, Annalen der Physik, 288 (1894) 275-299.
[2. 126] L. Braun, Über die Absorption von Stickstoff und von Wasserstoff in wässerigen Lösungen verschieden dissociierter Stoffe, Zeitschrift für Physikalische Chemie, 33 (1900) 721-739.
[2. 127] W. Knopp, Über die Löslichkeitsbeeinflussung von Wasserstoff und Stickoxydul in wässerigen Lösungen verschieden dissoziierter Stoffe, Zeitschrift für Physikalische Chemie, 48 (1904) 97-108.
[2. 128] G. Huefner, Study of the absorption of nitrogen and hydrogen in aqueous solutions, Z Phys Chem Stoechiom Verwandtschaftsl, 57 (1907) 611-625.
[2. 129] A. Findlay, B. Shen, CLVI.—The influence of colloids and fine suspensions on the solubility of gases in water. Part II. Solubility of carbon dioxide and of hydrogen, Journal of the Chemical Society, Transactions, 101 (1912) 1459-1468.
[2. 130] W. Ipatiew, S. Drushina-Artemowitsch, W. Tichomirow, Löslichkeit des Wasserstoffs in Wasser unter Druck, Berichte der deutschen chemischen Gesellschaft (A and B Series), 65 (1932) 568-571.
[2. 131] R. Wiebe, V. Gaddy, The solubility of hydrogen in water at 0, 50, 75 and 100° from 25 to 1000 atmospheres, Journal of the American Chemical Society, 56 (1934) 76-79.
[2. 132] H. Pray, CE Schweickert u. BH Minnich, Ind. Eng. Chem, 44 (1952) 1146.
[2. 133] H. Pray, E.F. Stephan, The solubility of hydrogen in uranyl sulphate solutions at elevated temperatures, in, Battelle Memorial Inst., Columbus, Ohio, 1953.
[2. 134] W.d. Wet, Determination of gas solubilities in water and some organc liquids, JS Afr Chem Inst, 17 (1964) 9-13.
[2. 135] P. Ruetschi, R. Amlie, Solubility of hydrogen in potassium hydroxide and sulfuric acid. Salting-out and hydration, The Journal of Physical Chemistry, 70 (1966) 718-723.
[2. 136] L.D. Longo, M. Delivoria-Papadopoulos, G.G. Power, E.P. Hill, R. Forster 2nd, Diffusion equilibration of inert gases between maternal and fetal placental capillaires, American Journal of Physiology-Legacy Content, 219 (1970) 561-569.
[2. 137] J. Gerecke, H. Bittrich, The solubility of H2, CO2 and NH3 in an aqueous electrolyte solution, Wiss Z Tech Hochsch Chem Carl Shorlemmer Leuna Merseburg, 13 (1971) 115-122.
[2. 138] J. Jung, O. Knacke, D. Neuschut, Solubility of carbon monoxide and hydrogen in water at temperatures up to 300 degrees c, Chemie ingenieur technik, 43 (1971) 112-&.

[2. 139] W. Schröder, Untersuchungen über die Temperaturabhängigkeit der Gaslöslichkeit in Wasser, Chemie Ingenieur Technik, 45 (1973) 603-608.
[2. 140] T.E. Crozier, S. Yamamoto, Solubility of hydrogen in water, sea water, and sodium chloride solutions, Journal of Chemical and Engineering Data, 19 (1974) 242-244.
[2. 141] L.I. Gordon, Y. Cohen, D.R. Standley, The solubility of molecular hydrogen in seawater, Deep Sea Research, 24 (1977) 937-941.
[2. 142] R.W. Cargill, Solubility of helium and hydrogen in some water+ alcohol systems, Journal of the Chemical Society, Faraday Transactions 1: Physical Chemistry in Condensed Phases, 74 (1978) 1444-1456.
[2. 143] P. Gillespie, G. Wilson, GPA Research Report RR-41 Gas Processors Association, Tulsa, OK, (1980).
[2. 144] V.R. Choudhary, M.G. Parande, P.H. Brahme, Simple apparatus for measuring solubility of gases at high pressures, Industrial & Engineering Chemistry Fundamentals, 21 (1982) 472-474.
[2. 145] R. Dohrn, G. Brunner, Phase equilibria in ternary and quaternary systems of hydrogen, water and hydrocarbons at elevated temperatures and pressures, Fluid phase equilibria, 29 (1986) 535-544.
[2. 146] J. Alvarez, R. Crovetto, R. Fernández-Prini, The dissolution of N2 and of H2 in water from room temperature to 640 K, Berichte der Bunsengesellschaft für physikalische Chemie, 92 (1988) 935-940.
[2. 147] G. Kling, G. Maurer, The solubility of hydrogen in water and in 2-aminoethanol at temperatures between 323 K and 423 K and pressures up to 16 MPa, The Journal of Chemical Thermodynamics, 23 (1991) 531-541.
[2. 148] U. Jáuregui-Haza, E. Pardillo-Fontdevila, A. Wilhelm, H. Delmas, Solubility of hydrogen and carbon monoxide in water and some organic solvents, Latin American applied research, 34 (2004) 71-74.
[2. 149] A. Ellis, R. Golding, The solubility of carbon dioxide above 100 degrees C in water and in sodium chloride solutions, American Journal of Science, 261 (1963) 47-60.
[2. 150] S. Takenouchi, G.C. Kennedy, The solubility of carbon dioxide in NaCl solutions at high temperatures and pressures, American journal of science, 263 (1965) 445-454.
[2. 151] S. Drummond, Boiling and mixing of hydrothermal fluids: Effects on mineral deposition, in, Ph. D. thesis, Pennsylvania State University, 1981.
[2. 152] M. Gehrig, H. Lentz, E. Franck, The system water—carbon dioxide—sodium chloride to 773 K and 300 MPa, Berichte der Bunsengesellschaft für physikalische Chemie, 90 (1986) 525-533.
[2. 153] F. Gu, Solubility of carbon dioxide in aqueous sodium chloride solution under high pressure, J. Chem. Eng. Chin. Univ, 12 (1998) 118-123.
[2. 154] J. Rosenqvist, A.D. Kilpatrick, B.W. Yardley, Solubility of carbon dioxide in aqueous fluids and mineral suspensions at 294 K and subcritical pressures, Applied geochemistry, 27 (2012) 1610-1614.
[2. 155] V. Savary, G. Berger, M. Dubois, J.-C. Lacharpagne, A. Pages, S. Thibeau, M. Lescanne, The solubility of CO2+ H2S mixtures in water and 2 M NaCl at 120° C and pressures up to 35 MPa, International Journal of Greenhouse Gas Control, 10 (2012) 123-133.
[2. 156] S.-X. Hou, G.C. Maitland, J.M. Trusler, Phase equilibria of (CO2+ H2O+ NaCl) and (CO2+ H2O+ KCl): Measurements and modeling, The Journal of Supercritical Fluids, 78 (2013) 78-88.

[2. 157] H. Guo, Y. Huang, Y. Chen, Q. Zhou, Quantitative Raman Spectroscopic Measurements of CO2 Solubility in NaCl Solution from (273.15 to 473.15) K at p=(10.0, 20.0, 30.0, and 40.0) MPa, Journal of Chemical & Engineering Data, 61 (2015) 466-474.
[2. 158] S.D. Cramer, The solubility of oxygen in brines from 0 to 300 C, Industrial & Engineering Chemistry Process Design and Development, 19 (1980) 300-305.
[2. 159] P.M. Armenante, H.T. Karlsson, Salting-out parameters for organic acids, Journal of Chemical and Engineering Data, 27 (1982) 155-156.
[2. 160] A.J. Elliot, M.P. Chenier, D.C. Ouellette, Solubilities of hydrogen and oxygen in concentrated lithium salt solutions, Fusion engineering and design, 13 (1990) 29-31.
[2. 161] Y. Iwai, H. Eya, Y. Itoh, Y. Aral, K. Takeuchi, Measurement and correlation of solubilities of oxygen in aqueous solutions containing salts and sucrose, Fluid phase equilibria, 83 (1993) 271-278.
[2. 162] J.W. Gibbs, On the equilibrium of heterogeneous substances, American Journal of Science, (1878) 441-458.
[2. 163] G.N. Lewis, The law of physico-chemical change, in: Proceedings of the American Academy of Arts and Sciences, JSTOR, 1901, pp. 49-69.
[2. 164] M. Michelsen, J. Mollerup, Thermodynamic models: fundamentals & computational aspects. 2004, Holte, Denmark: Tie-Line Publications.
[2. 165] S. Chabab, P. Paricaud, C. Coquelet, Détermination des propriétés thermodynamiques des fluides - Fluides purs, Techniques de l'ingénieur Thermodynamique et énergétique, base documentaire : TIB216DUO (2020).
[2. 166] S. Chabab, P. Paricaud, C. Coquelet, Détermination des propriétés thermodynamiques des fluides - Mélanges, Techniques de l'ingénieur Thermodynamique et énergétique, base documentaire : TIB216DUO (2020).
[2. 167] J.-C. De Hemptinne, J.-M. Ledanois, Select thermodynamic models for process simulation: A practical guide using a three steps methodology, Editions Technip, 2012.
[2. 168] I. Søreide, C.H. Whitson, Peng-Robinson predictions for hydrocarbons, CO2, N2, and H2 S with pure water and NaCI brine, Fluid Phase Equilibria, 77 (1992) 217-240.
[2. 169] D.-Y. Peng, D.B. Robinson, A new two-constant equation of state, Ind. Eng. Chem. Fundam., 15 (1976) 59.
[2. 170] G. Soave, Equilibrium constants from a modified Redlich-Kwong equation of state, Chem. Eng. Sci., 27 (1972) 1197-1203.
[2. 171] D.-Y. Peng, D.B. Robinson, A new two-constant equation of state, Industrial & Engineering Chemistry Fundamentals, 15 (1976) 59-64.
[2. 172] M. Wertheim, Fluids with highly directional attractive forces. I. Statistical thermodynamics, Journal of statistical physics, 35 (1984) 19-34.
[2. 173] L. Blum, Mean spherical model for asymmetric electrolytes: I. Method of solution, Molecular Physics, 30 (1975) 1529-1535.
[2. 174] M. Born, Volumen und hydratationswärme der ionen, Zeitschrift für Physik, 1 (1920) 45-48.
[2. 175] C. Held, T. Reschke, S. Mohammad, A. Luza, G. Sadowski, ePC-SAFT revised, Chemical Engineering Research and Design, 92 (2014) 2884-2897.
[2. 176] B. Maribo-Mogensen, K. Thomsen, G.M. Kontogeorgis, An electrolyte CPA equation of state for mixed solvent electrolytes, AIChE Journal, 61 (2015) 2933-2950.
[2. 177] D.K. Eriksen, G. Lazarou, A. Galindo, G. Jackson, C.S. Adjiman, A.J. Haslam, Development of intermolecular potential models for electrolyte solutions using an electrolyte SAFT-VR Mie equation of state, Molecular Physics, 114 (2016) 2724-2749.

[2. 178] S. Ahmed, N. Ferrando, J.-C. De Hemptinne, J.-P. Simonin, O. Bernard, O. Baudouin, Modeling of mixed-solvent electrolyte systems, Fluid Phase Equilibria, 459 (2018) 138-157.
[2. 179] R. Inchekel, J.-C. de Hemptinne, W. Fürst, The simultaneous representation of dielectric constant, volume and activity coefficients using an electrolyte equation of state, Fluid Phase Equilibria, 271 (2008) 19-27.
[2. 180] B. Maribo-Mogensen, G.M. Kontogeorgis, K. Thomsen, Comparison of the Debye–Hückel and the Mean Spherical Approximation Theories for Electrolyte Solutions, Industrial & Engineering Chemistry Research, 51 (2012) 5353-5363.
[2. 181] X. Courtial, N. Ferrando, J.-C. De Hemptinne, P. Mougin, Electrolyte CPA equation of state for very high temperature and pressure reservoir and basin applications, Geochimica et Cosmochimica Acta, 142 (2014) 1-14.
[2. 182] W. Fürst, H. Renon, Representation of excess properties of electrolyte solutions using a new equation of state, AIChE Journal, 39 (1993) 335-343.
[2. 183] G.M. Kontogeorgis, E.C. Voutsas, I.V. Yakoumis, D.P. Tassios, An equation of state for associating fluids, Industrial & engineering chemistry research, 35 (1996) 4310-4318.
[2. 184] G.M. Kontogeorgis, G.K. Folas, Thermodynamic models for industrial applications: from classical and advanced mixing rules to association theories, John Wiley & Sons, 2009.
[2. 185] G.K. Folas, J. Gabrielsen, M.L. Michelsen, E.H. Stenby, G.M. Kontogeorgis, Application of the Cubic-Plus-Association (CPA) Equation of State to Cross-Associating Systems, Ind. Eng. Chem. Res., 44 (2005) 3823-3833.
[2. 186] F.X. Ball, H. Planche, W. Fürst, H. Renon, Representation of deviation from ideality in concentrated aqueous solutions of electrolytes using a mean spherical approximation molecular model, AIChE journal, 31 (1985) 1233-1240.
[2. 187] J.A. Myers, S.I. Sandler, R.H. Wood, An equation of state for electrolyte solutions covering wide ranges of temperature, pressure, and composition, Industrial & engineering chemistry research, 41 (2002) 3282-3297.
[2. 188] J.-P. Simonin, O. Bernard, L. Blum, Real ionic solutions in the mean spherical approximation. 3. Osmotic and activity coefficients for associating electrolytes in the primitive model, The Journal of Physical Chemistry B, 102 (1998) 4411-4417.
[2. 189] M. Uematsu, E. Frank, Static dielectric constant of water and steam, Journal of Physical and Chemical Reference Data, 9 (1980) 1291-1306.
[2. 190] J.v.d. Waals, J. Platteeuw, Clathrate solutions, Advances in chemical physics, (1958) 1-57.

Chapter 3: Article 1: Thermodynamic study of the CO_2 – H_2O – NaCl system: Measurements of CO_2 solubility and modeling of phase equilibria using Soreide and Whitson, electrolyte CPA and SIT models

French summary / Chapitre 3 – Article 1 : Étude thermodynamique du système CO_2 - H_2O - NaCl : Mesures de la solubilité du CO_2 et modélisation des équilibres entre phases à l'aide des modèles Soreide et Whitson, CPA électrolyte et SIT

L'étude thermodynamique du système CO_2-H_2O-NaCl est d'une grande importance, que ce soit dans un contexte environnemental dans le cadre du Captage et Stockage du dioxyde de Carbone (CSC) ou dans un contexte économique tel que la récupération assistée du pétrole par injection de CO_2, ou le stockage souterrain massif et réversible à usage industriel (méthanation, fermentation, traitement de l'eau, carbonatation de boissons...). Dans ce travail, en utilisant un nouveau dispositif basé sur la méthode "statique-analytique", des mesures de la solubilité du CO_2 dans une solution aqueuse de chlorure de sodium ont été effectuées à des molalités comprises entre 1 et 3 m, à des températures comprises entre 50 et 100 °C et à des pressions allant jusqu'à 230 bars. Pour la partie modélisation, une version pour les électrolytes de l'équation d'état PR-CPA (Peng-Robinson Cubic Plus Association) a été développée sous le nom "e-PR-CPA", ainsi qu'un modèle modifié de Soreide et Whitson (m-SW) a été utilisé et amélioré. Ces deux modèles utilisant l'approche phi-phi sont comparés à deux modèles géochimiques (Corvisier 2013 et Duan el al. 2006) utilisant l'approche gamma-phi, ainsi qu'aux données bibliographiques et mesurées. Les données mesurées sont en bon accord avec les données de la littérature et les prédictions du modèle. Dans les conditions de stockage géologique, les modèles e-PR-CPA et Duan estiment la solubilité légèrement mieux (écart absolu moyen inférieur à 6,6 %) que le modèle m-SW et le modèle géochimique (AAD inférieur à 7,6 %).

Thermodynamic study of the CO_2 – H_2O – NaCl system: Measurements of CO_2 solubility and modeling of phase equilibria using Soreide and Whitson, electrolyte CPA and SIT models

Salaheddine Chabab[a], Pascal Theveneau[a], Jérôme Corvisier[b], Christophe Coquelet[a,*], Patrice Paricaud[c], Céline Houriez[a] and Elise El Ahmar[a]

[a]*Mines ParisTech, PSL, CTP - Centre of Thermodynamics of Processes, 35 rue Saint Honoré, 77305 Fontainebleau Cedex, France*

[b]*Mines ParisTech, PSL University, Centre de Géosciences, 35 rue Saint Honoré, 77305 Fontainebleau Cedex, France*

[c]*L'Unité Chimie & Procédés (UCP), ENSTA ParisTech, 828 Boulevard des Maréchaux, 91762 Palaiseau cedex, France*

International Journal of Greenhouse Gas Control 91 (2019) 102825

Contents lists available at ScienceDirect

International Journal of Greenhouse Gas Control

journal homepage: www.elsevier.com/locate/ijggc

Thermodynamic study of the CO_2 – H_2O – NaCl system: Measurements of CO_2 solubility and modeling of phase equilibria using Soreide and Whitson, electrolyte CPA and SIT models

Salaheddine Chabab[a], Pascal Théveneau[a], Jérôme Corvisier[b], Christophe Coquelet[a,*], Patrice Paricaud[c], Céline Houriez[a], Elise El Ahmar[a]

[a] *Mines ParisTech, PSL, CTP - Centre of Thermodynamics of Processes, 35 rue Saint Honoré, 77305 Fontainebleau Cedex, France*
[b] *Mines ParisTech, PSL University, Centre de Géosciences, 35 rue Saint Honoré, 77305 Fontainebleau Cedex, France*
[c] *L'Unité Chimie & Procédés (UCP), ENSTA Paris, 828 Boulevard des Maréchaux, 91762 Palaiseau cedex, France*

ARTICLE INFO

Keywords:
CO_2/brine solubility
CCS
Electrolyte CPA EoS
Measurement
Modeling

ABSTRACT

The thermodynamic study of the CO_2-H_2O-NaCl system is of great importance whether in an environmental context as part of Carbon Capture and Storage (CCS) or in an economic context such as enhanced oil recovery by CO_2 injection, or massive and reversible underground storage for industrial use (methanation, fermentation, water treatment, carbonation of drinks, etc.). In this work, using a new set-up based on the "static-analytic" method, measurements of CO_2 solubility in aqueous sodium chloride solution were performed at molalities between 1 and 3 m, at temperatures between 50 and 100 °C and pressures up to 230 bar. For the modeling part, an electrolyte version of the PR-CPA (Peng-Robinson Cubic Plus Association) equation of state was developed under the name "e-PR-CPA", as well as modified Soreide and Whitson (m-SW) model was used and improved. These two models using the phi-phi approach are compared with two geochemical models (Corvisier 2013 and Duan el al. 2006) using the gamma-phi approach, and against the literature and measured data. The measured data are in good agreement with the literature data and model predictions. Under geological storage conditions, the e-PR-CPA and Duan models estimate solubility slightly better (Average Absolute Deviation less than 6.6%) than the m-SW model and the geochemical model (AAD less than 7.6%).

Abstract

The thermodynamic study of the CO_2-H_2O-NaCl system is of great importance whether in an environmental context as part of Carbon Capture and Storage (CCS) or in an economic context such as enhanced oil recovery by CO_2 injection, or massive and reversible underground storage for industrial use (methanation, fermentation, water treatment, carbonation of drinks, etc.). In this work, using a new set-up based on the "static-analytic" method, measurements of CO_2 solubility in aqueous sodium chloride solution were performed at molalities between 1 and 3 m, at temperatures between 50 and 100 °C and pressures up to 230 bar. For the modeling part, an electrolyte version of the PR-CPA (Peng-Robinson Cubic Plus Association) equation of state was developed under the name "e-PR-CPA", as well as modified Soreide and Whitson (m-SW) model was used and improved. These two models using the phi-phi approach are compared with two geochemical models (Corvisier 2013 and Duan el al. 2006) using the gamma-phi approach, and against the literature and measured data. The measured data are in good agreement with the literature data and model predictions. Under geological storage conditions, the e-PR-CPA and Duan models estimate solubility slightly better (Average Absolute Deviation less than 6.6%) than the m-SW model and the geochemical model (AAD less than 7.6%).

Keywords: CO_2/brine solubility, CCS, Electrolyte CPA EoS, Measurement, Modeling

3.1 Introduction

Carbon dioxide emissions, which is the main greenhouse gas (in terms of quantity) produced by human activity, are constantly increasing, mainly due to the exploitation and use of fossil fuels. One of the possible solutions, that is of great interest to industrial actors in the gas sector, is to capture, transport and store carbon dioxide in deep geological formations (salt caverns, saline aquifers, oil and gas fields, etc.). The latter solution can be combined with enhanced oil recovery by CO_2 injection. In an economic context, the reversible storage of carbon dioxide (especially in salt caverns) is also a very good solution to meet the high demand for this gas in many applications (methanation, fermentation, water treatment, carbonation of drinks, etc.).

As part of the ANR FLUIDSTORY[1] project, the feeding of an Electrolysis-Methanation-Oxycombustion (EMO) unit requires massive quantities of CO_2. Therefore, the storage of CO_2 in salt caverns is necessary. Compared to above-ground storage facilities (gas tanks), geological storage facilities are less costly [3. 1] and are protected by a cover rock several hundred meters thick that can withstand high storage pressures [3. 2], which increases the amount of gas stored while maintaining higher safety standards. The design and optimization of the storage facility, as well as the monitoring of the temperature, pressure and quantity of gas in the geological reservoir, require very accurate models under the thermodynamic conditions of the storage.

The presence of brine in salt caverns and deep aquifers completely changes the thermodynamic behavior of the stored gas (salting-out effect) due to the existence of electrolytes (NaCl, KCl, $MgCl_2$, etc.) [3. 3] dissolved in the residual water of the cavern or deep aquifer, so studying these systems becomes very complicated. Na+ and Cl- are the main species found in the salts of most geological formations. The sodium chloride solution is therefore considered to be a representative model of brine [3. 4]. Therefore, the thermodynamic study of the CO_2-H_2O-NaCl ternary system is of great industrial interest.

In the literature, the CO_2-H_2O system is widely studied (experimental measurements and modeling) over a wide temperature and pressure range up to the critical points of the mixture (Todheide and Franck [3. 5] and Takenouchi and Kennedy [3. 6]). At high pressure, the phase equilibria of the CO_2-H_2O-NaCl system is less studied. As a result, recently many studies [3. 7, 8, 9, 10, 11, 12]

[1] FluidSTORY project: Massive and reversible underground storage of fluid energy carriers (O_2, CO_2, CH_4).

have been conducted to address the lack of data on this system. In the same way, an experimental apparatus has been developed in this work for the measurement of the solubility of CO_2 in an aqueous solution of sodium chloride, as well as a modeling study for this system was carried out.

This paper is organized as follows: In Section 2 the experimental set-up is described and the measured data are reported. In Section 3, three models are presented, based on two different approaches. The first approach is a symmetric approach (phi-phi) using the same equation of state (EoS) for the two existing phases (liquid-liquid equilibrium and/or vapor-liquid equilibrium); the first equation of state used and improved is the Soreide and Whitson EoS [3. 3]; the second equation of state is an electrolyte version of the PR-CPA EoS which has been developed in this work under the name e-PR-CPA. The second approach tested is an asymmetric approach (gamma-phi) using a geochemical model implemented in the CHESS/HYTEC software (Corvisier, 2013 [3. 13]; Corvisier et al., 2013 [3. 14]). Finally, in Section 4, the results of the three models are presented and compared against literature, measured data, and the well-known DUAN model (Duan et al. [3. 15]).

3.2 Experimental

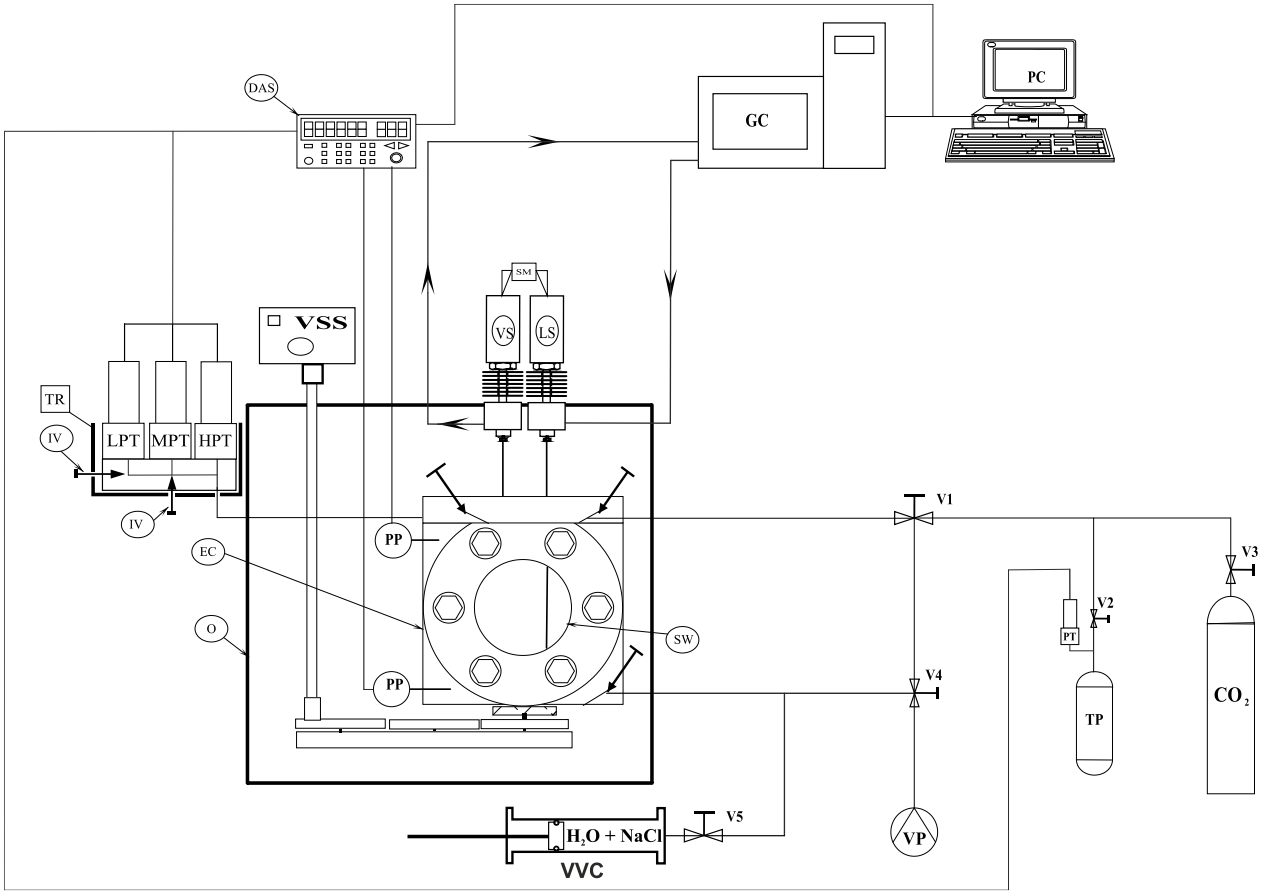

Figure 3.1 : Schematic representation of the apparatus for measuring the solubility of CO2 in NaCl brine. DAS: data acquisition system, EC: equilibrium cell, GC: gas chromatography, HPT: high pressure transducer, LPT: low pressure transducer, LS: liquid ROLSI® Sampler-Injector, MPT: medium pressure transducer, O: oven, PP: platinum resistance thermometer probe, PT: pressure transducer, IV: homemade shut off valve, SM: samplers monitoring, SW: sapphire window, TP: thermal press, TR: temperature regulator, Vi: valve i, VP: vacuum pump, VS: vapor ROLSI® Sampler-Injector, VSS: variable speed stirrer and VVC: Variable Volume Cell.

3.2.1 Materials

In Table 3.1, we list the suppliers of the two chemicals and the purities (given by the suppliers). Carbon dioxide (CO_2, CAS Number: 124-38-9) was purchased from Messer with a certified volume

purity greater than 99.995%. Sodium chloride (NaCl, CAS Number: 7647-14-5) was purchased from Fisher Chemical with a certified purity of 99.6%.Water was deionized and degassed before the preparation of the brine (water + NaCl).

Table 3.1 : Purities and suppliers of the chemicals used in this work

Chemicals	Purity	Analytical Method	Supplier
CO_2	99.995 vol%	Gas Chromatography	MESSER
NaCl	99.6%	None	Fisher Chemical

3.2.2 Apparatus description

Figure 3.1 illustrates the experimental set-up for the measurement of CO_2 solubility in brine. The principle of this apparatus is similar to that described by El Ahmar et al. [3. 16], and is based on the "static-analytic" method. It consists of an Equilibrium Cell (EC) with a volume of 235 cm^3, with two Sapphire Windows (SW), and positioned in an Oven (O) to maintain a constant temperature. The equilibrium cell is equipped with three pressure transducers for Low (LPT), Medium (MPT) and High (HPT) pressure, two Platinum resistance thermometer Probes (PP) and two ROLSI® (Rapid On-Line Sampler-Injector, French patent number 0304073) capillary samplers, one for the vapor phase and the other for the liquid phase. The LPT and MPT pressure transducers are isolated at 30 and 100 bar respectively using the home made shut off Valve (IV). The signals received by the Data Acquisition System (DAS) from pressure transducers and temperature probes are processed by the PC via the LTC10 interface. The feeding of the equilibrium cell by the saline solution (water + NaCl) is done by a Variable Volume Cell (VVC). Depending on the desired pressure, CO_2 is introduced either directly from the cylinder or from the Thermal Press (TP) for higher pressures. The system is agitated by a Variable Speed Stirrer (VSS). Samples are analyzed by a gas chromatograph (Shimadzu GC-2014) equipped with a Thermal Conductivity Detector (TCD) to capture CO_2 and water signals. The transfer line between the ROLSI® and the GC is overheated in order to avoid salt deposition on the ROLSI® mobile part, as well as a pre-column has been added to protect the separation column. The packed column used for the separation of CO_2 and water is Porapak Q, 80/100 mesh, 2m×1/8 in. Silcosteel (Restek, France).

3.2.3 Calibrations

Due to the large volume of the equilibrium cell, the temperature is measured at two locations (top and bottom of the cell) in order to know the precise temperature of the equilibrium cell and to check the thermal gradients. These temperature measurements are carried out by two platinum resistance thermometers (100 Ω), which are calibrated against a 25-Ohm platinum resistance thermometer (model 5628, Fluke (Hart Scientific)) combined with an Agilent 34420A precision Ohmmeter, and calibrated by LNE (Laboratoire National de Métrologie et d'Essais). The calibration accuracies of the temperature probes at the top and bottom of the equilibrium cell are not higher than ±0.008 K and ±0.007 K respectively, and are composed of two contributions: the uncertainty related to the standard probe and the uncertainty related to the polynomial equation established between the values transmitted by the probes and the values of the standard probe. The LPT, MPT and HPT pressure transducers were calibrated against pressure automated calibration equipment (PACE 5000, GE Sensing and Inspection Technologies). Above 100 bar, the HPT pressure transducer was calibrated against a dead weight pressure balance (Desgranges & Huot 5202S, CP 0.3–40MPa, Aubervilliers, France). The calibration accuracies of the LPT, MPT and HPT transducers are calculated in the same way as those of the temperature probes and are equal to ±0.2 kPa, ±0.2 kPa and ±0.3 kPa, respectively. The saline solution (water + NaCl) was prepared gravimetrically using a mass comparator (CC1200, Mettler-Toledo) with an uncertainty of 1 mg. Calibration of the thermal conductivity detector (TCD) was done by introducing and analyzing known quantities of compounds (water and CO_2) using suitable syringes. The calibration accuracy of the TCD is less than ±1.3% on the mole number of CO_2 and less than ±1.6% on the mole number of water, and it consists of the uncertainty associated with injection by syringe and the accuracy related to the polynomial equation established between the specific area of the peak obtained (S_1) and the number of moles (n_1). The uncertainty related to the repeatability of measurements is the most important, especially for solubility (xCO_2). The total uncertainties on temperature, pressure and composition, including all sources of error (calibration and repeatability) are reported in Table 3.2.

3.2.4 Experimental procedure and results

For each measured point, the following procedure was followed: setting the target temperature, evacuating the loading lines and the equilibrium cell and introducing the saline solution through the variable volume cell until approximately one third of the cell was filled. Then, the CO_2 is

introduced from the top of the cell until the desired pressure is reached. Stirring is started and thermodynamic equilibrium is reached in a few minutes. Once, the pressure and temperature are stabilized, several samples are taken from the liquid phase by the ROLSI® capillary sampler and sent via the transfer line to the GC for analysis. The data are processed by deducting the mole number n_i of each component *i* (water or CO_2) from the surface of the corresponding peak. Then, the salt-free molar fraction $x_{CO_2}^{sf}$ of CO_2 is determined as follows:

$$x_{CO_2}^{sf} = \frac{n_{CO_2}}{n_{CO_2} + n_{H_2O}} \quad \textbf{(3.1)}$$

The true mole number can be obtained from the following expressions:

$$x_{CO_2} = \frac{n_{CO_2}}{n_{CO_2} + n_{H_2O} + m_s \cdot n_{H_2O} \cdot M_{H_2O}} \quad \textbf{(3.2)}$$

Because $n_{salt} = m_s \cdot n_{H_2O} \cdot M_{H_2O}$

where m_s is the NaCl molality and M_{H_2O} is the molar mass of water.

Consequently

$$x_{CO_2} = \frac{x_{CO_2}^{sf}}{x_{CO_2}^{sf} + \left(1 - x_{CO_2}^{sf}\right)\left(1 + m_s \cdot M_{H_2O}\right)} \quad \textbf{(3.3)}$$

The very small quantities withdrawn during sampling do not modify the thermodynamic equilibrium. Since some water is evaporated, there is no significant increase of the salt molality of the solution, therefore the molality of the solution has been considered constant. Another equilibrium point is measured by adding more CO_2 and so on until the desired maximum pressure is reached. Before starting a new isotherm or introducing a solution with a different molality than the one before, the equilibrium cell is cleaned and evacuated.

The experimental measurements were performed at molalities between 1 and 3 m, temperatures between 50 and 100°C and pressures up to 230 bar, and are listed in Table 3.2. The number of points measured for each isotherm is different because of some difficulties encountered such as the clogging of the ROLSI® capillary sampler by salt deposit or leaks in the circuit, which requires the shutdown and maintenance of the apparatus.

Table 3.2 : Experimental and calculated solubilities of carbon dioxide in the CO_2 + H_2O + NaCl system, expressed as "salt-free" mole fractions.

	Experimental data				calculation							
					m-SW model		e-PR-CPA model		Geoch. model		DUAN model	
m_{NaCl} (mol/kg_w)	T (K)	P (bar)	$x_{CO_2}^{sf}$	$u(x_{CO_2}^{sf})$ [a]	$x_{CO_2}^{sf}$	AD % [b]	$x_{CO_2}^{sf}$	AD % [b]	$x_{CO_2}^{sf}$	AD % [b]	$x_{CO_2}^{sf}$	AD % [b]
1.13	372.33	31.148	0.00390	2.0E-04	0.00414	6.08	0.00418	7.14	0.00435	11.67	0.00445	14.19
	372.31	60.500	0.00750	2.0E-04	0.00755	0.73	0.00755	0.70	0.00776	3.46	0.00784	4.48
	372.29	108.840	0.01130	2.5E-04	0.01190	5.34	0.01174	3.91	0.01190	5.31	0.01183	4.70
	372.29	151.920	0.01360	3.5E-04	0.01461	7.45	0.01428	5.00	0.01442	6.06	0.01411	3.75
	372.25	191.980	0.01570	6.0E-04	0.01644	4.73	0.01595	1.61	0.01614	2.79	0.01550	1.29
1.13	323.02	53.450	0.01030	3.0E-04	0.01088	5.59	0.01122	8.95	0.01130	9.72	0.01145	11.18
	322.97	75.550	0.01290	3.0E-04	0.01384	7.32	0.01414	9.61	0.01402	8.67	0.01418	9.95
	323.03	100.350	0.01510	7.5E-04	0.01591	5.36	0.01611	6.70	0.01586	5.04	0.01618	7.16
	323.04	145.080	0.01700	4.5E-04	0.01756	3.28	0.01761	3.60	0.01740	2.33	0.01709	0.54
1.00	373.38	16.983	0.00237	1.0E-04	0.00230	3.07	0.00233	1.72	0.00247	4.05	0.00254	6.96
	373.37	32.527	0.00426	2.0E-04	0.00436	2.56	0.00440	3.30	0.00461	8.25	0.00470	10.49
	373.41	68.182	0.00833	2.0E-04	0.00847	1.70	0.00843	1.26	0.00869	4.30	0.00874	4.97
3.01	342.82	30.391	0.00441	1.0E-04	0.00405	8.18	0.00421	4.62	0.00398	9.83	0.00419	4.99
	342.81	72.559	0.00880	2.0E-04	0.00829	5.83	0.00840	4.53	0.00793	9.91	0.00811	7.88
	342.82	100.910	0.01057	3.0E-04	0.01021	3.44	0.01023	3.24	0.00968	8.38	0.00978	7.43
3.01	372.39	25.556	0.00292	8.0E-05	0.00264	9.44	0.00276	5.46	0.00261	10.58	0.00277	5.10

372.42	71.417	0.00707	1.5E-04	0.00661	6.46	0.00676	4.41	0.00643	9.06	0.00654	7.49
372.41	100.517	0.00878	3.0E-04	0.00854	2.71	0.00864	1.58	0.00825	5.99	0.00826	5.93
372.43	152.433	0.01141	2.5E-04	0.01102	3.42	0.01100	3.55	0.01063	6.86	0.01034	9.35
372.45	199.597	0.01258	3.0E-04	0.01254	0.32	0.01242	1.23	0.01214	3.51	0.01152	8.42
372.45	229.817	0.01337	3.0E-04	0.01330	0.52	0.01312	1.81	0.01292	3.34	0.01215	9.09
AAD %					**4.45**		**4.00**		**6.62**		**6.92**

[a] u: standard uncertainties, $u(T) = 0.02\ K$ and $u(P) = 5\ kPa$. [b] AD %: absolute deviation, AD % $= 100 \cdot \left| \frac{x_{CO_2}^{cal} - x_{CO_2}^{exp}}{x_{CO_2}^{exp}} \right|$, AAD %: average absolute deviation, AAD % $= \frac{100}{N_{exp}} \sum_{i=1}^{N_{exp}} \left(\left| \frac{x_{CO_2 i}^{cal} - x_{CO_2 i}^{exp}}{x_{CO_2 i}^{exp}} \right| \right)$.

3.3 Thermodynamic modeling

3.3.1 Soreide and Whitson EoS

The first thermodynamic model used in this work is the cubic Equation of State (EoS) proposed by Soreide and Whitson [3. 3], which is a revised form of the well-known Peng-Robinson EoS (PR-EoS) [3. 17]. The Soreide-Whitson model is widely used in the oil and gas field especially for systems in the presence of water or brine, and is implemented in several modeling software like reservoir simulators such as Eclipse 300 (by Schlumberger), IHRRS (by Total) and IPM (by Petex), and thermophysical properties calculators like Simulis Thermodynamics (by Prosim), etc.

To describe the phase equilibria of gas-water and gas-brine systems, Soreide and Whitson (SW) proposed two modifications to the PR-EoS. The expression of the equation of state (PR EoS) remains the same, while the alpha function and the mixing rules were modified (see Chapter 2). This last modification concerns the use of two different binary interaction coefficients (k_{ij}), one for the aqueous phase k_{ij}^{AQ} and the other for the non-aqueous (gas-rich) phase k_{ij}^{NA}. These two parameters are respectively adjusted on gas solubility data and water content data of gas-water-NaCl systems. The k_{ij}^{NA} is generally constant or slightly dependant on temperature, however, the k_{ij}^{AQ} depends on temperature and molality.

It should be noted that the use of two different k_{ij} makes the model inconsistent (which makes it equivalent to a gamma-phi approach), this limitation is effective especially near to the critical points region of the system (which is above 265 °C according to Todheide and Franck [3. 5]), and does not really represent a problem for reservoir simulation since the maximum temperature in geological formations is about 150 °C. The problem of inconsistency that may occur is on the implementation of the model in the simulators knowing that in the original model, salinity is considered static, therefore it is not taken into account in the derivative of the attractive term a, whereas it must be considered dynamic.

$$\left.\frac{\partial a}{\partial n_{w,w}}\right|^{dynamic} = \left.\frac{\partial a}{\partial n_{w,w}}\right|^{static} - \left.\frac{\partial a}{\partial m_s}\right|_{n_{j,w}} \left.\frac{\partial m_s}{\partial n_{w,w}}\right|_{n_{j\neq i,w}} \quad \textbf{(3.4)}$$

Petitfrere et al. [3. 18] considered a dynamic salinity (Equation 3.4), for more details see the original paper [3. 18]) and proposed some modifications to the implementation of the SW model to make it consistent and compared it to the original implementation by the simulation of CO_2 injection process in a saline aquifer with their simulation software (IHRRS). They showed that

the simulation results are not sensitive to this inconsistency problem; the most important thing is the correct prediction of mutual solubilities. But it is preferable to implement this model according to the approach they proposed in order to be able to do the stability analysis (to know if there is a phase split in each cell and also to initialize the flash calculations).

Yan et al. [3. 7] showed that the Soreide and Whitson model underestimates the solubility of carbon dioxide at high molalities, and they proposed a better correlation for $k^{AQ}_{CO_2,w}$ by refitting it to solubility data of CO_2 in water and NaCl brine. Soreide and Whitson [3. 3] and Yan et al. [3. 7] included only the experimental data of water content of the CO_2-H_2O system to adjust the binary interaction parameters, and they did not include the experimental data of water content for the CO_2-H_2O-NaCl system since they did not exist until 2013. The phase equilibria (liquid and vapor phase) for this system were recently measured by Hou et al. [3. 8]. In this work these data were added to our database and used to adjust the binary interaction parameters $k^{NA}_{CO_2,w}$ and $k^{AQ}_{CO_2,w}$. The new expressions for these parameters are given by

$$\left(k^{NA}_{CO_2,w}\right)_{New} = 0.68208385571 \times 10^{-3}T - 2.066623464504 \times 10^{-2} \quad \textbf{(3.5)}$$

$$\left(k^{AQ}_{CO_2,w}\right)_{New} = \left(\frac{T}{T_{c,CO_2}}\right)\left[a + b\left(\frac{T}{T_{c,CO_2}}\right) + c\left(\frac{T}{T_{c,CO_2}}\right)m_s\right] + m_s^2\left[d + e\left(\frac{T}{T_{c,CO_2}}\right)\right] + f \quad \textbf{(3.6)}$$

where T is the temperature in K, and $T_{c,CO_2} = 304.13$ K is the CO_2 critical temperature. Coefficients a, b, c, d, e and f are listed in Table 3.3. For $k^{NA}_{CO_2,w}$, temperature dependence has been added since it has been observed that $k^{NA}_{CO_2,w}$ varies slightly with a linear trend with respect to temperature and this modification improves the representation of the water content (decrease of AAD(y_w) by 1.5%). In this work, the Soreide and Whitson model with the new parameters is called m-SW.

Table 3.3 : Coefficients of the $\left(k^{AQ}_{CO_2,w}\right)_{New}$ correlation (Equation 3.6)

a	0.43575155
b	$-5.766906744 \cdot 10^{-2}$
c	$8.26464849 \cdot 10^{-3}$
d	$1.29539193 \cdot 10^{-3}$
e	$-1.6698848 \cdot 10^{-3}$
f	-0.47866096

3.3.2 e-PR-CPA EoS

The second thermodynamic model developed in this work is the e-PR-CPA (electrolyte Peng-Robinson Cubic Plus Association EoS). The idea of CPA (Cubic Plus Association) EoS [3. 19] is to present the contribution of intermolecular interactions between molecules with a cubic equation of state (Peng-Robinson (PR) or Soave-Redlich-Kwong (SRK) [3. 20]) and to add the Wertheim associative term [3. 21] in order to take into account the association phenomenon (hydrogen bonding in solutions). For the cubic term, the PR (1978) EoS [3. 22] was chosen in the continuity of previous work (Hajiw el al. 2015 [3. 23] and Wang et al. 2018 [3. 24, 25]) and because it better represents liquid density [3. 17] by comparing it with the SRK EoS.

The representation of electrostatic forces (long range interactions) can be done by one of the two theories: the complete Debye-Huckel theory (DH) used by the Sadowski [3. 26], Kontogeorgis [3. 27] groups, etc. and which treats ions as point charges; the Mean Spherical Approximation (MSA) theory which is used by various research groups (Jackson [3. 28], De Hemptinne [3. 29], Fürst [3. 30], etc.) and which considers ions as charged hard spheres. A very good comparison of the two theories was made by Maribo-Mogensen et al. [3. 31] shows that numerically the two theories behave in a very similar way. They also showed that only MSA correctly predicts the increase in screening length by increasing the ion diameter, since in DH the screening length is independent of the diameter. In this work we have chosen the MSA theory.

The electrolyte contribution in the e-PR-CPA model is represented by two terms: the first term comes from the MSA theory [3. 32] for the representation of ion-ion long range interactions and the second term is the Born term [3. 33] for the representation of short range interactions between solvent and ions (solvation).

The expression for the residual Helmholtz free energy of the e-PR-CPA model is as follows:

$$\frac{A^{res}_{e-PR-CPA}}{RT} = \frac{A^{PR}}{RT} + \frac{A^{Association}}{RT} + \frac{A^{MSA}}{RT} + \frac{A^{Born}}{RT} \qquad \textbf{(3.7)}$$

The non-electrolyte part of this model consists of two terms. Repulsive and attractive interactions are taken into account with the term $\frac{A^{PR}}{RT}$ of the PR EoS. The association phenomenon (self-association and cross-association) are represented by the term $\frac{A^{Association}}{RT}$ from Wertheim's theory. The different terms of equation 3.7 are detailed in Chapter 2.

The diameters σ_i of ions i used in the Born term and in the MSA term (see Chapter 2) are the same as the ones used to calculate the co-volume of the ions b_{ion}. In this work, we neglect the formation of ion pairs, that occur at very high temperatures (above 300°C) [3. 34]. The temperature in geological reservoirs, salt caverns and saline aquifers are generally not higher than 200°C [3. 35], so we can assume that NaCl is fully dissociated in the solution.

3. Parameterization of the e-PR-CPA model

The parameterization of the e-PR-CPA model consists of determining the five parameters (m_i, $a_{0,i}$, b_i, ε_i, β_i) of pure water and three parameters (m_{ion}, $a_{0,ion}$, σ_{ion}) for each ion. The adjustment of the parameters was carried out by a hybrid optimization program (simulated annealing combined with BFGS [3. 36]) by minimizing the following objective function:

$$F_{obj} = \frac{100}{N}\sum_{i=1}^{N}\left(\left|\frac{val_i^{cal} - val_i^{exp}}{val_i^{exp}}\right|\right) \quad \textbf{(3.8)}$$

where N represents the number of data, val corresponds to the thermodynamic property calculated by the model (cal) or measured experimentally (exp).

- Pure water

According to the terminology of Huang and Radosz [3. 37], the 4C association scheme with two electron donor sites and two electron acceptor sites has been applied in this work to describe water molecule. The parameters (m_i, $a_{0,i}$, b_i, ε_i, β_i) for pure water are obtained by adjusting to vapor pressure and saturated liquid density data correlated by NIST [3. 38]. The water parameters obtained in this work and those obtained previously by Hajiw et al. [3. 23] and Wang et al. [3. 24, 25] are reported in Table 3.4. As shown in Figure 3.2, the e-PR-CPA model can accurately describe the pure water VLE data, apart in the near critical region.

Table 3.4 : Pure water parameters (e-PR-CPA model), comparison with parameters from Hajiw et al. [3. 23] and parameters from Wang et al. [3. 24].

Water (4C)								
	m	a0 (Pa.m^6/mol^2)	b (m^3/mol)	ε (Pa.m^3/mol)	β	Range of Tr	AAD % [a]	
							P_{sat}	ρ_{liq}
Hajiw et al. 2015	0.6387	0.2174	1.52E-05	14639	6.83E-02	0.43-0.99	**1.04**	**2.46**
Wang et al. 2018	0.6740	0.1230	1.44E-05	17048	6.98E-02	0.43-0.99	**1.11**	**1.74**
This work	0.6755	0.1323	1.45E-05	16823	6.91E-02	0.43-0.99	**1.12**	**1.51**

[a] $AAD\% = \frac{100}{N}\sum_{i=1}^{N}\left(\left|\frac{val_i^{cal}-val_i^{exp}}{val_i^{exp}}\right|\right)$, val : P_{sat} or ρ_{liq}

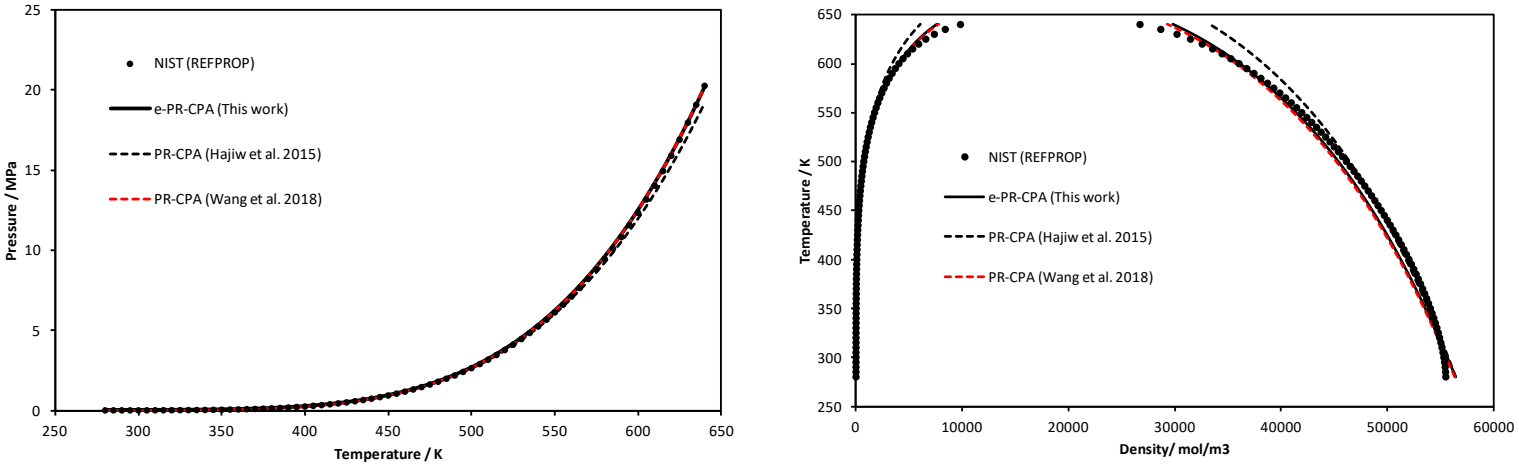

Figure 3.2 : Comparison of the e-PR-CPA model (with the three parameter sets in Table 3.4) with the NIST model. a) Water vapor pressure, b) Water density at saturation.

Over the entire temperature range, the parameters obtained in this work and those obtained by Wang et al. give the best results in terms of vapor pressure and density. It appears that the parameters of Hajiw et al. have been adjusted to the temperature range of the application of interest; however they better estimate the vapor pressure and density at temperatures below 500K. The third set of parameters (obtained in this work, Table 3.4) was chosen for the rest of the work.

- H_2O + NaCl system

There are three parameters (m_{ion}, $a_{0,ion}$, σ_{ion}) specific to each ion (Na^+ and Cl^-). To represent both the equilibrium properties and the excess properties, we have decided to adjust these parameters on saturation vapor pressure data and on osmotic coefficient data of the water + NaCl system. No binary interaction parameters were used for this system ($k_{Na^+-Cl^-} = k_{water-Na^+} = k_{water-Cl^-} = 0$). The optimized ion parameters and the results obtained by the e-PR-CPA model are shown in Table 3.5 and Figure 3.3-3.5 respectively.

Table 3.5 : The parameters of the Na^+ and Cl^- ions (e-PR-CPA model).

	m	a_0 (Pa.m^2/mol^2)	σ (Å)
Na^+	-1.5684	1.15236	1.0945
Cl^-	0.2489	0.93705	3.6391

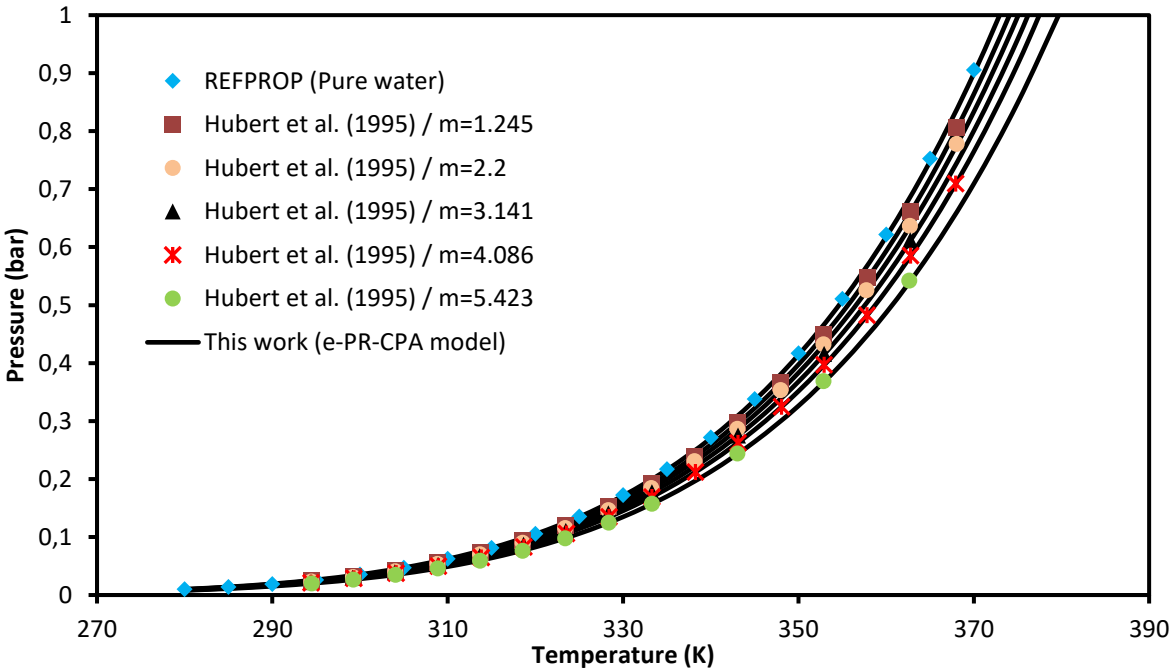

Figure 3.3 : Saturation vapor pressure of water + NaCl at low temperature and at different NaCl molalities. Comparison of the e-PR-CPA model with the experimental data of Hubert et al. [3. 39].

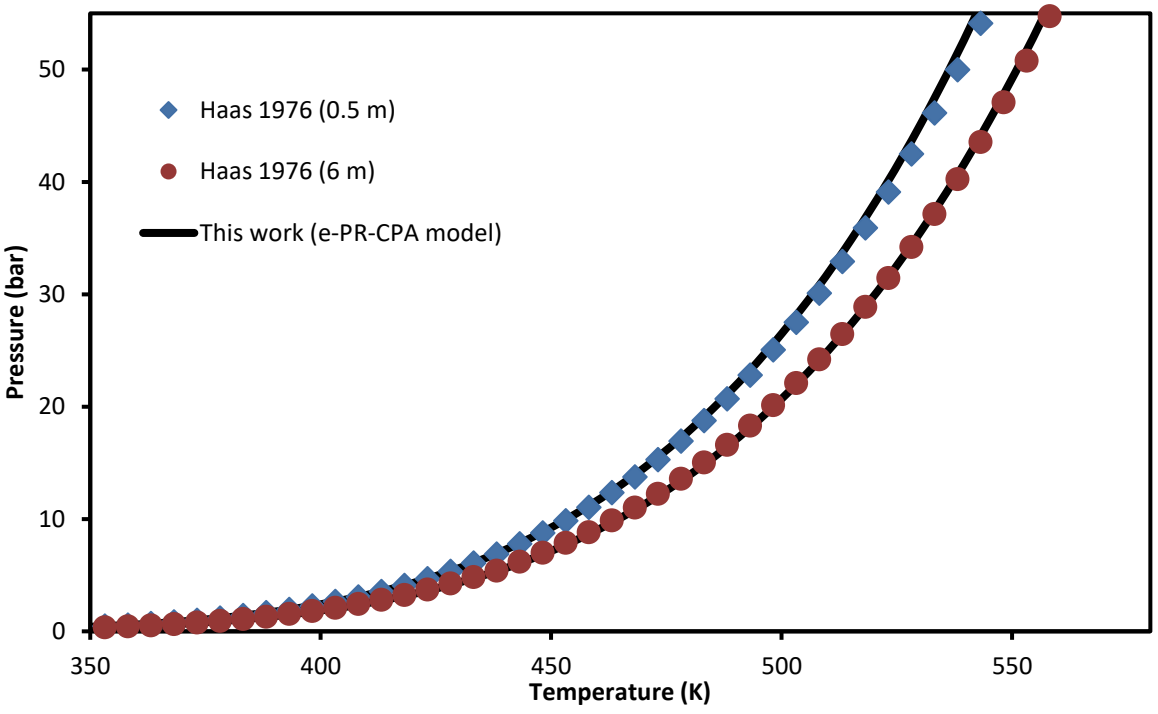

Figure 3.4: Saturation vapor pressure of water + NaCl at high temperature and at 0.5 and 6 moles/kgw of NaCl. Comparison of the e-PR-CPA model with the data correlated by Hass [3. 40].

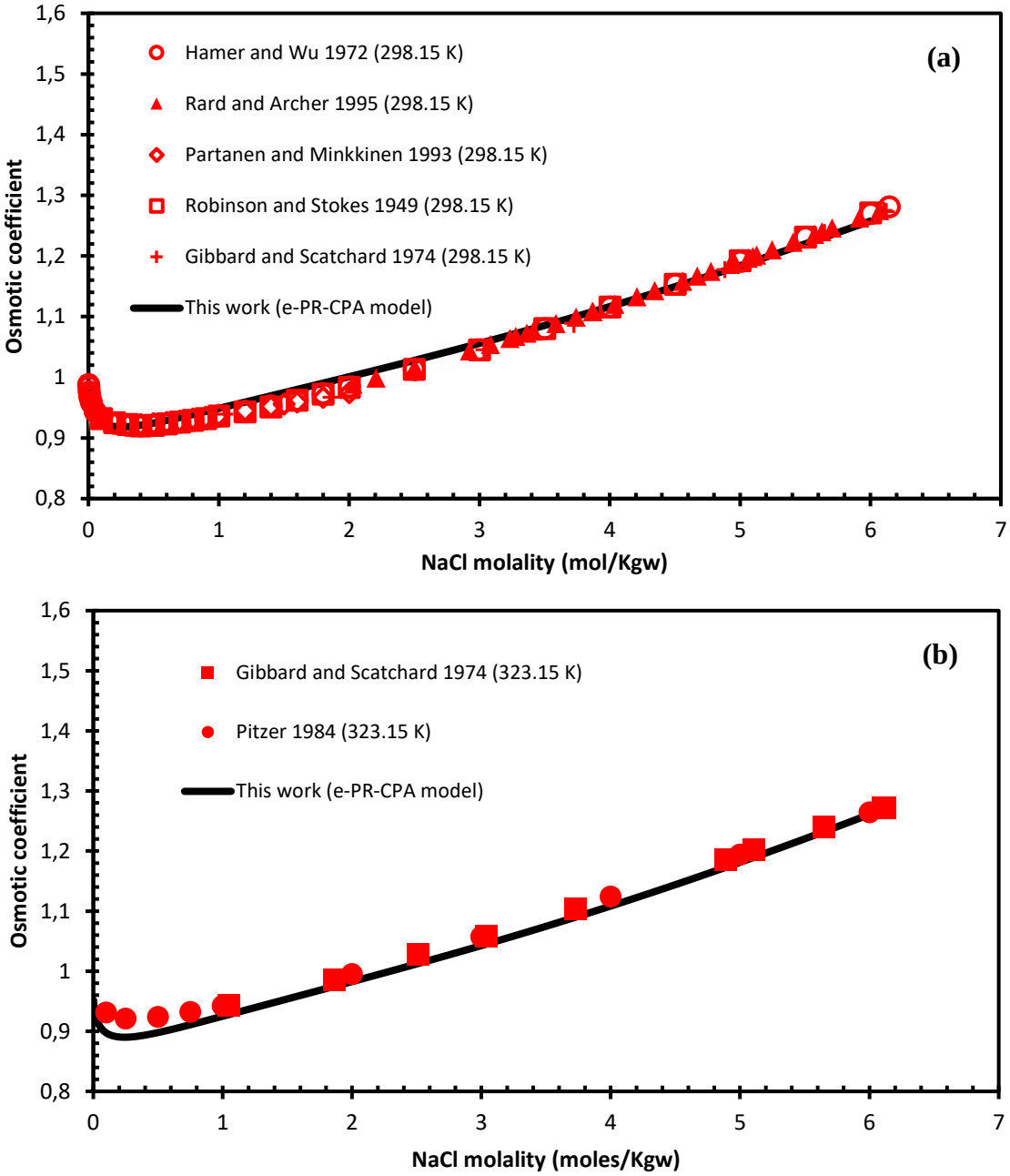

Figure 3.5: Osmotic coefficient of water + NaCl versus NaCl molality at 298.15 K (a) and 323.15 K (b). Comparison of the results of the e-PR-CPA model with the experimental data from [3. 41, 42, 43, 44, 45, 46].

The AAD of the vapor pressures and osmotic coefficients of the H_2O-NaCl system calculated for temperatures up to 300°C and molalities up to 6m NaCl are shown in Table 3.6 and are reproduced within an AAD of 1.87% and 2.02% respectively.

Table 3.6 : AAD (%) of the vapor pressure and osmotic coefficient calculated with the e-PR-CPA model.

	Number of data	Range of T (K)	Maximal Molality	AAD (%)	References
Vapor pressure	448	294 - 573	6	1.87	[3. 39, 40]
Osmotic coefficient	196	298 - 573	6.24	2.02	[3. 41, 42, 43, 44, 45, 46]

3.3.3 Geochemical model

The third model tested in this work is a geochemical model implemented in CHESS/HYTEC software (Corvisier, 2013 [3. 13]; Corvisier et al., 2013 [3. 14]). It implies a dissymmetrical approach $\gamma - \varphi$:

$$m_i^{aq}\gamma_i^{aq}\mathrm{K}_i^g(T,P^{sat})\exp\left(v_i^{\infty}\frac{P-P^{sat}}{RT}\right) = \mathrm{y}_i^g\varphi_i^g P \qquad \textbf{(3.9)}$$

where m_i^{aq} is the molality (mol/kg of water) of the dissolved gaseous component i, γ_i^{aq} its activity coefficient, K_i^g the Henry's law constant at water saturation pressure, v_i^{∞} the molar volume of the dissolved gaseous component at infinite dilution, y_i^g the component mole fraction in the gas phase and φ_i^g its fugacity coefficient.

Let us recall that this model uses an important database and could solve a large set of mass balances and mass action laws to calculate the whole system speciation (i.e. pH, concentrations of species such as HCO_3^-, CO_3^{2-}, $NaCO_3^-$..., potential minerals dissolution/precipitation). It is also important that equations remain generic, in order that the model remains multi-component either for the gas phase and the electrolyte.

For the gas phase, the PR-SW EoS is then used with the classical mixing rule.

Aqueous activity coefficients can be calculated using various models, but as far as saline solutions with high ionic strength are concerned, specific models should be used, as for example the well-known Pitzer model (Pitzer 1973 [3. 47], Pitzer 1991 [3. 48]). The Specific Ion Theory model (SIT) already implemented in CHESS/HYTEC software is simpler and allows obtaining satisfactory results on such systems. SIT theory first mentioned by Bronsted (Bronsted 1922) [3. 49] and later by Scatchard (Scatchard 1936 [3. 50]) and Guggenheim (Guggenheim &

Turgeon 1955 [3. 51]) takes short-distance forces into account by adding terms to the Debye-Hückel law (Debye & Hückel 1923 [3. 52]). The theoretical details of this approach are explained in Grenthe's work (Grenthe & Puigdomenech 1997 [3. 53]). The fundamental equation of the SIT model is given by:

$$ln(\gamma_i^{aq}) = \frac{-Az_i^2\sqrt{I}}{1+1.5\sqrt{I}} + \sum_j m_j^{aq}\,\varepsilon_{ij} \qquad \textbf{(3.10)}$$

where A the first Debye-Hückel parameter (function of the temperature), I the ionic strength of the solution, z_i the charge of the aqueous species i, and ε_{ij} binary interaction parameters between aqueous species i and j.

Best Henry's law constant, molar volume for its pressure correction and gas binary interaction parameters for CO_2 have been selected from the literature or fitted in a previous work (Hajiw et al. 2018 [3. 54]). Aqueous binary interaction parameters for the SIT model have been fitted on experimental data.

- $\varepsilon_{H^+Cl^-}$ and $\varepsilon_{Na^+Cl^-}$ are equal to -0.062 and -0.021 respectively, using HCl and NaCl solutions activity measurements (Schneider et al. 2004 [3. 55], Sakaida & Kakiuchi 2011 [3. 56], Khoshkbarchi & J.H. Vera 1996 [3. 57])
- $\varepsilon_{CO_2Na^+}$ varying with temperature (from 0.261 at 25°C to -0.624 at 200°C), using numerous CO_2 solubility measurements in NaCl solutions.

3.4 Results and discussions

3.4.1 H_2O + CO_2 binary system

The molecular representations of carbon dioxide and water with the association sites assigned to each of these molecules are shown in Figure 3.6. For the H_2O-CO_2 binary system, solvation was considered by assuming that CO_2 has only one electron acceptor (ea) site (type 0ed-1ea) and that H_2O has 4 association sites (type 4C) with two electron donor (ed) sites and two electron acceptor sites. However, the modified combining rules m-CR1 (Equation 2.44, Chapter 2) are used.

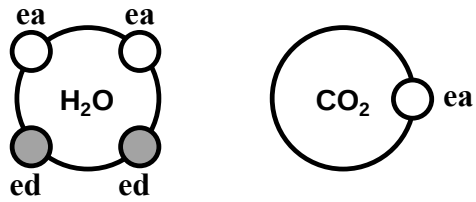

Figure 3.6 : Molecular representations of water and carbon dioxide in terms of electron donor/acceptor sites. ed: electron donor site, ea: electron acceptor site

In order to investigate the influence of the temperature, the binary interaction parameter $k_{H_2O-CO_2}$ and the cross association volume $\beta_{H_2O-CO_2}$ of the H_2O-CO_2 binary system were optimized on solubility data (Wiebe and Gaddy 1939 [3. 58], Yan et al. 2011 [3. 7] and Hou et al. 2013 [3. 59]) simultaneously for each temperature (in the range of 323 - 423 K). Figure 3.7 shows the trend of these two parameters with respect to temperature. To reproduce this trend, a 1st degree (Equation 3.11) and 2nd degree (Equation 3.12) polynomial equations have been proposed for $k_{H_2O-CO_2}$ and $\beta_{H_2O-CO_2}$ respectively.

$$k_{H_2O-CO_2} = 1.522403212 \times 10^{-3}T - 0.339526533 \quad \textbf{(3.11)}$$

$$\beta_{H_2O-CO_2} = 6.982115486 \times 10^{-6}T^2 - 4.334449524 \times 10^{-3}T + 0.849767346 \quad \textbf{(3.12)}$$

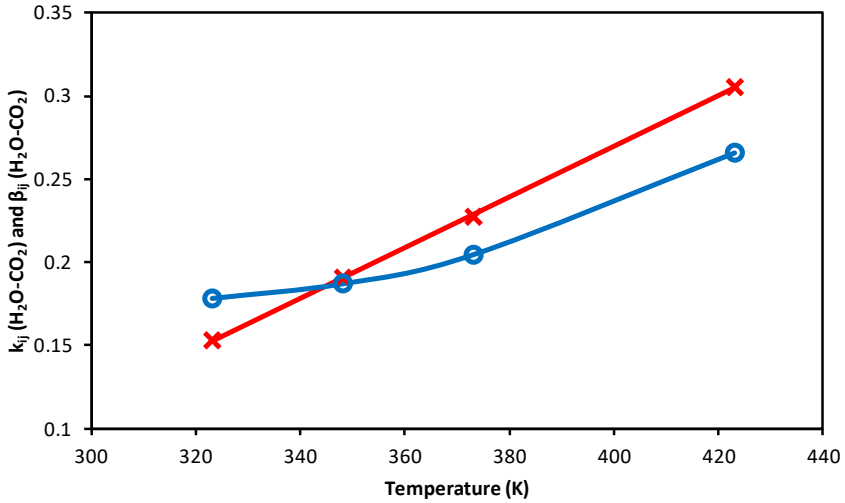

Figure 3.7 : Influence of temperature on $k_{H_2O-CO_2}$ (×) and on $\beta_{H_2O-CO_2}$ (o) for the H_2O-CO_2 system. Symbols represent optimized parameter values; solid lines represent correlations (Equations 3.11-3.12).

The CO_2 solubility in water and water content of the H_2O-CO_2 system are shown in Figure 3.8. The symbols represent the experimental data and the lines (solid, dotted and dashed) represent the calculations done by the e-PR-CPA, Geochemical and m-SW models, respectively. The predictions (calculations outside the adjustment range) of CO_2 solubility and water content at 298.15 K with the e-PR-CPA model are shown in Figure 3.8-c and 3.8-d and are compared with the calculations obtained by the m-SW and the geochemical models. The three models can accurately describe the CO_2 solubility in water and the water content. The CO_2 solubility in water is better represented with the e-PR-CPA model. However, the geochemical model and the m-SW model give slightly better results for the calculation of the water content since for the later two different binary interaction coefficients are used for each phase.

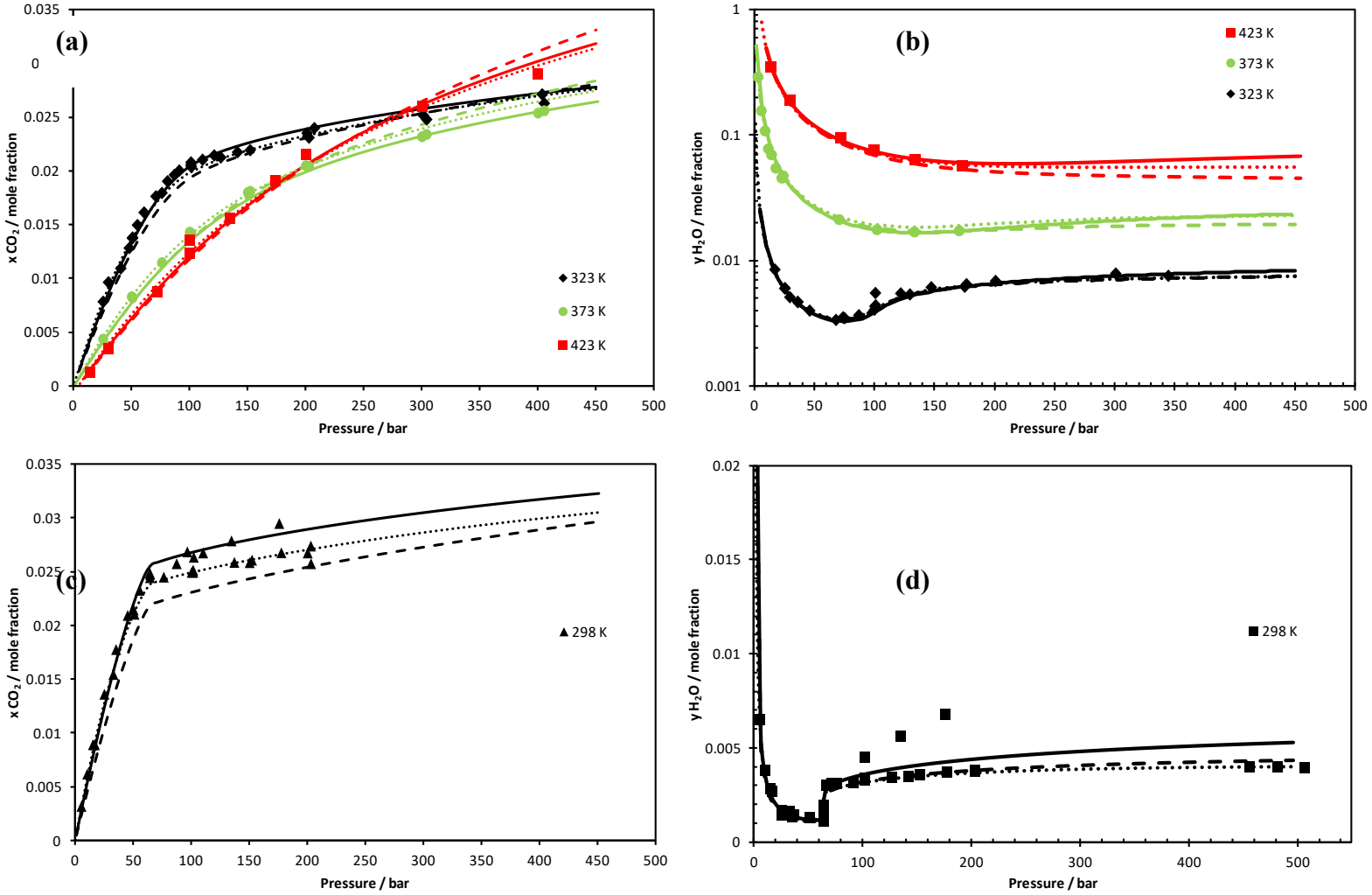

Figure 3.8 : CO_2-H_2O binary system: Calculation of CO_2 solubility in water (a and c) and water content (b and d) at 298, 323, 373 and 423 K by e-PR-CPA (solid line), m-SW (dashed line) and geochemical (dotted line) models. The symbols are literature data: (a): [3. 6, 7, 58, 59, 60, 61, 62], (b): [3. 59, 61, 63, 64, 65, 66], (c): [3. 59, 67, 68, 69, 70, 71], and (d): [3. 59, 67, 68, 69, 70, 72].

3.4.2 Prediction of the phase equilibria of the CO_2-H_2O system at very high pressure and temperature.

The ability to extrapolate the e-PR-CPA model outside the adjustment range was investigated by predicting the liquid-vapor equilibria of the CO_2-H_2O system at very high pressures (up to 3000 bar) and temperatures (up to 573 K). This binary system is classified as type III according to Scott and van Konynenburg [3. 73] classification. The Predictions of the e-PR-CPA model compared with experimental data from the literature are shown in Figure 3.9. There is a mixture critical point at 548 K and 573 K. In all pressure/temperature ranges, the solubilities of carbon dioxide in water and water content are well estimated. Note that the experimental data for the vapor phase at 473 K are not consistent, and the model predictions are between two independent sets of experimental data (Todheide and Franck [3. 5] and Takenouchi and Kennedy [3. 6]).

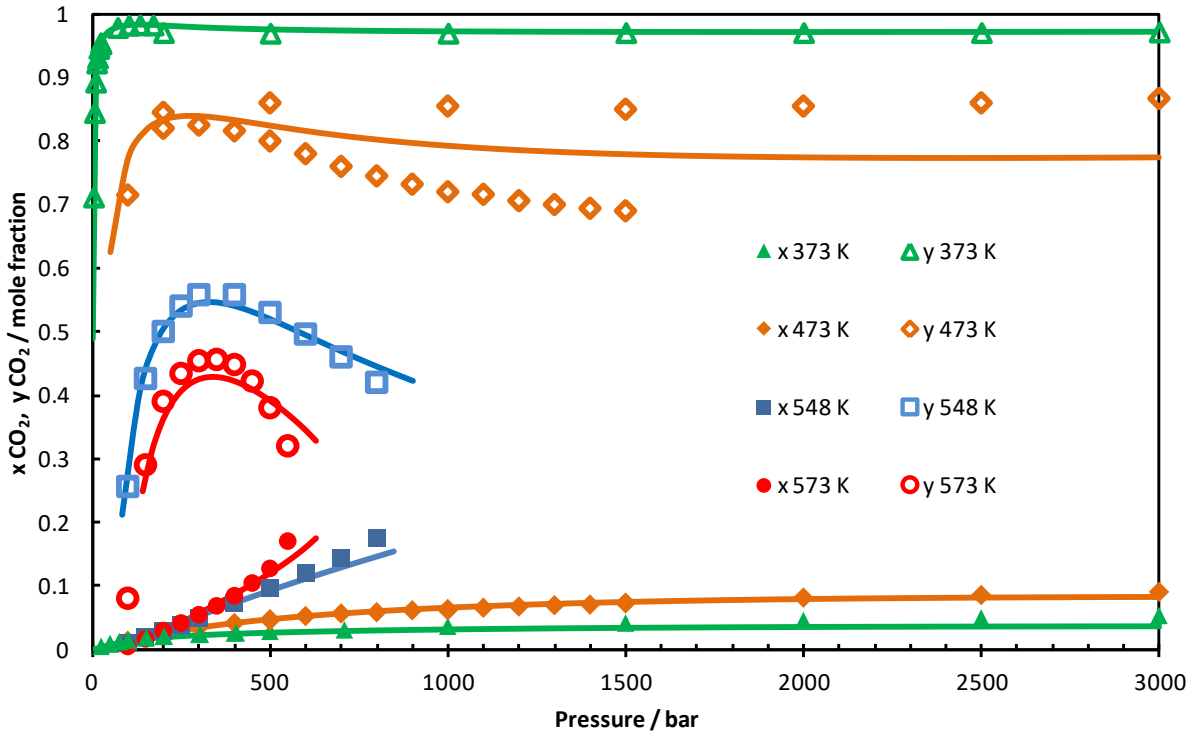

Figure 3.9 : CO_2-H_2O system: Prediction of liquid-vapor equilibria at very high temperature and pressure by the e-PR-CPA model. The symbols are literature data: [3. 5, 6].

3.4.3 H_2O + CO_2 + NaCl system

In Figure 3.10, the calculation results of the solubility of CO_2 in high molality NaCl brine (4m and 6m) by the Soreide and Whitson (SW) model were presented using two sets of binary interaction parameters (BIPs): the original BIPs and the BIPs proposed in this work (m-SW).

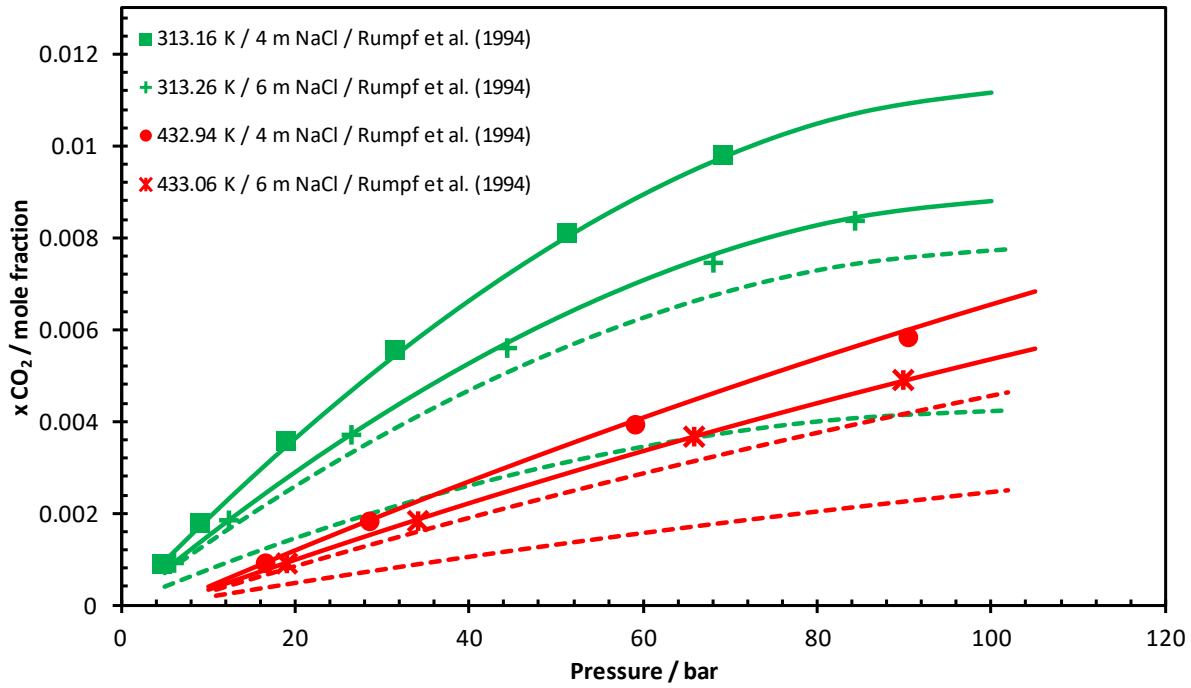

Figure 3.10 : CO_2-H_2O-NaCl system: Calculation of CO_2 solubility in high molality NaCl brine at 313 K and at 433 K by the Soreide and Whitson (SW) model using the original kij (dashed line) and the kij proposed in this work (solid line). Literature data from Rumpf et al. [3. 74].

Comparing these results with literature data, a significant improvement was made with the new BIPs (m-SW), especially at high molality.

The description of phase equilibria in the presence of electrolytes with the e-PR-CPA model requires the introduction of binary interaction parameters $k_{gas-ions}$ between CO_2 and the ions (Na^+ and Cl^-). These parameters ($k_{CO_2-Na^+}$ and $k_{CO_2-Cl^-}$) are obtained by adjusting the model parameters to solubility data (Rumpf et al. 1994 [3. 74], Koschel et al. 2003 [3. 4] and Yan et al. 2011 [3. 7]) of carbon dioxide in brine (H_2O + NaCl). To be in good agreement with the experimental data, we noticed that the $k_{gas-ions}$ are slightly dependent on molality (Figure 3.11). Since, the effect of temperature is already taken into account in $k_{H_2O-CO_2}$ and $\beta_{H_2O-CO_2}$, a simple linear dependence of $k_{gas-ions}$ on molality was sufficient to have good results.

$$k_{CO_2-Na^+} = -0.563937723 \times m_s - 4.352740149 \quad \textbf{(3.13)}$$

$$k_{CO_2-Cl^-} = 0.347571193 \times m_s + 4.762185508 \quad \textbf{(3.14)}$$

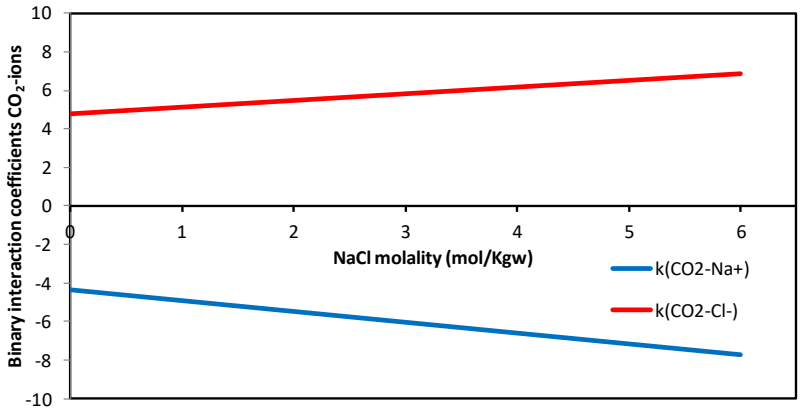

Figure 3.11 : Influence of molality on k_{CO_2-ions} for the H_2O-CO_2-NaCl system.

In Figure 3.12, the calculations done by e-PR-CPA, m-SW and geochemical models were compared with the experimental data (from literature and from this work) for the H_2O-CO_2-NaCl system. The experimental data measured in this work are in good agreement with the literature data (Figure 3.12-a) and also with model predictions (Figure 3.12-b). It should be noted that none of the measured data was included in the model parameterizations. The three models are in good agreement with the experimental data, and are able to estimate solubilities at high pressures and temperatures and for molalities up to saturation (~6m).

To compare the predictions of the three models over a wide range of temperature, pressure and molality, existing data in the open literature were collected [3. 4, 7, 8, 9, 10, 11, 12, 74, 75, 76, 77, 78, 79, 80, 81, 82, 83, 84, 85, 86, 87, 88, 89, 90, 91, 92, 93, 94, 95, 96, 97, 98, 99, 100, 101, 102, 103, 104, 105, 106, 107, 108]. The calculation was made for all the collected points (1150) and also at reduced temperature and pressure conditions in order to evaluate the predictions under the geological conditions of the storage. Calculations by the well-known DUAN model (Duan et al. [3. 15]) were also done and compared with the other models. The Absolute Average Deviations (AAD) from the literature data in the different temperature and pressure ranges obtained with the models are summarized in Table 3.7. For all data, the geochemical model and the Duan model estimate solubility better than the m-SW and e-PR-CPA models, however, under storage conditions the e-PR-CPA model and the Duan model estimate solubility with an AAD less than 6.6%, while the m-SW model and the geochemical model estimate solubility with an AAD less than 7.6%. These results can be explained by the fact that the e-PR-CPA model and the m-SW model were adjusted only on data at temperatures between 313 and 433 K and therefore no liquid-liquid equilibrium data were included in the adjustment of these two models.

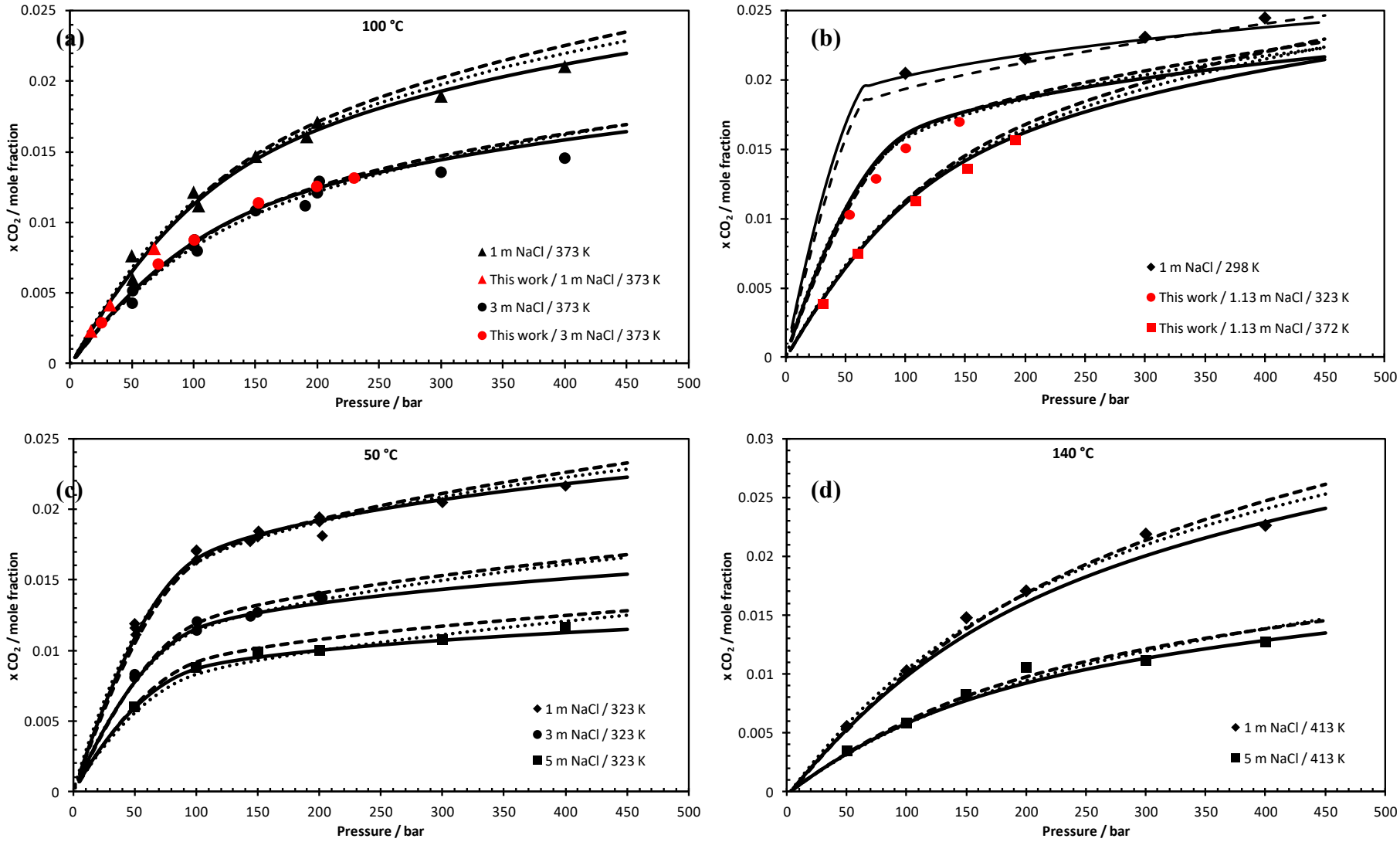

Figure 3.12 : CO_2-H_2O-NaCl system: Calculation of CO_2 solubility by e-PR-CPA (solid line), m-SW (dashed line) and geochemical (dotted line) models. The black symbols (a, b, c and d) are the literature data [3. 4, 7, 11, 12], and the red symbols (a and b) are the measured data (Table 3.2).

Table 3.7 : Solubility of CO_2 in the CO_2-H_2O-NaCl system. AAD between experimental literature data and model predictions at different temperature and pressure ranges.

Selected data	Temperature (K)	Pressure (bars)	NaCl molality (mol/kgw)	Number of experimental points	AAD (%)			
					e-PR-CPA	m-SW	CHESS (Geoch.)	DUAN
All data	273.15 - 523.15	0.1 - 600	0 - 7.14	1150	10.2	10.2	6.7	6.4
Data at reduced temperature	297.00 - 433.08	1.9 - 600	0 - 7.14	725	7.0	7.3	7.5	6.6
Storage conditions	297.00 - 433.08	50 - 600	0 - 6.00	506	6.6	7.5	7.6	6.5

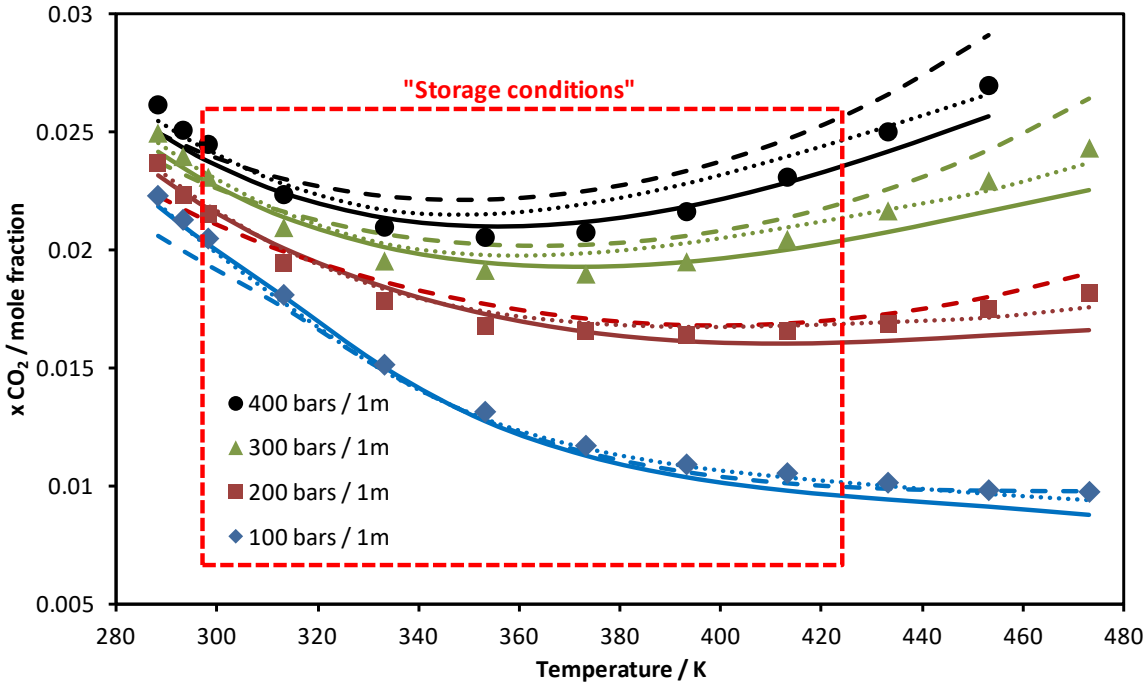

Figure 3.13 : CO_2-H_2O-NaCl system: Calculation of CO_2 solubility at different temperatures and pressures by e-PR-CPA (solid line), m-SW (dashed line) and geochemical (dotted line) models. The symbols are the literature data from Guo et al. [3. 11].

The purpose of this comparison is to facilitate the choice of the appropriate model for an engineering application. The Duan model is widely used for the CO_2-brine system, but it is limited to a molality of 4.3 m (mol/kgw), therefore for storage applications in salt caverns (saturated brine), it is necessary to take the risk of extrapolation beyond the 4.3 m, which is not recommended with this type of empirical model. In this case, it is preferable to use the e-PR-CPA model (very accurate at high temperature and pressure, see Figures 3.12 and 3.13) or the geochemical model or Soreide and Whitson with the parameters proposed in this work (m-SW). To evaluate the models according to thermodynamic conditions (T and P), in Figure 3.13, calculations over a wide temperature and pressure range (at 1 m NaCl, more or less the salinity condition of aquifers) are presented and compared with literature data that have not been included in the model parameterization. At low temperature (below T_{c,CO_2}), where CO_2 is liquid (at high pressure), it is preferable to use the gamma-phi approach using the geochemical model, since in this approach each phase is represented by a specific model (SIT for the liquid phase, PR for the vapor phase). For reservoir simulation, it is necessary to carry out the stability test before the equilibrium calculation in each cell, this can only be done with an equation of state (phi-phi approach), it is known that for reservoir simulation, the number of points to be calculated is enormous (it can exceed one million points), which is why SAFT and CPA models are not used for this type of application given the high calculation time when comparing with cubic EoS. The m-SW model is best suited for reservoir simulation, and it is suggested to implement it according to the approach proposed by Petitfrere et al. [3. 18] to solve the inconsistency problem and therefore use second order methods for the calculation of phase equilibria (Michelsen [3. 109]). Finally, the common advantage of the models studied in this work is that they can generate reliable data without the need for more experimental measurements, which are generally complicated due to the presence of salts (corrosion, clogging, etc.) and require a lot of time and investment.

3.5 Conclusions

In this work, measurements of the solubility of carbon dioxide in NaCl brine were carried out by a new set-up based on the "static-analytic" method. A modification of the sampling procedure to avoid salt deposition in the sampler was made. The validation of this set-up was done by comparing some obtained results with the literature data. All measurements are intended to complement the existing data for this system, to evaluate and validate the developed models, and also to check the feasibility of sampling in saline solution. Our goal is to do measurement of solubility of mixture of gas.

The modeling of phase equilibria was carried out by four models using different approaches.

1- An improvement of the Soreide and Whitson model (m-SW) was made by proposing new correlations for binary interaction parameters. This model is implemented in many simulation software, so the old parameters can easily be replaced by those proposed in this work.

2- An electrolyte version of the PR-CPA model has been developed (e-PR-CPA) and parameterized on vapor pressure and osmotic coefficient data, to represent both equilibrium data and excess properties. For gas-water and gas-brine mixtures, the binary interaction parameters were adjusted on CO_2 solubility data.

3- A geochemical model implemented in CHESS/HYTEC software using an asymmetric "gamma-phi" approach was tested.

The liquid-vapor equilibria of the CO_2-H_2O system at very high pressure and temperature (up to the critical points of the mixture) were calculated by the e-PR-CPA model. CO_2 solubility and water content are well predicted, which proves the extrapolation quality with this model far from the adjustment range. The measurements performed in this work are in good agreement with the literature data and also with the model predictions. The e-PR-CPA, m-SW, geochemical and DUAN models reproduce the measured data with AAD of 4%, 4.5%, 6.6% and 6.9% respectively. A comparison of these models with all the existing literature data covering the geological storage conditions was carried out. In the storage condition the e-PR-CPA model and the Duan model reproduce solubilities with an AAD less than 6.6%, while the geochemical model and the m-SW model reproduce solubilities with an AAD less than 7.6%.

Finally, model predictions over a wide temperature and pressure range were compared with literature data to allow the evaluation of each model in a specific region (low and high pressure and temperature).

Nomenclature

a	energy parameter (Pa m^6 mol^{-2})
A	Helmholtz free energy, or Debye-Hückel parameter
A_i, B_i	site A or B in molecule i
b	molar co-volume (m^3/mol)
D	dielectric constant
D_0	vacuum permittivity (F/m)
e	elementary charge (C)
ea	electron acceptor site
ed	electron donor site
g	radial distribution function
I	ionic strength (mol/kgw)
k	binary interaction parameter
K	Henry's law constant
m	molality (mol/kgw), or e-PR-CPA parameter
M	Molar mass (kg/mol)
n	number of mole
N_{Av}	Avogadro number
P	pressure (Pa)
R	ideal gas constant (J mol^{-1} K^{-1})
T	temperature (K)
v	molar volume (m^3/mol)
V	volume (m^3)
x	liquid molar fraction
X	site fraction
y	vapor molar fraction
Z	electric charge

Greek letters

ε	CPA association energy (Pa m^3 mol^{-1}), or SIT binary interaction parameter
β	bonding volume
Δ	association strength
ρ	molar density (mol/m^3)
σ	ion diameter
γ	activity coefficient
φ	fugacity coefficient
ω	acentric factor
Γ	screening length

Subscripts

c	critical
g	gas
i, j	compound
liq	liquid
r	reduced
s	salt
sat	saturation
w	water

Superscripts

AQ	aqueous phase
cal	calculated value
exp	experimental value
g	gas
NA	non-aqueous phase
sf	salt-free
∞	infinite dilution

Abbreviations

BIP	Binary Interaction Parameter
CPA	Cubic Plus Association
DH	Debye-Hückel
EoS	Equation of State
MSA	Mean Spherical Approximation
NIST	National Institute of Standards and Technology
PR	Peng-Robinson
SIT	Specific Ion Theory
SW	Soreide and Whitson

Acknowledgments

Financial support from Agence Nationale de la Recherche (ANR) through the project FluidSTORY (n° 7747, ID ANR-15-CE06-0015) is gratefully acknowledged.

References

[3. 1] P. Berest, Stockage souterrain des gaz et hydrocarbures : des perspectives pour la transition énergétique, Encyclopédie de l'Environnement [en ligne ISSN 2555-0950], (2019).
[3. 2] O. Kruck, F. Crotogino, R. Prelicz, T. Rudolph, Assessment of the potential, the actors and relevant business cases for large scale and seasonal storage of renewable electricity by hydrogen underground storage in Europe, (2013).
[3. 3] I. Søreide, C.H. Whitson, Peng-Robinson predictions for hydrocarbons, CO2, N2, and H2 S with pure water and NaCI brine, Fluid Phase Equilibria, 77 (1992) 217-240.
[3. 4] D. Koschel, J.-Y. Coxam, L. Rodier, V. Majer, Enthalpy and solubility data of CO 2 in water and NaCl (aq) at conditions of interest for geological sequestration, Fluid phase equilibria, 247 (2006) 107-120.
[3. 5] K. Tödheide, E. Franck, Das Zweiphasengebiet und die kritische Kurve im System Kohlendioxid–Wasser bis zu Drucken von 3500 bar, Zeitschrift für Physikalische Chemie, 37 (1963) 387-401.
[3. 6] S. Takenouchi, G.C. Kennedy, The binary system H 2 O-CO 2 at high temperatures and pressures, American Journal of Science, 262 (1964) 1055-1074.
[3. 7] W. Yan, S. Huang, E.H. Stenby, Measurement and modeling of CO2 solubility in NaCl brine and CO2–saturated NaCl brine density, International Journal of Greenhouse Gas Control, 5 (2011) 1460-1477.
[3. 8] S.-X. Hou, G.C. Maitland, J.M. Trusler, Phase equilibria of (CO2+ H2O+ NaCl) and (CO2+ H2O+ KCl): Measurements and modeling, The Journal of Supercritical Fluids, 78 (2013) 78-88.
[3. 9] H. Zhao, M.V. Fedkin, R.M. Dilmore, S.N. Lvov, Carbon dioxide solubility in aqueous solutions of sodium chloride at geological conditions: Experimental results at 323.15, 373.15, and 423.15 K and 150bar and modeling up to 573.15 K and 2000bar, Geochimica et Cosmochimica Acta, 149 (2015) 165-189.
[3. 10] K. Gilbert, P.C. Bennett, W. Wolfe, T. Zhang, K.D. Romanak, CO 2 solubility in aqueous solutions containing Na+, Ca 2+, Cl−, SO 4 2− and HCO 3-: The effects of electrostricted water and ion hydration thermodynamics, Applied Geochemistry, 67 (2016) 59-67.
[3. 11] H. Guo, Y. Huang, Y. Chen, Q. Zhou, Quantitative Raman Spectroscopic Measurements of CO2 Solubility in NaCl Solution from (273.15 to 473.15) K at p=(10.0, 20.0, 30.0, and 40.0) MPa, Journal of Chemical & Engineering Data, 61 (2015) 466-474.
[3. 12] H. Messabeb, F.o. Contamine, P. Cézac, J.P. Serin, E.C. Gaucher, Experimental Measurement of CO2 Solubility in Aqueous NaCl Solution at Temperature from 323.15 to 423.15 K and Pressure of up to 20 MPa, Journal of Chemical & Engineering Data, 61 (2016) 3573-3584.
[3. 13] J. Corvisier, Modeling water-gas-rock interactions using CHESS/HYTEC, in: Goldschmidt Conference, Florence–Italy, 2013.
[3. 14] J. Corvisier, A.-F. Bonvalot, V. Lagneau, P. Chiquet, S. Renard, J. Sterpenich, J. Pironon, Impact of co-injected gases on CO2 storage sites: Geochemical modeling of experimental results, Energy Procedia, 37 (2013) 3699-3710.
[3. 15] Z. Duan, R. Sun, C. Zhu, I.-M. Chou, An improved model for the calculation of CO2 solubility in aqueous solutions containing Na+, K+, Ca2+, Mg2+, Cl−, and SO42−, Marine Chemistry, 98 (2006) 131-139.
[3. 16] E. El Ahmar, B. Creton, A. Valtz, C. Coquelet, V. Lachet, D. Richon, P. Ungerer, Thermodynamic study of binary systems containing sulphur dioxide: Measurements and molecular modelling, Fluid Phase Equilibria, 304 (2011) 21-34.

[3. 17] D.-Y. Peng, D.B. Robinson, A new two-constant equation of state, Ind. Eng. Chem. Fundam., 15 (1976) 59.
[3. 18] M. Petitfrere, L. Patacchini, R. de Loubens, Three-phase EoS-based Reservoir Simulation with Salinity Dependent Phase-equilibrium Calculations, in: ECMOR XV-15th European Conference on the Mathematics of Oil Recovery, 2016.
[3. 19] G.M. Kontogeorgis, E.C. Voutsas, I.V. Yakoumis, D.P. Tassios, An equation of state for associating fluids, Industrial & engineering chemistry research, 35 (1996) 4310-4318.
[3. 20] G. Soave, Equilibrium constants from a modified Redlich-Kwong equation of state, Chemical engineering science, 27 (1972) 1197-1203.
[3. 21] M. Wertheim, Fluids with highly directional attractive forces. I. Statistical thermodynamics, Journal of statistical physics, 35 (1984) 19-34.
[3. 22] D.B. Robinson, D.-Y. Peng, The characterization of the heptanes and heavier fractions for the GPA Peng-Robinson programs, Gas Processors Association, 1978.
[3. 23] M. Hajiw, A. Chapoy, C. Coquelet, Hydrocarbons - water phase equilibria using the CPA equation of state with a group contribution method, The Canadian Journal of Chemical Engineering, 93 (2015) 432-442.
[3. 24] T. Wang, E. El Ahmar, C. Coquelet, G.M. Kontogeorgis, Improvement of the PR-CPA equation of state for modelling of acid gases solubilities in aqueous alkanolamine solutions, Fluid Phase Equilibria, 471 (2018) 74-87.
[3. 25] T. Wang, P. Guittard, C. Coquelet, E. El Ahmar, O. Baudouin, G. Kontogeorgis, Corrigendum to" Improvement of the PR-CPA equation of state for modelling of acid gases solubilities in aqueous alkanolamine solutions"[Fluid Phase Equilibria, Vol. 471, 2018, 74-87], Fluid Phase Equilibria, 485 (2019) 126-127.
[3. 26] C. Held, T. Reschke, S. Mohammad, A. Luza, G. Sadowski, ePC-SAFT revised, Chemical Engineering Research and Design, 92 (2014) 2884-2897.
[3. 27] B. Maribo-Mogensen, K. Thomsen, G.M. Kontogeorgis, An electrolyte CPA equation of state for mixed solvent electrolytes, AIChE Journal, 61 (2015) 2933-2950.
[3. 28] D.K. Eriksen, G. Lazarou, A. Galindo, G. Jackson, C.S. Adjiman, A.J. Haslam, Development of intermolecular potential models for electrolyte solutions using an electrolyte SAFT-VR Mie equation of state, Molecular Physics, 114 (2016) 2724-2749.
[3. 29] S. Ahmed, N. Ferrando, J.-C. De Hemptinne, J.-P. Simonin, O. Bernard, O. Baudouin, Modeling of mixed-solvent electrolyte systems, Fluid Phase Equilibria, 459 (2018) 138-157.
[3. 30] R. Inchekel, J.-C. de Hemptinne, W. Fürst, The simultaneous representation of dielectric constant, volume and activity coefficients using an electrolyte equation of state, Fluid Phase Equilibria, 271 (2008) 19-27.
[3. 31] B. Maribo-Mogensen, G.M. Kontogeorgis, K. Thomsen, Comparison of the Debye–Hückel and the Mean Spherical Approximation Theories for Electrolyte Solutions, Industrial & Engineering Chemistry Research, 51 (2012) 5353-5363.
[3. 32] L. Blum, Mean spherical model for asymmetric electrolytes: I. Method of solution, Molecular Physics, 30 (1975) 1529-1535.
[3. 33] M. Born, Volumen und hydratationswärme der ionen, Zeitschrift für Physik, 1 (1920) 45-48.
[3. 34] A. Anderko, K.S. Pitzer, Equation-of-state representation of phase equilibria and volumetric properties of the system NaCl-H2O above 573 K, Geochimica et Cosmochimica Acta, 57 (1993) 1657-1680.
[3. 35] D. Tong, J.M. Trusler, D. Vega-Maza, Solubility of CO2 in aqueous solutions of CaCl2 or MgCl2 and in a synthetic formation brine at temperatures up to 423 K and pressures up to 40 MPa, Journal of Chemical & Engineering Data, 58 (2013) 2116-2124.
[3. 36] W.H. Press, FORTRAN Numerical Recipes: Numerical recipes in FORTRAN 90: the art of parallel scientific computing, Cambridge University Press, 1996.

[3. 37] S.H. Huang, M. Radosz, Equation of state for small, large, polydisperse, and associating molecules, Industrial & Engineering Chemistry Research, 29 (1990) 2284-2294.
[3. 38] W. Wagner, A. Pruß, The IAPWS formulation 1995 for the thermodynamic properties of ordinary water substance for general and scientific use, Journal of physical and chemical reference data, 31 (2002) 387-535.
[3. 39] N. Hubert, Y. Gabes, J.-B. Bourdet, L. Schuffenecker, Vapor pressure measurements with a nonisothermal static method between 293.15 and 363.15 K for electrolyte solutions. Application to the H2O+ NaCl system, Journal of Chemical and Engineering Data, 40 (1995) 891-894.
[3. 40] J.L. Haas Jr, Thermodynamics properties of the coexisting phases and thermochemical properties of the NaCl component in boiling NaCl solutions, US, Geol. Surv., Bull.;(United States), 1421 (1976).
[3. 41] W.J. Hamer, Y.C. Wu, Osmotic coefficients and mean activity coefficients of uni-univalent electrolytes in water at 25° C, Journal of Physical and Chemical Reference Data, 1 (1972) 1047-1100.
[3. 42] J.A. Rard, D.G. Archer, Isopiestic Investigation of the Osmotic and Activity Coefficients of Aqueous NaBr and the Solubility of NaBr. cntdot. 2H2O (cr) at 298.15 K: Thermodynamic Properties of the NaBr+ H2O System over Wide Ranges of Temperature and Pressure, Journal of Chemical and Engineering Data, 40 (1995) 170-185.
[3. 43] J. llmari Partanen, P.O. Minkkinen, Thermodynamic Activity Quantities in Aqueous Sodium and Potassium Chloride Solutions at 298.15 K up to a Molality of 2.0 mol kg _1, Acta Chemica Scandinavica, 47 (1993) 768-776.
[3. 44] R.A. Robinson, R.H. Stokes, Tables of osmotic and activity coefficients of electrolytes in aqueous solution at 25 C, Transactions of the Faraday Society, 45 (1949) 612-624.
[3. 45] H.F. Gibbard Jr, G. Scatchard, R.A. Rousseau, J.L. Creek, Liquid-vapor equilibrium of aqueous sodium chloride, from 298 to 373. deg. K and from 1 to 6 mol kg-1, and related properties, Journal of Chemical and Engineering Data, 19 (1974) 281-288.
[3. 46] K.S. Pitzer, J.C. Peiper, R. Busey, Thermodynamic properties of aqueous sodium chloride solutions, Journal of Physical and Chemical Reference Data, 13 (1984) 1-102.
[3. 47] K.S. Pitzer, Thermodynamics of electrolytes. I. Theoretical basis and general equations, The Journal of Physical Chemistry, 77 (1973) 268-277.
[3. 48] K.S. Pitzer, Ion interaction approach: theory and data correlation, Activity coefficients in electrolyte solutions, 2 (1991) 75-153.
[3. 49] J.N. Brønsted, Studies on solubility. IV. The principle of the specific interaction of ions, Journal of the American Chemical Society, 44 (1922) 877-898.
[3. 50] G. Scatchard, Concentrated Solutions of Strong Electrolytes, Chemical Reviews, 19 (1936) 309-327.
[3. 51] E. Guggenheim, J. Turgeon, Specific interaction of ions, Transactions of the Faraday Society, 51 (1955) 747-761.
[3. 52] P. Debye, E. Hückel, De la theorie des electrolytes. I. abaissement du point de congelation et phenomenes associes, Physikalische Zeitschrift, 24 (1923) 185-206.
[3. 53] I. Grenthe, I. Puigdomenech, B. Allard, Modelling in aquatic chemistry, OECD Publishing, 1997.
[3. 54] M. Hajiw, J. Corvisier, E. El Ahmar, C. Coquelet, Impact of impurities on CO 2 storage in saline aquifers: Modelling of gases solubility in water, International Journal of Greenhouse Gas Control, 68 (2018) 247-255.
[3. 55] A.C. Schneider, C. Pasel, M. Luckas, K.G. Schmidt, J.-D. Herbell, Determination of hydrogen single ion activity coefficients in aqueous HCl solutions at 25 C, Journal of solution chemistry, 33 (2004) 257-273.

[3. 56] H. Sakaida, T. Kakiuchi, Determination of single-ion activities of H+ and Cl– in aqueous hydrochloric acid solutions by use of an ionic liquid salt bridge, The Journal of Physical Chemistry B, 115 (2011) 13222-13226.
[3. 57] M.K. Khoshkbarchi, J.H. Vera, Measurement and correlation of ion activity in aqueous single electrolyte solutions, AIChE journal, 42 (1996) 249-258.
[3. 58] R. Wiebe, V. Gaddy, The solubility in water of carbon dioxide at 50, 75 and 100, at pressures to 700 atmospheres, Journal of the American Chemical Society, 61 (1939) 315-318.
[3. 59] S.-X. Hou, G.C. Maitland, J.M. Trusler, Measurement and modeling of the phase behavior of the (carbon dioxide+ water) mixture at temperatures from 298.15 K to 448.15 K, The Journal of Supercritical Fluids, 73 (2013) 87-96.
[3. 60] A. Bamberger, G. Sieder, G. Maurer, High-pressure (vapor+ liquid) equilibrium in binary mixtures of (carbon dioxide+ water or acetic acid) at temperatures from 313 to 353 K, The Journal of Supercritical Fluids, 17 (2000) 97-110.
[3. 61] R. Dohrn, A. Bünz, F. Devlieghere, D. Thelen, Experimental measurements of phase equilibria for ternary and quaternary systems of glucose, water, CO2 and ethanol with a novel apparatus, Fluid Phase Equilibria, 83 (1993) 149-158.
[3. 62] P. Ahmadi, A. Chapoy, CO2 solubility in formation water under sequestration conditions, Fluid Phase Equilibria, 463 (2018) 80-90.
[3. 63] J. Briones, J. Mullins, M. Thies, B.-U. Kim, Ternary phase equilibria for acetic acid-water mixtures with supercritical carbon dioxide, Fluid Phase Equilibria, 36 (1987) 235-246.
[3. 64] A.D. King Jr, C. Coan, Solubility of water in compressed carbon dioxide, nitrous oxide, and ethane. Evidence for hydration of carbon dioxide and nitrous oxide in the gas phase, Journal of the American Chemical Society, 93 (1971) 1857-1862.
[3. 65] K. Jackson, L.E. Bowman, J.L. Fulton, Water solubility measurements in supercritical fluids and high-pressure liquids using near-infrared spectroscopy, Analytical Chemistry, 67 (1995) 2368-2372.
[3. 66] G. Müller, E. Bender, G. Maurer, Das Dampf-Flüssigkeitsgleichgewicht des ternären Systems Ammoniak-Kohlendioxid-Wasser bei hohen Wassergehalten im Bereich zwischen 373 und 473 Kelvin, Berichte der Bunsengesellschaft für physikalische Chemie, 92 (1988) 148-160.
[3. 67] A. Valtz, A. Chapoy, C. Coquelet, P. Paricaud, D. Richon, Vapour–liquid equilibria in the carbon dioxide–water system, measurement and modelling from 278.2 to 318.2 K, Fluid phase equilibria, 226 (2004) 333-344.
[3. 68] M. King, A. Mubarak, J. Kim, T. Bott, The mutual solubilities of water with supercritical and liquid carbon dioxides, The Journal of Supercritical Fluids, 5 (1992) 296-302.
[3. 69] T. Nakayama, H. Sagara, K. Arai, S. Saito, High pressure liquid・ liquid equilibria for the system of water, ethanol and 1, 1-difluoroethane at 323.2 K, Fluid Phase Equilibria, 38 (1987) 109-127.
[3. 70] P. Gillespie, G. Wilson, GPA Research Report RR-48, Gas Processors Association, Tulsa, (1982).
[3. 71] H. Greenwood, H. Barnes, section 17: Binary mixtures of volatile components, Geological Society of America Memoirs, 97 (1966) 385-400.
[3. 72] R. Wiebe, V. Gaddy, Vapor phase composition of carbon dioxide-water mixtures at various temperatures and at pressures to 700 atmospheres, Journal of the American Chemical Society, 63 (1941) 475-477.
[3. 73] P. Van Konynenburg, R. Scott, Critical lines and phase equilibria in binary van der Waals mixtures, Philosophical Transactions of the Royal Society of London. Series A, Mathematical and Physical Sciences, 298 (1980) 495-540.

[3. 74] B. Rumpf, H. Nicolaisen, C. Öcal, G. Maurer, Solubility of carbon dioxide in aqueous solutions of sodium chloride: experimental results and correlation, Journal of solution chemistry, 23 (1994) 431-448.
[3. 75] J.J. Mackenzie, Ueber die Absorption der Gase durch Salzlösungen, Annalen der Physik, 237 (1877) 438-451.
[3. 76] M. Setschenow, Action de l'acide carbonique sur les solutions dessels a acides forts. Etude absortiometrique, Ann. Chim. Phys, 25 (1892) 226-270.
[3. 77] K.A. Kobe, J.S. Williams, Confining liquids for gas analysis: solubility of carbon dioxide in salt solutions, Industrial & Engineering Chemistry Analytical Edition, 7 (1935) 37-38.
[3. 78] A.E. Markham, K.A. Kobe, The solubility of carbon dioxide and nitrous oxide in aqueous salt solutions, Journal of the American Chemical Society, 63 (1941) 449-454.
[3. 79] H.S. Harned, R. Davis Jr, The ionization constant of carbonic acid in water and the solubility of carbon dioxide in water and aqueous salt solutions from 0 to 50, Journal of the American Chemical Society, 65 (1943) 2030-2037.
[3. 80] W. Rosenthal, thesis, in: Faculty of Science, University of Strasbourg, 1954.
[3. 81] A. Ellis, R. Golding, The solubility of carbon dioxide above 100 degrees C in water and in sodium chloride solutions, American Journal of Science, 261 (1963) 47-60.
[3. 82] S.Y. Yeh, R.E. Peterson, Solubility of carbon dioxide, krypton, and xenon in aqueous solution, Journal of pharmaceutical sciences, 53 (1964) 822-824.
[3. 83] S. Takenouchi, G.C. Kennedy, The solubility of carbon dioxide in NaCl solutions at high temperatures and pressures, American journal of science, 263 (1965) 445-454.
[3. 84] K. ONDA, E. SADA, T. KOBAYASHI, S. KITO, K. ITO, Salting-out parameters of gas solubility in aqueous salt solutions, Journal of Chemical Engineering of Japan, 3 (1970) 18-24.
[3. 85] Y.H. Li, T.F. Tsui, The solubility of CO2 in water and sea water, Journal of Geophysical research, 76 (1971) 4203-4207.
[3. 86] S. Malinin, N. Savelyeva, Experimental investigations of CO2 solubility in NaCl and CaCl2 solutions at temperature of 25, 50 and 75 Degrees and elevated CO2 pressure, Geochem. Int, 9 (1972) 643.
[3. 87] S. Malinin, N. Kurovskaya, Solubility of CO2 in chloride solutions at elevated temperatures and CO2 pressures, Geochem. Int, 12 (1975) 199-201.
[3. 88] A. Yasunishi, F. Yoshida, Solubility of carbon dioxide in aqueous electrolyte solutions, Journal of Chemical and Engineering Data, 24 (1979) 11-14.
[3. 89] S. Drummond, Boiling and mixing of hydrothermal fluids: Effects on mineral deposition, in, Ph. D. thesis, Pennsylvania State University, 1981.
[3. 90] G. Burmakina, L. Efanov, M. Shnet, CO2 SOLUBILITY IN AQUEOUS-SOLUTIONS OF SOME ELECTROLYTES AND SUCROSE, ZHURNAL FIZICHESKOI KHIMII, 56 (1982) 1159-1161.
[3. 91] S. Cramer, Solubility of methane, carbon dioxide, and oxygen in brines from 0/sup 0/to 300/sup 0/C, in, Bureau of Mines, Pittsburgh, PA, 1982.
[3. 92] M. Gehrig, H. Lentz, E. Franck, The system water—carbon dioxide—sodium chloride to 773 K and 300 MPa, Berichte der Bunsengesellschaft für physikalische Chemie, 90 (1986) 525-533.
[3. 93] J.A. Nighswander, N. Kalogerakis, A.K. Mehrotra, Solubilities of carbon dioxide in water and 1 wt.% sodium chloride solution at pressures up to 10 MPa and temperatures from 80 to 200. degree. C, Journal of Chemical and Engineering Data, 34 (1989) 355-360.
[3. 94] S. He, J.W. Morse, The carbonic acid system and calcite solubility in aqueous Na-K-Ca-Mg-Cl-SO4 solutions from 0 to 90°C, Geochimica et Cosmochimica Acta, 57 (1993) 3533-3554.

[3. 95] G. Vazquez, F. Chenlo, G. Pereira, CO2 diffusivity in nacl and cuso4 aqueous-solutions, Afinidad, 51 (1994) 369-374.
[3. 96] G. Vázquez, F. Chenlo, G. Pereira, J. Peaguda, SOLUBILITY OF CO2 IN AQUEOUS-SOLUTIONS OF NACL, CUSO4, KL AND NABR, in: Anales de Quimica, REAL SOC ESPAN QUIMICA FACULTAD DE FISICA QUIMICA CIUDAD UNIV, 3 MADRID, SPAIN, 1994, pp. 324-328.
[3. 97] D.-Q. Zheng, T.-M. Guo, H. Knapp, Experimental and modeling studies on the solubility of CO2, CHC1F2, CHF3, C2H2F4 and C2H4F2 in water and aqueous NaCl solutions under low pressures, Fluid Phase Equilibria, 129 (1997) 197-209.
[3. 98] J. Kiepe, S. Horstmann, K. Fischer, J. Gmehling, Experimental determination and prediction of gas solubility data for CO2+ H2O mixtures containing NaCl or KCl at temperatures between 313 and 393 K and pressures up to 10 MPa, Industrial & Engineering Chemistry Research, 41 (2002) 4393-4398.
[3. 99] S. Bando, F. Takemura, M. Nishio, E. Hihara, M. Akai, Solubility of CO2 in aqueous solutions of NaCl at (30 to 60) C and (10 to 20) MPa, Journal of Chemical & Engineering Data, 48 (2003) 576-579.
[3. 100] G. Ferrentino, D. Barletta, F. Donsì, G. Ferrari, M. Poletto, Experimental measurements and thermodynamic modeling of CO2 solubility at high pressure in model apple juices, Industrial & Engineering Chemistry Research, 49 (2010) 2992-3000.
[3. 101] Y. Liu, M. Hou, G. Yang, B. Han, Solubility of CO2 in aqueous solutions of NaCl, KCl, CaCl2 and their mixed salts at different temperatures and pressures, The Journal of supercritical fluids, 56 (2011) 125-129.
[3. 102] J. Rosenqvist, A.D. Kilpatrick, B.W. Yardley, Solubility of carbon dioxide in aqueous fluids and mineral suspensions at 294 K and subcritical pressures, Applied geochemistry, 27 (2012) 1610-1614.
[3. 103] V. Savary, G. Berger, M. Dubois, J.-C. Lacharpagne, A. Pages, S. Thibeau, M. Lescanne, The solubility of CO2+ H2S mixtures in water and 2 M NaCl at 120° C and pressures up to 35 MPa, International Journal of Greenhouse Gas Control, 10 (2012) 123-133.
[3. 104] C. Langlais, Impacts géochimiques de la présence d'oxygène sur les saumures en conditions de stockage géologique de CO2 : caractérisation de solubilités, in, 2013.
[3. 105] P.J. Carvalho, L.M. Pereira, N.P. Gonçalves, A.J. Queimada, J.A. Coutinho, Carbon dioxide solubility in aqueous solutions of NaCl: Measurements and modeling with electrolyte equations of state, Fluid Phase Equilibria, 388 (2015) 100-106.
[3. 106] E. Mohammadian, H. Hamidi, M. Asadullah, A. Azdarpour, S. Motamedi, R. Junin, Measurement of CO2 solubility in NaCl brine solutions at different temperatures and pressures using the potentiometric titration method, Journal of Chemical & Engineering Data, 60 (2015) 2042-2049.
[3. 107] R. Jacob, B.Z. Saylor, CO2 solubility in multi-component brines containing NaCl, KCl, CaCl2 and MgCl2 at 297 K and 1–14 MPa, Chemical Geology, 424 (2016) 86-95.
[3. 108] B. Liborio, Dissolution du dioxyde de carbone dans des solutions aqueuses d'électrolyte dans le contexte du stockage géologique : approche thermodynamique, in, 2017.
[3. 109] M.L. Michelsen, The isothermal flash problem. Part II. Phase-split calculation, Fluid phase equilibria, 9 (1982) 21-40.

Chapter 4: Article 2: Measurements and modeling of high-pressure O_2 and CO_2 solubility in brine (H_2O+NaCl) between 303 and 373 K and pressures up to 36 MPa

French summary / Chapitre 4 – Article 2 : Mesures et modélisation de la solubilité à haute pression de l'O_2 et du CO_2 dans la saumure (H_2O+NaCl) entre 303 et 373 K et à des pressions allant jusqu'à 36 MPa

L'étude de la solubilité de l'oxygène dans l'eau naturelle, qui est généralement saline, est importante pour plusieurs domaines scientifiques et d'ingénierie. Des applications telles que le stockage géologique du gaz (contenant de l'O_2, par exemple les fumées) ou de l'énergie (stockage de l'énergie par air comprimé) fonctionnent à haute pression. Cependant, à ce jour, il n'existe pas de données sur la solubilité de l'O_2 à haute pression dans la saumure, ce qui a conduit les chercheurs à développer des modèles pour prédire cette importante propriété. Pour pallier ce manque de données, la solubilité de l'O_2 dans la saumure a été mesurée à l'aide de deux techniques différentes, à des molalités comprises entre 0,5 et 4 m (NaCl), des températures entre 303 et 373 K et des pressions allant jusqu'à 36 MPa. Afin de valider les méthodes expérimentales, des mesures de la solubilité du CO_2 dans une saumure hautement concentrée (6 m de NaCl) à des températures comprises entre 303 et 373 K et à des pressions allant jusqu'à 39,5 MPa, ont également été effectuées dans le cadre de ce travail. Ces mesures ont permis d'évaluer des modèles existants tels que le modèle bien connu de Geng et Duan, et le modèle récemment développé par Zheng et Mao (ZM). Les modèles e-PR-CPA, Soreide-Whitson et géochimiques utilisés dans nos travaux précédents ont également été utilisés pour traiter les nouvelles données. Ces trois derniers modèles ont été paramétrés sur la base des données de solubilité de l'O_2 mesurées et rapportées dans la littérature, et de nouveaux paramètres optimisés du modèle ZM ont été proposés. Ces modèles reproduisent très bien l'effet de la température, de la pression et de la concentration de NaCl sur la solubilité avec un écart absolu moyen inférieur à 5% par rapport aux données mesurées.

Measurements and modeling of high-pressure O_2 and CO_2 solubility in brine (H_2O+NaCl) between 303 and 373 K and pressures up to 36 MPa

Salaheddine Chabab[a], Pezhman Ahmadi[b], Pascal Théveneau[a], Christophe Coquelet[a], Antonin Chapoy[b,a], Jérôme Corvisier[c] and Patrice Paricaud[d,a]

[a]*Mines ParisTech, PSL University, Centre of Thermodynamics of Processes, 35 rue Saint Honoré, 77305 Fontainebleau Cedex, France*

[b]*Hydrates, Flow Assurance & Phase Equilibria Research Group, Institute of GeoEnergy Engineering, Heriot-Watt University, Edinburgh EH14 4AS, Scotland,UK*

[c]*Mines ParisTech, PSL University, Centre de Géosciences, 35 rue Saint Honoré, 77305 Fontainebleau Cedex, France*

[d]*Unité Chimie & Procédés (UCP), ENSTA Paris, 828 Boulevard des Maréchaux, 91762 Palaiseau cedex, France*

Journal of chemical & engineering data

pubs.acs.org/jced Article

Measurements and Modeling of High-Pressure O_2 and CO_2 Solubility in Brine (H_2O + NaCl) between 303 and 373 K and Pressures up to 36 MPa

Salaheddine Chabab, Pezhman Ahmadi, Pascal Théveneau, Christophe Coquelet,* Antonin Chapoy, Jérôme Corvisier, and Patrice Paricaud

Cite This: *J. Chem. Eng. Data* 2021, 66, 609–620 Read Online

ACCESS | Metrics & More | Article Recommendations | Supporting Information

ABSTRACT: Knowledge of the solubility of oxygen in natural water, which is generally saline, is important for several scientific and engineering fields. Applications such as geological storage of gas (containing O_2, e.g., flue gas) or energy (compressed air energy storage) operate at high pressure. However, to date, there is no high-pressure O_2 solubility data in brine, which has led researchers to develop models to predict this important property. To overcome the lack of data, solubility of O_2 in brine has been measured using two different techniques, at molalities between 0.5 and 4 mol/kg_w (NaCl), temperatures between 303 and 373 K, and pressures up to 36 MPa. In order to validate the experimental methods, measurements of the solubility of CO_2 in a highly concentrated brine (6 mol/kg_w of NaCl) at temperatures between 303 and 373 K and pressures up to 39.5 MPa were performed also in this work. These measurements allowed the evaluation of existing models such as the well-known Geng and Duan model and the model recently developed by Zheng and Mao (ZM). The e-PR-CPA, Søreide−Whitson, and geochemical models used in our previous work were also used to process the new data. These last three models have been parameterized on measured and reported literature O_2 solubility data, and new optimized parameters of the ZM model have been proposed. These models reproduce the effect of temperature, pressure, and NaCl concentration on solubility with an average absolute deviation less than 5% from the measured data.

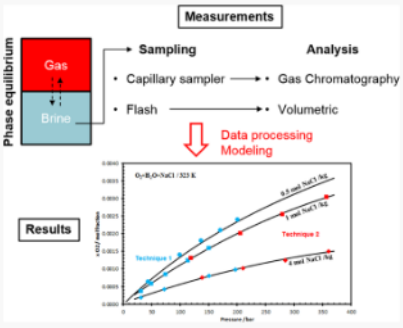

Abstract

Knowledge of the solubility of oxygen in natural water, which is generally saline, is important for several scientific and engineering fields. Applications such as geological storage of gas (containing O_2, e.g. flue gas) or energy (Compressed Air Energy Storage) operate at high pressure. However, to date, there is no high-pressure O_2 solubility data in brine, which has led researchers to develop models to predict this important property. To overcome this lack of data, solubility of O_2 in brine has been measured using two different techniques, at molalities between 0.5 and 4 m (NaCl), temperatures between 303 and 373 K and pressures up to 36 MPa. In order to validate the experimental methods, measurements of the solubility of CO_2 in highly concentrated brine (6m NaCl) at temperatures between 303 and 373 K and pressures up to 39.5 MPa, were performed also in this work. These measurements allowed the evaluation of existing models such as the well-known Geng and Duan model, and the model recently developed by Zheng and Mao (ZM). The e-PR-CPA, Soreide-Whitson, and geochemical models used in our previous work were also used to process the new data. These last three models have been parameterized on measured and reported literature O_2 solubility data, and new optimized parameters of the ZM model have been proposed. These models reproduce very well the effect of temperature, pressure and NaCl concentration on solubility with an average absolute deviation less than 5% from the measured data.

Keywords: O_2, CO_2, brine, solubility, Underground Gas Storage, CAES, Electrolyte CPA EoS, Measurement, Modeling

4.1 Introduction

Knowledge of the solubility of oxygen in natural water, which is generally saline, is important for several scientific and engineering fields such as hydrometallurgy [4. 1], bioprocess engineering [4. 2], oceanography and geochemistry [4. 3], etc. Underground gas and energy storage is one of the geochemical applications that require the knowledge of the phase equilibrium of the O_2 + water + salt mixture, since oxygen is generally always present in gas streams, whether as impurity as in the case of flue gases storage in the context of Carbon Capture and Storage (CCS), or in large quantities as in the case of Compressed Air Energy Storage (CAES). Due to its very high reactivity in the aqueous phase, oxygen can participate in geochemical reactions such as the oxidation of pyrite possibly present in the geological formation or can be used by micro-organisms leading to the contamination of the stored products [4. 4].

The oxycombustion process uses oxygen as an oxidant instead of air for energy production while avoiding NOx emissions and facilitating the recovery of CO_2 from the flue gases since they are mostly enriched by the latter. This technology needs large quantities of oxygen and requires the centralization of oxygen production and storage. In the framework of the ANR FLUIDSTORY project, an innovative concept (Electrolysis-Methanation-Oxycombustion (EMO) unit) [4. 5] for energy storage concerns the supply of oxycombustion with oxygen from water electrolysis using renewable electricity, and with methane produced by methanation using hydrogen from electrolysis as well and CO_2 recovered from oxycombustion flue gases. To manage the time laps between the production and use of these energy carriers (H_2, O_2, CH_4, and CO_2), the underground storage in salt caverns is suggested since it is considered to be the most suitable technique for massive gas storage. The risks related to the reactivity of oxygen, which are discussed earlier, must be considered in the case of storage of oxygen (pure or mixed) in salt caverns. Accurate determination of oxygen solubility in the aqueous phase (residual brine in the caverns) under the thermodynamic conditions of storage (temperature, pressure, and salinity) is therefore necessary.

Several experimental studies exist for the solubility of O_2 in pure and saline water. Existing data for these systems have been well reviewed by Battino [4. 6], and recently by Geng and Duan [4. 7] and Zheng and Mao [4. 8]. These reviews have shown that there is a great lack of high pressure solubility data especially for O_2 solubility in saline water which has only been studied at atmospheric pressure and low temperature ($\leq$ 318 K). This lack of data has prompted

researchers to develop models (Geng and Duan [4. 7], Li et al. [4. 9], Valderrama et al. [4. 10], Zheng and Mao [4. 8]) to estimate solubilities outside the range of available experimental data. Due to their unavailability to date, no data of O_2 solubility in salt water at high pressure were included in the adjustment of these models, hence the need for high pressure solubility measurements of O_2 in brine, and more specifically in NaCl brine since sodium and chloride are the main species present in natural saline water.

In this work, the solubility of O_2 in H_2O+NaCl with two different techniques was measured under geological storage conditions (temperature $303 \leq T\,(K) \leq 373$, pressure up to 36 MPa and NaCl molality $0.5 \leq m_{NaCl}\,(mol/kg_w) \leq 4$). CO_2 solubility measurements at very high molality (6 m_{NaCl}) were also performed to complete our previous work [4. 11] and also to validate the measurement technique. The modeling of literature data and the measured solubilities of this study, was performed using several models (e-PR-CPA, Soreide and Whitson, and geochemical models) developed and presented in our recent work [4. 11]. In order to improve the accuracy of the model proposed by Zheng and Mao, the model parameters were readjusted on experimental data including the new measured data.

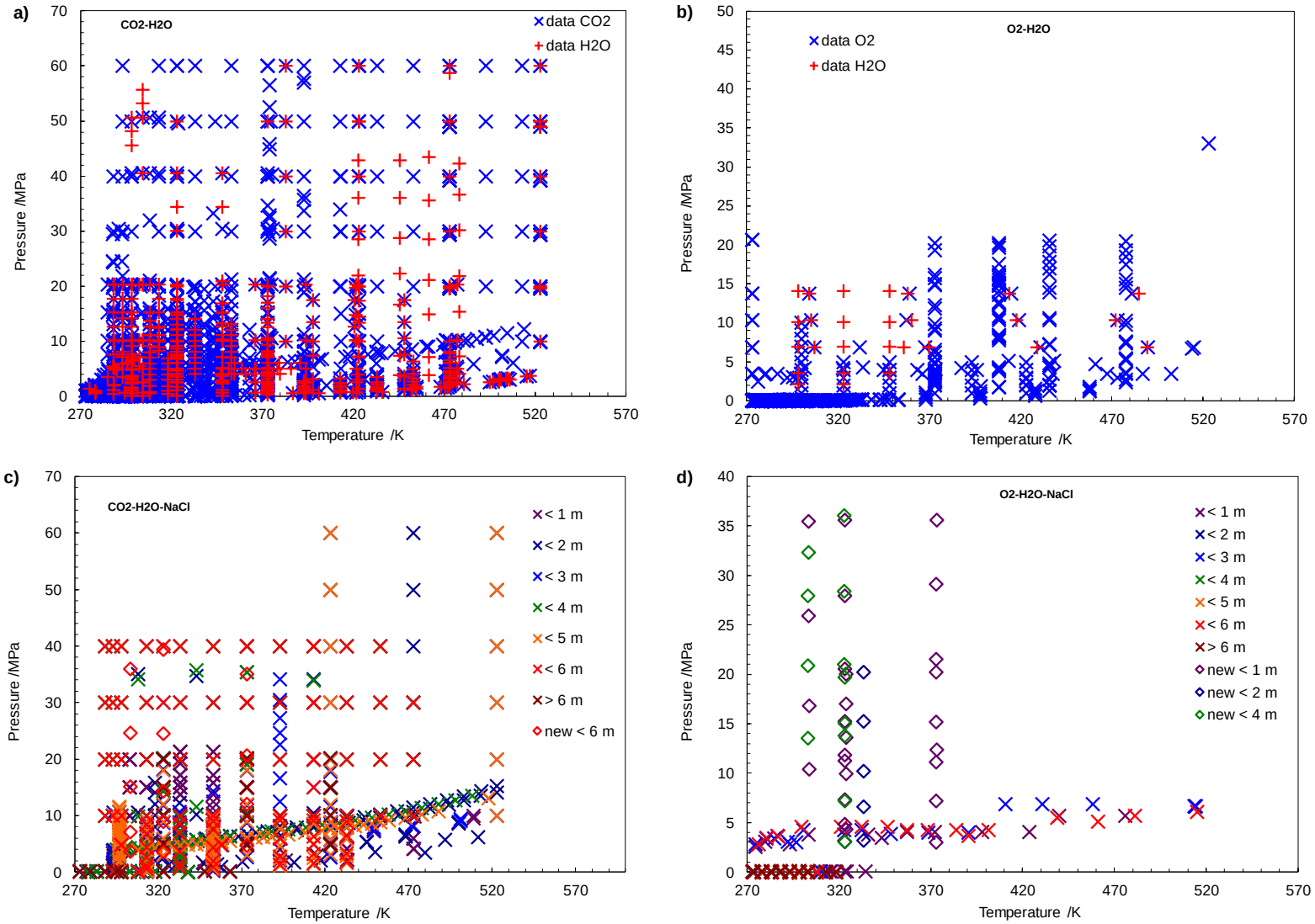

Figure 4.1 : Distribution of literature (×) and new measured (◊) solubility data. (a): CO_2+H_2O system (solubility and water content); (b): O_2+H_2O system (solubility and water content); (c): CO_2 solubility in NaCl brine; (d): O_2 solubility in NaCl brine.

4.2 Experimental

4.2.1 Literature and measured solubility data of CO_2 and O_2 in water and brine

In the literature, several reviews of CO_2 [4. 12, 13, 14] and O_2 [4. 6, 7, 8] solubility data in water and brine are available. To list the literature data and those measured in this work, the distribution of these data sets are presented in Figure 4.1 as a function of temperature, pressure and NaCl molality. As shown in this figure, data on the solubility of CO_2 in H_2O+NaCl (Figure 4.1.a and 4.1.c) and the solubility of O_2 in H_2O (Figure 4.1.b) are widely available. However, the measurements made in this work fill the lack of solubility data in brine at high pressure especially for O_2 (Figure 4.1.d).

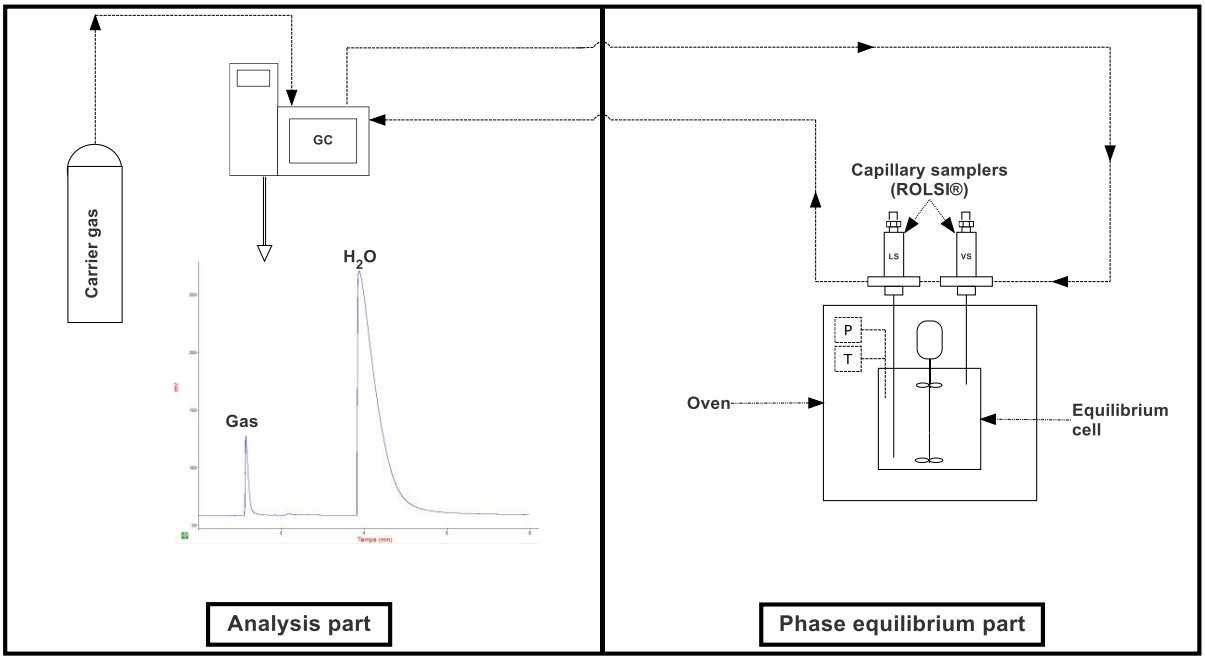

Figure 4.2 : Simplified schematic representation of the "static-analytic" apparatus for phase equilibria measurement.

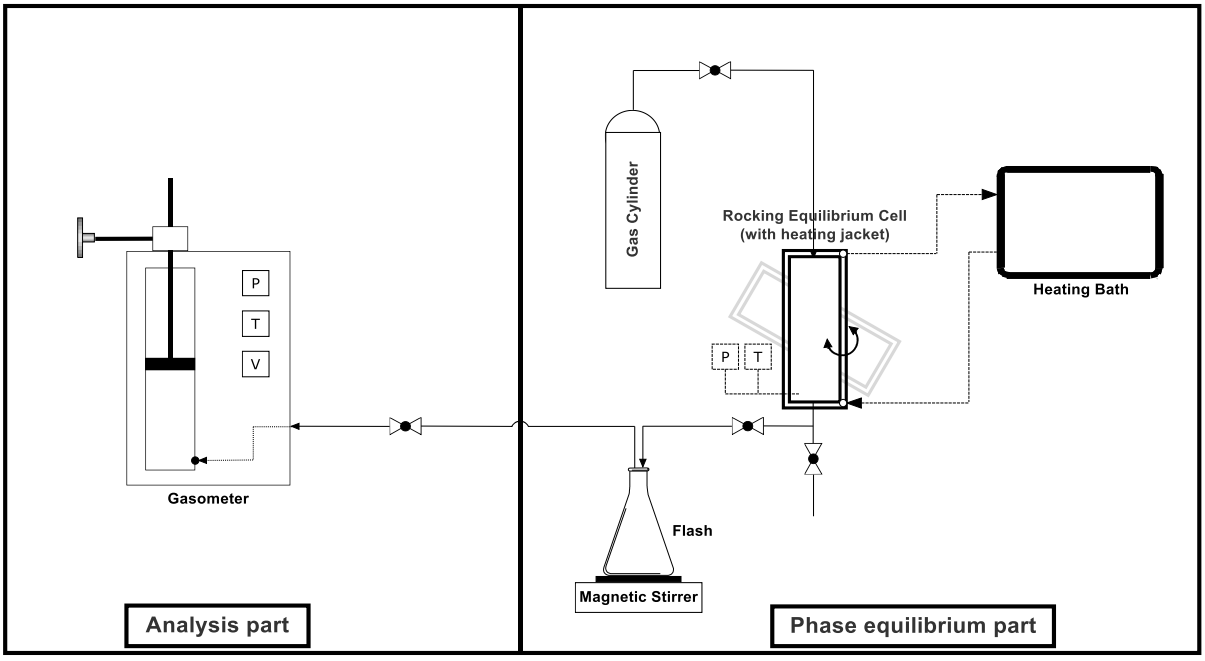

Figure 4.3 : Simplified schematic representation of the "Rocking cell" apparatus for solubility measurement.

4.2.2 Materials

In Table 4.1, the suppliers of the chemicals (CO_2, O_2 and NaCl) and the given purities are listed. Carbon dioxide (CO_2, CAS Number: 124-38-9) and oxygen (O_2, CAS Number: 7782-44-7) were purchased from BOC with a certified volume purity greater than 99.995%. Sodium Chloride (NaCl, CAS Number: 7647-14-5) was purchased from Fisher Chemical with a certified purity of 99.6%. Water (H_2O, CAS Number: 7732-18-5) was deionized and degassed before the preparation of the brine (H_2O + NaCl).

Table 4.1 : Chemical samples used for experimental work (CAS Registry Number, mole fraction purity and suppliers of chemicals).

Chemicals	CAS Reg. No.	Purity	Analysis method	Supplier
CO_2	124-38-9	99.995 mol%	GC[a]	BOC
O_2	7782-44-7	99.995 mol%	GC[a]	BOC / Air Liquide
NaCl	7647-14-5	99.6%	None	Fisher Chemical
H_2O (ultrapure)	7732-18-5	18.2 MΩ·cm		MilliporeTM (direct-Q5)

a: Gas Chromatography

4.2.3 Apparatus and method

4.2.3.1 Static-analytic setup

The first setup used in this work is based on the static-analytic method and is described in detail in our recent work [4. 11]. However, in Figure 4.2, a simplified description of this technique is illustrated. It consists of an equilibrium cell positioned in an oven for temperature control, and equipped with pressure transducers, temperature probes and two ROLSI® (Rapid On-Line Sampler-Injector, French patent number 0304073) capillary samplers for each phase (liquid and vapor). After setting the temperature and charging the cell with the salt solution and the gas up to the desired pressure, the thermodynamic equilibrium is reached in some dozens of minutes after continuous agitation, assuming that the equilibrium is verified by the stabilization of the temperature and pressure in the cell. Several samples are then taken by the liquid ROLSI® and sent through a transfer line to GC (Gas Chromatography) to determine the mole fraction of gas and water.

4.2.3.2 Rocking cell setup (volumetric technique)

The rocking cell setup illustrated in Figure 4.3 is based on a volumetric technique. It is the same as that presented by Chapoy et al. [4. 15] and recently used by Ahmadi and Chapoy [4. 14]. It consists of a rocking equilibrium cell with a volume of 350 cm^3 mounted on an adjustable rotary axis of the pneumatic rocking system and surrounded by a heating jacket connected to a thermostat bath to maintain a constant temperature. The cell is equipped with a Quartzdyne pressure transducer and a platinum resistance thermometer placed in the heating jacket of the cell. Since the temperature probe is not placed inside the cell, the real temperature in the cell is determined by calibration with respect to the jacket temperature.

For each measured point, the following procedure was followed: setting the target temperature, introducing 300 cm^3 of the saline solution and evacuating the equilibrium cell to remove the air. Then, the gas is introduced until the desired pressure is reached. The gas injection line is disconnected to allow the shaking of the system by the rocking system. Once the pressure and temperature are stabilized, the rocking is stopped and the cell is locked in a vertical position to take a sample of the aqueous phase. The gas injection line is reconnected to the cell, the flash tank is connected to the bottom of the cell to collect the sample, and the gasometer (VINCI TECHNOLOGIES) is connected to the flash tank. During sampling, the gas is injected continuously to maintain a constant pressure. The gas is separated from the liquid at the flash

tank and transferred to the gasometer. The volume difference at constant pressure and temperature is then determined using the gasometer and knowing the density of the pure gas, the mass of the gas is deduced. The mass of the brine is determined gravimetrically using a balance. Finally, by knowing the quantities of gas and brine in the sample, the solubility of the gas is obtained. The calculation procedure is described in detail by Ahmadi and Chapoy [4. 14]. More gas is added to increase the pressure, and the procedure is repeated to measure another equilibrium point.

4.2.4 Experimental results

In this section, measurements concerning the high-pressure solubility of CO_2 and O_2 in H_2O + NaCl are presented. The standard uncertainties u (T), u (P) and u (x) of the measurements performed by the static-analytic setup were calculated by the NIST method [4. 16]. The calibration (the polynomial correlation) uncertainty and repeatability uncertainty are the two sources of uncertainties involved in the calculation of u (T) and u (P). The third source of uncertainty was associated with the injection of the pure compound by the syringe during GC calibration, u (x). For the measurements carried out with the Rocking Cell apparatus, the uncertainties for temperature, pressure and composition were calculated in the same way as that of Ahmadi and Chapoy [4. 14], since the same installation and the same calibrations were used. The standard uncertainties for temperature $u(T)$ and pressure $u(P)$ are 0.02 K and 0.005 MPa respectively for the static-analytic setup and 0.17 K and 0.068 MPa respectively for the rocking cell setup. The standard uncertainties related to the measurement of the composition u (x_{CO_2}) and u (x_{O_2}) are listed with the results in Tables 4.2 and 4.3. The gas solubility is expressed as "salt-free" mole fractions: $x_{gas} = m_{gas}/(m_{gas} + 1000/M_{H_2O})$, m_{gas} is the gas molality (in mol/kg_w), and M_{H_2O} is the molecular weight of water (in g/mol) .

4.2.4.1 CO_2 solubility in H_2O + NaCl

The experimental measurements of the CO_2+H_2O+NaCl system were performed by the rocking cell setup at molality of 6 m (mol NaCl/kg_w), temperatures between 303 and 373 K and pressures up to 39.5 MPa and are listed in Table 4.2. These measurements were used to validate the experimental setup by comparing some obtained results with literature data from Messabeb et al. [4. 13] and Zhao et al. [4. 17] (Figure 4.4), and also to complement the existing data for this system, especially at high pressure.

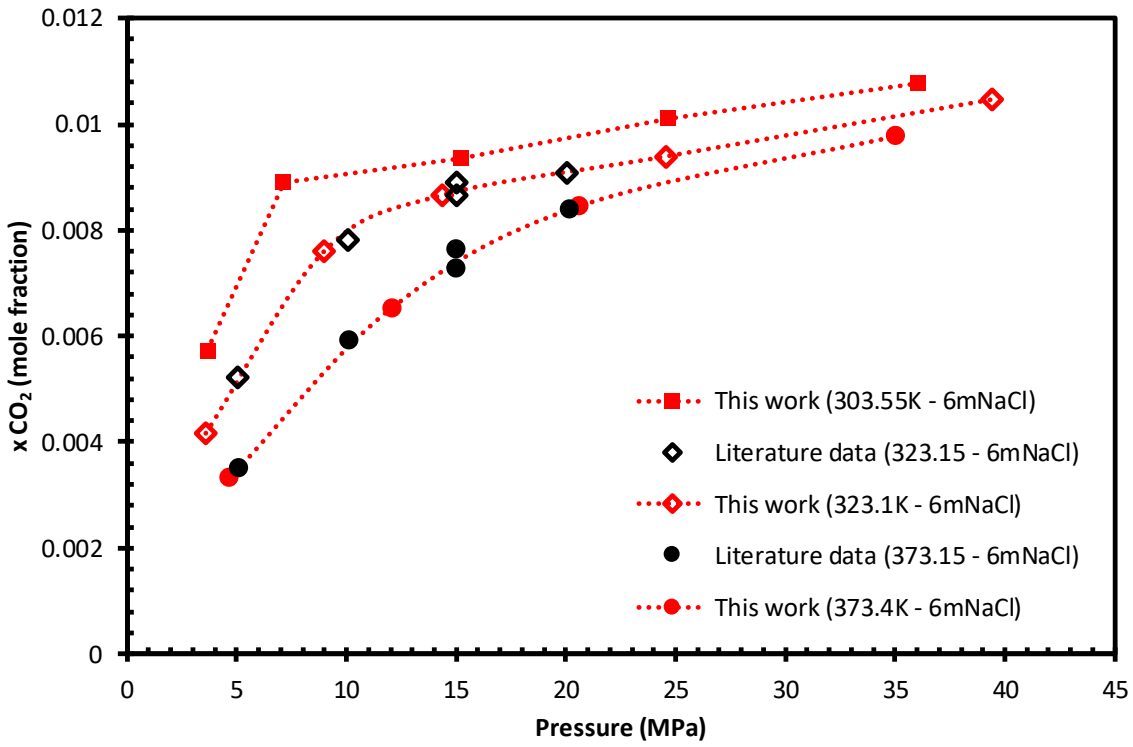

Figure 4.4 : CO_2+H_2O+NaCl system : Experimental CO_2 solubility in 6m NaCl-brine at 323 K and 373 K. The black symbols are the literature data [4. 13, 17], and the red symbols with dotted lines (to guide the eye) are the measured data.

Table 4.2 : Measured solubility of CO_2 in the H_2O + NaCl at 6 mol/kg$_w$ NaCl by the rocking cell setup, expressed as "salt-free" mole fractions x_{CO_2} and their standard uncertainties $u(x_{CO_2})$. $u(m_{NaCl}) = 0.002$ mol/kg$_w$, $u(T) = 0.17\ K$ and $u(P) = 0.068\ MPa$.

Equilibrium	T (K)	P (MPa)	x_{CO_2}	$u(x_{CO_2})$
Vapor-Liquid (VLE)	303.55	3.6721	0.00572	0.00010
VLE	303.55	7.1333	0.00890	0.00008
Liquid-Liquid (LLE)	303.55	15.1857	0.00936	0.00010
LLE	303.55	24.6777	0.01012	0.00010
LLE	303.55	36.0196	0.01077	0.00010
VLE	323.10	3.5818	0.00418	0.00010
VLE	323.10	8.9744	0.00760	0.00007
VLE	323.10	14.3618	0.00866	0.00009
VLE	323.10	24.5798	0.00939	0.00010
VLE	323.10	39.4477	0.01046	0.00010
VLE	373.29	4.676	0.00333	0.00010
VLE	373.39	12.0603	0.00654	0.00006
VLE	373.39	20.5905	0.00846	0.00008
VLE	373.39	35.0185	0.00978	0.00010

4.2.4.2 O_2 solubility in H_2O + NaCl

The solubility of O_2 in H_2O+NaCl was measured with both apparatus (technique 1: static-analytic, technique 2: rocking cell (volumetric)). The experimental results obtained at molalities between 0.5 and 4 m, temperatures between 303 and 373 K and pressures up to 36 MPa, are listed in Table 4.3. For validation purpose, some measurements were made with both techniques under the same experimental conditions (T, P, mNaCl). As shown in Figure 4.5, the two datasets are consistent and follow similar trends, which validates both measurement techniques (including equipment and calibration).

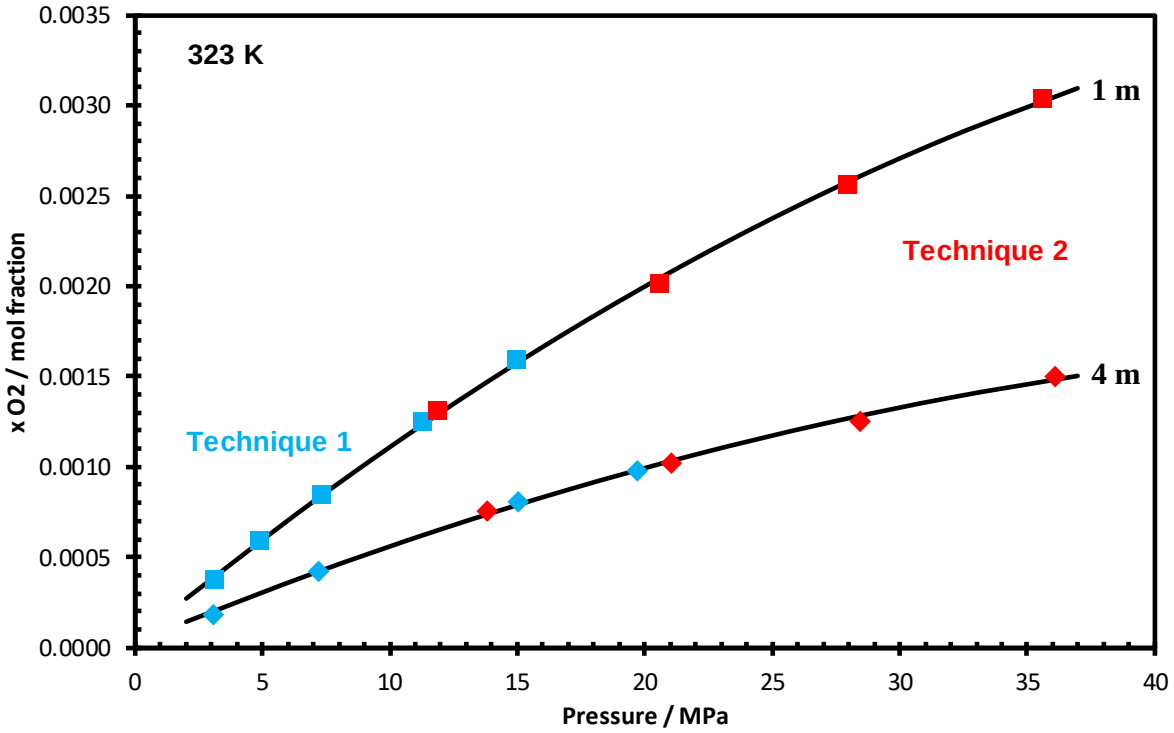

Figure 4.5 : O_2+H_2O+NaCl system : Validation of measured O_2 solubility data in 1m and 4m NaCl-brine at 323 K. The blue and red symbols represent data measured by the Technique 1 and 2 respectively. The solid lines represent a trend line to guide the eye.

Table 4.3 : Measured solubility of O_2 in the H_2O + NaCl, expressed as "salt-free" mole fractions x_{O_2} and their standard uncertainties $u(x_{O_2})$. $u(m_{NaCl}) = 0.002$ mol/kg$_w$, for

Technique 1: $u(T) = 0.02\ K$ and $u(P) = 0.005\ MPa$; For Technique 2: $u(T) = 0.17\ K$ and $u(P) = 0.068\ MPa$.

Technique	m_{NaCl} (mol/kg_w)	T (K)	P (MPa)	x_{O_2}	$u(x_{O_2})$
Technique 1: static-analytic	0.5	324.00	4.3540	0.00064	0.000020
		323.95	9.9310	0.00140	0.000100
		323.94	13.6330	0.00180	0.000100
		323.93	17.0180	0.00210	0.000100
		323.93	20.0710	0.00240	0.000100
	1	323.16	3.1210	0.00038	0.000010
		323.17	7.3479	0.00085	0.000020
		323.14	4.8790	0.00059	0.000010
		323.14	11.2857	0.00125	0.000040
		323.17	15.2399	0.00160	0.000050
	4	323.18	3.0720	0.00018	0.000010
		323.16	7.2104	0.00042	0.000010
		323.13	15.0404	0.00080	0.000030
		323.16	19.6893	0.00098	0.000030
	1*	372.92	3.0516	0.00029	0.000010
		373.11	7.2294	0.00070	0.000010
		373.07	11.1250	0.00106	0.000020
		373.10	15.1719	0.00139	0.000020
		373.09	20.2617	0.00175	0.000040
	2	333.30	3.1964	0.00029	0.000010
		333.53	6.6156	0.00057	0.000010
		333.53	10.2178	0.00083	0.000060
		333.52	15.2950	0.00118	0.000040
		333.53	20.2640	0.00146	0.000080
Technique 2: rocking cell (volumetric)	1	303.74	10.4249	0.00141	0.000050
		303.74	16.8653	0.00206	0.000053
		303.55	25.9464	0.00290	0.000055
		303.55	35.4577	0.00350	0.000058
	1	323.20	11.8555	0.00131	0.000050
		323.20	20.5567	0.00201	0.000054
		323.20	27.9341	0.00256	0.000055
		323.20	35.6287	0.00304	0.000056
	1	373.10	29.1304	0.00245	0.000054
		373.10	21.5461	0.00197	0.000054
		373.19	12.3554	0.00129	0.000053

	373.19	35.5839	0.00286	0.000055
4	303.26	13.5379	0.00078	0.000050
	303.26	20.8808	0.00112	0.000053
	303.26	27.9272	0.00134	0.000053
	303.64	32.3123	0.00153	0.000054
4	323.10	13.8274	0.00075	0.000050
	323.01	21.0325	0.00102	0.000053
	323.01	28.4305	0.00125	0.000054
	323.01	36.0630	0.00150	0.000054

* Initial NaCl molality must have increased due to experimental error (see explanation in Section 4.2.).

4.3 Thermodynamic modeling

The models used in this work are fully programmed and parameterized, and are described in detail in our recent work [4. 11]. These models are based on two thermodynamic approaches:

- Asymmetric (gamma-phi) approach:

Being simple and fast, the gamma-phi approach is the most used approach by geochemists for correlating gas solubility data in water and brine. This approach consists of using an equation of state for the gas phase and an activity coefficient model for the liquid phase. Among the best known works are those of Duan et al. [4. 18, 19] and Spycher et al. [4. 20, 21] on the solubility of CO_2 in water/brine, and those of Geng and Duan [4. 7] and Valderrama et al. [4. 10] on the solubility of O_2 in water/brine.

The geochemical model implemented in CHESS/HYTEC software (Corvisier, 2013 [4. 22]; Corvisier et al., 2013 [4. 23]) was used, as well as the model proposed by Zheng and Mao [4. 8] was reparameterized by including the new measured data from this work.

- Symmetric (phi-phi) approach:

Unlike the asymmetric approach, the symmetric approach consists in representing all the fluid phases (liquid and vapor) of the system with a single equation of state. Using this approach, two types of equations of state (cubic and non-cubic) were used.

The first EoS is the Soreide-Whitson model [4. 24] (revision of the PR model) which is widely used in reservoir engineering (mixture of gas, oil, water, salts, etc.), and is implemented in several modeling and simulation software (Eclipse 300 - Schlumberger, IPM - Petex, Simulis Thermodynamics – Prosim France, etc.).

The second EoS used is the e-PR-CPA (electrolyte Peng-Robinson Cubic Plus Association) model that was presented in our previous work [4. 11]. With this model, all molecular and electrolyte interactions are taken into account. In the e-PR-CPA model, the PR cubic EoS has been selected to represent attractive and dispersive interactions, and the Wertheim's theory (used in SAFT and CPA type EoS) has been considered to account for the association phenomenon. Concerning electrolyte interactions, the long-range interactions (between ions) are taken into account by the MSA (Mean Spherical Approximation) theory, and the phenomenon of solvation of the ions by the solvent (water) is considered by the Born term.

4.4 Results and discussions

4.4.1 CO_2 + H_2O + NaCl system

The solubility of CO_2 in the CO_2 + H_2O + NaCl system was modeled by the Soreide and Whitson models (SW, with improved binary interaction parameters, see Chabab et al. [4. 11]) and the e-PR-CPA model using the phi-phi approach, as well as the geochemical model using the gamma-phi approach. For the e-PR-CPA model the solvation of CO_2 by water molecules was considered by attributing to CO_2 a single electron acceptor association site and to H_2O four association sites (2 electron donor sites and 2 electron acceptor sites). The predictions were compared with data from the literature and those measured in this work. This was done under geological storage conditions, either in saline aquifers (low or medium salinity) or in salt caverns (saturated brine). An example of modeling results at different salinities (in terms of molality), ranging from pure water to saline water with very high salt concentration (close to saturation ~ 6m NaCl), is shown in figure 4.6. The model predictions are in good agreement with the literature and measured solubility data. In Table 4.6, calculations of CO_2 solubility in water and NaCl brine generated by the e-PR-CPA model over a wide range of temperature, pressure and molality are listed.

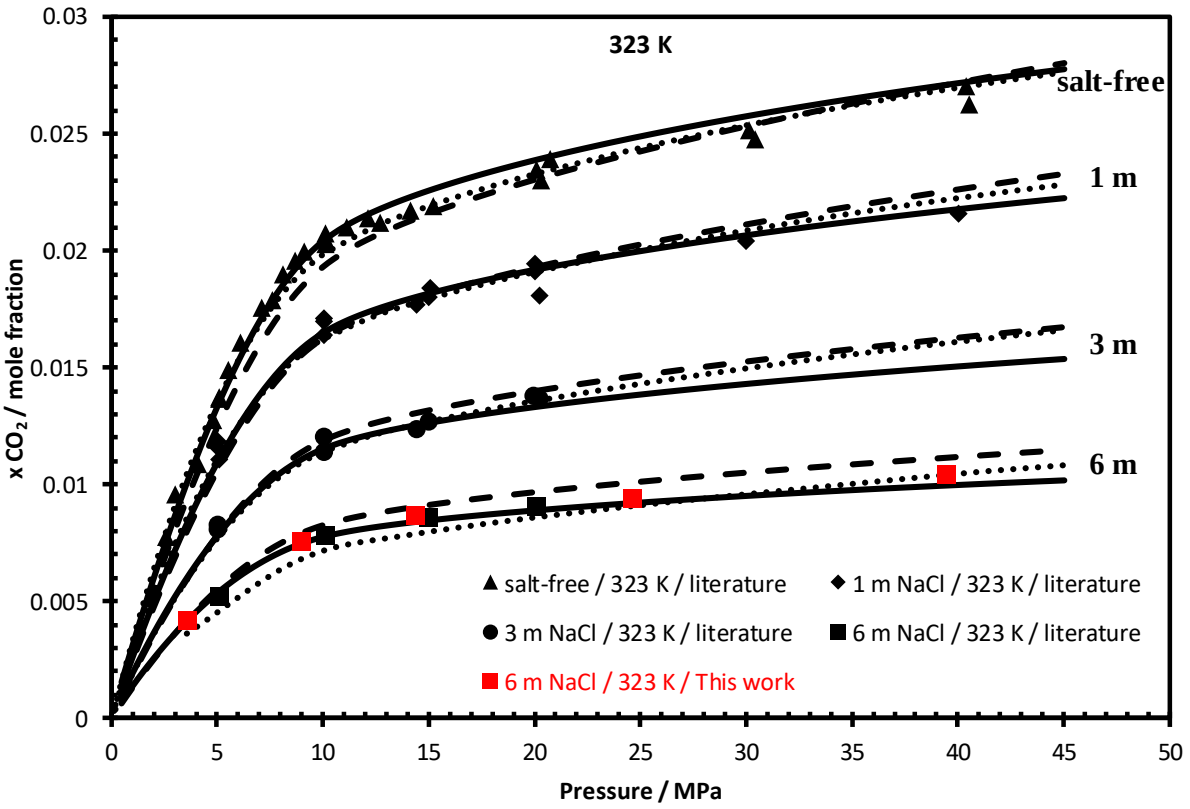

Figure 4.6 : CO_2+H_2O+NaCl system : Prediction of CO_2 solubility at different NaCl molality m (mol/kg_w) by e-PR-CPA (solid line), SW (dashed line) and geochemical (dotted line) models. The black symbols are the literature data [4. 13, 14, 25, 26, 27, 28, 29, 30, 31], and the red symbols are the measured data (Table 4.2).

4.4.2 O_2 + H_2O + NaCl system

In order to check more or less the consistency of the measured solubilities of O_2 in water + NaCl, we verified the linearity of the experimental data in terms of $Ln(P/xO_2)$ as a function of P, following the Krichevsky-Kasarnovsky [4. 32] approach. This linearity condition can be easily demonstrated from the gamma-phi approach, by considering the fugacity coefficient of the gas (Li et al. [4. 9]) or by neglecting it (assuming that the vapor phase is ideal, see Descamps et al. [4. 33]).

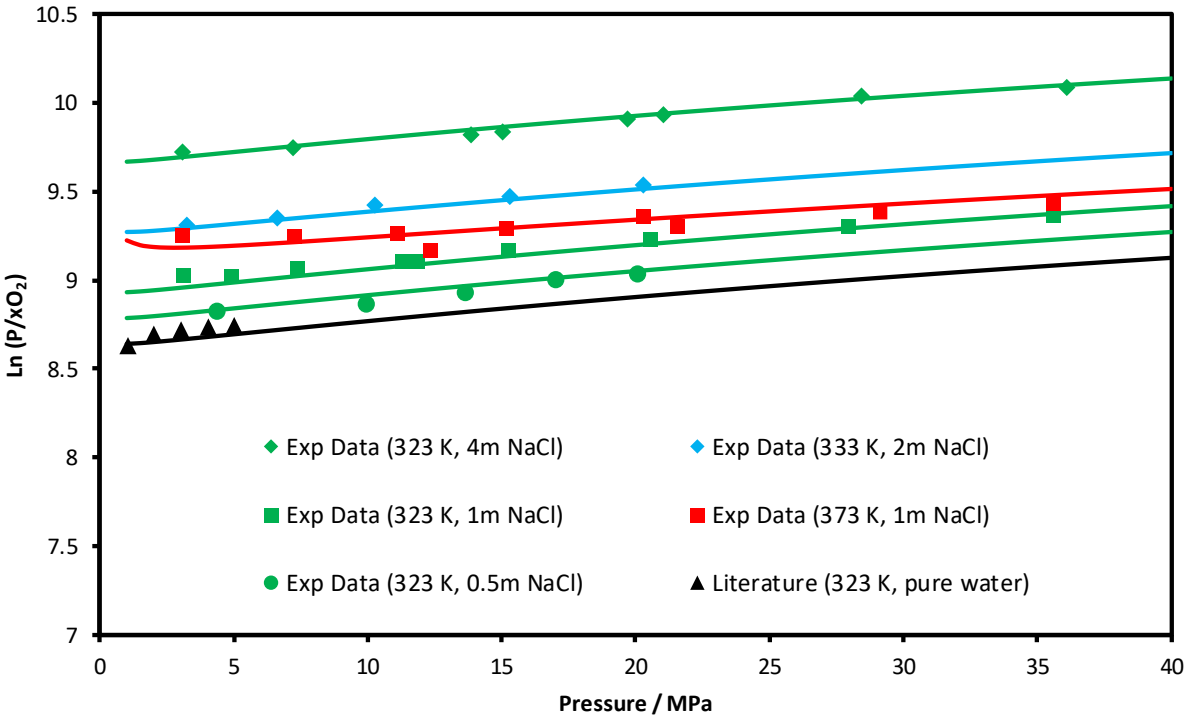

Figure 4.7 : Solubility of O_2 in H_2O + NaCl at different NaCl molality m (mol/kg$_w$). The black symbols are the literature data [4. 34], the red symbols are the measured data (Table 4.3), and the solid lines are the prediction by e-PR-CPA model.

In Figure 4.7, the linearity of the experimental data was checked and compared with the predictions of the e-PR-CPA model. All measurements appear to be consistent and linear except for the isotherm at 373 K (1m NaCl). This inconsistency with respect to this isotherm can be explained by the fact that the points were not measured at the same molality, since we used two different techniques. The deviations concern only the measurements made with the technique 1 at 373 K (1m), assuming that the initial molality has increased, since by mistake, after filling the cell with the prepared brine solution (at 1m), we evacuated it at high temperature (373 K). This allowed the water to evaporate more and increase the molality.

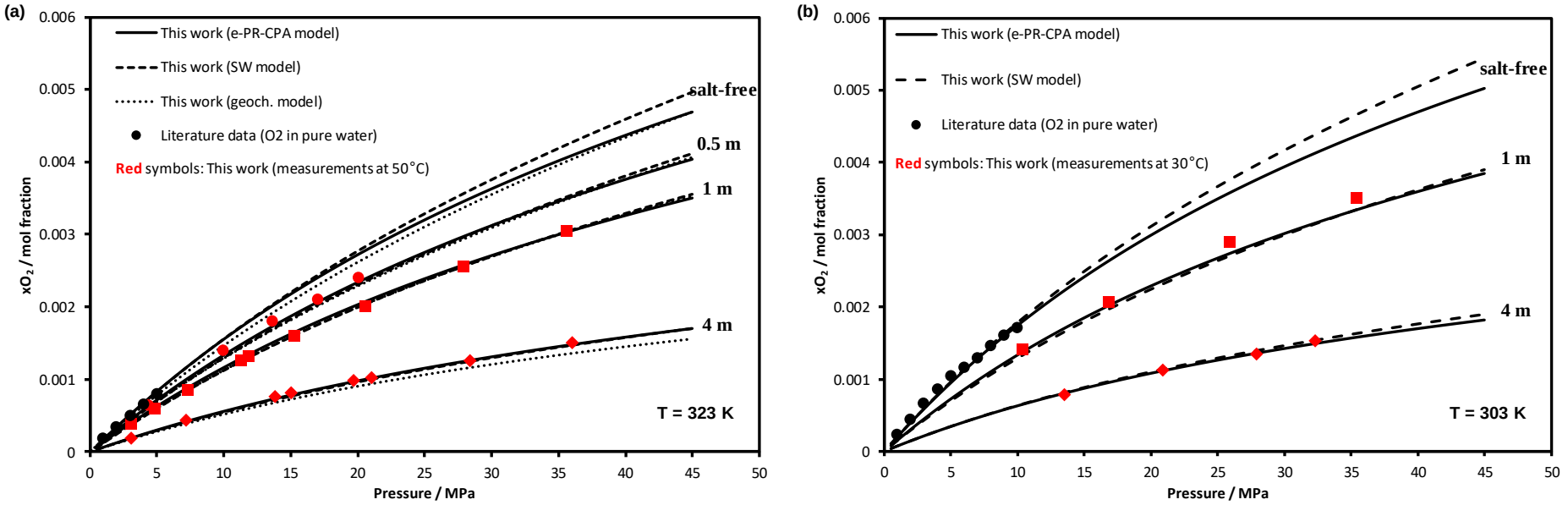

Figure 4.8 : O_2+H_2O+NaCl system : Prediction of O_2 solubility at different NaCl molality m (mol/kg_w) by e-PR-CPA (solid line), SW (dashed line) and geochemical (dotted line) models. The black symbols are the literature data ((a) : [4. 34], (b) : [4. 35]), and the red symbols are the measured data (Table 4.3).

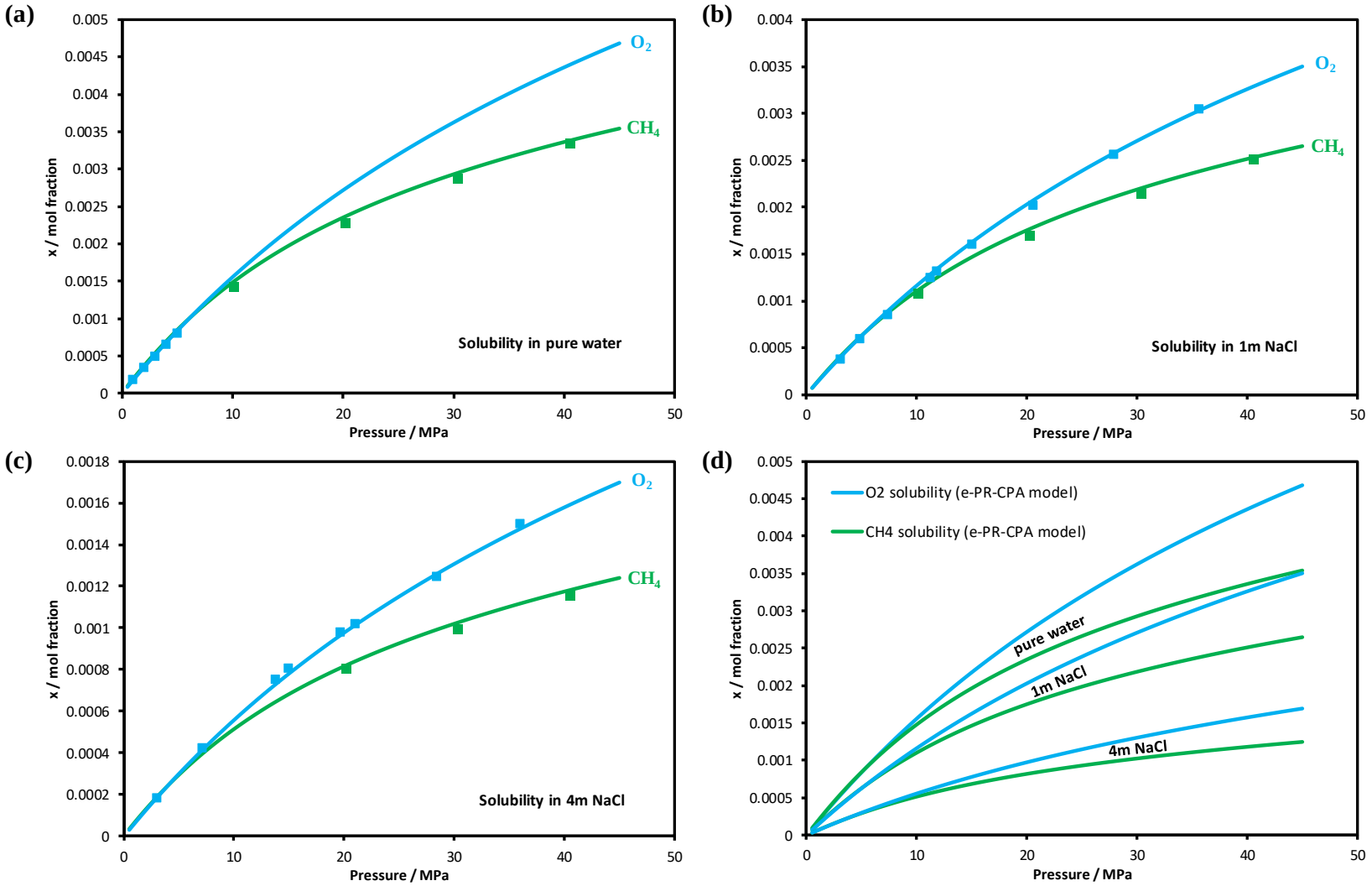

Figure 4.9 : Comparison of O_2 and CH_4 solubilities in pure water (a) and NaCl brine (water+NaCl; b: 1m; c: 4m; d: 0-4m; m=mol/kgw) at 323 K. The symbols represent the experimental data (O_2 in water: [4. 34]; O_2 in brine: from this work (Table 3); CH_4 in water and brine: [4. 36]) and the solid lines represent the predictions by the e-PR-CPA model.

The solubility of O_2 in H_2O + NaCl was also modeled by the three models. The binary interaction parameters of the different models were fitted to the literature and measured data. For the e-PR-CPA model, the cross-association (solvation) between O_2 molecules and H_2O molecules was not considered (no Lewis Acid-Lewis Base interaction), since O_2 is not considered as an associative species. Therefore, only the binary interaction parameters $k_{O_2-H_2O}$ and k_{O_2-ion} were adjusted. As in our previous work [4. 11], we considered temperature dependence in k_{gas-H_2O} and salt molality dependence in $k_{gas-ion}$.

$$k_{O_2-H_2O} = 9.51493975 \times 10^{-11} T^2 + 3.22791135 \times 10^{-3} T - 0.726309790 \quad \textbf{(4.1)}$$

$$k_{O_2-Na^+} = -1.49034322 \times m_{NaCl} + 0.10603754 \quad \textbf{(4.2)}$$

$$k_{O_2-Cl^-} = 1.286649425 \times m_{NaCl} - 0.62173576 \quad \textbf{(4.3)}$$

The "asymmetric" binary interaction parameters (one for each phase) of the Soreide and Whitson (SW) model depend on temperature (in K) and salt molality. In the original paper of the SW model [4. 24], there is no expression of these parameters for O_2. We propose the following expression (the same is used for N_2 in the original paper) whose coefficients (Table 4.4) have been fitted to solubility and water content data:

$$\left(k^{AQ}_{O_2,H_2O}\right)_{SW} = A_0(1 + \alpha_0 {m_{NaCl}}^{0.8}) + A_1 \frac{T}{T_{c,O_2}}(1 + \alpha_1 {m_{NaCl}}^{0.8}) \quad \textbf{(4.4)}$$

$$\left(k^{NA}_{O_2,H_2O}\right)_{SW} = 0.58165 \quad \textbf{(4.5)}$$

Table 4.4 : Coefficients of the binary interaction parameter $\left(k^{AQ}_{O_2,H_2O}\right)_{SW}$ of the SW model (Equation 4.4)

A_0	α_0	A_1	α_1	$T_{c,O_2}\ (K)$
-1.1677444	3.361921×10^{-2}	0.4666067	8.4573057×10^{-2}	154.581

The geochemical model, based on a dissymmetrical approach, solves a large set of mass balances and mass action laws to calculate the whole system speciation (i.e. aqueous, gaseous and solid quantities and activities/fugacities). Equations shall remain generic, in order that the

model handles multi-components either for the gas phase and the electrolyte. For the gas phase, the PR-SW EoS is used with the classical mixing rule. For the aqueous solution and particularly for saline solutions with high ionic strength, activity coefficients can be calculated using Specific Ion Theory (SIT) showing satisfactory results.

It requires a thermodynamic database and simulations presented here are run along with the Thermoddem database including Henry's constants and parameters for PR-SW EoS (Blanc et al. 2012 [4. 37]), and parameters for molar volume of the dissolved gaseous component at infinite dilution (Shock et al. 1989 [4. 38]; Schulte et al. 2001 [4. 39]). Gas binary interaction parameters for PR-SW and aqueous binary interactions parameters for SIT have been fitted on experimental data.

- $k_{CO_2H_2O}$ and $k_{O_2H_2O}$ are equal to 0.193 and 0.591 respectively.
- $\varepsilon_{H^+Cl^-}$ and $\varepsilon_{Na^+Cl^-}$ are equal to -0.097 and -0.035 using HCl and NaCl solutions activity measurements (Schneider et al., 2004 [4. 40]; Sakaida and Kakiuchi, 2011 [4. 41]; Khoshkbarchi and Vera, 1996 [4. 42]).
- $\varepsilon_{CO_2Na^+}$ varies with temperature (from 0.085 at 298 K to 0.077 at 473 K) and $\varepsilon_{O_2Na^+}$ as well (from 0.124 at 298 K to 0.107 at 473 K) using numerous CO_2 and O_2 solubility measurements in NaCl solutions.

As shown in Figure 4.8, comparing with measured and literature [4. 34, 35] data, the models capture qualitatively (salting-out effect) and quantitatively very well the effect of NaCl on solubility over a wide range of pressure and molality. The e-PR-CPA, SW, and geochemical models respectively reproduce the O_2 solubility with an average absolute deviation of 2.8%, 2.9%, and 4.3% from the measured data. It should be noted that the geochemical model has been fitted to all literature and measured data, and most of these data are at low pressure and temperature, therefore it is more accurate at low pressure. The e-PR-CPA and SW models have been adjusted on high pressure data (≥1 MPa), hence they estimate the solubility at high pressure more precisely. The calculated values for solubility of O_2 in water and NaCl brine estimated using the e-PR-CPA model over a wide range of temperature, pressure and molality are listed in Table 4.7. In Figure 4.9, the solubility of O_2 in pure water and NaCl brine was compared with that of CH_4 under the same conditions of temperature (323 K) and NaCl molality (0, 1 and 4 mol/kg of water). The e-PR-CPA model also predicts well the solubility of CH_4 in pure water and brine an average absolute deviation of 1.9% and BIAS of 0.8%. The binary interaction coefficients for CH_4–H_2O are provided in Equations 6-8. In Figure 9, it is observed

that the solubility in pure water and brine of O_2 becomes more important than that of CH_4 at high pressure, which is not the case at lower pressures (<5 MPa). Moreover, the binary gas/water interaction parameters are more important for O_2 (between 0.24 and 0.48 for temperatures between 298 and 373 K) than CH_4 (between 0.11 and 0.29 for temperatures between 298 and 373 K). This can perhaps be explained by the difference in polarizability between the molecules of O_2 (1.6 Å3) and CH_4 (2.6 Å3) [4. 43]: O_2 is less polarizable, so the attractive water-gas interactions are less strong for O_2 than for CH_4.

$$k_{CH_4-H_2O} = -8.270968 \times 10^{-6}T^2 + 8.012843 \times 10^{-3}T - 1.543212 \quad \textbf{(4.6)}$$

$$k_{CH_4-\mathrm{Na}^+} = -0.93612817 \times m_{NaCl} - 2.78121097 \quad \textbf{(4.7)}$$

$$k_{CH_4-\mathrm{Cl}^-} = 0.66659884 \times m_{NaCl} + 2.46759704 \quad \textbf{(4.8)}$$

The difference in solubility of CH_4 and O_2 can be explained by their size. The critical volume of methane (98.62 cm3/mol [4. 44]) is larger than that of oxygen (73.36 cm3/mol [4. 44]), which is related to the size of the molecule. Therefore, methane requires more energy than oxygen to form a cavity in the aqueous phase. The same remark was given by Battino and Seybold [4. 45] to explain the mystery of the solubilities of O_2 and N_2 in water.

The interaction parameters $\lambda_{O_2-Na^+}$ and $\xi_{O_2-Na^+-Cl^-}$ of the Zheng and Mao (ZM) [4. 8] model have been readjusted by including the new measured data. In Table 4.5, the old and new parameters are listed, and the comparison of the O_2 solubility predictions using the two sets of parameters is shown in Figure 4.10. With the new parameters, the solubility calculation by the ZM model has been improved by reproducing the new measured data with an absolute average deviation of 4% instead of 11% (with the original parameters).

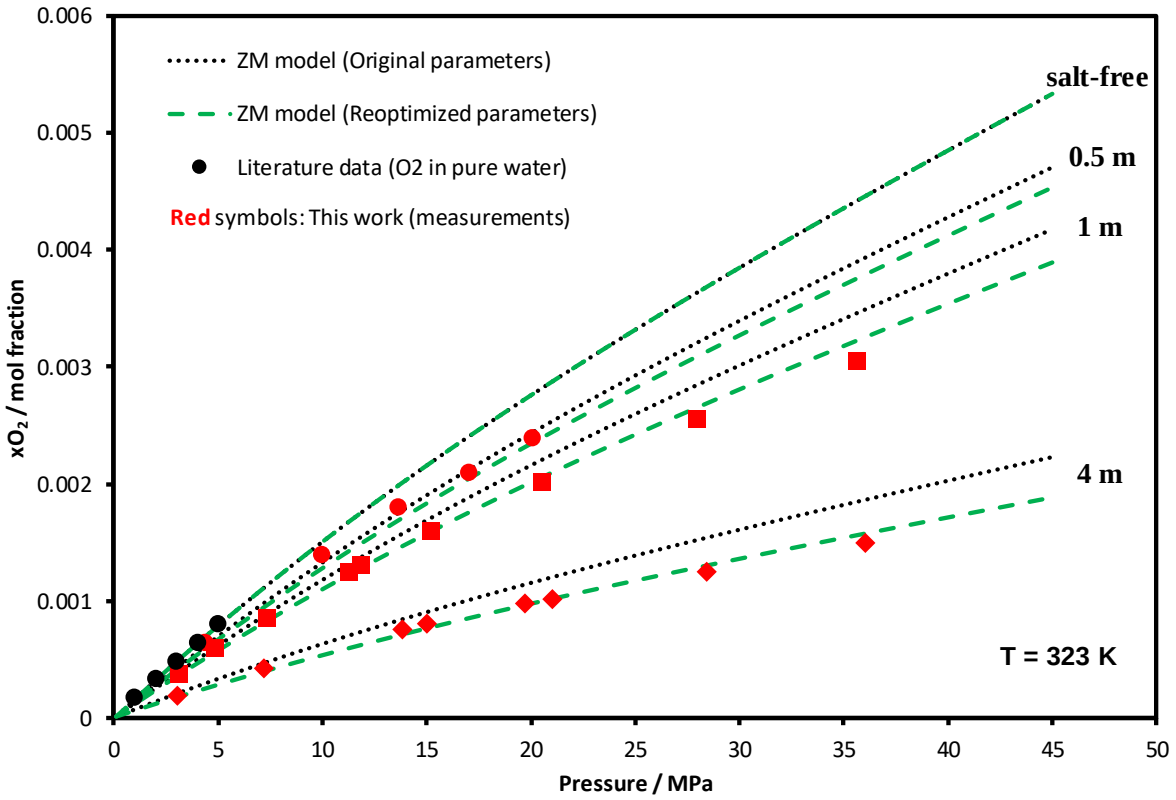

Figure 4.10 : O_2+H_2O+NaCl system : Calculation of O_2 solubility at different NaCl molality m (mol/kg_w) by the Zheng and Mao (ZM) model using original (dotted line) and reoptimized (dashed line) parameters (Table 4.4). The black symbols are the literature data [4. 34], and the red symbols are the measured data (Table 4.3).

Table 4.5 : Zheng and Mao model interaction parameters for the O_2 solubility in NaCl brine

ZM model parameters	$\lambda_{O_2-Na^+}$	$\xi_{O_2-Na^+-Cl^-}$	AAD (%) [a]
Original [4. 8]	$0.4670997 - 0.10500795 \times 10^{-2}T$	$-0.90085535 \times 10^{-2}$	11.23
Reoptimized (this work)	$0.33428760 - 5.14803685 \times 10^{-4}T$	$-1.8659617215 \times 10^{-2}$	3.97

[a] AAD %: average absolute deviation (from the data measured in this work), AAD % $= \frac{100}{N_{exp}} \sum_{i=1}^{N_{exp}} \left(\left| \frac{x_{O_2\ i}^{cal} - x_{O_2\ i}^{exp}}{x_{O_2\ i}^{exp}} \right| \right)$

In Figure 4.11, one of the isotherms measured in this work was compared with the predictions of the well-known Geng and Duan [4. 7] model. The predictions are somewhat acceptable (underestimation of the O_2 solubility in brine), but can be improved by readjusting the model parameters by including the new data.

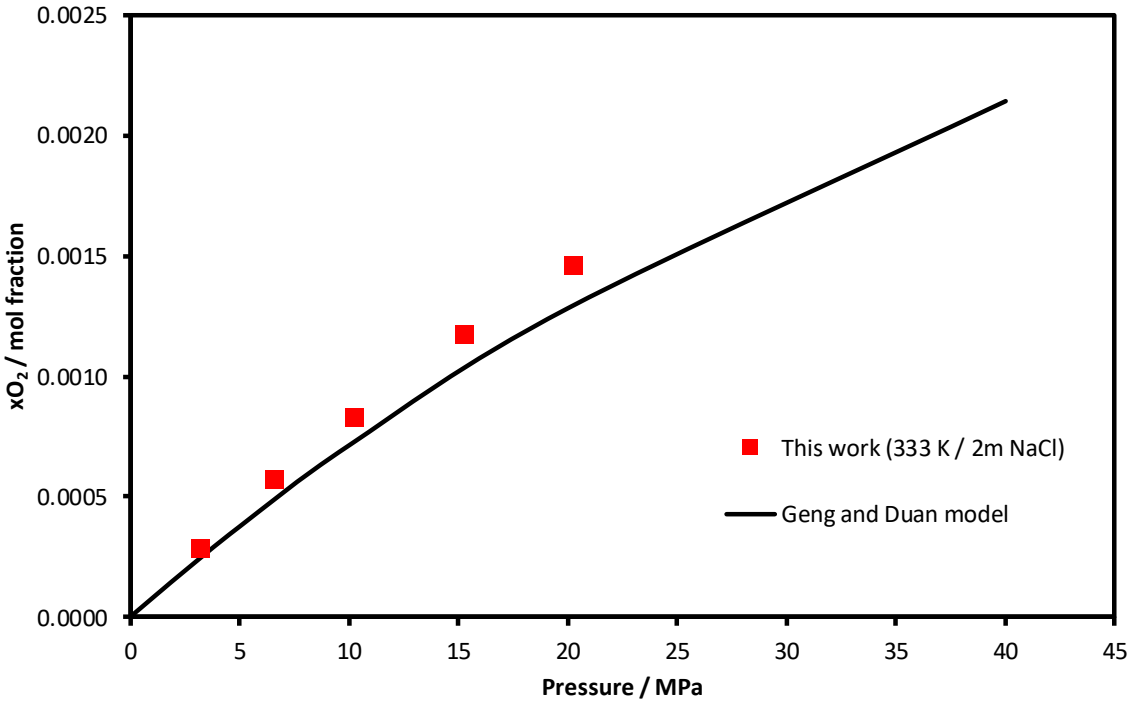

Figure 4.11 : Geng and Duan [4. 7] model predictions of O_2 solubility compared with data measured at 333 K (2 mol/kg$_w$).

The water content in the O_2-rich gas phase (O_2+H_2O system) was also studied. In Figure 4.12, the water content predictions with the e-PR-CPA, SW, and geochemical models are compared with data from the literature. All three models estimate water content very well, with a slight advantage of models with asymmetric parameters (SW and geochemical), since the gas and liquid phases are not represented by the same parameters (SW) or not by the same method (geochemical model: activity coefficient for the liquid phase and fugacity coefficient for the gas phase). However, the symmetric approach with a consistent model is preferable for reservoir simulation, since it is indispensable to perform stability analysis before each phase equilibrium calculation, especially for multi-component and multiphase systems, and this can only be achieved by consistent equations of state.

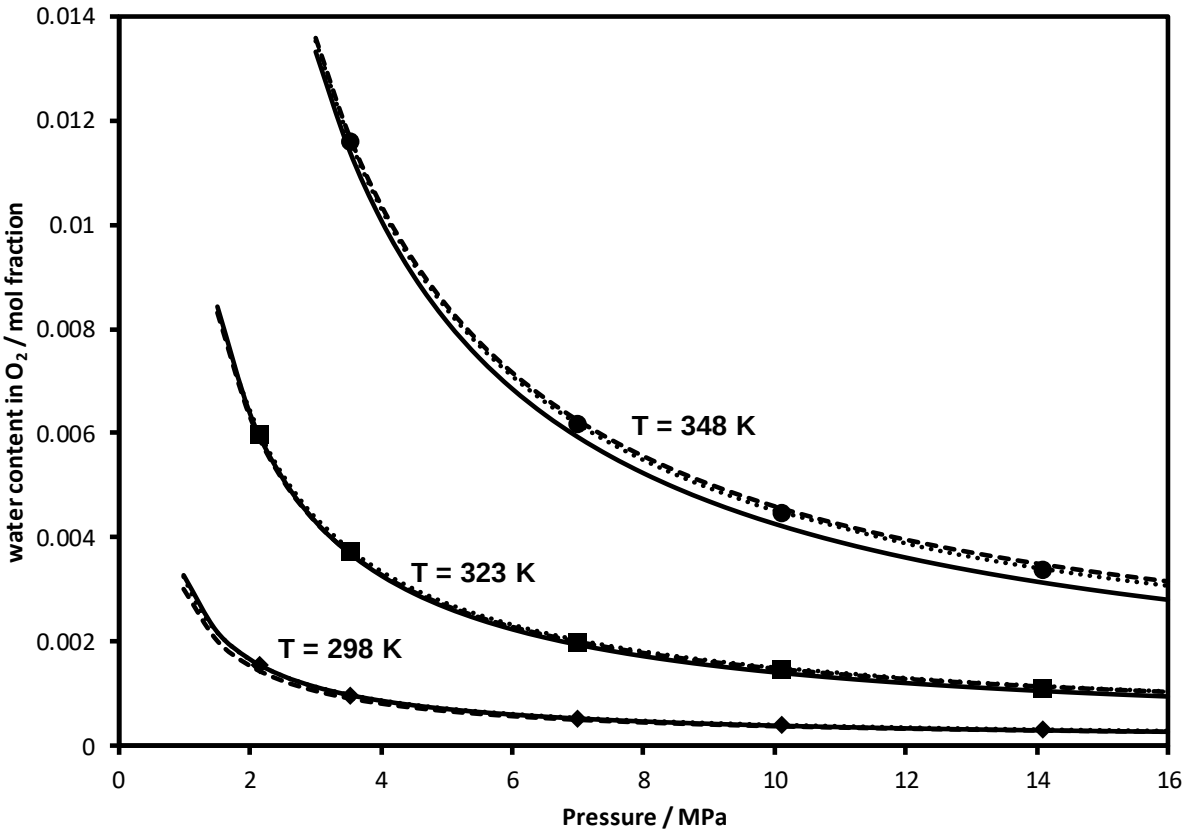

Figure 4.12 : Prediction of the water content in O_2 as a function of pressure at different temperatures by e-PR-CPA (solid line), SW (dashed line) and geochemical (dotted line) models. The data (symbols) are from Wylie and Fisher [4. 46].

Table 4.6 : Calculated solubility (in terms of salt-free mole fraction) of CO_2 in water + NaCl by the e-PR-CPA model.

T (K)	P (MPa)										
	0.5	1	1.5	2	2.5	5	7.5	10	20	30	40
						m = 0 mol/kg$_w$					
298.15	0.0026071	0.0051592	0.0076315	0.0100157	0.0123029	0.0219331	0.0260020	0.0267641	0.0289212	0.0304761	0.0317156
323.15	0.0015179	0.0030297	0.0044946	0.0059105	0.0072753	0.0132646	0.0176968	0.0203868	0.0238630	0.0257476	0.0271639
348.15	0.0010060	0.0020677	0.0031003	0.0041031	0.0050756	0.0094650	0.0130360	0.0157862	0.0211499	0.0236370	0.0253887
373.15	0.0006943	0.0015454	0.0023768	0.0031884	0.0039798	0.0076298	0.0107615	0.0133851	0.0198747	0.0232152	0.0254892
398.15	0.0004135	0.0011700	0.0019123	0.0026402	0.0033536	0.0067011	0.0096804	0.0122985	0.0197113	0.0240867	0.0271035
423.15		0.0007646	0.0014820	0.0021886	0.0028841	0.0061950	0.0092250	0.0119765	0.0204854	0.0261166	0.0301548
						m = 1 mol/kg$_w$					
298.15	0.0020898	0.0041110	0.0060464	0.0078914	0.0096411	0.0167806	0.0196909	0.0202372	0.0217807	0.0228878	0.0237641
323.15	0.0012838	0.0025517	0.0037722	0.0049444	0.0060672	0.0109098	0.0144041	0.0164926	0.0192009	0.0206815	0.0217991
348.15	0.0008745	0.0017875	0.0026715	0.0035264	0.0043518	0.0080342	0.0109781	0.0132164	0.0175550	0.0195934	0.0210484
373.15	0.0006111	0.0013438	0.0020570	0.0027507	0.0034249	0.0065051	0.0091105	0.0112689	0.0165551	0.0193021	0.0212072
398.15	0.0003727	0.0010122	0.0016377	0.0022490	0.0028463	0.0056241	0.0080632	0.0101829	0.0161051	0.0196119	0.0220768
423.15	0.0000707	0.0006658	0.0012500	0.0018234	0.0023860	0.0050388	0.0074314	0.0095771	0.0160909	0.0203769	0.0234984
						m = 3 mol/kg$_w$					
298.15	0.0013911	0.0027150	0.0039635	0.0051359	0.0062319	0.0105444	0.0122345	0.0125530	0.0134516	0.0140925	0.0145954
323.15	0.0009505	0.0018786	0.0027638	0.0036063	0.0044063	0.0077786	0.0101352	0.0115180	0.0133161	0.0143071	0.0150576
348.15	0.0006847	0.0013909	0.0020702	0.0027230	0.0033495	0.0060994	0.0082464	0.0098512	0.0129306	0.0143914	0.0154456
373.15	0.0004901	0.0010650	0.0016219	0.0021608	0.0026822	0.0050331	0.0069838	0.0085759	0.0124162	0.0144176	0.0158241
398.15	0.0003044	0.0007988	0.0012802	0.0017487	0.0022046	0.0043005	0.0061094	0.0076597	0.0119131	0.0144198	0.0162011
423.15	0.0000792	0.0005228	0.0009566	0.0013805	0.0017949	0.0037277	0.0054422	0.0069586	0.0124162	0.0144176	0.0158241
						m = 6 mol/kg$_w$					
298.15	0.0008408	0.0016311	0.0023675	0.0030511	0.0036834	0.0061082	0.0070310	0.0072036	0.0076868	0.0080267	0.0082891
323.15	0.0006713	0.0013220	0.0019372	0.0025179	0.0030650	0.0053256	0.0068629	0.0077496	0.0088918	0.0095170	0.0099869
348.15	0.0005225	0.0010607	0.0015751	0.0020662	0.0025347	0.0045579	0.0061016	0.0072359	0.0093742	0.0103783	0.0110996
373.15	0.0003793	0.0008300	0.0012642	0.0016823	0.0020847	0.0038745	0.0053301	0.0064993	0.0092584	0.0106721	0.0116600

398.15	0.0002222	0.0006054	0.0009768	0.0013366	0.0016852	0.0032688	0.0046112	0.0057445	0.0087798	0.0105282	0.0117589
423.15		0.0003612	0.0006831	0.0009966	0.0013017	0.0027095	0.0039377	0.0050084	0.0081112	0.0100731	0.0114898

Table 4.7 : Calculated solubility (in terms of salt-free mole fraction) of O_2 in water + NaCl by the e-PR-CPA model.

T (K)	P (MPa)										
	0.5	1	1.5	2	2.5	5	7.5	10	20	30	40
					m = 0 mol/kg$_w$						
298.15	0.0001066	0.0002119	0.0003152	0.0004166	0.0005160	0.0009861	0.0014145	0.0018062	0.0030853	0.0040474	0.0048137
323.15	0.0000880	0.0001768	0.0002641	0.0003500	0.0004346	0.0008377	0.0012105	0.0015560	0.0027181	0.0036245	0.0043612
348.15	0.0000759	0.0001569	0.0002367	0.0003155	0.0003931	0.0007657	0.0011137	0.0014396	0.0025592	0.0034562	0.0041972
373.15	0.0000636	0.0001424	0.0002201	0.0002969	0.0003727	0.0007382	0.0010822	0.0014067	0.0025388	0.0034638	0.0042374
398.15	0.0000438	0.0001243	0.0002040	0.0002827	0.0003606	0.0007372	0.0010936	0.0014316	0.0026238	0.0036116	0.0044452
423.15		0.0000904	0.0001756	0.0002599	0.0003434	0.0007479	0.0011324	0.0014982	0.0027986	0.0038860	0.0048091
					m = 1 mol/kg$_w$						
298.15	0.0000824	0.0001636	0.0002433	0.0003215	0.0003982	0.0007604	0.0010903	0.0013917	0.0023752	0.0031148	0.0037041
323.15	0.0000658	0.0001320	0.0001971	0.0002612	0.0003242	0.0006247	0.0009025	0.0011600	0.0020271	0.0027052	0.0032580
348.15	0.0000547	0.0001128	0.0001701	0.0002265	0.0002822	0.0005494	0.0007992	0.0010333	0.0018397	0.0024893	0.0030292
373.15	0.0000444	0.0000984	0.0001517	0.0002043	0.0002563	0.0005071	0.0007436	0.0009670	0.0017501	0.0023953	0.0029400
398.15	0.0000303	0.0000827	0.0001346	0.0001859	0.0002366	0.0004824	0.0007156	0.0009372	0.0017246	0.0023849	0.0029493
423.15	0.0000063	0.0000591	0.0001114	0.0001632	0.0002145	0.0004637	0.0007013	0.0009282	0.0017428	0.0024354	0.0030333
					m = 3 mol/kg$_w$						
298.15	0.0000494	0.0000981	0.0001458	0.0001926	0.0002385	0.0004553	0.0006525	0.0008325	0.0014199	0.0018621	0.0022152
323.15	0.0000394	0.0000790	0.0001179	0.0001563	0.0001940	0.0003737	0.0005399	0.0006942	0.0012147	0.0016240	0.0019598
348.15	0.0000321	0.0000661	0.0000995	0.0001325	0.0001650	0.0003213	0.0004677	0.0006050	0.0010806	0.0014673	0.0017919
373.15	0.0000253	0.0000556	0.0000855	0.0001150	0.0001442	0.0002853	0.0004186	0.0005449	0.0009907	0.0013629	0.0016812
398.15	0.0000169	0.0000448	0.0000724	0.0000997	0.0001267	0.0002578	0.0003827	0.0005018	0.0009289	0.0012929	0.0016093
423.15	0.0000047	0.0000310	0.0000571	0.0000830	0.0001086	0.0002335	0.0003532	0.0004679	0.0008845	0.0012457	0.0015638
					m = 6 mol/kg$_w$						
298.15	0.0000242	0.0000481	0.0000714	0.0000944	0.0001168	0.0002229	0.0003194	0.0004074	0.0006943	0.0009104	0.0010830

323.15	0.0000219	0.0000440	0.0000658	0.0000871	0.0001082	0.0002084	0.0003012	0.0003873	0.0006785	0.0009084	0.0010977
348.15	0.0000191	0.0000394	0.0000594	0.0000792	0.0000986	0.0001923	0.0002800	0.0003625	0.0006491	0.0008837	0.0010819
373.15	0.0000153	0.0000339	0.0000522	0.0000704	0.0000883	0.0001752	0.0002574	0.0003354	0.0006122	0.0008452	0.0010464
398.15	0.0000097	0.0000267	0.0000436	0.0000603	0.0000768	0.0001572	0.0002338	0.0003071	0.0005716	0.0007993	0.0009993
423.15		0.0000171	0.0000326	0.0000480	0.0000633	0.0001377	0.0002092	0.0002779	0.0005293	0.0007498	0.0009462

4.5 Conclusions

The solubility of O_2 in NaCl brine was measured using two different techniques: the first one is based on the static-analytic method (liquid phase sampling and GC analysis) and the second one is a rocking cell setup (liquid phase sampling, gas/brine separation, gravimetric and volumetric analysis of brine and gas). For validation purpose, the measurements carried out using both techniques were compared, and consistency of results was verified. The solubility of CO_2 in NaCl brine (at high concentration) was also measured using the second technique. These measurements are intended to complement our previous work (on CO_2 solubility in brine), and also to validate the measurement technique by comparing some measurements with literature data. It was challenging to be able to measure such a low solubility (of O_2) with small samples using GC with the first technique. This gave us more confidence in this static analytical technique and recently allowed us to also use it to measure the solubility of Hydrogen in brine [4. 47] which is also very difficult to measure.

The new measured solubility data were used to evaluate and improve existing or developed models. The e-PR-CPA and SW equations of state (phi-phi approach) were tested, and a geochemical model and the recently proposed model by Zheng and Mao (ZM) (gamma-phi approach) were used to process measured and literature O_2 solubility data. The measurements carried out also show the need to readjust the well-known Geng and Duan model by including these new data. The predictions of the water content in the gas phase (O_2-rich) by the three models (e-PR-CPA, SW, and geochemical) were evaluated by comparing them with literature data. All three models gave similar results. For CO_2, the solubility data were processed by the three models as well, whose parameterization was already done in our previous work.

All models capture very well the effect of temperature, pressure, and NaCl concentration on the solubility of O_2 and CO_2 with an absolute average deviation less than 5% with respect to the measured data. Each of these models can be used for solubility estimation, criteria such as accuracy, simplicity and speed of calculation can be considered in selecting the appropriate model and approach. Finally, we provided tables of solubility data of O_2 and CO_2 in water and NaCl brine, generated by the e-PR-CPA model.

Acknowledgments

Financial support from Agence Nationale de la Recherche (ANR) through the project FluidSTORY (n° 7747, ID ANR-15-CE06-0015) is gratefully acknowledged.

References

[4. 1] D. Tromans, Oxygen solubility modeling in inorganic solutions: concentration, temperature and pressure effects, Hydrometallurgy, 50 (1998) 279-296.
[4. 2] M. Jamnongwong, K. Loubiere, N. Dietrich, G. Hébrard, Experimental study of oxygen diffusion coefficients in clean water containing salt, glucose or surfactant: consequences on the liquid-side mass transfer coefficients, Chemical engineering journal, 165 (2010) 758-768.
[4. 3] G. Ming, D. Zhenhao, Prediction of oxygen solubility in pure water and brines up to high temperatures and pressures, Geochimica et Cosmochimica Acta, 74 (2010) 5631-5640.
[4. 4] R. Roffey, Microbial problems during long-term storage of petroleum products underground in rock caverns, International biodeterioration, 25 (1989) 219-236.
[4. 5] N. Kezibri, C. Bouallou, Conceptual design and modelling of an industrial scale power to gas-oxy-combustion power plant, International Journal of Hydrogen Energy, 42 (2017) 19411-19419.
[4. 6] R. Battino, IUPAC solubility data series, Oxygen and ozone, 7 (1981).
[4. 7] M. Geng, Z. Duan, Prediction of oxygen solubility in pure water and brines up to high temperatures and pressures, Geochimica et Cosmochimica Acta, 74 (2010) 5631-5640.
[4. 8] J. Zheng, S. Mao, A thermodynamic model for the solubility of N2, O2 and Ar in pure water and aqueous electrolyte solutions and its applications, Applied Geochemistry, (2019).
[4. 9] D. Li, C. Beyer, S. Bauer, Solubility of Nitrogen and Oxygen Gas in Aqueous NaCl Solutions for Elevated Temperatures and Pressures, in: The Third Sustainable Earth Sciences Conference and Exhibition, European Association of Geoscientists & Engineers, 2015, pp. 1-5.
[4. 10] J.O. Valderrama, R.A. Campusano, L.A. Forero, A new generalized Henry-Setschenow equation for predicting the solubility of air gases (oxygen, nitrogen and argon) in seawater and saline solutions, Journal of Molecular Liquids, 222 (2016) 1218-1227.
[4. 11] S. Chabab, P. Théveneau, J. Corvisier, C. Coquelet, P. Paricaud, C. Houriez, E. El Ahmar, Thermodynamic study of the CO2–H2O–NaCl system: Measurements of CO2 solubility and modeling of phase equilibria using Soreide and Whitson, electrolyte CPA and SIT models, International Journal of Greenhouse Gas Control, 91 (2019) 102825.
[4. 12] S. Mao, D. Zhang, Y. Li, N. Liu, An improved model for calculating CO2 solubility in aqueous NaCl solutions and the application to CO2–H2O–NaCl fluid inclusions, Chemical Geology, 347 (2013) 43-58.
[4. 13] H. Messabeb, F.o. Contamine, P. Cézac, J.P. Serin, E.C. Gaucher, Experimental Measurement of CO2 Solubility in Aqueous NaCl Solution at Temperature from 323.15 to 423.15 K and Pressure of up to 20 MPa, Journal of Chemical & Engineering Data, 61 (2016) 3573-3584.
[4. 14] P. Ahmadi, A. Chapoy, CO2 solubility in formation water under sequestration conditions, Fluid Phase Equilibria, 463 (2018) 80-90.
[4. 15] A. Chapoy, M. Nazeri, M. Kapateh, R. Burgass, C. Coquelet, B. Tohidi, Effect of impurities on thermophysical properties and phase behaviour of a CO2-rich system in CCS, International Journal of Greenhouse Gas Control, 19 (2013) 92-100.
[4. 16] B.N. Taylor, C.E. Kuyatt, Guidelines for evaluating and expressing the uncertainty of NIST measurement results, (1994).
[4. 17] H. Zhao, M.V. Fedkin, R.M. Dilmore, S.N. Lvov, Carbon dioxide solubility in aqueous solutions of sodium chloride at geological conditions: Experimental results at 323.15, 373.15, and 423.15 K and 150bar and modeling up to 573.15 K and 2000bar, Geochimica et Cosmochimica Acta, 149 (2015) 165-189.

[4. 18] Z. Duan, R. Sun, An improved model calculating CO2 solubility in pure water and aqueous NaCl solutions from 273 to 533 K and from 0 to 2000 bar, Chemical geology, 193 (2003) 257-271.
[4. 19] Z. Duan, R. Sun, C. Zhu, I.-M. Chou, An improved model for the calculation of CO2 solubility in aqueous solutions containing Na+, K+, Ca2+, Mg2+, Cl−, and SO42−, Marine Chemistry, 98 (2006) 131-139.
[4. 20] N. Spycher, K. Pruess, J. Ennis-King, CO2-H2O mixtures in the geological sequestration of CO2. I. Assessment and calculation of mutual solubilities from 12 to 100 C and up to 600 bar, Geochimica et cosmochimica acta, 67 (2003) 3015-3031.
[4. 21] N. Spycher, K. Pruess, CO2-H2O Mixtures in the Geological Sequestration of CO2. II. Partitioning in Chloride Brines at 12–100 C and up to 600 bar, Geochimica et Cosmochimica Acta, 69 (2005) 3309-3320.
[4. 22] J. Corvisier, Modeling water-gas-rock interactions using CHESS/HYTEC, in: Goldschmidt Conference, Florence–Italy, 2013.
[4. 23] J. Corvisier, A.-F. Bonvalot, V. Lagneau, P. Chiquet, S. Renard, J. Sterpenich, J. Pironon, Impact of co-injected gases on CO2 storage sites: Geochemical modeling of experimental results, Energy Procedia, 37 (2013) 3699-3710.
[4. 24] I. Søreide, C.H. Whitson, Peng-Robinson predictions for hydrocarbons, CO2, N2, and H2S with pure water and NaCl brine, Fluid Phase Equilibria, 77 (1992) 217-240.
[4. 25] H. Guo, Y. Huang, Y. Chen, Q. Zhou, Quantitative Raman Spectroscopic Measurements of CO2 Solubility in NaCl Solution from (273.15 to 473.15) K at p=(10.0, 20.0, 30.0, and 40.0) MPa, Journal of Chemical & Engineering Data, 61 (2015) 466-474.
[4. 26] D. Koschel, J.-Y. Coxam, L. Rodier, V. Majer, Enthalpy and solubility data of CO 2 in water and NaCl (aq) at conditions of interest for geological sequestration, Fluid phase equilibria, 247 (2006) 107-120.
[4. 27] W. Yan, S. Huang, E.H. Stenby, Measurement and modeling of CO2 solubility in NaCl brine and CO2–saturated NaCl brine density, International Journal of Greenhouse Gas Control, 5 (2011) 1460-1477.
[4. 28] A. Bamberger, G. Sieder, G. Maurer, High-pressure (vapor+ liquid) equilibrium in binary mixtures of (carbon dioxide+ water or acetic acid) at temperatures from 313 to 353 K, The Journal of Supercritical Fluids, 17 (2000) 97-110.
[4. 29] S.-X. Hou, G.C. Maitland, J.M. Trusler, Measurement and modeling of the phase behavior of the (carbon dioxide+ water) mixture at temperatures from 298.15 K to 448.15 K, The Journal of Supercritical Fluids, 73 (2013) 87-96.
[4. 30] R. Dohrn, A. Bünz, F. Devlieghere, D. Thelen, Experimental measurements of phase equilibria for ternary and quaternary systems of glucose, water, CO2 and ethanol with a novel apparatus, Fluid Phase Equilibria, 83 (1993) 149-158.
[4. 31] R. Wiebe, V. Gaddy, The solubility in water of carbon dioxide at 50, 75 and 100, at pressures to 700 atmospheres, Journal of the American Chemical Society, 61 (1939) 315-318.
[4. 32] I. Krichevsky, J. Kasarnovsky, Partial Molal Quantities in an Infinitely Dilute Solution, Journal of the American Chemical Society, 57 (1935) 2171-2172.
[4. 33] C. Descamps, C. Coquelet, C. Bouallou, D. Richon, Solubility of hydrogen in methanol at temperatures from 248.41 to 308.20 K, Thermochimica acta, 430 (2005) 1-7.
[4. 34] A. Broden, R. Simonson, Solubility of oxygen, Svensk Papperstidning, 17 (1978) 541-544.
[4. 35] Z.-Q. Tan, G.-H. Gao, Y.-X. Yu, C. Gu, Solubility of oxygen in aqueous sodium carbonate solution at pressures up to 10 MPa, Fluid phase equilibria, 180 (2001) 375-382.
[4. 36] T.D. O'Sullivan, N.O. Smith, Solubility and partial molar volume of nitrogen and methane in water and in aqueous sodium chloride from 50 to 125. deg. and 100 to 600 atm, J. Phys. Chem., 74 (1970) 1460-1466.

[4. 37] P. Blanc, A. Lassin, P. Piantone, M. Azaroual, N. Jacquemet, A. Fabbri, E.C. Gaucher, Thermoddem: A geochemical database focused on low temperature water/rock interactions and waste materials, Applied geochemistry, 27 (2012) 2107-2116.
[4. 38] E.L. Shock, H.C. Helgeson, D.A. Sverjensky, Calculation of the thermodynamic and transport properties of aqueous species at high pressures and temperatures: Standard partial molal properties of inorganic neutral species, Geochimica et Cosmochimica Acta, 53 (1989) 2157-2183.
[4. 39] M.D. Schulte, E.L. Shock, R.H. Wood, The temperature dependence of the standard-state thermodynamic properties of aqueous nonelectrolytes, Geochimica et Cosmochimica Acta, 65 (2001) 3919-3930.
[4. 40] A.C. Schneider, C. Pasel, M. Luckas, K.G. Schmidt, J.-D. Herbell, Determination of hydrogen single ion activity coefficients in aqueous HCl solutions at 25 C, Journal of solution chemistry, 33 (2004) 257-273.
[4. 41] H. Sakaida, T. Kakiuchi, Determination of single-ion activities of H+ and Cl–in aqueous hydrochloric acid solutions by use of an ionic liquid salt bridge, The Journal of Physical Chemistry B, 115 (2011) 13222-13226.
[4. 42] M.K. Khoshkbarchi, J.H. Vera, Measurement and correlation of ion activity in aqueous single electrolyte solutions, AIChE journal, 42 (1996) 249-258.
[4. 43] U. Hohm, K. Kerl, Temperature dependence of mean molecular polarizability of gas molecules, Mol. Phys., 58 (1986) 541-550.
[4. 44] E. Lemmon, I.H. Bell, M. Huber, M. McLinden, NIST Standard Reference Database 23: Reference Fluid Thermodynamic and Transport Properties-REFPROP, Version 10.0, National Institute of Standards and Technology, (2018).
[4. 45] R. Battino, P.G. Seybold, The O2/N2 ratio gas solubility mystery, J. Chem. Eng. Data, 56 (2011) 5036-5044.
[4. 46] R.G. Wylie, R.S. Fisher, Molecular interaction of water vapor and oxygen, Journal of Chemical & Engineering Data, 41 (1996) 175-180.
[4. 47] S. Chabab, P. Théveneau, C. Coquelet, J. Corvisier, P. Paricaud, Measurements and predictive models of high-pressure H2 solubility in brine (H2O+NaCl) for underground hydrogen storage application, Int. J. Hydrogen Energy, 45 (2020) 32206-32220.

Chapter 5: Article 3: Measurements and predictive models of high-pressure H_2 solubility in brine (H_2O+NaCl) for Underground Hydrogen Storage application

French summary / Chapitre 5 – Article 3 : Mesures et modèles prédictifs de la solubilité à haute pression de l'H_2 dans la saumure (H_2O+NaCl) pour le stockage souterrain de l'hydrogène

Dans le cadre du stockage souterrain d'hydrogène, le gaz stocké est en contact direct avec la saumure (saumure résiduelle de la caverne ou eau de formation des aquifères profonds). Par conséquent, la connaissance des équilibres entre les phases (solubilité de l'hydrogène dans la saumure et teneur en eau dans la phase riche en hydrogène) dans le réservoir géologique est nécessaire pour l'étude de la mobilité et de la réactivité de l'hydrogène, ainsi que pour le contrôle, la surveillance et l'optimisation du stockage. L'absence de données mesurées de la solubilité de l'H_2 à haute pression dans la saumure a récemment conduit les scientifiques à développer des modèles prédictifs ou à générer des pseudo-données à l'aide de la simulation moléculaire. Cependant, des mesures expérimentales sont nécessaires pour l'évaluation et la validation des modèles. Dans ce travail, un appareil expérimental basé sur la méthode "statique-analytique" développée et utilisée dans nos travaux précédents pour la mesure de la solubilité de gaz dans la saumure a été utilisé. De nouvelles données de solubilité d'H_2 dans H_2O+NaCl ont été mesurées plus ou moins dans les conditions géologiques du stockage, à des températures comprises entre 323 et 373 K, des molalités de NaCl entre 0 et 5m, et des pressions allant jusqu'à 230 bars. Ces données ont été utilisées pour paramétrer et évaluer trois modèles (modèles géochimiques, SW et e-PR-CPA) testés dans le cadre de ce travail. Des tableaux de solubilité et de teneur en eau ont été générés par le modèle e-PR-CPA, et une formulation simple (relation de type Setschenow) pour des calculs rapides et précis (dans la gamme d'ajustement de ses coefficients) de la solubilité d'H_2 dans l'eau et la saumure a été proposée. Finalement, les modèles développés estiment très bien la teneur en eau dans la phase riche en hydrogène et capturent et calculent avec précision l'effet « salting-out » sur la solubilité de l'H_2.

Measurements and predictive models of high-pressure H_2 solubility in brine (H_2O+NaCl) for Underground Hydrogen Storage application

Salaheddine Chabab[a], Pascal Théveneau[a], Christophe Coquelet[a,*], Jérôme Corvisier[b] and Patrice Paricaud[c,a]

[a]*Mines ParisTech, PSL University, Centre of Thermodynamics of Processes, 35 rue Saint Honoré, 77305 Fontainebleau Cedex, France*

[b]*Mines ParisTech, PSL University, Centre de Géosciences, 35 rue Saint Honoré, 77305 Fontainebleau Cedex, France*

[c]*Unité Chimie & Procédés (UCP), ENSTA Paris, 828 Boulevard des Maréchaux, 91762 Palaiseau cedex, France*

INTERNATIONAL JOURNAL OF HYDROGEN ENERGY 45 (2020) 32206–32220

Available online at www.sciencedirect.com

ScienceDirect

journal homepage: www.elsevier.com/locate/he

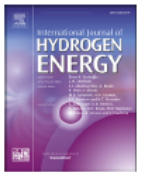

Measurements and predictive models of high-pressure H_2 solubility in brine (H_2O+NaCl) for underground hydrogen storage application

Salaheddine Chabab [a], *Pascal Théveneau* [a], *Christophe Coquelet* [a,*], *Jérôme Corvisier* [b], *Patrice Paricaud* [c,a]

[a] Mines ParisTech, PSL University, Centre of Thermodynamics of Processes, 35 Rue Saint Honoré, Fontainebleau Cedex, 77305, France
[b] Mines ParisTech, PSL University, Centre de Géosciences, 35 Rue Saint Honoré, Fontainebleau Cedex, 77305, France
[c] Unité Chimie & Procédés (UCP), ENSTA Paris, 828 Boulevard des Maréchaux, Palaiseau Cedex, 91762, France

HIGHLIGHTS

- High-pressure H_2 solubility in NaCl brine was measured using gas chromatography.
- Data consistency was verified and some measurements were compared with the literature.
- Models and correlations are proposed to estimate H_2 solubility in water and brine.
- Developed models accurately estimate H_2 solubility and predict water content.

ARTICLE INFO

Article history:
Received 10 July 2020
Received in revised form
20 August 2020
Accepted 23 August 2020
Available online 16 September 2020

Keywords:
Underground hydrogen storage
H_2 solubility in brine
Water content
Electrolyte CPA EoS
Søreide and Whitson EoS
Geochemical model

ABSTRACT

In the context of Underground Hydrogen Storage (UHS), the stored gas is in direct contact with brine (residual brine from the cavern or formation water of deep aquifers). Therefore, knowledge of the phase equilibria (solubility of hydrogen in brine and water content in the hydrogen-rich phase) in the geological reservoir is necessary for the study of hydrogen mobility and reactivity, as well as the control, monitoring and optimization of the storage. The absence of measured data of high-pressure H_2 solubility in brine has recently led scientists to develop predictive models or to generate pseudo-data using molecular simulation. However, experimental measurements are needed for model evaluation and validation. In this work, an experimental apparatus based on the "static-analytic" method developed and used in our previous work for the measurement of gas solubility in brine was used. New solubility data of H_2 in H_2O+NaCl were measured more or less under the geological conditions of the storage, at temperatures between 323 and 373 K, NaCl molalities between 0 and 5m, and pressures up to 230 bar. These data were used to parameterize and evaluate three models (Geochemical, SW, and e-PR-CPA models) tested in this work. Solubility and water content tables were generated by the e-PR-CPA model, as well as a simple formulation (Setschenow-type relationship) for quick and accurate calculations (in the fitting range) of H_2 solubility in water and brine was proposed. Finally, the developed models estimate very well the water content in hydrogen-rich phase and capture and calculate precisely the salting-out effect on H_2 solubility.

Abstract

In the context of Underground Hydrogen Storage (UHS), the stored gas is in direct contact with brine (residual brine from the cavern or formation water of deep aquifers). Therefore, knowledge of the phase equilibria (solubility of hydrogen in brine and water content in the hydrogen-rich phase) in the geological reservoir is necessary for the study of hydrogen mobility and reactivity, as well as the control, monitoring and optimization of the storage. The absence of measured data of high-pressure H_2 solubility in brine has recently led scientists to develop predictive models or to generate pseudo-data using molecular simulation. However, experimental measurements are needed for model evaluation and validation. In this work, an experimental apparatus based on the "static-analytic" method developed and used in our previous work for the measurement of gas solubility in brine was used. New solubility data of H_2 in H_2O+NaCl were measured more or less under the geological conditions of the storage, at temperatures between 323 and 373 K, NaCl molalities between 0 and 5m, and pressures up to 230 bar. These data were used to parameterize and evaluate three models (Geochemical, SW, and e-PR-CPA models) tested in this work. Solubility and water content tables were generated by the e-PR-CPA model, as well as a simple formulation (Setschenow-type relationship) for quick and accurate calculations (in the fitting range) of H_2 solubility in water and brine was proposed. Finally, the developed models estimate very well the water content in hydrogen-rich phase and capture and calculate precisely the salting-out effect on H_2 solubility.

Keywords: Underground Hydrogen Storage, H2 solubility in brine, water content, Electrolyte CPA EoS, Søreide and Whitson EoS, geochemical model.

5.1 Introduction

Hydrogen (H_2) is considered to be a renewable energy carrier with promising prospects for energy transition. It can be used directly in fuel cells for transport and mobility applications, or as a complement to existing energy resources such as the production of synthetic methane by combining it with CO_2 through methanation, and the injection into existing Natural Gas (NG) networks with the aim of reducing consumption (in the short term) and stopping the use (in the long term) of fossil fuels. To manage the intermittent nature of renewable energy sources such as wind and solar power, surplus electricity can be stored in chemical form by producing H_2 through water electrolysis (power-to-gas concept). In order to balance the temporal differences between production and demand, storage of pure or blended (e.g. with NG [5. 1, 2]) hydrogen is necessary.

Hydrogen can be stored in gaseous form in gas cylinders, in liquid form in cryogenic tanks, or in solid form by adsorption, absorption or by reacting with some chemical compounds [5. 3]. However, the most studied and used technology for hydrogen large-scale storage is underground storage in geological formations such as salt caverns, deep aquifers, and depleted gas fields. In addition to their huge storage capacity (in terms of volume and pressure), underground hydrogen storage remains more cost-effective and safer than other storage techniques [5. 4, 5].

Hydrogen storage in salt caverns has been done successfully for decades. However, none of this storage has been done for energetic purposes, since the stored hydrogen was mainly dedicated to the chemical and petrochemical industry. Large quantities of hydrogen are used [5. 6] in refineries (50%) to remove/recover sulfur from fuels using hydrotreating (hydrogenation process), and in the Haber process (32%) for ammonia (NH3) synthesis by combining nitrogen (N2) and hydrogen (H2). Currently, four sites for hydrogen storage in salt caverns are operational worldwide: three in the USA (Clemens Dome, Moss Bluff, Spindletop) and one in the UK (Teesside). Several projects are in progress or have just been completed studying for energy purposes the storage of pure hydrogen in salt caverns (H2STORE, HyUnder, HyStock, Rostock H, STOPIL H2, etc.) and in gas fields (SunStorage and HyChico projects) or possibly mixed with CO_2 in deep saline aquifers (Underground bio-methanation concept [5. 7]) or with CH_4 (SunStorage and HyChico projects). A benchmarking study of the different options for high-pressure hydrogen storage was carried out as part of the European project HyUnder [5. 8]. This comparative study concluded that, according to the different techno-economic and safety

factors, storage in salt caverns is first in the ranking, followed by storage in depleted gas fields and storage in deep saline aquifers. Finally, hydrogen (especially pure) storage in salt caverns is preferred for several reasons [5. 9]: the least expensive of all forms of storage, less cushion gas than storage in porous media, the possibility of several injection/withdrawal cycles, and a positive experience feedback.

Underground Hydrogen Storage (UHS) is much less studied than the underground natural gas storage, therefore in most existing hydrogen storage sites, the pressure does not exceed more or less than 150 bar. This is explained by its high mobility due to its small size [5. 10], as well as its high reactivity (redox reactions) by possibly participating in certain microbial processes: sulfate-reduction, methanogenesis, acetogenesis, and iron-reduction [5. 11, 12]. Most of these types of reactions can take place in the aqueous medium, i.e. in the residual brine after the solution mining of salt caverns or in the formation water of deep aquifers. The study of the mobility and reactivity of hydrogen is therefore necessary for the total control of the storage of this molecule, as well as for the reduction of the safety factors used (just by feedback), and consequently a more efficient and economical storage. In order to be able to perform chemical speciation calculations and study its mobility, it is therefore necessary to determine precisely the solubility of hydrogen in the aqueous phase under the thermodynamic storage conditions (temperature, pressure and salinity). Finally, the simulation and control of storage facilities, as well as the monitoring of hydrogen (temperature, pressure and quantity) in the reservoir (salt cavern or aquifer), requires knowledge of phase diagrams (solubility and water content of hydrogen) [5. 13].

The solubility of hydrogen in water has been extensively studied at different pressures (P) and temperatures (T) in the past, as well as in saline water only under atmospheric P−T conditions. However, there are no high-pressure data of hydrogen solubility in saline water [5. 14]. This can be justified by the complexity and dangerousness of this type of measurements, which are characterized by high pressure, high flammability of H_2, and presence of salt (risk of corrosion and leakage). To overcome this lack of data, recently “predictive” models adjusted on a limited number of data (available experimental data and/or molecular simulation data) have been proposed. Li et al. [5. 15] proposed a model to predict the solubility of hydrogen in brine under geological storage conditions. The parameters of their model were adjusted on H_2 solubility data in brine at atmospheric pressure and high-pressure H_2 solubility data in pure water. Lopez-Lazaro et al. [5. 13] performed Monte Carlo simulations to generate pseudo-experimental data,

which were then correlated using an equation of state (Soreide and Whitson model [5. 16]). An inconsistency between the two studies was identified, which was totally expected, given the different approaches used and the lack of experimental data. However, further experimental measurements are needed to evaluate these predictions and refine existing models by including "real" high-pressure solubility data.

In this work, the solubility of hydrogen in brine (H_2O+NaCl) was measured analytically with the apparatus used in our previous work on the carbon dioxide and oxygen solubility in brine [5. 17, 18]. The measurements were carried out more or less under the geological storage conditions (temperature $323 \leq T\ (K) \leq 373$, pressure up to 200 bar and NaCl molality $0 \leq m_{NaCl}$ (mol/kgw) ≤ 5). These new data, as well as existing literature data, were used to parameterize the models developed and presented in our previous work [5. 17, 18] using different thermodynamic approaches (gamma-phi and phi-phi).

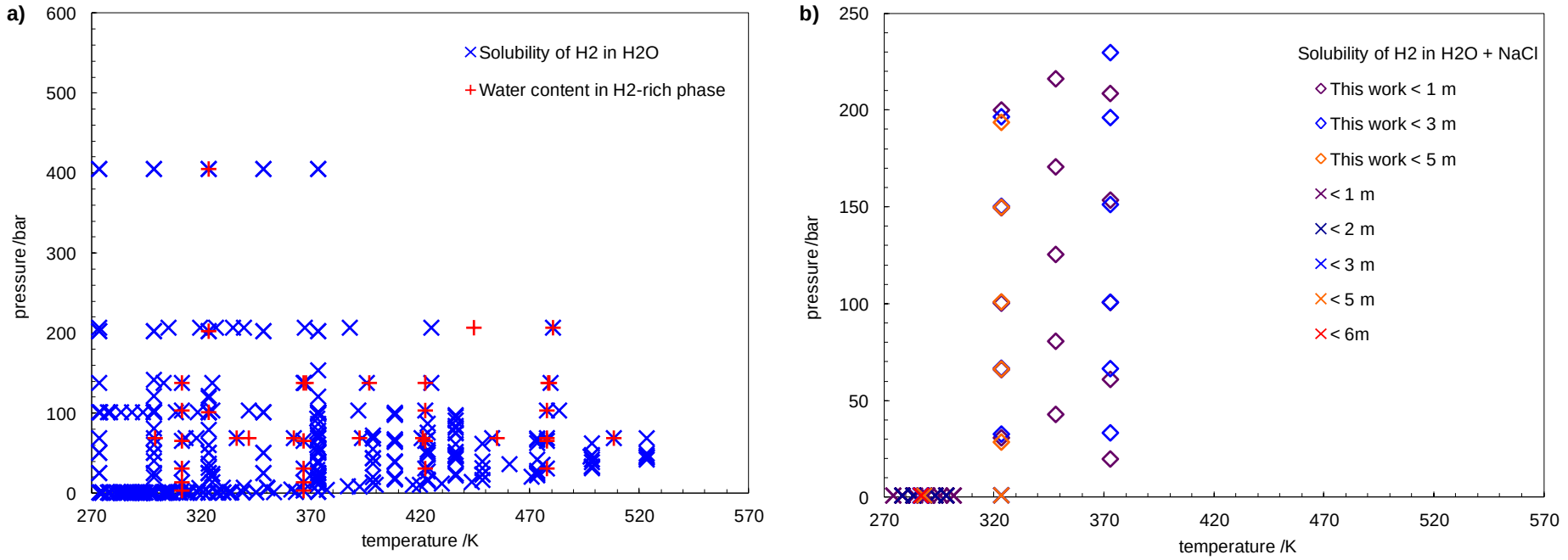

Figure 5.1 : Distribution of literature solubility data (×) and this work (◊). (a): H_2-H_2O system (solubility and water content); (b): H_2 solubility in NaCl brine.

5.2 Experimental

5.2.1 Literature and measured (this work) solubility data of H_2 in water and brine

In the literature, there are numerous data on the solubility of hydrogen in pure water, the majority of which come from very old studies. These data were collected, listed in Table 5.1, and presented in Figure 5.1.a as function of temperature and pressure. The Wiebe and Gaddy [5. 19] data are the most reliable according to IUPAC's [5. 20] evaluation of experimental data, and largely cover the pressure and temperature range of geological storage conditions.

The solubility of hydrogen in brine is less studied than in pure water. In Table 5.2, hydrogen solubility data in water + salt (NaCl, KCl, $CaCl_2$, Na_2SO_4 and $MgSO_4$) are listed. All these data found are old and limited to low temperature and atmospheric pressure. It is therefore necessary to overcome this lack of data especially for the H_2+H_2O+NaCl system which is the most important since Na^+ and Cl^- are the predominant species present in natural saline water. The measurements carried out in this work for the H_2+H_2O+NaCl system as well as data from the literature are presented in Figure 5.1.b as function of temperature, pressure and NaCl molality.

Table 5.1 : Literature experimental data for H_2 solubility in pure water

Reference	Year	Tmin/K	Tmax/K	Pmin/bar	Pmax/bar
Bunsen [5. 21]	1855	277.15	296.75	1.021	1.042
Timofejew [5. 22]	1890	274.55	298.85	1.020	1.046
Bohr and Bock [5. 23]	1891	273.20	373.15	1.019	2.030
Winkler [5. 24]	1891	273.65	323.25	1.020	1.138
Steiner [5. 25]	1894	288.20	288.20	1.030	1.030
Braun [5. 26]	1900	278.15	298.15	1.022	1.045
Geffcken [5. 27]	1904	288.15	298.15	1.030	1.045
Knopp [5. 28]	1904	293.15	293.15	1.037	1.037
Hufner [5. 29]	1907	293.15	293.34	1.037	1.037
Findlay and Shen [5. 30]	1912	298.15	298.15	1.009	1.840
Muller [5. 31]	1913	289.35	290.35	1.032	1.033
Ipatiew et al. [5. 32]	1932	273.65	318.15	20.265	141.855
Wiebe and Gaddy [5. 19]	1934	273.15	373.15	25.331	1013.250
Morrison and Billett [5. 33]	1952	285.65	345.65	1.028	1.350
Pray et al. [5. 34]	1952	324.82	588.71	6.900	24.150
Zoss [5. 35]	1952	273.15	606.48	34.500	207.000
Pray and Stephan [5. 36]	1953	373.15	435.93	14.133	100.308
Wet [5. 37]	1964	291.65	304.55	1.035	1.059
Ruetschi and Amlie [5. 38]	1966	303.15	303.15	1.056	1.056
Shoor et al. [5. 39]	1969	298.15	333.15	1.045	1.213

Longo et al. [5. 40]	1970	310.15	310.15	1.076	1.076
Power and Stegall [5. 41]	1970	310.15	310.15	1.076	1.076
Gerecke and Bittrich [5. 42]	1971	298.15	298.15	1.045	1.045
Jung et al. [5. 43]	1971	373.15	423.15	9.962	85.844
Schroder [5. 44]	1973	298.15	373.15	101.300	101.300
Crozier and Yamamoto [5. 45]	1974	274.60	302.47	1.013	1.013
Gordon et al. [5. 46]	1977	273.29	302.40	1.013	1.013
Cargill [5. 47]	1978	277.70	344.83	1.022	1.350
Gillespie and Wilson [5. 48]	1980	310.93	588.71	3.450	138.000
Choudhary et al. [5. 49]	1982	323.15	373.15	25.331	101.325
Dohrn and Brunner [5. 50]	1986	473.15	623.15	100.000	300.000
Alvarez et al. [5. 51]	1988	318.90	497.50	4.360	45.940
Kling and Maurer [5. 52]	1991	323.15	423.15	31.800	153.700
Jauregui-Haza et al. [5. 53]	2004	353.00	373.00	1.486	2.025

Table 5.2 : Literature experimental data for H_2 solubility in saline water

Reference	Year	Max Molality	Tmin/K	Tmax/K	Pmin/bar	Pmax/bar
Steiner [5. 25]	1894	5.3 m NaCl	286.32	286.95	1.028	1.029
Braun [5. 26]	1900	1.1 m NaCl	278.15	298.15	1.022	1.045
Gerecke & Bittrich [5. 42]	1971	4.3 m NaCl	288.15	298.15	1.030	1.045
Crozier & Yamamoto [5. 45]	1974	0.5 m NaCl	274.03	301.51	1.013	1.013
Steiner [5. 25]	1894	4.0 m KCl	291.77	292.38	1.035	1.036
Knopp [5. 28]	1904	2.1 m KCl	293.15	293.15	1.037	1.037
Gerecke et Bittrich [5. 42]	1971	1.0 m KCl	288.15	288.15	1.030	1.030
Steiner [5. 25]	1894	3.2 m $CaCl_2$	290.83	291.67	1.034	1.035
Steiner [5. 25]	1894	1.4 m Na_2SO_4	291.56	291.72	1.035	1.035
Steiner [5. 25]	1894	2.6 m $MgSO_4$	290.25	291.41	1.033	1.034

5.2.2 Materials

Table 5.3 : Chemicals used in this work: purities and suppliers

Chemicals	Purity	Analytical Method	Supplier
H_2 (Hydrogen 5.0)	99.999 vol%	GC: Gas Chromatography	Messer
NaCl	99.6%	None	Fisher Chemical

In Table 5.3, the suppliers of Hydrogen (H_2, CAS Number: 1333-74-0) and Sodium Chloride (NaCl, CAS Number: 7647-14-5) and the given purities are listed. Water was deionized and degassed before the preparation of the brine (water + NaCl).

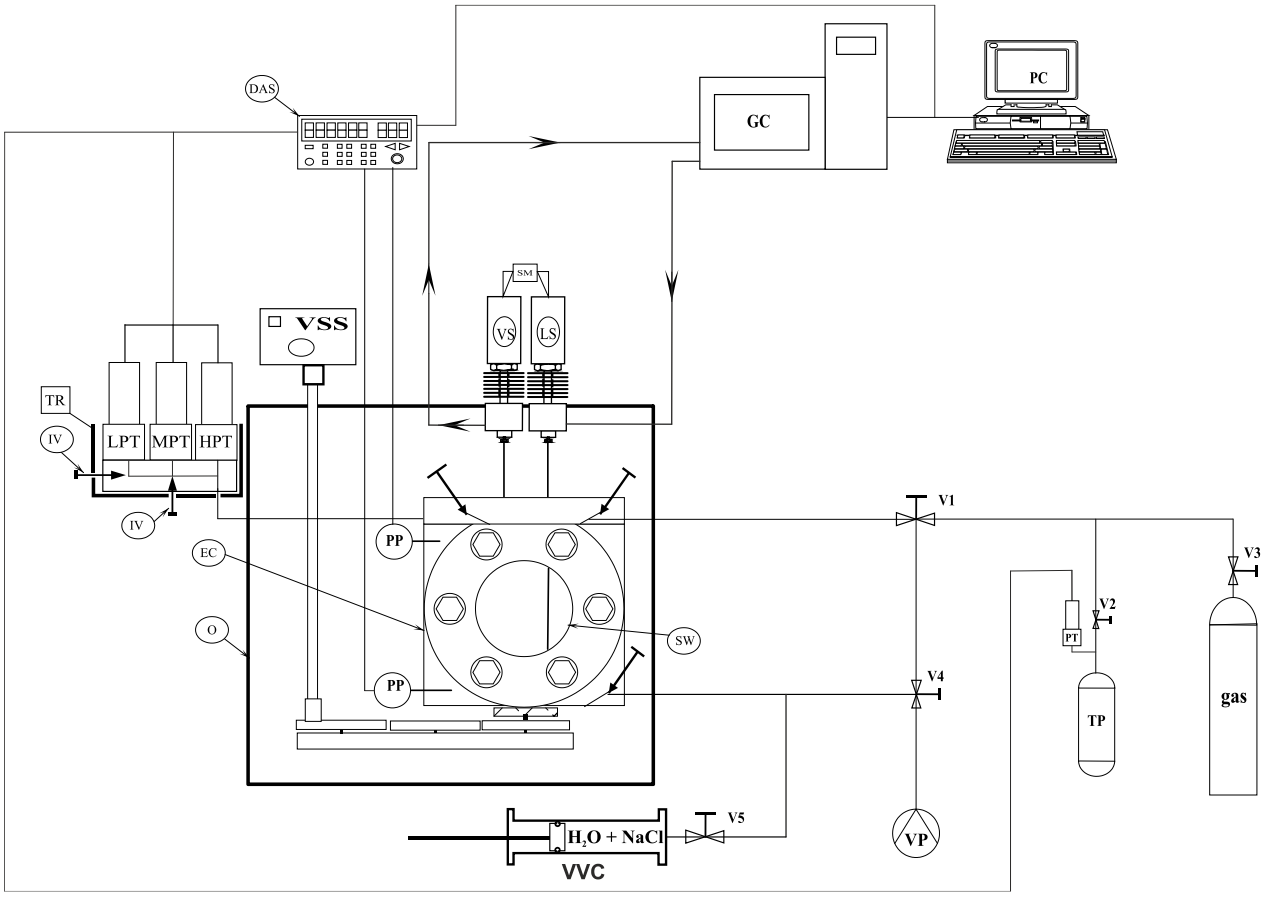

Figure 5.2 : Schematic representation of the static-analytic apparatus [5. 17] used to measure the solubility of gas (H_2) in NaCl brine. DAS: data acquisition system, EC: equilibrium cell, GC: gas chromatography, HPT: high pressure transducer, LPT: low pressure transducer, LS: liquid ROLSI® capillary Sampler-Injector, MPT: medium pressure transducer, O: oven, PP: platinum resistance thermometer probe, PT: pressure transducer, IV: homemade shut off valve, SM: samplers monitoring, SW: sapphire window, TP: thermal press, TR: temperature regulator, Vi: valve i, VP: vacuum pump, VS: vapor ROLSI® capillary Sampler-Injector, VSS: variable speed stirrer and VVC: Variable Volume Cell.

5.2.3 Apparatus and method

The experimental method used for this work has already been employed to measure the solubility of CO_2 [5. 17, 18] and O_2 [5. 18] in NaCl brine. However, a brief description of this technique will be presented (for more details, see Chabab et al. [5. 17, 18]).

The technique based on the "static-analytic" method is illustrated in Figure 5.2 and consists of:

1- Performing the Equilibrium in a Cell (EC) placed in an Oven (O) to control the temperature, and equipped with a Variable Speed Stirrer (VSS), pressure and temperature sensors, and ROLSI® (Rapid On-Line Sampler-Injector, French patent number 0304073) capillary samplers. The desired pressure is less controlled than the temperature, and is obtained by adding through a manual valve (V1) the necessary quantity of gas to the saline solution previously loaded in the cell.

2- Taking a sample from the liquid phase by the ROLSI® and transferring it to the analytical part once the thermodynamic equilibrium (temperature and pressure stabilization) has been reached.

3- Quantification of non-electrolyte compounds (H_2 and H_2O) by GC analysis.

This last step depends on GC detector calibration, which is carried out under the same measurement conditions, to convert the areas obtained by integration of the chromatogram peaks into numbers of moles. It should be noted that Argon was used as carrier gas. Using the mole number of H_2 (n_{H_2}) and H_2O (n_{H_2O}), the solubility of H_2 in the saline solution in terms of "salt-free" mole fraction x_{H_2} is determined:

$$x_{H_2} = \frac{n_{H_2}}{n_{H_2} + n_{H_2O}} \tag{5.1}$$

The solubility in terms of "salt-free" mole fraction x_{H_2} can be converted in terms of molality m_{H_2} (in mol/kgw) easily by the following relationship:

$$m_{H_2} = \frac{1000\, x_{H_2}}{M_{H_2O}(1 - x_{H_2})} \tag{5.2}$$

or in terms of "true" mole fraction by

$$x_{H_2}^{true} = \frac{n_{H_2}}{n_{H_2} + n_{H_2O} + n_s} = \frac{n_{H_2}}{n_{H_2} + n_{H_2O} + m_s n_{H_2O} M_{H_2O}} = \frac{x_{H_2}}{x_{H_2} + \left(1 - x_{H_2}\right)\left(1 + m_s M_{H_2O}\right)} \tag{5.3}$$

where n_s and m_s are respectively the mole number and molality (in mol/kgw) of the salt (NaCl), and M_{H_2O} is the molecular weight of water (in g/mol).

To check repeatability and to obtain data that are more representative of the real solubility, the procedure described above is repeated several times.

5.2.4 Experimental results

Experimental measurements of H_2 solubility in H_2O+NaCl were carried out at temperatures between 323 K and 373 K, at pressures up to 230 bar and at NaCl molalities (m=mol/kgw) equal to 0 (pure water), 1m, 3m and 5m. These measurements are presented in Table 5.4, knowing that the reported data (P, T, x_{H_2}) with the associated uncertainties are an average of several repeated measurements. The method proposed by NIST [5. 54] was used to estimate measurement uncertainties. The uncertainties related to the TCD calibration (determination of mole numbers) and repeatability, are taken into account in the calculation of the total uncertainty on composition $u(x_{H_2})$, by the following relationship:

$$u(x_{H_2}) = \pm\sqrt{u^2_{calibration}(x_{H_2}) + u^2_{repeatability}(x_{H_2})} \quad \textbf{(5.4)}$$

Since the composition x_{H_2} is determined from the values of the other independent measurands (number of moles of the compounds: n_{H_2} and n_{H_2O}), the law of propagation of uncertainty should apply [5. 55, 56, 57, 58]:

$$\begin{aligned} u(x_{H_2}) &= \pm\sqrt{\left(\frac{\partial x_{H_2}}{\partial n_{H_2}}\right)^2 u^2(n_{H_2}) + \left(\frac{\partial x_{H_2}}{\partial n_{H_2O}}\right)^2 u^2(n_{H_2O}) + u^2_{repeatability}(x_{H_2})} \\ &= \pm\sqrt{\left(\frac{1 - x_{H_2}}{n_{H_2} + n_{H_2O}}\right)^2 u^2(n_{H_2}) + \left(\frac{x_{H_2}}{n_{H_2} + n_{H_2O}}\right)^2 u^2(n_{H_2O}) + u^2_{repeatability}(x_{H_2})} \end{aligned} \quad \textbf{(5.5)}$$

The uncertainty $u(n_i)$ involved in the calculation of the mole number n_i takes into account the injection of the constituents by the syringe (for GC calibration) $u_{inj}(n_i)$ and the polynomial equation $u_{pol.eq}(n_i)$ relating the surface area S (obtained by integration of the chromatogram) and the mole number n:

$$u(n_i) = \sqrt{u^2_{inj}(n_i) + u^2_{pol.eq}(n_i)} \quad \textbf{(5.6)}$$

The calculation of $u_{repeatability}(x)$, $u_{inj}(n_i)$ and $u_{pol.eq}(n_i)$ are described in detail by Soo [5. 56], Zhang [5. 57] and El Abbadi [5. 58]. In the same way repeatability and calibration

(polynomial equation) are the two sources of error on the measurement of pressure $u(P)$ and temperature $u(T)$ uncertainties.

Since the water content in the H_2-rich phase is very low, and considering the vapor phase as ideal, the Krichevsky-Kasarnovsky [5. 59] equation $\left(ln\left(\frac{f_g}{x_g}\right) = ln(K_H) + PF = f(P)\right)$ derived from the gamma-phi approach is reduced to: $\left(ln\left(\frac{P}{x_g}\right) = f(P)\right)$, where f_g, x_g and K_H are respectively the fugacity, the mole fraction and the Henry constant of the gas, PF is the Poynting Factor and $f(P)$ is a linear function with respect to the pressure P.

In Figure 5.3, the measured data were plotted as $ln\left(\frac{P}{x_{H_2}}\right) = f(P)$ to check their linearity. By comparing with the predictions of the e-PR-CPA model (see next section), in general, one can observe a good linearity even by neglecting the fugacity coefficient and water content. Only a few points at low pressure are slightly shifted, this is due to the fact that the water content is not negligible at low pressure and also to the experimental protocol. The H_2 solubility in pure water was measured to validate the calibration by comparing with literature data. Figure 5.3 shows that the obtained measurements are in good agreement with the literature data.

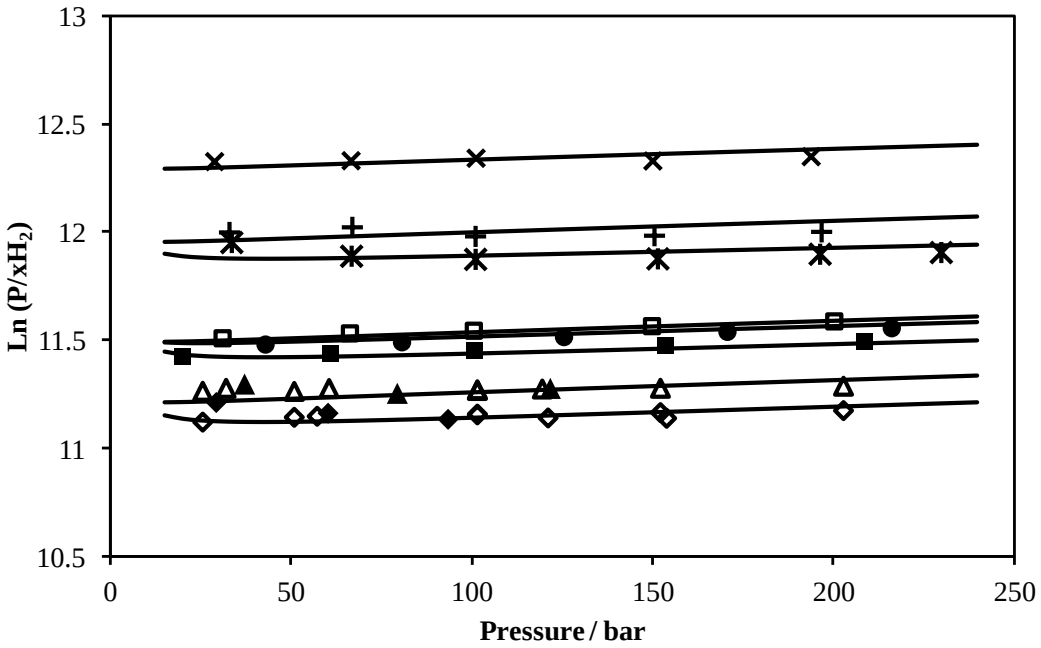

Figure 5.3: Solubility of H_2 in H_2O + NaCl. Literature data [5. 20, 49, 52] are represented by black symbols (△: 323 K – pure water; ◊: 373K – pure water) and measured ones (Table 5.4) are represented by colored symbols (▲: 323 K – pure water; □: 323 K – 1m; +: 323 K – 3m; ×: 323 K – 5m; ●: 348 K – 1m; ◆: 373K – pure water; ■: 373 K – 1m; ✱: 373 K – 3m). The solid lines represent the predictions of the e-PR-CPA model.

Table 5.4: Measured solubility of H_2 in the H_2O + NaCl solutions, expressed as "salt-free" mole fractions (Equation 5.1). $u(T) = 0.02$ K and $u(P) = 5$ kPa.

m_{NaCl} (mol/kg_w)	T (K)	P (bar)	x_{H_2}	$u(x_{H_2})$
0	323.18	37.108	0.000461	2.0E-05
	323.18	79.366	0.001030	3.0E-05
	323.19	121.706	0.001544	4.0E-05
	372.71	29.272	0.000396	2.5E-05
	372.73	60.213	0.000857	3.5E-05
	372.72	93.426	0.001368	6.0E-05
1	323.20	30.828	0.000309	1.0E-05
	323.21	66.068	0.000648	2.0E-05
	323.21	100.354	0.000972	3.5E-05
	323.21	149.657	0.001419	4.0E-05
	323.21	200.093	0.001855	6.0E-05
	347.90	42.907	0.000444	1.0E-05
	347.91	80.673	0.000827	2.0E-05
	347.90	125.504	0.001255	4.0E-05
	347.90	170.730	0.001667	4.5E-05
	347.91	216.205	0.002076	6.0E-05
	372.73	19.884	0.000217	1.0E-05
	372.76	60.987	0.000659	2.0E-05
	372.76	100.677	0.001071	3.5E-05
	372.78	153.553	0.001595	4.5E-05
	372.72	208.620	0.002132	7.0E-05
3	323.20	32.736	0.000201	1.5E-05
	323.18	66.733	0.000400	2.0E-05
	323.20	100.832	0.000631	2.0E-05
	323.21	150.342	0.000938	3.5E-05
	323.20	196.595	0.001204	4.0E-05
	372.75	33.387	0.000215	1.5E-05
	372.74	66.536	0.000456	1.5E-05
	372.74	100.855	0.000702	3.0E-05
	372.76	151.296	0.001050	4.0E-05
	372.75	196.178	0.001333	4.0E-05
	372.76	229.720	0.001549	5.0E-05
5	323.19	28.623	0.000127	5.0E-06

323.19	66.385	0.000293	1.0E-05
323.19	100.979	0.000440	1.0E-05
323.20	149.900	0.000662	2.0E-05
323.19	193.702	0.000838	3.5E-05

5.3 Thermodynamic modeling

Asymmetric and symmetric thermodynamic approaches were used for modeling liquid-vapor equilibria of the binary H_2+H_2O and ternary H_2+H_2O+NaCl.

5.3.1 Approaches and models

In the asymmetric approach, the non-ideality of the vapor phase is taken into account by considering fugacity coefficients in the vapor phase, which are obtained by using an equation of state. However the non-ideality of the liquid phase is considered with a G-excess model through the activity coefficients. Based on this approach, the **Geochemical model** implemented in CHESS/HYTEC software and proposed by Corvisier [5. 60, 61] was tested.

In the symmetric approach, the two phases (liquid and vapor) in equilibrium are represented by the same model (Equation of State (EoS)). Based on this approach, two equations of state (**SW** and **e-PR-CPA**) were tested.

These three models (Geochemical, SW, and e-PR-CPA models) were presented in details in our previous work [5. 17, 18], however a brief description of the models and their parameters resulting from this work are given hereafter.

A. Geochemical model

This model solves a large set of mass balances and mass action laws to calculate the whole system speciation (i.e. aqueous, gaseous and solid quantities and activities/fugacities). Nevertheless, to handle multi-components either for the gas phase and the electrolyte, equations shall remain generic. For the gas phase, the PR-SW EoS is used with the classical mixing rule. For the aqueous solution and particularly for saline solutions with high ionic strength, activity coefficients are calculated using Specific Ion Theory (SIT) showing satisfactory results.

Simulations presented here are run along with the Thermoddem database including parameters for PR-SW EoS (Blanc et al. [5. 62]) with the addition of the Henry's constant for H_2 (Harvey [5. 63]), and parameters for molar volume of the dissolved gaseous component at infinite

dilution (Shock et al. [5. 64]). Gas binary interaction parameters for PR-SW and aqueous binary interactions parameters for SIT have been fitted on experimental data.

- $k_{H_2H_2O}$ is equal to 0.445.
- $\varepsilon_{H^+Cl^-}$ and $\varepsilon_{Na^+Cl^-}$ are equal to -0.097 and -0.035 using HCl and NaCl solutions activity measurements (Schneider et al. [5. 65], Sakaida and Kakiuchi [5. 66]; Khoshkbarchi and Vera [5. 67]).
- $\varepsilon_{H_2Na^+}$ vary with temperature (from 0.090 at 25°C to 0.108 at 100°C) using H_2 solubility measurements in NaCl solutions.

B. Soreide and Whitson (SW) EoS

The Soreide and Whitson [5. 16] EoS is widely used in oil and gas applications especially for gas/water/salt systems, and is available in several thermophysical calculators and reservoir simulators. This EoS does not consider the salt (NaCl) as a compound, but takes into account its presence by adding a dependence of the model parameters (water alpha function $\alpha_w(T)$ and the aqueous phase binary interaction parameter k_{ij}^{AQ}) to the NaCl molality. The use of two binary interaction parameters (k_{ij}^{AQ} for the aqueous phase and k_{ij}^{NA} for the non-aqueous phase) makes the model inconsistent (similar to an asymmetric approach) and very empirical (to be used just within the range of parameter fit). Concerning $k_{H_2-H_2O}^{AQ}$ and $k_{H_2-H_2O}^{NA}$, we have taken the expression recently proposed by Lopez-Lazaro et al. [5. 13] which performs well when compared with our new data and readjusted its coefficients on H_2 solubility data in brine (including those obtained in this work) and on water content data.

$$\left(k_{H_2-H_2O}\right)_{SW} = A_0\left(1+\alpha_0 {m_{NaCl}}^{\beta_0}\right) + A_1\frac{T}{T_{c,H_2}}\left(1+\alpha_1 {m_{NaCl}}^{\beta_1}\right) + A_2\exp\left(A_3\frac{T}{T_{c,H_2}}\right) \tag{5.7}$$

The coefficients A_x, α_x and β_x given by Lopez-Lazaro et al. [5. 13] and those proposed in this work are listed in Table 5.5. The H_2 critical temperature $T_{c,H_2} = 33.145\ K$ was taken from REFPROP 10.0 [5. 68]. The readjustment of the coefficients has led to a significant improvement (comparing with the coefficients given by Lopez-Lazaro et al.) in the estimation of the solubility of H_2 in water and NaCl-brine (AAD of 2.6% instead of 4.3%), and of the water content in the H_2-rich phase (AAD of 2.5% instead of 6.6%).

Table 5.5: Optimized coefficients of the binary interaction parameters in aqueous $k^{AQ}_{H_2-H_2O}$ and non-aqueous $k^{NA}_{H_2-H_2O}$ phases (Equation 5.7).

		Lopez-Lazaro et al. [5. 13]		This work	
		$k^{AQ}_{H_2-H_2O}$	$k^{NA}_{H_2-H_2O}$	$k^{AQ}_{H_2-H_2O}$	$k^{NA}_{H_2-H_2O}$
A_0		-2.513	2.5	-2.34	-0.3776
A_1		0.181	-0.179	0.166	0.08385
A_2		-12.723	-	-12.69	-
A_3		-0.499	-	-0.474	-
α_0		6.8×10^{-4}	-	3.88×10^{-3}	-
α_1		0.038	-	0.049	-
β_0		0.443	-	0.443	-
β_1		0.799	-	0.799	-
AAD (%)	x_{H_2}	4.3		2.6	
	y_{H_2O}	6.6		2.5	

C. e-PR-CPA EoS

Unlike the SW EoS, the e-PR-CPA (electrolyte Peng-Robinson Cubic Plus Association) EoS takes into account the presence of salt theoretically. This model considers molecular interactions (attraction, dispersion, and association) by the PR (Peng-Robinson) cubic term [5. 69] and the Wertheim's association theory [5. 70], and ionic interactions ion/ion by the MSA (Mean Spherical Approximation) theory [5. 71] and ion/solvent (solvation phenomenon) by the Born term [5. 72]. The expression of the residual Helmholtz free energy of the e-PR-CPA EoS is as follows:

$$\frac{A^{res}_{e-PR-CPA}}{RT} = \frac{A^{PR}}{RT} + \frac{A^{Association}}{RT} + \frac{A^{MSA}}{RT} + \frac{A^{Born}}{RT} \quad \textbf{(5.8)}$$

The expression of the residual Helmholtz energy A^{res} is the key function in equilibrium thermodynamics, because all other thermodynamic properties (pressure, fugacity coefficient, enthalpy, etc.) are calculable from the partial derivatives of A^{res} with respect to temperature, volume, and mole number. Further details on the different terms of Equation 5.8 and their

calculation methods as well as the model parameterization (for pure H_2O and H_2O+NaCl) are presented in our previous paper [5. 17].

Since H_2 is not considered as an associative species, the solvation (cross-association interaction) of H_2 by H_2O molecules was not considered (no Lewis Acid − Lewis Base interaction). Only the binary interaction parameters (of the cubic term PR) of the $H_2 - H_2O$, $H_2 - Na^+$, and $H_2 - Cl^-$ pairs were considered in the fit. Temperature dependence was considered in the $H_2 - H_2O$ interaction, and salt concentration dependence was considered in the $H_2 -$ ion interactions.

$$k_{H_2-H_2O} = -2.51 \times 10^{-5}\, T^2 + 2.24 \times 10^{-2}\, T - 4.44 \quad \textbf{(5.9)}$$

$$k_{H_2-Na^+} = -1.58\, m_{NaCl} - 5.7 \quad \textbf{(5.10)}$$

$$k_{H_2-Cl^-} = 0.96\, m_{NaCl} + 4.87 \quad \textbf{(5.11)}$$

5.3.2 H_2+H_2O system: H_2 solubility and water content

The models presented above were used to process data of H_2 solubility in pure water. In Figure 5.4, literature data and "validation" measurements are presented together with calculated solubilities at 323 and 373 K. Compared to experimental data, all three models estimate accurately the solubility of H_2 in pure water at different temperatures and pressures. The solubility is higher at 373 K, this can be better visualized by studying the effect of temperature on the solubility. In Figure 5.5, isobaric solubility data smoothed by IUPAC [5. 20] (with an accuracy of ± 1 or 2%) between 51 and 203 bar are compared with model predictions. The models reproduce very well the effect of temperature on solubility at different fixed pressures, and estimate well the minimum solubility temperature which is close to 329 (± 2) K.

The prediction of water content in the H_2-rich phase by the developed models was also investigated. Gillespie and Wilson [5. 48] data were used in the adjustment of the SW EoS and geochemical model. However, for the e-PR-CPA model, it is not necessary to include them in the parameter fitting for a good representation of the vapor phase. With a zero binary interaction parameter ($k_{H_2-H_2O} = 0$), the e-PR-CPA model reproduces the Gillespie and Wilson [5. 48] data with an Average Absolute Deviation (AAD) of 3.1% over a wide range of temperature (311 − 478 K) and pressure (3 − 138 bar), whereas with a non-zero $k_{H_2-H_2O}$ (Equation 5.9), the model reproduces the same water content data with an AAD of 2.8%. The calculation of water

content with CPA-type models is not very sensitive to variations in binary interaction parameters, which was also observed by Hajiw et al. [5. 73] using the GC-PR-CPA model. This is a great advantage of CPA-type models, as only gas solubility data are needed to parameterize the model and hence predict water content.

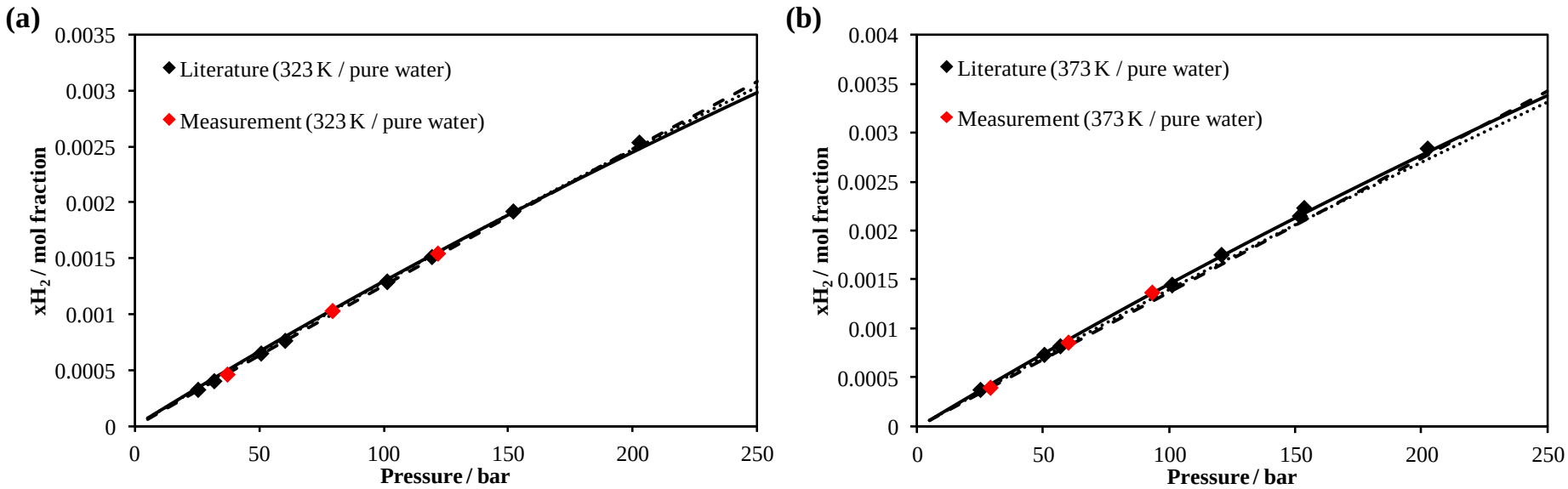

Figure 5.4 : Solubility of H_2 in H_2O at 323 K (a) and 373 K (b). Literature data [5. 20, 49, 52] are represented by black symbols (◆) and measured ones (Table 5.4) are represented by red symbols (◆). The solid, dotted and dashed lines represent the H_2 solubilities calculated by the e-PR-CPA, SW, and geochemical models, respectively.

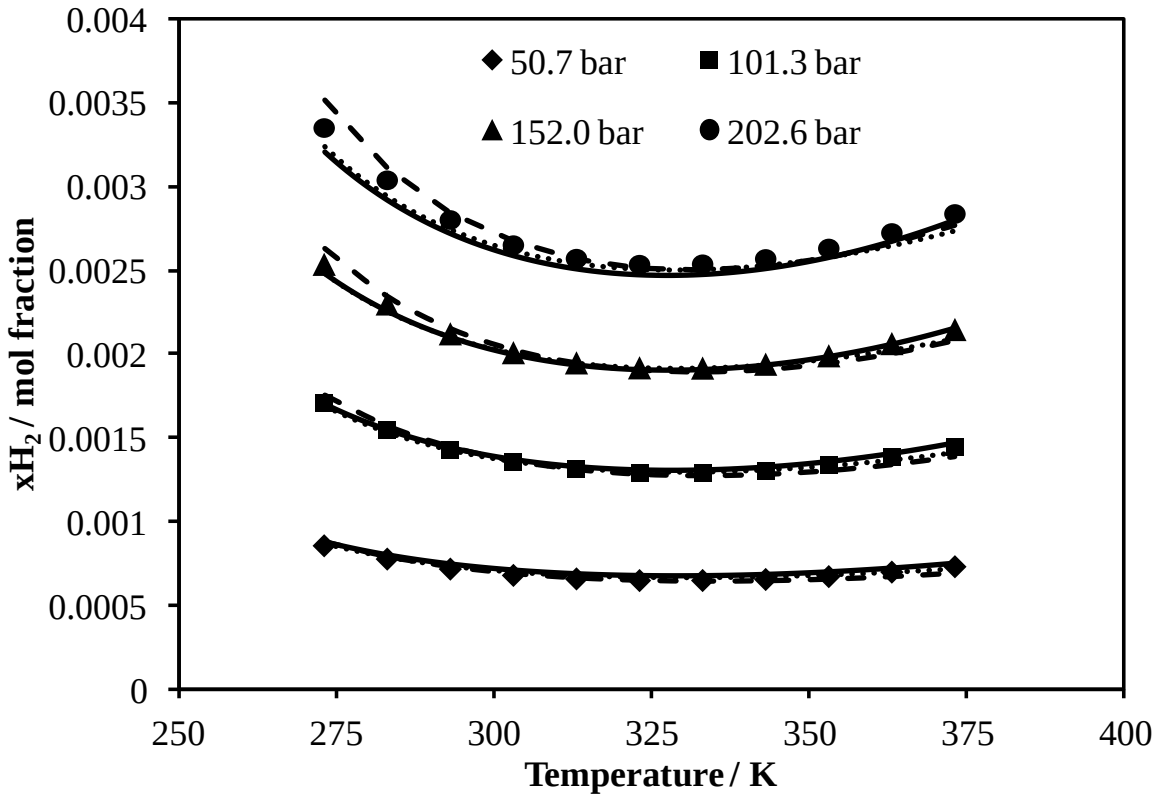

Figure 5.5 : Isobars of solubility of H_2 in H_2O showing solubility minimum temperatures at 50, 100, 150 and 200 atm. Comparison of data smoothed by IUPAC [5. 20] represented by black symbols, with predictions by e-PR-CPA, SW, and geochemical models represented by solid, dotted, and dashed lines, respectively.

In Figure 5.6, one can show that all models are able to predict the water contents, although only H_2 solubility data were used to determine the e-PR-CPA model interaction parameters. All three models can be used to generate data with high accuracy especially in the parameter fitting range, however due to its theoretical background, the e-PR-CPA model can be used with a high level of confidence for the prediction of water content outside the parameter fitting range. In Table 5.6, predictions of water content in the H_2+H_2O binary system are generated with the e-PR-CPA model at different temperatures and pressures.

Table 5.6 : H_2+H_2O binary system: Predicted water content y_{H_2O} in H_2-rich phase by the e-PR-CPA model.

P (bar)	T (K)					
	298.15	323.15	348.15	373.15	398.15	423.15
2	0.01607391	0.06204187	0.19388235	0.50968425		
3	0.01073722	0.04142540	0.12952971	0.34180465	0.77743831	
4	0.00806878	0.03111404	0.09729662	0.25720417	0.58886005	
5	0.00646768	0.02492622	0.07793854	0.20623041	0.47400614	
6	0.00540027	0.02080058	0.06502553	0.17215844	0.39671208	0.80424530
7	0.00463784	0.01785348	0.05579820	0.14777733	0.34114267	0.69524713
8	0.00406600	0.01564304	0.04887564	0.12946735	0.29926734	0.61233208
9	0.00362125	0.01392374	0.04349020	0.11521191	0.26657938	0.54713811
10	0.00326544	0.01254825	0.03918107	0.10379850	0.24035410	0.49453249
11	0.00297432	0.01142282	0.03565489	0.09445423	0.21884731	0.45119016
12	0.00273173	0.01048494	0.03271605	0.08666320	0.20089066	0.41486231
13	0.00252646	0.00969133	0.03022907	0.08006782	0.18567212	0.38397358
14	0.00235051	0.00901108	0.02809719	0.07441248	0.17260976	0.35738747
15	0.00219802	0.00842151	0.02624940	0.06950956	0.16127564	0.33426351
16	0.00206459	0.00790564	0.02463248	0.06521826	0.15134806	0.31396673
17	0.00194687	0.00745045	0.02320569	0.06143086	0.14258047	0.29600849
18	0.00184222	0.00704583	0.02193736	0.05806350	0.13478078	0.28000665
19	0.00174859	0.00668379	0.02080247	0.05504999	0.12779709	0.26565799
20	0.00166432	0.00635795	0.01978103	0.05233732	0.12150770	0.25271891
21	0.00158808	0.00606315	0.01885682	0.04988260	0.11581397	0.24099140
22	0.00151877	0.00579513	0.01801659	0.04765068	0.11063510	0.23031289
23	0.00145548	0.00555042	0.01724940	0.04561256	0.10590427	0.22054866
24	0.00139747	0.00532610	0.01654611	0.04374403	0.10156574	0.21158609
25	0.00134410	0.00511972	0.01589906	0.04202478	0.09757266	0.20333035
26	0.00129484	0.00492922	0.01530176	0.04043759	0.09388534	0.19570098
27	0.00124923	0.00475282	0.01474868	0.03896782	0.09046995	0.18862930
28	0.00120687	0.00458902	0.01423510	0.03760290	0.08729748	0.18205630
29	0.00116744	0.00443651	0.01375692	0.03633199	0.08434290	0.17593104
30	0.00113063	0.00429417	0.01331060	0.03514570	0.08158451	0.17020926
35	0.00097815	0.00370444	0.01146140	0.03022994	0.07014866	0.14645440
40	0.00086380	0.00326211	0.01007428	0.02654184	0.06156294	0.12858457
45	0.00077486	0.00291803	0.00899524	0.02367247	0.05487974	0.11465357
50	0.00070370	0.00264273	0.00813187	0.02137636	0.04952962	0.10348815
55	0.00064549	0.00241746	0.00742536	0.01949726	0.04514979	0.09433894
60	0.00059697	0.00222971	0.00683650	0.01793097	0.04149814	0.08670488
65	0.00055592	0.00207081	0.00633813	0.01660535	0.03840692	0.08023824
70	0.00052074	0.00193459	0.00591088	0.01546884	0.03575625	0.07469013
75	0.00049024	0.00181651	0.00554051	0.01448363	0.03345816	0.06987772
80	0.00046355	0.00171317	0.00521637	0.01362138	0.03144663	0.06566369

85	0.00044001	0.00162196	0.00493029	0.01286039	0.02967116	0.06194288
90	0.00041907	0.00154087	0.00467594	0.01218379	0.02809247	0.05863342
95	0.00040034	0.00146829	0.00444830	0.01157827	0.02667951	0.05567060
100	0.00038348	0.00140295	0.00424336	0.01103315	0.02540747	0.05300262
105	0.00036822	0.00134382	0.00405789	0.01053982	0.02425623	0.05058751
110	0.00035435	0.00129005	0.00388923	0.01009122	0.02320934	0.04839089
115	0.00034168	0.00124094	0.00373519	0.00968152	0.02225320	0.04638436
120	0.00033007	0.00119590	0.00359394	0.00930585	0.02137649	0.04454424
125	0.00031938	0.00115445	0.00346394	0.00896013	0.02056967	0.04285060
130	0.00030951	0.00111617	0.00334390	0.00864092	0.01982470	0.04128660
135	0.00030037	0.00108072	0.00323271	0.00834525	0.01913471	0.03983787
140	0.00029189	0.00104778	0.00312943	0.00807062	0.01849381	0.03849209
145	0.00028398	0.00101710	0.00303323	0.00781484	0.01789694	0.03723865
150	0.00027660	0.00098846	0.00294340	0.00757604	0.01733968	0.03606834
155	0.00026969	0.00096165	0.00285934	0.00735257	0.01681822	0.03497312
160	0.00026322	0.00093650	0.00278049	0.00714299	0.01632920	0.03394598
165	0.00025713	0.00091286	0.00270639	0.00694604	0.01586967	0.03298074
170	0.00025140	0.00089060	0.00263662	0.00676061	0.01543703	0.03207196
175	0.00024599	0.00086961	0.00257080	0.00658571	0.01502899	0.03121481
180	0.00024088	0.00084976	0.00250861	0.00642046	0.01464349	0.03040498
185	0.00023605	0.00083098	0.00244975	0.00626409	0.01427871	0.02963867
190	0.00023146	0.00081318	0.00239396	0.00611589	0.01393301	0.02891243
195	0.00022711	0.00079628	0.00234101	0.00597523	0.01360493	0.02822319
200	0.00022298	0.00078021	0.00229068	0.00584155	0.01329315	0.02756819

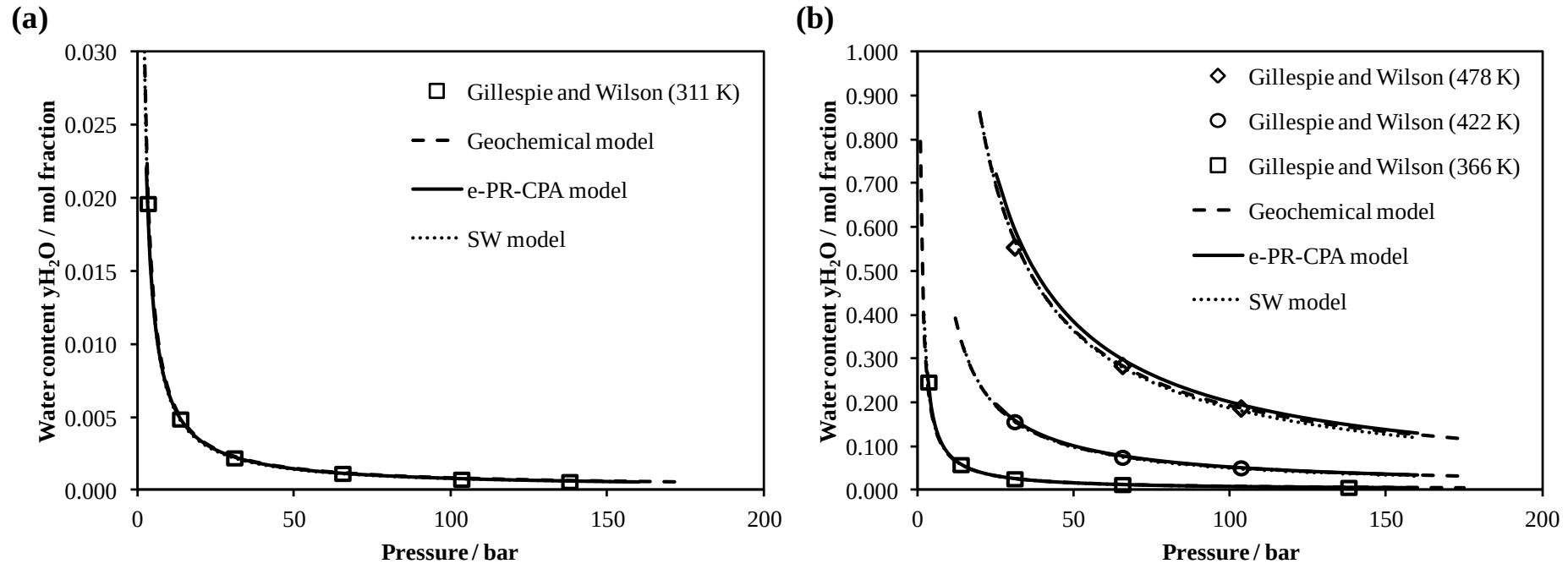

Figure 5.6 : Water content in H_2-rich phase at (a): 311 K; (b): 366, 422, and 478 K. Comparison of literature data [5. 48] represented by black symbols, with predictions with the e-PR-CPA, SW, and geochemical models represented by solid, dotted, and dashed lines, respectively.

5.3.3 H_2+H_2O+NaCl system: H_2 solubility

As with all gases, the presence of salt in water is expected to decrease the solubility of hydrogen (salting-out effect) in a manner proportional to the concentration of the salt until the solution is saturated. Both atmospheric pressure data of H_2 solubilities in H_2O+NaCl from literature as well as new high pressure data measured in this work were included in the parameterization of the models (Geochemical, SW, and e-PR-CPA). The modeling results are shown in Figure 5.7. The three models correlate solubility data at different temperatures (323−373 K) and pressures (up to 230 bar) with high accuracy and capture accurately the salting-out effect over a wide range of NaCl concentration (from salt-free solution to highly concentrated brine).

Given its very good performance and predictive capability, the e-PR-CPA model was used to predict solubility minimum temperatures in the presence of NaCl. In Figure 5.8.a, isothermal data (at 323, 348 and 373 K) of the solubility of H_2 in water and brine (1m NaCl) as a function of pressure are presented and compared with the model calculations. In Figure 5.8.b, the prediction of the evolution of H_2 solubility as function of temperature at 152 bar (which is a pressure more or less representative of hydrogen geological storage conditions) is compared with salt-free data and measured data around 152 bar. Since the calculated solubilities are in very good agreement with the IUPAC (in pure water) and measured (in brine) data, accurate H_2 solubility values in water and brine were generated at different temperatures, pressures and NaCl molalities with the e-PR-CPA model and listed in Table 5.8.

Correlation for H_2 solubility in water and NaCl-brine:

For quick calculations of the solubility of H_2 in water and brine, a simple correlation taking into account the effect of temperature, pressure and molality has been developed. The proposed correlation is based on a Setschenow-type relationship, and is defined by:

$$ln\left(\frac{x_{H_2}}{x_{H_2}^0}\right) = a_1 m_{NaCl}^2 + a_2 m_{NaCl} \quad \textbf{(5.12)}$$

Knowing the solubility $x_{H_2}^0$ of H_2 in pure water at system temperature and pressure, the solubility x_{H_2} of H_2 in brine at a molality m_{NaCl} is therefore easily obtained by Equation 5.12. The solubility data (from IUPAC) of H_2 in pure water were correlated by the following equation:

$$x_{H_2}^0 = b_1 PT + \frac{b_2 P}{T} + b_3 P + b_4 P^2 \quad \textbf{(5.13)}$$

In Equation 5.13, the temperature T is in K and the pressure P is in bar. The coefficients a_i and b_i in Equations 5.12 and 5.13 are listed in Table 5.7.

Table 5.7: Coefficients for Equations 5.12 and 5.13.

a_1	a_2	b_1	b_2	b_3	b_4
0.018519	-0.30185103	3.338844×10^{-7}	0.0363161	-0.00020734	$-2.1301815 \times 10^{-9}$

The correlation for solubility in brine (Equation 5.12) is reduced to the correlation for solubility in pure water (Equation 5.13) when the molality is equal to 0.

When compared with IUPAC and measured data, the two correlations developed are capable of estimating the solubility in pure water and brine with high precision (see Figure 5.9) with an AAD of 0.5% and 2% respectively, and an overall AAD of 1%. However, it is recommended to use the two correlations only in the range of their coefficients adjustments, which are:

- For H_2 solubility in pure water (Equation 5.13): 273.15 < T (K) < 373.15; 1 < P (bar) < 203
- For H_2 solubility in NaCl-brine (Equation 5.12): 323.15 < T (K) < 373.15; 10 < P (bar) < 230; 0 < molality (mol/kgw) < 5

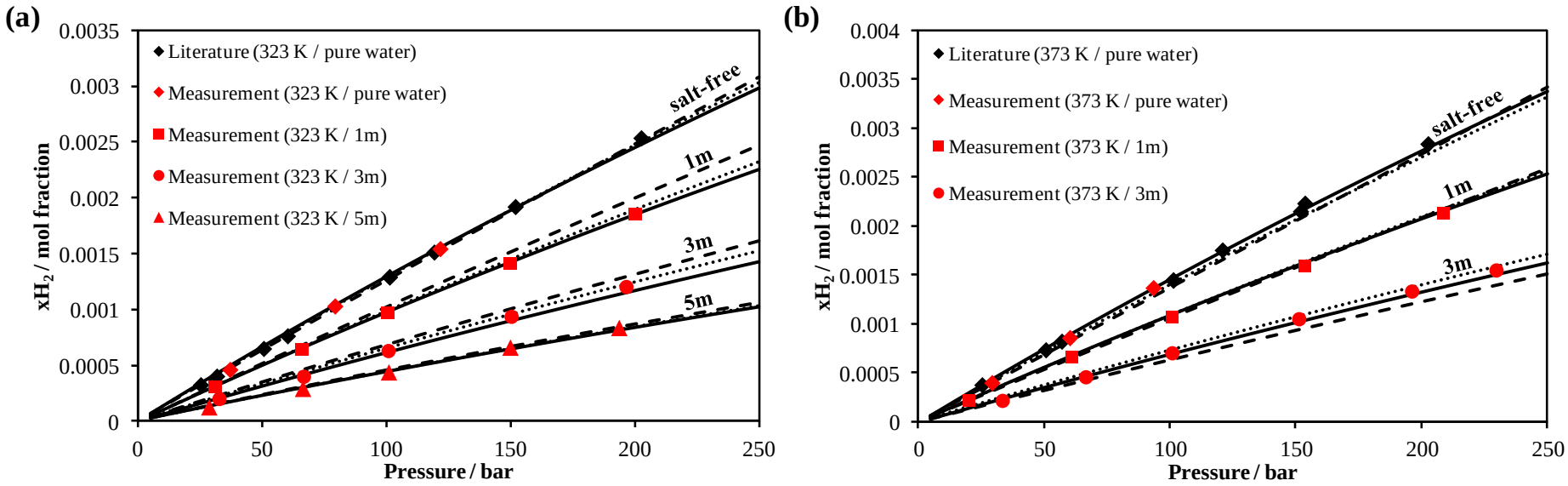

Figure 5.7 : Solubility of H_2 in H_2O + NaCl at 323 K (a) and 373 K (b) and different NaCl molalities. Literature data [5. 20, 49, 52] are represented by black symbols and measured ones (Table 5.4) are represented by red symbols. The solid, dotted and dashed lines represent the H_2 solubilities calculated by the e-PR-CPA, SW, and geochemical models, respectively.

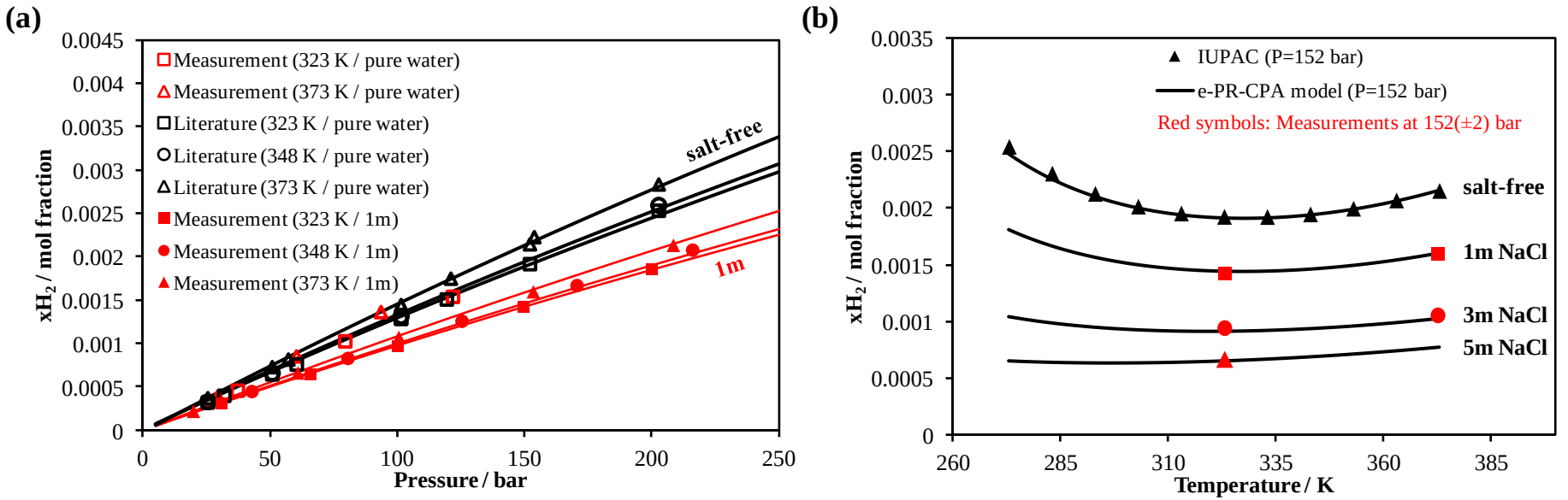

Figure 5.8 : Effect of temperature, pressure and NaCl concentration (molality) on H_2 solubility. Comparison of literature [5. 20, 49, 52] and some measured (Table 5.4) data with e-PR-CPA (solid lines) model predictions.

Table 5.8 : Calculated solubility (in terms of salt-free mole fraction) of H_2 in water + NaCl by the e-PR-CPA model.

T (K)	P (bar)										
	5	10	15	20	25	50	75	100	200	300	400
						m = 0 mol/kgw					
298.15	0.0000732	0.0001463	0.0002190	0.0002911	0.0003628	0.0007144	0.0010550	0.0013854	0.0026164	0.0037247	0.0047326
323.15	0.0000669	0.0001351	0.0002029	0.0002702	0.0003371	0.0006654	0.0009839	0.0012932	0.0024473	0.0034877	0.0044335
348.15	0.0000649	0.0001348	0.0002043	0.0002733	0.0003419	0.0006789	0.0010062	0.0013242	0.0025127	0.0035852	0.0045602
373.15	0.0000619	0.0001390	0.0002155	0.0002917	0.0003674	0.0007393	0.0011007	0.0014522	0.0027674	0.0039554	0.0050353
398.15	0.0000487	0.0001385	0.0002279	0.0003168	0.0004051	0.0008395	0.0012618	0.0016728	0.0032122	0.0046038	0.0058690
423.15		0.0001151	0.0002242	0.0003326	0.0004405	0.0009709	0.0014870	0.0019894	0.0038732	0.0055776	0.0071276
						m = 1 mol/kgw					
298.15	0.0000549	0.0001097	0.0001642	0.0002183	0.0002721	0.0005357	0.0007910	0.0010387	0.0019614	0.0027920	0.0035470
323.15	0.0000506	0.0001021	0.0001533	0.0002041	0.0002547	0.0005028	0.0007436	0.0009776	0.0018525	0.0026432	0.0033638
348.15	0.0000491	0.0001017	0.0001539	0.0002058	0.0002575	0.0005112	0.0007580	0.0009981	0.0018988	0.0027159	0.0034625
373.15	0.0000467	0.0001038	0.0001606	0.0002171	0.0002732	0.0005495	0.0008186	0.0010808	0.0020672	0.0029654	0.0037883
398.15	0.0000374	0.0001024	0.0001671	0.0002315	0.0002955	0.0006109	0.0009184	0.0012185	0.0023505	0.0033852	0.0043359
423.15	0.0000091	0.0000858	0.0001622	0.0002382	0.0003139	0.0006867	0.0010508	0.0014066	0.0027525	0.0039874	0.0051257
						m = 3 mol/kgw					
298.15	0.0000334	0.0000668	0.0001000	0.0001330	0.0001657	0.0003263	0.0004820	0.0006330	0.0011965	0.0017049	0.0021678
323.15	0.0000319	0.0000642	0.0000964	0.0001284	0.0001601	0.0003163	0.0004682	0.0006159	0.0011703	0.0016741	0.0021357
348.15	0.0000314	0.0000648	0.0000980	0.0001310	0.0001639	0.0003256	0.0004832	0.0006369	0.0012166	0.0017472	0.0022360
373.15	0.0000301	0.0000662	0.0001021	0.0001379	0.0001735	0.0003489	0.0005203	0.0006877	0.0013222	0.0019067	0.0024480
398.15	0.0000245	0.0000650	0.0001053	0.0001454	0.0001853	0.0003824	0.0005753	0.0007641	0.0014827	0.0021486	0.0027686
423.15	0.0000082	0.0000548	0.0001012	0.0001474	0.0001934	0.0004206	0.0006435	0.0008621	0.0016970	0.0024751	0.0032033
						m = 5 mol/kgw					
298.15	0.0000227	0.0000453	0.0000678	0.00009019	0.00011241	0.0002214	0.0003271	0.0004298	0.0008131	0.0011596	0.0014756
323.15	0.0000227	0.0000458	0.0000688	0.00009163	0.00011433	0.0002260	0.0003346	0.0004404	0.0008383	0.0012013	0.00153497

348.15	0.0000231	0.00004764	0.00007209	0.00009642	0.00012063	0.0002399	0.0003562	0.00046986	0.0008998	0.00129521	0.00166131
373.15	0.0000223	0.00004934	0.00007623	0.000103	0.00012964	0.0002611	0.0003897	0.00051558	0.00099429	0.0014379	0.0018512
398.15	0.00001797	0.0000484	0.0000787	0.00010888	0.00013893	0.0002874	0.00043296	0.00057574	0.0011212	0.00163005	0.00210691
423.15	0.00000496	0.00003989	0.0000747	0.00010937	0.00014392	0.00031479	0.00048262	0.00064754	0.00128025	0.00187407	0.00243355

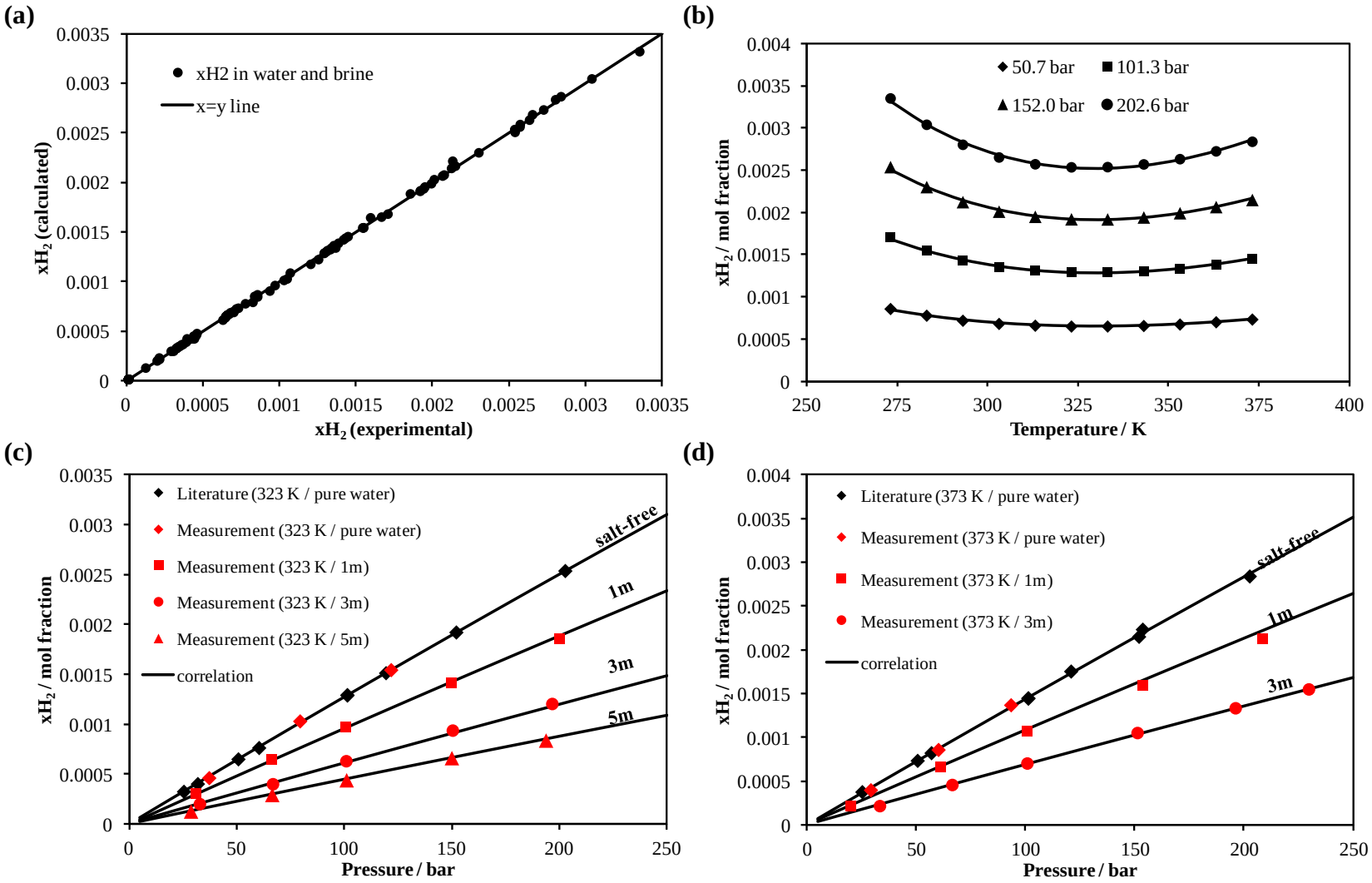

Figure 5.9: Calculated Solubility (solid lines) of H_2 in H_2O + NaCl using correlation (Equations 5.12 and 5.13). (a): measured vs calculated x_{H_2}; (b): Isobars of H_2 solubility in pure water; (c) and (d): Isotherms of solubility of H_2 in water and brine at different molalities. Literature data [5. 20, 49, 52] are represented by black symbols and measured ones (Table 5.4) are represented by red symbols.

5.4 Conclusions

Knowledge of high pressure hydrogen solubility in brine is of great importance especially for Underground Hydrogen Storage (UHS), however, a literature review has shown that there are no published experimental data at high pressure to date due to technical and safety challenges. The "static-analytic" apparatus developed and validated in our previous work has been used to perform original measurements of H_2 solubility in H_2O+NaCl at high pressure (up to 230 bar) and at different temperatures (323 and 373 K) and molality (from salt-free to highly concentrated NaCl brine). The GC calibration was verified by performing measurements of H_2 solubility in pure water which were compared with available literature data. The consistency of the measured data was verified with a Krichevsky-Kasarnovsky type approach. Some medium uncertainties were observed at low pressure (low solubility) due to the necessity of using two syringes of different volumes for calibration (one for small quantities and the other for large quantities). The new H_2 solubility data will serve to improve the models implemented in the various reservoir simulation software (e.g. the nonisothermal multiphase flow and reactive transport simulator OpenGeoSys [5. 15]) for the simulation of hydrogen storage.

For the processing of these new measured data, three models (Geochemical, SW, and e-PR-CPA models) using different thermodynamic approaches were used. The new data were used in the parameterization of these models, and in the evaluation of recently published pseudo-data from molecular simulation or "predictive" models. The tested models can describe very well the solubility of H_2 in water and brine as well as the water content in the H_2-rich phase under different thermodynamic conditions. Accurate data tables of water content and H_2 solubility in H_2O±NaCl were generated with the e-PR-CPA model at different temperature, pressure and molality. Moreover, a simple Setschenow-type correlation has been proposed which is very efficient if used in the coefficient fitting range. Finally, the models and correlations proposed in this work can be used to calculate the solubility of hydrogen under geological storage conditions, however one method may be chosen over another, depending on the simplicity, accuracy, and degree of prediction (within or outside the fitting range).

Acknowledgments

Financial support from Géodénergies through the project "Rostock H" is gratefully acknowledged. Institut CARNOT "M.I.N.E.S." (Hytrend Project) is also gratefully acknowledged.

References

[5. 1] M.W. Melaina, O. Antonia, M. Penev, Blending hydrogen into natural gas pipeline networks. a review of key issues, in, National Renewable Energy Laboratory, 2013.
[5. 2] Z. Shi, K. Jessen, T.T. Tsotsis, Impacts of the subsurface storage of natural gas and hydrogen mixtures, International Journal of Hydrogen Energy, 45 (2020) 8757-8773.
[5. 3] A. Züttel, Hydrogen storage methods, Naturwissenschaften, 91 (2004) 157-172.
[5. 4] A. Ozarslan, Large-scale hydrogen energy storage in salt caverns, International Journal of Hydrogen Energy, 37 (2012) 14265-14277.
[5. 5] R. Tarkowski, Underground hydrogen storage: Characteristics and prospects, Renewable and Sustainable Energy Reviews, 105 (2019) 86-94.
[5. 6] N. Bader, R. Bleischwitz, A.N. Madsen, P.D. Andersen, EU policies and cluster development of hydrogen communities, Bruges European Economic Research papers, (2008).
[5. 7] G. Strobel, B. Hagemann, T.M. Huppertz, L. Ganzer, Underground bio-methanation: Concept and potential, Renewable and Sustainable Energy Reviews, 123 (2020) 109747.
[5. 8] O. Kruck, F. Crotogino, Benchmarking of selected storage options, Hannover, Germany, (2013).
[5. 9] F. Crotogino, Larger scale hydrogen storage, in: Storing energy, Elsevier, 2016, pp. 411-429.
[5. 10] M. Bai, K. Song, Y. Sun, M. He, Y. Li, J. Sun, An overview of hydrogen underground storage technology and prospects in China, Journal of Petroleum Science and Engineering, 124 (2014) 132-136.
[5. 11] V. Reitenbach, L. Ganzer, D. Albrecht, B. Hagemann, Influence of added hydrogen on underground gas storage: a review of key issues, Environmental Earth Sciences, 73 (2015) 6927-6937.
[5. 12] B. Hagemann, M. Rasoulzadeh, M. Panfilov, L. Ganzer, V. Reitenbach, Hydrogenization of underground storage of natural gas, Computational Geosciences, 20 (2016) 595-606.
[5. 13] C. Lopez-Lazaro, P. Bachaud, I. Moretti, N. Ferrando, Predicting the phase behavior of hydrogen in NaCl brines by molecular simulation for geological applicationsPrédiction par simulation moléculaire des équilibres de phase de l'hydrogène dans des saumures de NaCl pour des applications géologiques, Bulletin de la Société Géologique de France, 190 (2019).
[5. 14] E.F. Bazarkina, I.-M. Chou, A.F. Goncharov, N.N. Akinfiev, The Behavior of H2 in Aqueous Fluids under High Temperature and Pressure, Elements: An International Magazine of Mineralogy, Geochemistry, and Petrology, 16 (2020) 33-38.
[5. 15] D. Li, C. Beyer, S. Bauer, A unified phase equilibrium model for hydrogen solubility and solution density, International Journal of Hydrogen Energy, 43 (2018) 512-529.
[5. 16] I. Søreide, C.H. Whitson, Peng-Robinson predictions for hydrocarbons, CO2, N2, and H2S with pure water and NaCl brine, Fluid Phase Equilibria, 77 (1992) 217-240.
[5. 17] S. Chabab, P. Théveneau, J. Corvisier, C. Coquelet, P. Paricaud, C. Houriez, E. El Ahmar, Thermodynamic study of the CO2–H2O–NaCl system: Measurements of CO2 solubility and modeling of phase equilibria using Soreide and Whitson, electrolyte CPA and SIT models, International Journal of Greenhouse Gas Control, 91 (2019) 102825.
[5. 18] S. Chabab, P. Ahmadi, P. Theveneau, C. Coquelet, A. Chapoy, J. Corvisier, P. Paricaud, R. Burgass, C. Houriez, E. El Ahmar, Solubility of Gases in Brine for Underground Gas Storage Application: Experimental Measurements and Modeling, in: 2019 AIChE Annual Meeting, AIChE, 2019.
[5. 19] R. Wiebe, V. Gaddy, The solubility of hydrogen in water at 0, 50, 75 and 100° from 25 to 1000 atmospheres, Journal of the American Chemical Society, 56 (1934) 76-79.
[5. 20] C.L. Young, Hydrogen and deuterium, Solubility Data Series, 5 (1981) 428-429.

[5. 21] R. Bunsen, Ueber das Gesetz der Gasabsorption, Justus Liebigs Annalen der Chemie, 93 (1855) 1-50.
[5. 22] W. Timofejew, Über die Absorption von Wasserstoff und Sauerstoff in Wasser und Alkohol, Zeitschrift für Physikalische Chemie, 6 (1890) 141-152.
[5. 23] C. Bohr, J. Bock, Bestimmung der Absorption einiger Gase in Wasser bei den Temperaturen zwischen 0 und 100°, Annalen der Physik, 280 (1891) 318-343.
[5. 24] L. Winkler, The solubility of gases in water (first treatise), Ber. Dtsch. Chem. Ges, 24 (1891) 89-101.
[5. 25] P. Steiner, Ueber die Absorption des Wasserstoffs im Wasser und in wässerigen Lösungen, Annalen der Physik, 288 (1894) 275-299.
[5. 26] L. Braun, Über die Absorption von Stickstoff und von Wasserstoff in wässerigen Lösungen verschieden dissociierter Stoffe, Zeitschrift für Physikalische Chemie, 33 (1900) 721-739.
[5. 27] G. Geffcken, Beiträge zur kenntnis der löslichkeitsbeeinflussung, Zeitschrift für Physikalische Chemie, 49 (1904) 257-302.
[5. 28] W. Knopp, Über die Löslichkeitsbeeinflussung von Wasserstoff und Stickoxydul in wässerigen Lösungen verschieden dissoziierter Stoffe, Zeitschrift für Physikalische Chemie, 48 (1904) 97-108.
[5. 29] G. Huefner, Study of the absorption of nitrogen and hydrogen in aqueous solutions, Z Phys Chem Stoechiom Verwandtschaftsl, 57 (1907) 611-625.
[5. 30] A. Findlay, B. Shen, CLVI.—The influence of colloids and fine suspensions on the solubility of gases in water. Part II. Solubility of carbon dioxide and of hydrogen, Journal of the Chemical Society, Transactions, 101 (1912) 1459-1468.
[5. 31] C. Müller, Die Absorption von Sauerstoff, Stickstoff und Wasserstoff in wässerigen Lösungen von Nichtelektrolyten, Zeitschrift für Physikalische Chemie, 81 (1913) 483-503.
[5. 32] W. Ipatiew, S. Drushina‐Artemowitsch, W. Tichomirow, Löslichkeit des Wasserstoffs in Wasser unter Druck, Berichte der deutschen chemischen Gesellschaft (A and B Series), 65 (1932) 568-571.
[5. 33] T. Morrison, F. Billett, 730. The salting-out of non-electrolytes. Part II. The effect of variation in non-electrolyte, Journal of the Chemical Society (Resumed), (1952) 3819-3822.
[5. 34] H. Pray, CE Schweickert u. BH Minnich, Ind. Eng. Chem, 44 (1952) 1146.
[5. 35] L. Zoss, A Study of the Hydrogen and Water and Oxygen and Water Systems at Various Temperatures and Pressures, in, Ph. D. thesis, Purdue University, West Lafayette, IN, 1952.
[5. 36] H. Pray, E.F. Stephan, The solubility of hydrogen in uranyl sulphate solutions at elevated temperatures, in, Battelle Memorial Inst., Columbus, Ohio, 1953.
[5. 37] W.d. Wet, Determination of gas solubilities in water and some organc liquids, JS Afr Chem Inst, 17 (1964) 9-13.
[5. 38] P. Ruetschi, R. Amlie, Solubility of hydrogen in potassium hydroxide and sulfuric acid. Salting-out and hydration, The Journal of Physical Chemistry, 70 (1966) 718-723.
[5. 39] S. Shoor, R.D. Walker Jr, K. Gubbins, Salting out of nonpolar gases in aqueous potassium hydroxide solutions, The Journal of Physical Chemistry, 73 (1969) 312-317.
[5. 40] L.D. Longo, M. Delivoria-Papadopoulos, G.G. Power, E.P. Hill, R. Forster 2nd, Diffusion equilibration of inert gases between maternal and fetal placental capillaires, American Journal of Physiology-Legacy Content, 219 (1970) 561-569.
[5. 41] G.G. Power, H. Stegall, Solubility of gases in human red blood cell ghosts, Journal of Applied Physiology, 29 (1970) 145-149.
[5. 42] J. Gerecke, H. Bittrich, The solubility of H2, CO2 and NH3 in an aqueous electrolyte solution, Wiss Z Tech Hochsch Chem Carl Shorlemmer Leuna Merseburg, 13 (1971) 115-122.
[5. 43] J. Jung, O. Knacke, D. Neuschut, Solubility of carbon monoxide and hydrogen in water at temperatures up to 300 degrees c, Chemie ingenieur technik, 43 (1971) 112-&.

[5. 44] W. Schröder, Untersuchungen über die Temperaturabhängigkeit der Gaslöslichkeit in Wasser, Chemie Ingenieur Technik, 45 (1973) 603-608.
[5. 45] T.E. Crozier, S. Yamamoto, Solubility of hydrogen in water, sea water, and sodium chloride solutions, Journal of Chemical and Engineering Data, 19 (1974) 242-244.
[5. 46] L.I. Gordon, Y. Cohen, D.R. Standley, The solubility of molecular hydrogen in seawater, Deep Sea Research, 24 (1977) 937-941.
[5. 47] R.W. Cargill, Solubility of helium and hydrogen in some water+ alcohol systems, Journal of the Chemical Society, Faraday Transactions 1: Physical Chemistry in Condensed Phases, 74 (1978) 1444-1456.
[5. 48] P. Gillespie, G. Wilson, GPA Research Report RR-41 Gas Processors Association, Tulsa, OK, (1980).
[5. 49] V.R. Choudhary, M.G. Parande, P.H. Brahme, Simple apparatus for measuring solubility of gases at high pressures, Industrial & Engineering Chemistry Fundamentals, 21 (1982) 472-474.
[5. 50] R. Dohrn, G. Brunner, Phase equilibria in ternary and quaternary systems of hydrogen, water and hydrocarbons at elevated temperatures and pressures, Fluid phase equilibria, 29 (1986) 535-544.
[5. 51] J. Alvarez, R. Crovetto, R. Fernández‐Prini, The dissolution of N2 and of H2 in water from room temperature to 640 K, Berichte der Bunsengesellschaft für physikalische Chemie, 92 (1988) 935-940.
[5. 52] G. Kling, G. Maurer, The solubility of hydrogen in water and in 2-aminoethanol at temperatures between 323 K and 423 K and pressures up to 16 MPa, The Journal of Chemical Thermodynamics, 23 (1991) 531-541.
[5. 53] U. Jáuregui-Haza, E. Pardillo-Fontdevila, A. Wilhelm, H. Delmas, Solubility of hydrogen and carbon monoxide in water and some organic solvents, Latin American applied research, 34 (2004) 71-74.
[5. 54] B.N. Taylor, C.E. Kuyatt, Guidelines for evaluating and expressing the uncertainty of NIST measurement results, (1994).
[5. 55] B.N. Taylor, Guidelines for Evaluating and Expressing the Uncertainty of NIST Measurement Results (rev, Diane Publishing, 2009.
[5. 56] C.-B. Soo, Experimental thermodynamic measurements of biofuel-related associating compounds and modeling using the PC-SAFT equation of state, in, 2011.
[5. 57] F. Zhang, Développement d'un dispositif expérimental original et d'un modèle prédictif pour l'étude thermodynamique des composés soufrés, in, Paris, ENMP, 2015.
[5. 58] J. El Abbadi, Etude des propriétés thermodynamiques des nouveaux fluides frigorigènes, in, PSL Research University, 2016.
[5. 59] I. Krichevsky, J. Kasarnovsky, Partial Molal Quantities in an Infinitely Dilute Solution, Journal of the American Chemical Society, 57 (1935) 2171-2172.
[5. 60] J. Corvisier, Modeling water-gas-rock interactions using CHESS/HYTEC, in: Goldschmidt Conference, Florence–Italy, 2013.
[5. 61] J. Corvisier, A.-F. Bonvalot, V. Lagneau, P. Chiquet, S. Renard, J. Sterpenich, J. Pironon, Impact of co-injected gases on CO2 storage sites: Geochemical modeling of experimental results, Energy Procedia, 37 (2013) 3699-3710.
[5. 62] P. Blanc, A. Lassin, P. Piantone, M. Azaroual, N. Jacquemet, A. Fabbri, E.C. Gaucher, Thermoddem: A geochemical database focused on low temperature water/rock interactions and waste materials, Applied geochemistry, 27 (2012) 2107-2116.
[5. 63] A.H. Harvey, Semiempirical correlation for Henry's constants over large temperature ranges, AIChE journal, 42 (1996) 1491-1494.
[5. 64] E.L. Shock, H.C. Helgeson, D.A. Sverjensky, Calculation of the thermodynamic and transport properties of aqueous species at high pressures and temperatures: Standard partial

molal properties of inorganic neutral species, Geochimica et Cosmochimica Acta, 53 (1989) 2157-2183.
[5. 65] A.C. Schneider, C. Pasel, M. Luckas, K.G. Schmidt, J.-D. Herbell, Determination of hydrogen single ion activity coefficients in aqueous HCl solutions at 25 C, Journal of solution chemistry, 33 (2004) 257-273.
[5. 66] H. Sakaida, T. Kakiuchi, Determination of single-ion activities of H+ and Cl–in aqueous hydrochloric acid solutions by use of an ionic liquid salt bridge, The Journal of Physical Chemistry B, 115 (2011) 13222-13226.
[5. 67] M.K. Khoshkbarchi, J.H. Vera, Measurement and correlation of ion activity in aqueous single electrolyte solutions, AIChE journal, 42 (1996) 249-258.
[5. 68] E. Lemmon, I.H. Bell, M. Huber, M. McLinden, NIST Standard Reference Database 23: Reference Fluid Thermodynamic and Transport Properties-REFPROP, Version 10.0, National Institute of Standards and Technology, (2018).
[5. 69] D.-Y. Peng, D.B. Robinson, A new two-constant equation of state, Industrial & Engineering Chemistry Fundamentals, 15 (1976) 59-64.
[5. 70] M. Wertheim, Fluids with highly directional attractive forces. I. Statistical thermodynamics, Journal of statistical physics, 35 (1984) 19-34.
[5. 71] L. Blum, Mean spherical model for asymmetric electrolytes: I. Method of solution, Molecular Physics, 30 (1975) 1529-1535.
[5. 72] M. Born, Volumen und hydratationswärme der ionen, Zeitschrift für Physik, 1 (1920) 45-48.
[5. 73] M. Hajiw, A. Chapoy, C. Coquelet, Hydrocarbons–water phase equilibria using the CPA equation of state with a group contribution method, The Canadian Journal of Chemical Engineering, 93 (2015) 432-442.

Chapter 6: Article 4: Hydrate Stability of carbon dioxide + oxygen binary mixture ($CO_2 + O_2$) in pure water: Measurements and modeling

French summary / Chapitre 6 – Article 4 : Stabilité des hydrates du mélange binaire de dioxyde de carbone + oxygène ($CO_2 + O_2$) dans l'eau pure : Mesures et modélisation

La connaissance des conditions de dissociation des hydrates de gaz mixtes est d'une grande importance pour la compréhension scientifique (par exemple, les clathrate d'hydrates dans le système solaire externe) et les applications d'ingénierie (par exemple, le maintien de l'écoulement, la réfrigération et les procédés de séparation). Dans ce travail, les points de dissociation des hydrates du mélange CO_2+O_2 ont été mesurés à différentes fractions molaires d'O_2 (11%, 32% et 50%) en utilisant la méthode de recherche de pression isochorique. La consistance de ces nouvelles données a été vérifiée à l'aide de la relation de Clausius-Clapeyron. Les mesures effectuées pour des pressions allant jusqu'à 19 MPa permettent de pallier le manque de données pour ce système, et permettent également d'évaluer les prédictions des modèles allant de l'hydrate de CO_2 pur à l'hydrate d'O_2 pur. Pour prédire les courbes de stabilité des hydrates de gaz, dans ce travail, la théorie bien établie des hydrates de van der Waals et Platteeuw (vdWP) est combinée à une équation d'état de type CPA pour les électrolytes (e-PR-CPA EoS) qui a été utilisée avec succès pour représenter avec une grande précision les équilibres des phases fluides (y compris la solubilité des gaz et la teneur en eau) des systèmes complexes contenant du gaz, de l'eau et du sel. Le modèle résultant (e-PR-CPA + vdWP) a été appliqué avec succès aux systèmes O_2+H_2O et CO_2+H_2O+(NaCl) en le comparant avec les données de la littérature. Dans la plage de température étudiée (>270K), le modèle prédit comme attendu une structure d'hydrate de type I pour l'O_2, le CO_2 et leurs mélanges. Une excellente reproduction des données mesurées par ce modèle complet a été obtenue sans aucun paramètre ajustable supplémentaire.

Hydrate Stability of carbon dioxide + oxygen binary mixture ($CO_2 + O_2$) in pure water: Measurements and modeling

Salaheddine Chabab[a], Alain Valtz[a], Snaide Ahamada[a], Christophe Coquelet[a,*]

[a]*Mines ParisTech, PSL University, CTP-Centre of Thermodynamics of Processes, 35 rue Saint Honoré, 77305 Fontainebleau Cedex, France*

Journal of chemical & engineering data

pubs.acs.org/jced Article

Hydrate Stability of Carbon Dioxide + Oxygen Binary Mixture ($CO_2 + O_2$) in Pure Water: Measurements and Modeling

Salaheddine Chabab, Alain Valtz, Snaide Ahamada, and Christophe Coquelet*

Cite This: *J. Chem. Eng. Data* 2021, 66, 767−779 Read Online

ACCESS | Metrics & More | Article Recommendations | Supporting Information

ABSTRACT: Knowledge of the dissociation conditions of mixed-gas hydrate systems is of great importance for scientific understanding (e.g., clathrate hydrates in the outer solar system) and engineering applications (e.g., flow assurance, refrigeration, and separation processes). In this work, $CO_2 + O_2$ hydrate dissociation points were measured at different O_2 mole fractions (11, 32, and 50%) using the isochoric pressure search method. The consistency of these new data was verified using the Clausius−Clapeyron relationship. The measurements performed for pressures up to 19 MPa overcome the lack of data for this system and also allow us to evaluate the model predictions from pure CO_2 hydrate to pure O_2 hydrate. To predict gas hydrate stability curves, in this work, the well-established hydrate theory of van der Waals and Platteeuw (vdWP) is combined with an electrolyte CPA-type equation of state (e-PR-CPA EoS), which has been successfully used to represent with high accuracy the fluid phase equilibria (including gas solubility and water content) of complex systems containing gas, water, and salt. The resulting model (e-PR-CPA + vdWP) was applied to the $O_2 + H_2O$ and $CO_2 + H_2O$ + (NaCl) systems by comparing with the literature data. In the studied temperature range (>270 K), the model predicts, as expected, a hydrate structure of type I for O_2, CO_2, and their mixtures. An excellent reproduction of the measured data by this complete model was obtained without any additional adjustable parameters.

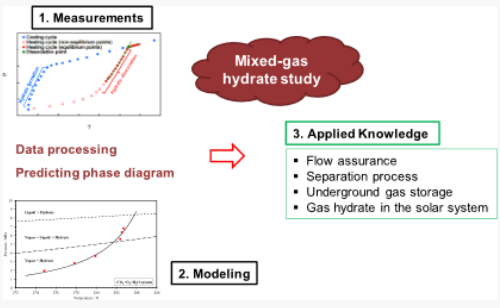

Abstract

Knowledge of the dissociation conditions of mixed-gas hydrate systems is of great importance for scientific understanding (e.g. Clathrate hydrates in the outer solar system) and engineering applications (e.g. flow assurance, refrigeration and separation processes). In this work, CO_2+O_2 hydrate dissociation points were measured at different O_2 mole fractions (11%, 32% and 50%) using isochoric pressure search method. The consistency of these new data was verified using the Clausius-Clapeyron relationship. The measurements performed for pressures up to 19 MPa overcome the lack of data for this system, and also allows to evaluate the model predictions from pure CO_2 hydrate to pure O_2 hydrate. To predict gas hydrate stability curves, in this work, the well-established hydrate theory of van der Waals and Platteeuw (vdWP) is combined with an electrolyte CPA-type Equation of State (e-PR-CPA EoS) which has been successfully used to represent with high accuracy the fluid phase equilibria (including gas solubility and water content) of complex systems containing gas, water and salt. The resulting model (e-PR-CPA + vdWP) was applied to the O_2+H_2O and CO_2+H_2O+(NaCl) systems by comparing with literature data. In the studied temperature range (>270K), the model predicts as expected a hydrate structure of type I for O_2, CO_2 and their mixtures. An excellent reproduction of the measured data by this complete model was obtained without any additional adjustable parameters.

6.1 Introduction

The growing integration of renewable energies, mainly intermittent (with issues of overcapacity and redundancy) in the short term (energy transition) and the total replacement of fossil hydrocarbons use in the long term, requires a flexible solution for large-scale energy storage. In the framework of the ANR (Agence Nationale de la Recherche) FLUIDSTORY project, a combination of Power-to-Gas (PtG) and Gas-to-Power (GtP) technologies with temporary underground gas storage is proposed as a solution for storing intermittent surplus renewable electricity while recovering and keeping CO_2 in a closed loop. To manage the temporal differences between the gas production from PtG and the gas consumption (GtP), this concept called EMO (Electrolysis-Methanation-Oxycombustion) involves the underground storage of these different energy carriers (O_2, H_2, CH_4, CO_2) in salt caverns built in very tight salt layers, with very large volumes, and which can withstand very high pressures (that can exceed 200 bars depending on the depth of the reservoir). Under certain temperature and pressure conditions (especially at temperatures below the critical temperature of CO_2 and at high pressure), CO_2 can be stable in the liquid state, which is not desired in underground storage because of the thermal effects on the rock (the salt layer) due to the phase transitions that the gas undergoes. The proposed solution is the storage of CO_2 and O_2 in the same cavern. The mixing of the two gases reduces the critical temperature of the mixture (CO_2+O_2) and keeps the gas in a supercritical state under the operating conditions of the storage. However, for the design and simulation of storage facilities and also for the evaluation of possible risks, it is necessary to study the thermophysical properties of this mixture.

In some cases, the temperature in the storage reservoir may be low enough to form hydrates in the wellhead or in surface facilities (pipes, compressors, etc.) [6. 1, 2]. The large temperature difference between the bottom of the reservoir and the wellhead is due to the thermal gradient that depends on the depth and nature of the geological formation and also due to the Joule-Thomson effect resulting from the rapid expansion (high flow rate) of the extracted gas. Kleinitz and Boehling [6. 3] presented temperatures of some underground storage facilities showing the necessity of injecting hydrate inhibitors in the reservoir to avoid blockage of the flow path and possibly the stoppage of production for maintenance purposes. To limit these flow assurance issues, it is crucial to know the temperature and pressure conditions under which gas hydrates are stable. In addition, important properties to be studied for such storage applications include the gas density and viscosity, its solubility in brine, as well as gas hydrate stability curves. In our recent work, we have studied the density of the CO_2+O_2 mixture [6. 4] and the solubility of

CO_2 [6. 5, 6], O_2 [6. 6] and H_2 [6. 7] in brine under underground storage conditions. Herein, in the continuity of the previous work, we are interested in the study of the dissociation points of the hydrates of CO_2, O_2 and their mixtures under the transport and storage conditions. Generally thermodynamic models are parameterized only on binary systems by optimizing binary interaction parameters, and therefore thanks to mixing rules, phase equilibria (fluid-fluid and hydrate-fluid) of multi-component (more than two compounds) systems can be predicted. This reduces the number of experiments required. However, a minimum of measurements must be performed to validate model predictions.

Several studies have reported dissociation point data for CO_2 and O_2 hydrates. However, to date there are no published data on the hydrates of the mixture of these two gases (CO_2+O_2). Chapoy et al. [6. 8] measured and modelled a representative CO_2-rich flue gas system in the presence of impurities (O_2, Ar and N_2). This study and other ones [6. 9, 10] showed that even in small concentrations, the presence of these impurities changes the phase diagram of the system. In a Joint Industry Project (JIP) report on the impact of impurities on the CCS chain, Chapoy et al. [6. 11] also reported four measurement points of hydrate dissociation of the CO_2+O_2 mixture (5mol% of O_2). The present work aims to complete this study by measuring and modelling the CO_2+O_2 system at different compositions (especially for compositions above 5% of O_2). The new data measured in the context of the transport and storage of CO_2 and O_2 containing streams can also be used for other applications, for instance: 1) hydrate separation processes, in particular CO_2 capture from oxy-combustion flue gas [6. 12] which mainly contain CO_2, O_2 and H_2O by gas hydrates formation since CO_2 hydrates are more stable than other gas hydrates (flue gas impurities) [6. 13]; 2) the study of mixed gas hydrates in the outer solar system [6. 14]; 3) and finally allowing the evaluation of predictive models.

In this work, CO_2+O_2 hydrate dissociation points were measured at different O_2 mole fractions (11%, 32% and 50%) using isochoric pressure search method. In the second section of this paper, the experimental apparatus is described and the measured data are presented and checked. To predict the stability conditions of single-gas and mixed-gas hydrate systems, in the third section, a complete model for calculating hydrate-fluid and fluid-fluid phase equilibria is presented. It consists of a combination of the well-established hydrate theory of van der Waals and Platteeuw (vdWP) [6. 15] with the e-PR-CPA Equation of State (EoS) [6. 5].

6.2 Experimental

6.2.1 Materials

In Table 6.1, the suppliers of Carbon dioxide (CO_2, CAS Number: 124-38-9) and Oxygen (O_2, CAS Number: 7782-44-7) and the given purities are listed. Water (H_2O, CAS Number: 7732-18-5) was deionized and degassed.

Table 6.1: Chemical samples used for experimental work (CAS Registry Number, mole fraction purity and suppliers of chemicals).

Chemicals	CAS Reg. No.	Supplier	Purity (mol %)	Analysis method[a]
Carbon dioxide	124-38-9	Air Liquide	99.995	GC
Oxygen	7782-44-7	Air Liquide	99.999	GC
Water (ultrapure)	7732-18-5	MilliporeTM (direct-Q5)	18.2 MΩ·cm	

[a] GC: Gas Chromatography

Three mixtures of CO_2+O_2 were considered in this study, their compositions are listed in Table 6.2. The mixtures were prepared in a gas reservoir considering the difference of total pressure. First, the gas reservoir is put under vacuum. CO_2 was first introduced into the gas reservoir and the pressure was recorded (*P1*). Afterwards, O_2 is introduced and pressure is recorded (*P2*). The temperature of the gas reservoir is selected in order to have a monophasic phase inside. Approximate composition is estimated using $x_{O2}=(P2-P1)/P2$. In order to have the accurate value of the gas mixture composition, a Gas Chromatograph (Varian, model CP 3800), equipped with a thermal conductivity detector (TCD) is used. WINILAB III software (Perichrom, France) is used for peaks integration and their analysis. The calibration of the GC detector is obtained after introduction of several known pure component volumes. Appropriate syringes are considered. A PORAPAK R (80/100 mesh, 1.2 m X 1/8" Silcosteel) packed column is used. A calibration curve between moles number introduced and GC peak surface is determined and accuracies are determined. The resulting relative accuracies concerning the mole numbers are 0.7 % for CO_2 and 0.8 % for O_2. The uncertainty of molar fractions (x_1) is determined by Equation 6.1:

$$u(x_1) = x_1(1 - x_1)\sqrt{\left(\frac{u(n_1)}{n_1}\right)^2 + \left(\frac{u(n_2)}{n_2}\right)^2} \quad \textbf{(6.1)}$$

with $u(x_1)$ the uncertainty on mole fraction for component 1 and $\frac{u(n_i)}{n_i}$ the relative uncertainty on mole number n_i of the component i calculated from GC calibration.

Table 6.2: Compositions of the studied CO_2+O_2 mixtures: Expected composition and real composition mole fractions

Mixture	Expected composition mole fractions		Real composition mole fractions (x)		Standard uncertainties u(xCO_2)
	O_2	CO_2	O_2	CO_2	
MIX1	0.3	0.7	0.3238	0.6762	0.0016
MIX2	0.1	0.9	0.1104	0.8896	0.0006
MIX3	0.5	0.5	0.4984	0.5016	0.0015

6.2.2 Apparatus and method

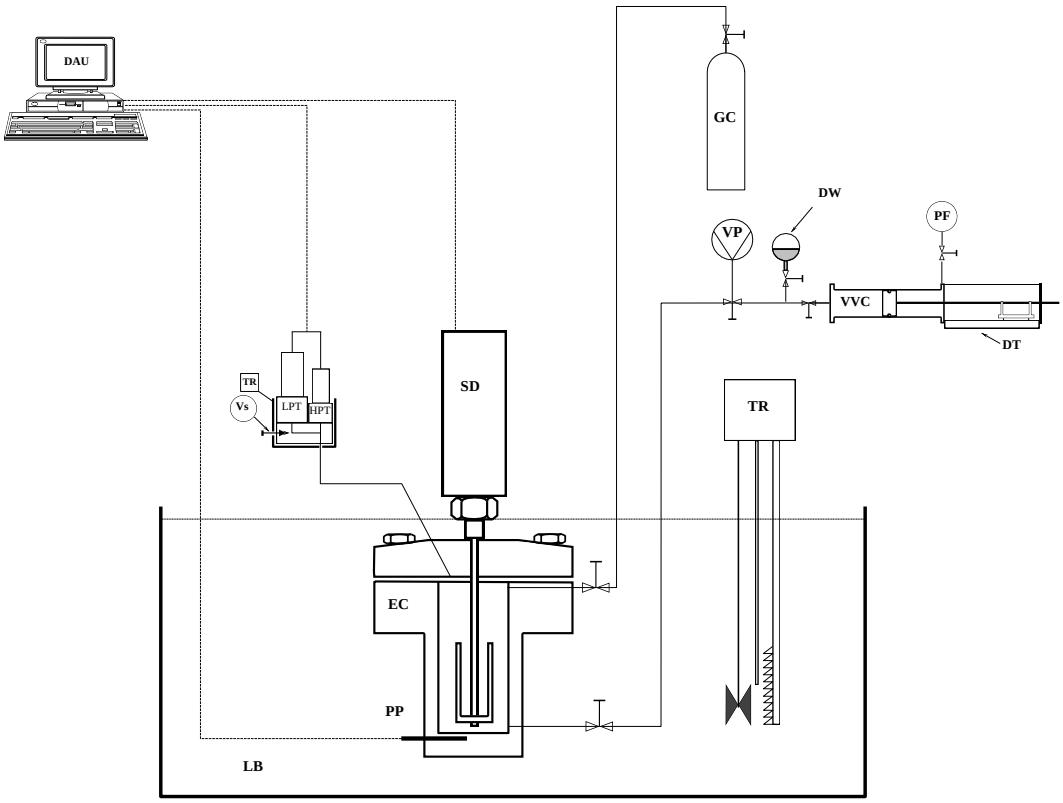

Figure 6.1: Schematic representation of the used apparatus. DW: degassed water; DAU: data acquisition unit; EC: equilibrium cell; GC: Gas cylinder; LPT: low pressure transducer; HPT: high pressure transducer; LB: liquid bath; PP: platinum probe; SD: stirring de-vice; TR: temperature regulator; VP: vacuum pump; VVC: variable volume cell; PF: pressurizing fluid; DT: displacement transducer.

The principle of the experimental apparatus used to measure dissociation points of gas hydrates of the CO_2+O_2 mixture is based on the isochoric pressure search method. The experimental device is illustrated in Figure 6.1 and is the same one used in the previous work at Armines - Mines ParisTech [6. 16, 17, 18]. It consists of a cylindrical constant volume (128 cm^3) equilibrium cell equipped with a Stirring Device (SD), two pressure transducers (LPT and HPT) to be more precise in each specific pressure range, a platinum resistance thermometer (PP) at the bottom of the cell (in aqueous phase) and introduced in a thermostatically controlled bath (LB) to maintain a constant temperature (TR). The evolution of temperature and pressure is monitored by means of a Data Acquisition Unit (DAU) connected to a DAU software to manage the stepwise variation of temperature and record the acquired data. The temperature probe (100 Ω) is calibrated against a 25-Ohm platinum resistance thermometer (model 5628, Fluke Hart Scientific) which is calibrated by LNE (Laboratoire National de Métrologie et d'Essais). The LPT and HPT pressure transducers were calibrated against pressure automated calibration equipment (PACE 5000, GE Sensing and Inspection Technologies) and a dead weight pressure balance (Desgranges & Huot 5202S, CP 0.3–40MPa, Aubervilliers, France), respectively.

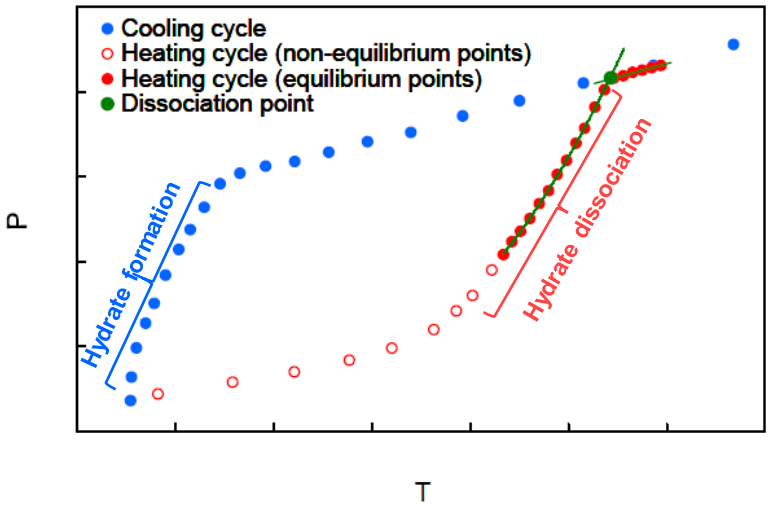

Figure 6.2: Measurement principle of gas hydrate dissociation points by isochoric pressure search method.

The measurement procedure summarized in Figure 6.2 consists of looking for the pressure at which the hydrates are completely dissociated. A gas mixture of a certain quantity and composition is introduced in the equilibrium cell which is previously evacuated and filled with a known quantity of water. The mixture is then strongly agitated (800 RPM). The temperature is decreased until the hydrate phase is formed (sudden pressure drop). The temperature is then

increased stepwise by 1K until the dissociation pressure of the hydrate phase is reached. For each step of temperature increase, equilibrium conditions are reached by allowing enough time at each step (8h/step). The hydrate dissociation point is determined by the intersection of the thermal expansion curve of the fluid and the equilibrium heating cycle curve. Once the hydrate dissociation point (P, T) is determined, more gas is added to the equilibrium cell to measure another point, and so on until enough experimental points are obtained. Finally, the equilibrium cell is emptied, cleaned and evacuated.

6.2.3 Experimental results

Table 6.3: Measured data of hydrate dissociation conditions of the CO_2+O_2 gas mixture and expanded uncertainties (k=2): 0.1≤*U(T)*≤0.6 K and 0.040≤*U(p)*≤0.251 MPa.

Mixture	Loaded water		AqFr (mole fraction)	Temperature [K]	Pressure [MPa]
	n_{H_2O} (mole)	V_{H_2O} (cm^3)			
MIX1	1.16050	20.97	0.902 ± 0.017	274.17	2.178
	1.16050	20.97	0.886 ± 0.018	277.00	3.017
	1.16050	20.97	0.836 ± 0.015	279.75	4.233
	1.16050	20.97	0.761 ± 0.013	282.17	6.054
	1.16050	20.97	0.671 ± 0.010	283.88	8.353
	1.16050	20.97	0.550 ± 0.007	284.96	11.194
	2.04400	36.94	0.838 ± 0.009	283.26	7.227
	2.04400	36.94	0.681 ± 0.006	285.38	13.245
	2.80600	50.71	0.583 ± 0.006	286.07	18.741
MIX2	1.09190	19.73	0.965 ± 0.017	274.85	1.955
	1.09190	19.73	0.910 ± 0.015	277.84	2.810
	1.09190	19.73	0.843 ± 0.014	279.92	3.632
	1.09190	19.73	0.676 ± 0.010	282.37	5.590
	1.09190	19.73	0.523 ± 0.007	282.53	6.370
	1.09190	19.73	0.452 ± 0.005	282.69	6.799
MIX3	1.15004	20.78	0.912 ± 0.019	283.25	11.261
	1.15004	20.78	0.865 ± 0.018	284.32	13.895
	1.15004	20.78	0.848 ± 0.018	285.01	15.985
	1.15004	20.78	0.956 ± 0.021	275.79	4.460
	1.15004	20.78	0.945 ± 0.020	278.98	6.299
	1.15004	20.78	0.916 ± 0.020	282.39	9.713

The expanded uncertainties $U = k \times u$ (with a coverage factor $k = 2$) are between 0.1 and 0.6 K for temperature ($U(T)$) and between 0.04 and 0.25 MPa for pressure ($U(P)$). The measured

data are listed in Table 6.3 and presented in Figure 6.3a. The aqueous fraction (AqFr, see Equation 6.2), which is the ratio between the number of moles of water n_{H_2O} and the total number of moles in the system (water and gas $n_{H_2O} + \sum n_{gas}$), was determined for each measured point.

$$AqFr = x_{H_2O} = \frac{n_{H_2O}}{n_{H_2O} + \sum_{gas} n_{gas}} \quad \textbf{(6.2)}$$

A consistency test was applied to the measured data. Using the Clausius-Clapeyron relation (Equation 6.3) [6. 19], the evolution of the enthalpy of dissociation of the hydrate as a function of temperature is examined. Given the small temperature range, we can consider that the compressibility factor does not vary significantly, and since the enthalpy of dissociation does not vary rapidly [6. 19], this equation can be used in a small dissociation temperature range to check the linearity of the measured data in terms of $ln(p)$ as a function of $1/T$.

$$\frac{dln(P)}{d\left(\frac{1}{T}\right)} = \frac{-\Delta H_{dis}}{Z\ R} \quad \textbf{(6.3)}$$

where P and T are respectively the hydrate dissociation pressure and temperature (in equilibrium with the vapor (or liquid) and aqueous phases), R the ideal gas constant, Z the compressibility factor and ΔH_{dis} the apparent enthalpy of dissociation of the hydrate phase.

The results of the consistency tests on the measured data are shown in Figure 6.3 (b, c and d). Overall the measured data are consistent. When a breakpoint is present, it means that we have gas hydrate when there is a phase split in the gas-rich phase (CO_2+O_2) including a vapor phase and a CO_2-rich liquid phase (other than the aqueous phase). In the modeling part (next section), the phase behavior (single-phase and two-phase) of the gas mixture in equilibrium with the aqueous phase and the hydrate phase is highlighted for the different CO_2+O_2 mixture compositions.

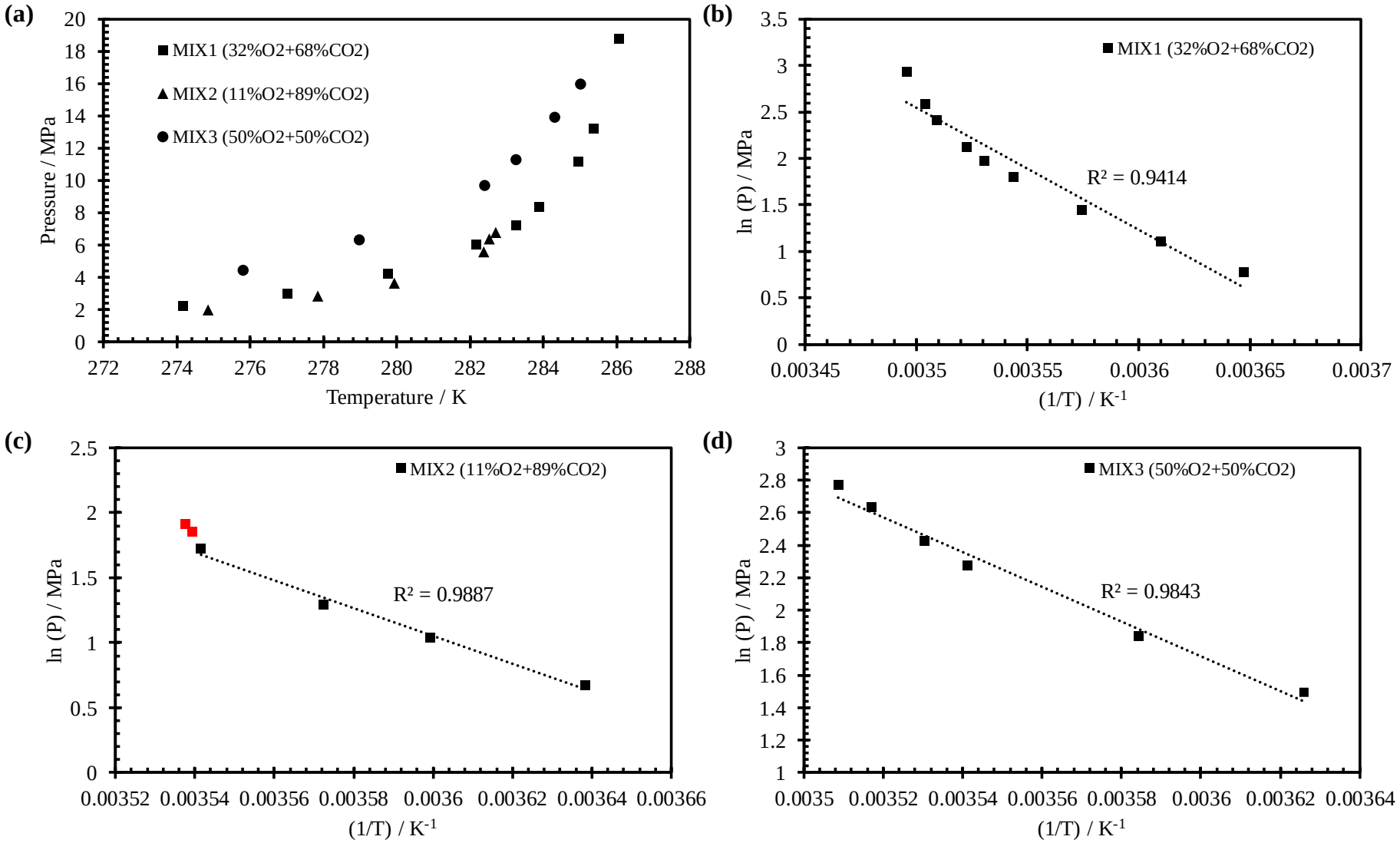

Figure 6.3: Hydrate dissociation points of the CO_2+O_2 gas mixture: measured data (a) and consistency tests (b, c and d). The red symbols (graph c) represent measurements where the gas mixture was in liquid-vapor equilibrium (see Figure 6.9b).

6.3 Thermodynamic modeling

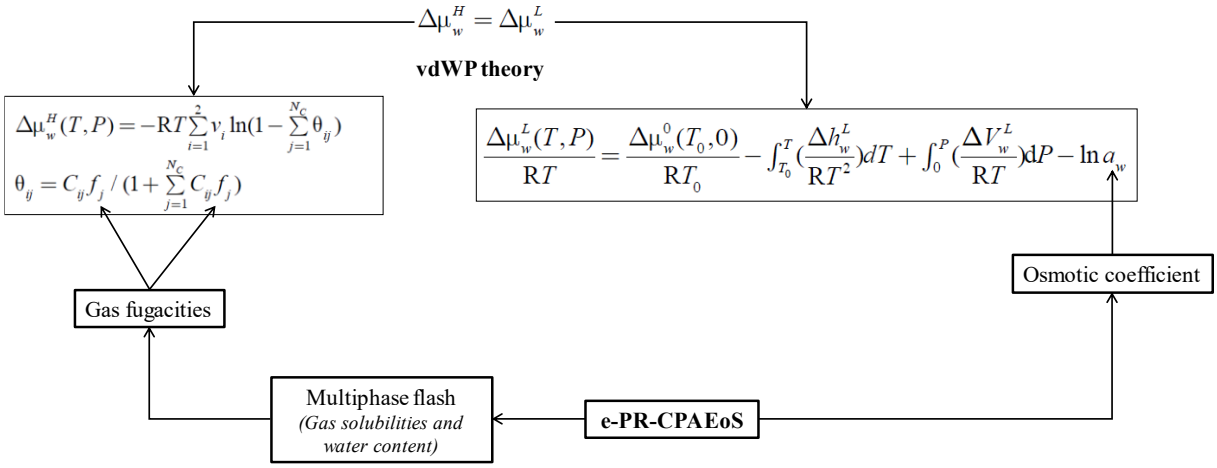

Figure 6.4: Schematic diagram of the approach used to calculate gas hydrate equilibria with the e-PR-CPA model combined with the Van der Waals and Platteeuw model.

6.3.1 Model presentation: procedure description and parameter estimation

Hydrate dissociation thermodynamic modeling is generally done by combining the solid van der Waals and Platteeuw theory [6. 15] for hydrate phase calculation with an Equation of State (EoS) for fluid phases (liquid and vapor) calculation and possibly with a G-excess model for water activity coefficient estimation. The hydrate dissociation curve represents the equilibrium of the hydrate phase with the aqueous phase and the gas-rich phase (which can be liquid and/or vapor), and this more or less limits the hydrate stability domain at thermodynamic equilibrium. The e-PR-CPA (electrolyte Peng-Robinson Cubic Plus Association) EoS recently developed and presented in our previous work [6. 5, 6, 7] has performed successfully in the prediction of liquid (gas solubility) and vapor (water content) phases of systems including water, gas (CO_2, O_2, H_2, CH_4, etc.) and salt (NaCl). Hence, this EoS has been chosen to calculate gas fugacities, fluid phase (aqueous and gaseous) equilibria, and the activity coefficient of water which is different from one if there are electrolytes (salts) or solvents (alcohols, glycols, etc.) in the aqueous solution.

For the calculation of fluid phase equilibria with an equation of state, it is necessary to know the overall composition (or feed composition) of the system. However, generally, mixed-gas hydrate data are provided in terms of "water-free" gas composition x'_{gas} ($\sum_{gas} x'_{gas} = 1$) and aqueous fraction AqFr ($= x_{H_2O}$) (see Equation 6.2) in order to study hydrates with a fixed global gas mixture composition. In order to be able to model mixed-gas hydrate systems, we provide

below the equations used to convert these "apparent" quantity (x'_{gas}) into "real" mole fractions x_i ($\sum_i x_i = 1$, $i =$ all non-electrolyte species).

Using Equation 6.2, the mole number of water is:

$$n_{H_2O} = \frac{AqFr \sum_{gas} n_{gas}}{1 - AqFr} \quad \textbf{(6.4)}$$

Considering a total mole number of 1 for the gas mixture ($\sum_{gas} n_{gas} = 1$ and $n_{gas} = x'_{gas}$), the Equation 6.4 becomes:

$$n_{H_2O} = \frac{AqFr}{1 - AqFr} \quad \textbf{(6.5)}$$

Finally, the real mole fractions are calculated by:

$$x_i = \frac{n_i}{n_{H_2O} + \sum_{gas} n_{gas}} = \frac{n_i}{n_{H_2O} + 1} = \frac{n_i}{\frac{AqFr}{1 - AqFr} + 1} \quad \textbf{(6.6)}$$

Applying Equation 6.6 to water and a gas *i*, we obtain:

$$x_{H_2O} = \frac{n_{H_2O}}{\frac{AqFr}{1 - AqFr} + 1} = \frac{\frac{AqFr}{1 - AqFr}}{\frac{AqFr}{1 - AqFr} + 1} = AqFr \quad \textbf{(6.7)}$$

$$x_{gas,i} = \frac{n_{gas,i}}{\frac{AqFr}{1 - AqFr} + 1} = \frac{x'_{gas,i}}{\frac{AqFr}{1 - AqFr} + 1} \quad \textbf{(6.8)}$$

The aqueous fraction has no effect on single-gas hydrate systems, since in two-phase thermodynamic equilibrium (which is always the case for gas-water systems), the calculation of the compositions in each phase of a binary system is independent of the global composition (using Gibbs' phase rules, the degree of freedom is two in this case, for example, in a liquid-vapor PT-flash calculation, the same results of liquid x and vapor y compositions are obtained for any global composition z stable in the liquid-vapor state). However, for mixed-gas hydrate systems, the degree of freedom is higher than two, hence calculations of the hydrate dissociation conditions are sensitive to the aqueous fraction, and the composition of the gas-rich phase can vary significantly from the overall composition if one of the gases is more absorbed than the other in the hydrate.

At thermodynamic equilibrium, one can write the equality of the chemical potential of water in the liquid phase and in the hydrate phase. As illustrated in the schematic of Figure 6.4, the e-PR-CPA model calculates gas fugacities and the osmotic coefficient of water which is then transformed into water activity (Equation 6.10), in order to calculate the chemical potential of water in the liquid and hydrate phases. A multiphase flash [6. 20, 21] is calculated at each step until the Hydrate-Liquid-Vapor (HLV) or Hydrate-Liquid-Liquid (HLL) equilibrium is reached. Newton's method was applied to find the dissociation pressure at fixed temperature and the dissociation temperature at fixed pressure. The different terms of the vdWP model (Figure 6.4) were calculated by the Munck et al. [6. 22] method.

The vdWP model derived from statistical thermodynamics is an established theory for the study of phase equilibria involving hydrates following the implementation proposed by Parrish and Prausnitz [6. 23]. Since then, several studies have been published using this approach, therefore the vdWP model is very well described in the literature. The equations proposed by Munck et al. [6. 22] have been used in this work for the calculation of the chemical potential of water in the liquid and hydrate phase. However, since we use a different equation of state, a reparameterization of the parameters used in the calculation of the Langmuir constant is necessary.

A. e-PR-CPA EoS

A detailed description of the e-PR-CPA EoS equations and parameterization is given in our previous work [6. 5]. However, we recall here the main terms and definitions of the parameters. For the modeling of complex systems including gas, water and ions, the e-PR-CPA EoS (expressed in terms of reduced residual Helmholtz free energy $\frac{A^{res}_{e-PR-CPA}}{RT}$ in Equation 6.9) combines several terms to represent the different types of interactions in these systems. For molecular interactions, the selection concerns the well-known cubic term of Peng-Robinson (PR) [6. 24] to describe attractive and repulsive forces between species, and the Wertheim's association theory [6. 25] used in SAFT and CPA –type EoS to describe association phenomena (self-association between identical molecules and cross-association between different molecules). For electrolyte interactions, the MSA theory (Mean Spherical Approximation) [6. 26] and the Born term [6. 27] were chosen to represent ion/ion and ion/solvent (solvation) interactions, respectively.

$$\frac{A^{res}_{e-PR-CPA}}{RT} = \frac{A^{PR}}{RT} + \frac{A^{Association}}{RT} + \frac{A^{MSA}}{RT} + \frac{A^{Born}}{RT} \quad \textbf{(6.9)}$$

Like most thermodynamic models, the parameterization of the e-PR-CPA EoS on pure and binary systems will allow to predict multicomponent (ternary, quaternary, etc.) systems. However, comparison with some experimental data is necessary to verify if the model is well adapted to the studied systems. Concerning fluid phase equilibria modeling, the e-PR-CPA EoS counts for pure compounds:

- Five parameters for the solvent (water): three parameters (m_i, $a_{0,i}$, b_i) to determine the energy parameter a_i and the co-volume b_i in the PR cubic term, and two parameters (association energy ε_i and bonding volume β_i) to calculate the Wertheim association term.
- Three parameters for each ion: three parameters (m_{ion}, $a_{0,ion}$ and ion diameter σ_{ion}) for the calculation of the energy parameter a_{ion} and the co-volume b_{ion} in the PR cubic term.
- No parameters for the gas (only the critical temperature T_c and pressure P_c and the acentric factor ω must be known, which is the case for all gases).

Halite is the main and almost "the only pure" mineral in salt layers where storage caverns are built, hence the water+NaCl mixture was chosen as a representative brine mixture. Before modeling phase equilibria involving fluid and hydrate phases, the osmotic coefficient ∅ of the aqueous electrolyte water+NaCl and the two-phase equilibria calculated by the e-PR-CPA must be verified. In Figure 6.5, the calculations at different salinities (in terms of NaCl molality: m=[mol/kg_w]) of the vapor pressure and the osmotic coefficient of the water+NaCl system by the e-PR-CPA EoS were compared with experimental literature data. As shown in the figure, the model accurately correlates these two properties and estimates their variation as a function of temperature and NaCl molality. The water activity a_w used to calculate the chemical potential of water in the liquid phase (see Figure 6.4) is easily obtained from the osmotic coefficient ∅ by the following relationship (Equation 6.10):

$$a_w = \exp\left[-\frac{M_{H_2O}}{1000}\left(\sum_{ion} m_{ion}\right)\emptyset\right] \quad \textbf{(6.10)}$$

where M_{H_2O} is the molar mass of water and m_{ion} is the molality of each ion (Na+ and Cl- in our case).

Concerning binary systems, generally a Binary Interaction Parameter (BIP or k_{ij} in the cubic term) is to be determined in particular for binaries whose species are not associative. However, for mixtures of associative compounds, when solvation is possible, the cross-association volume β_{ij} can be considered as a second adjustable parameter in order to improve the calculations [6. 28]. Since the e-PR-CPA EoS is reduced to the PR EoS in the case of systems that do not contain associative compounds and electrolytes (e.g. gas mixtures), it is possible to use parameters already available in the literature to represent this type of system. In Table 6.4, the different parameters of the e-PR-CPA model as well as the thermophysical properties used for their determination (by optimization) are presented.

The parameters of the pure compounds as well as the interaction parameters of the CO_2+H_2O+NaCl and O_2+H_2O+NaCl systems used in this work are from our previous work [6. 5, 6]. The binary interaction parameter ($k_{CO_2-O_2} = 0.114$) used to represent Vapor Liquid Equilibria (VLE) of the CO_2-O_2 binary system was taken from the work of Lasala et al. [6. 29].

In Figures 6.6 and 6.7, the predictions of the VLE of the CO_2+H_2O+NaCl, O_2+H_2O+NaCl and CO_2+O_2 systems by the e-PR-CPA EoS are compared to the experimental data. As shown in the figures, the e-PR-CPA EoS accurately estimates gas solubility in water and brine (Figures 6.6a and 6.6b) and water content in gas-rich phases (Figure 6.7a) and captures very well the salting-out effect of gas due to the presence of NaCl under different thermodynamic conditions. The complete study of these systems as well as precise solubility data tables are provided in our previous work [6. 6]. The VLE of the CO_2+O_2 gas mixture calculated by the same model which is reduced to the PR EoS (since there are no electrolytes or associative compounds) are quite good, however this representation can be improved especially in the region of the critical points of the mixture by using other mixing rules (see Lasala et al. [6. 29] and Ahamada et al. [6. 4]) or multiparametric EoS (e.g. EoS-CG), or adding a crossover treatment. All these options add additional parameters, which is not necessary for our study, as demonstrated by the prediction results obtained for multicomponent systems (see section 3.3).

The water activity and fluid phase equilibria are known, to model gas hydrate systems following the approach described earlier, it remains to determine the Langmuir constants C_{ij} of each gas j in a cavity of type i (two types of cavities exist for hydrates: small and large cavities).

B. Langmuir constant

The Langmuir constants quantify the interactions between guest (gas) and host (water) molecules in hydrate cavities. Generally, the formula (Equation 6.11) proposed by van der Waals and Platteeuw [6. 15] developed using the Lennard-Jones-Devonshire cell theory (considering a spherically symmetrical cell) is used to determine the Langmuir constants. For this, the Kihara potential [6. 30] (McKoy and Sinanoğlu [6. 31]) whose parameters are adjusted on experimental hydrate stability data is used to calculate the spherically symmetrical cell potential $W(r)$.

$$C_{ij}(T) = \frac{4\pi}{kT}\int_0^{\infty} \exp[-W(r)/kT] r^2 dr \quad \textbf{(6.11)}$$

where k is Boltzmann's constant, T is the temperature and r is the cell radius.

In order to avoid the numerical calculation of the integral in Equation 6.11, Parrish and Prausnitz [6. 23] proposed a simplified empirical expression (Equation 6.12) of the Langmuir constant which was then used and refined in subsequent studies (e.g. the notable work by Munck et al. [6. 22]).

$$C_{ij}(T) = \frac{A_{ij}}{T}\exp\left(\frac{B_{ij}}{T}\right) \quad \textbf{(6.12)}$$

In Equation 6.12, the A_{ij} and B_{ij} coefficients are specific to gas and cavity types (small or large) and are optimized on experimental gas hydrate data. In this work we have used similar empirical relationships inferred from the shape of the Langmuir constants (for each gas and cavity type) variation with respect to temperature. The coefficients of these formulations are determined by minimizing the absolute deviation between the calculated gas hydrate dissociation pressure or temperature data and the experimental data. The expressions of the Langmuir constants obtained for CO_2 and O_2 in Small and Large cavities are as follows:

$$C_{Small,CO_2} = 74832.46337816 \exp(-0.08827493\ T) \quad \textbf{(6.13)}$$

$$C_{Large,CO_2} = \frac{4.19 \times 10^{-7}}{T}\exp\left(\frac{2813}{T}\right) \quad \textbf{(6.14)}$$

$$C_{Small,O_2} = 0.04462485 \exp(-0.04019974\ T) \quad \textbf{(6.15)}$$

$$C_{Large,O_2} = 0.00132256 \exp(-0.02147978\ T) \quad \textbf{(6.16)}$$

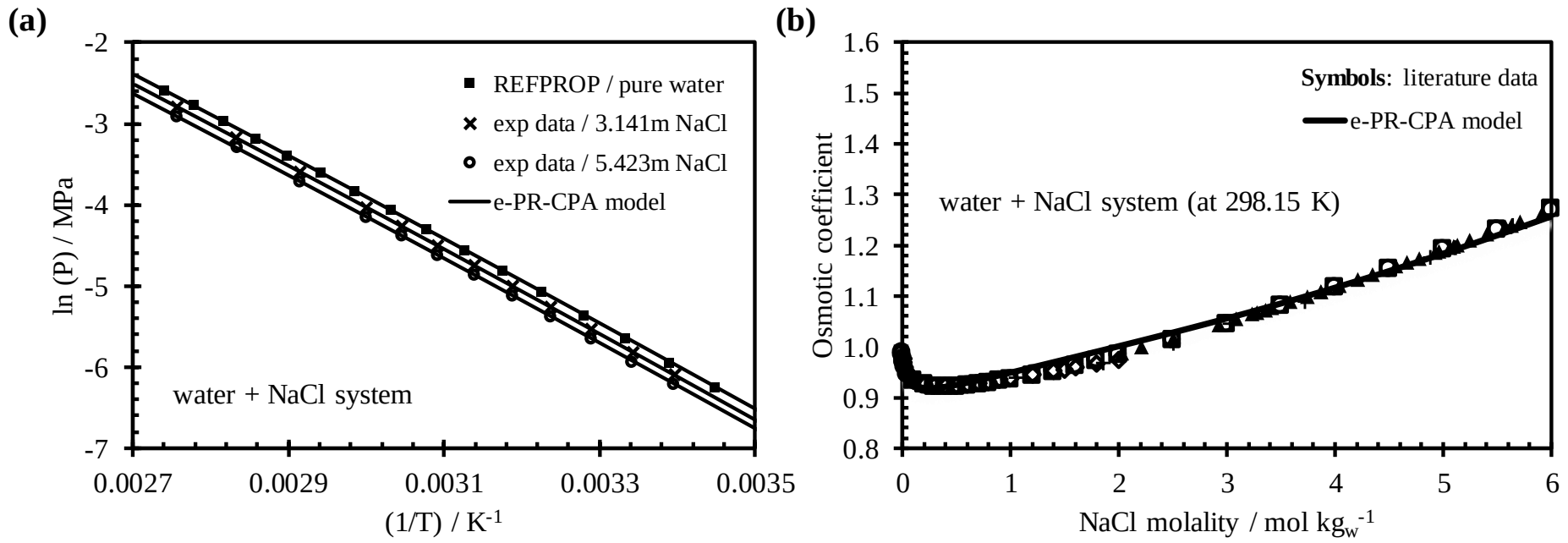

Figure 6.5: Saturation vapor pressure (a) and osmotic coefficient (b) of H_2O + NaCl system. Comparison of literature data (symbols) [6. 32, 33, 34, 35, 36, 37, 38] with predictions (solid lines) by e-PR-CPA EoS.

Table 6.4: e-PR-CPA EoS configuration: model parameters and properties used in the fitting.

		$\frac{A^{PR}}{RT}$	$\frac{A^{Association}}{RT}$	$\frac{A^{MSA}}{RT}+\frac{A^{Born}}{RT}$	Adjusted on:
Pure	gas	-	-	-	-
	ions	m_i, $a_{0,i}$	-	σ_{ion}	Vapor pressure and osmotic coefficient
	water	a_0, m, b	ε, β	-	Vapor pressure and density
Binary	gas-gas	$k_{gas-gas}$	-	-	Vapor Liquid Equilibria (VLE) data
	gas-water	$k_{gas-water}$	$\beta_{gas-water}$ (if solvation, e.g CO_2)	-	Gas solubility in water
	gas-ions	$k_{gas-anion}$ $k_{gas-cation}$	-	-	Gas solubility in water + salt

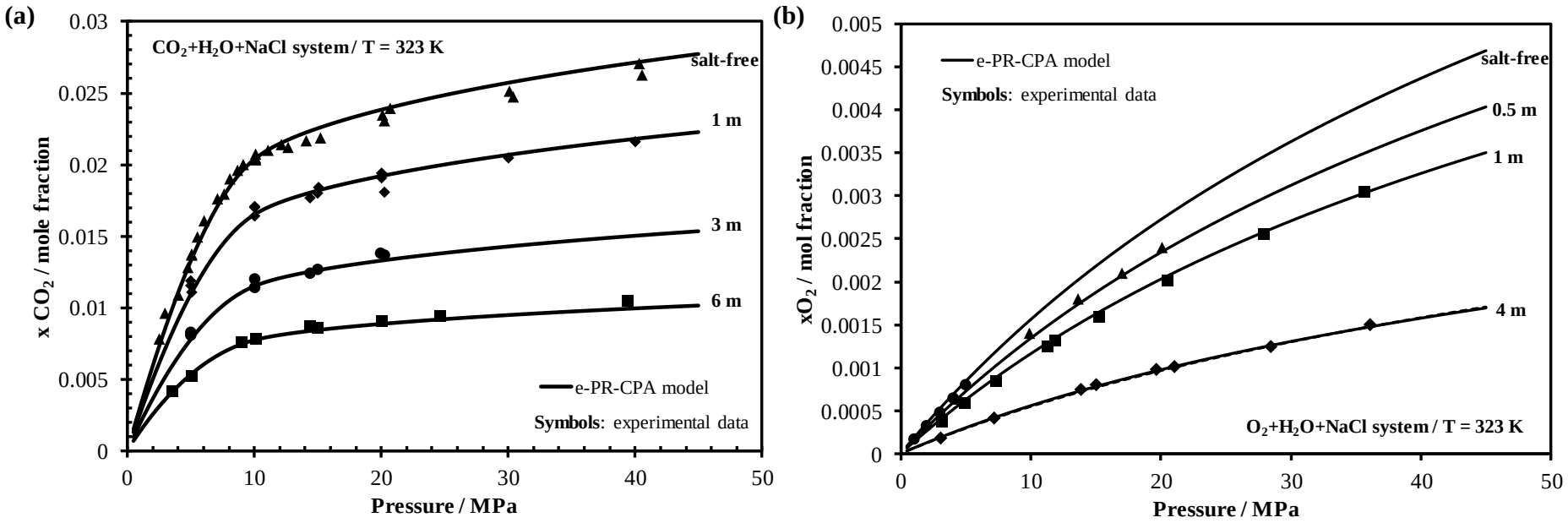

Figure 6.6: Comparison of experimental data (symbols) [6. 6, 39, 40, 41, 42, 43, 44, 45, 46, 47] with predicted CO_2 (a) and O_2 (b) solubilities in NaCl-brine at 323 K for different salt molalities using the e-PR-CPA EoS (solid lines).

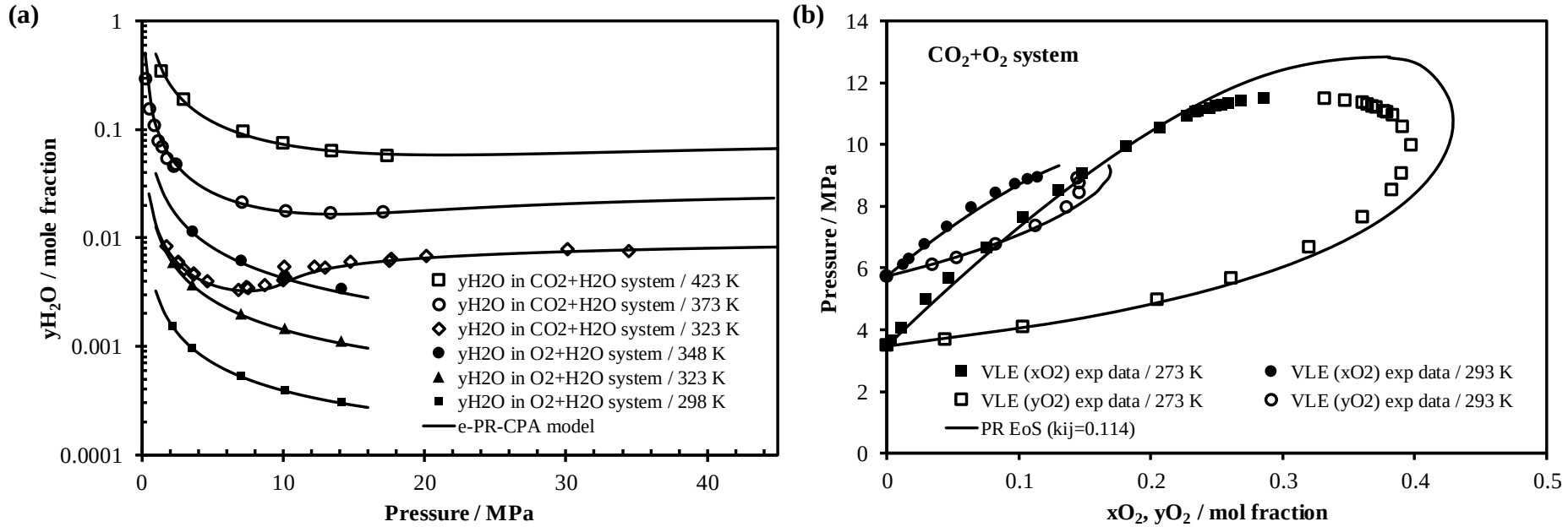

Figure 6.7: Water content in CO_2+H_2O and O_2+H_2O systems (a) and VLE of the CO_2+O_2 mixture (b) at different temperatures: Comparison of experimental data (symbols, (a): [6. 45, 46, 48, 49, 50, 51, 52]; (b): [6. 29]) with predictions (solid lines) using e-PR-CPA model (a) and PR EoS (b).

6.3.2 Hydrate stability of the O_2+H_2O and CO_2+H_2O+(NaCl) mixtures

Structures I and II are the most common forms of gas hydrates [6. 53]. From a modeling point of view, the most stable hydrate structure is the one with the lowest dissociation pressure. Pure CO_2 is well known to form hydrate of structure I. The (e-PR-CPA + vdWP) model predicts a type I hydrate structure for CO_2 hydrate and this is also the case for O_2. The latter is a subject of discussion, basically it has been considered in the past that O_2 forms type I hydrate (like any other small molecule) but later experimental studies [6. 54, 55] have shown that it rather forms type II hydrates. However, according to different studies carried out at different temperature ranges, it is found that O_2 at low temperatures (<270 K) forms type II hydrates and forms type I hydrates at higher temperatures [6. 56] which is the case in our study.

The modeling results of the stability conditions of O_2 hydrate in pure water and CO_2 hydrate in pure water and NaCl-brine are shown in Figure 6.8. By comparing with experimental literature data, the developed model (e-PR-CPA + vdWP) correlates accurately the gas hydrate data in pure water and also predicts well the inhibitory effect of NaCl on the stability of CO_2 hydrate at different concentrations (in terms of salt molality) which tends to destabilize the hydrate proportionally to its concentration. Model calculations are reliable over a wide range of temperature and pressure (up to 100 MPa) for gas hydrates in pure water. The high quality predictions of the effect of salt (NaCl) on CO_2 hydrates is due to the accurate representation of the salting-out effect by the e-PRCPA EoS and also to the excellent vdWP hydrate theory. In addition, it should be noted that the model has been successfully applied to other single-gas and mixed-gas hydrate systems (CH_4+H_2O, CH_4+H_2O+NaCl and CH_4+CO_2+H_2O etc.).

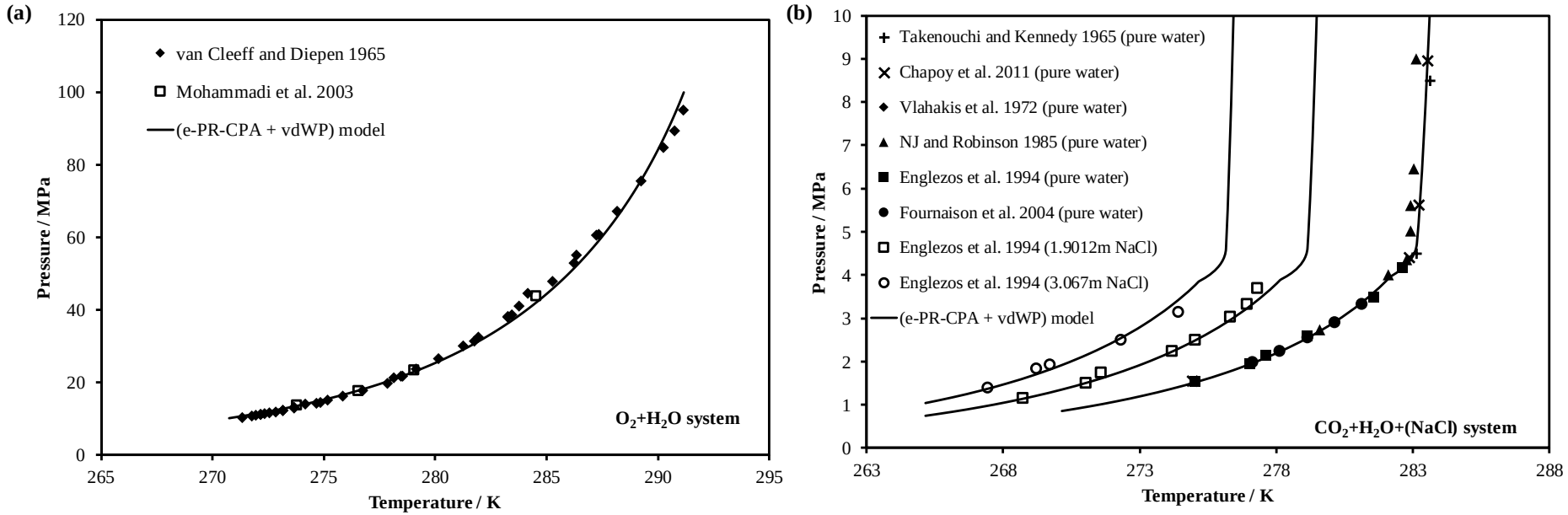

Figure 6.8: Hydrate dissociation conditions of the O_2+H_2O (a) and CO_2+H_2O+(NaCl) (b) mixtures: Comparison of literature experimental data with predictions using the (e-PR-CPA + vdWP) model.

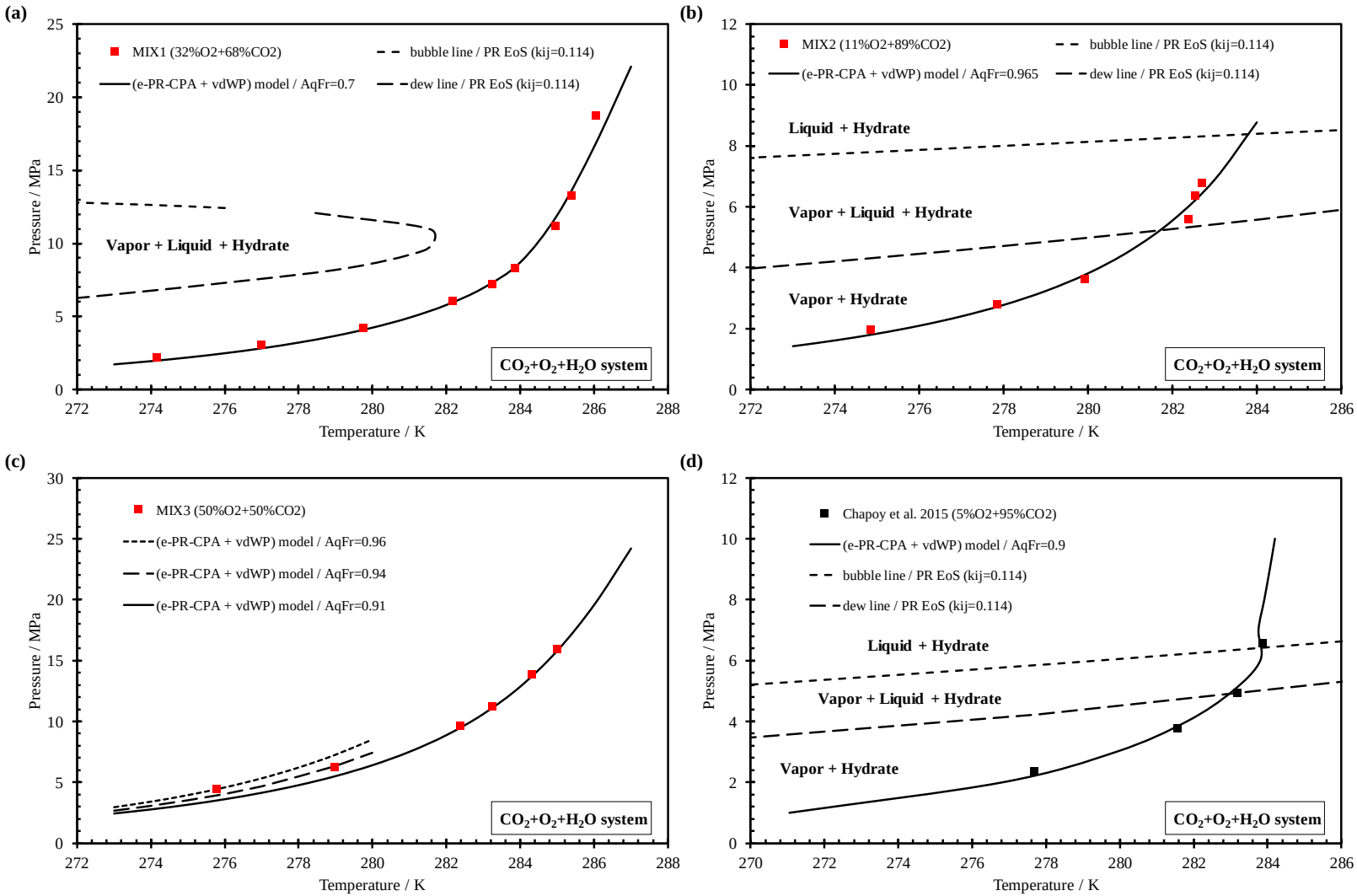

Figure 6.9: Hydrate dissociation conditions of the CO_2+O_2+H_2O ternary system at different O_2 "water-free" mole fractions 32% (a), 11% (b), 50% (c) and 5% (d): Comparison of measured (a, b and c, see Table 6.3) and literature [6. 11] (d) experimental data with predictions using the (e-PR-CPA + vdWP) model (solid lines). The bubble and dew lines of the different gas mixtures are determined by the PR EoS.

6.3.3 Hydrate stability of the CO_2+O_2+H_2O mixture

Concerning the mixed-gas hydrate system (CO_2+O_2), the (e-PR-CPA + vdWP) model also predicts a hydrate structure of type I. In Figure 6.9, the predictions of the hydrate stability conditions of this system are compared with the measured data (from this work, see Table 6.3) at different O_2 compositions (11%, 32% and 50% water-free mole fraction) and also with those of Chapoy et al. [6. 11] at 5% O_2. Remarkable accuracy in the predictions of this system at different gas mixture compositions from 5 to 50% O_2 is obtained. The calculations were performed at different fixed aqueous fractions AqFr in a very representative way of the experimental aqueous fractions listed in Table 6.3 which are not fixed (decreases with each increase in pressure by adding more gas mixture). It should be noted that no further adjustments were made, i.e. only the good representation of the single-gas hydrate systems and the VLE of the binary systems (gas-gas and gas-water) allowed the accurate prediction of the multi-component system (CO_2+O_2+H_2O), and this is thanks to the good theoretical basis of the coupling of the e-PR-CPA EoS with the vdWP theory. As shown in Figure 6.9, by plotting the gas hydrate dissociation curve and the phase envelope of the gas mixture obtained by the e-PR-CPA model, we can accurately identify the different types of coexisting phases (liquid, aqueous, vapor and gaseous) at each temperature and pressure condition, which is very useful. As shown in plots a, b, c and d of Figure 6.9, the addition of O_2 effectively decreases the critical point of the mixed-gas and shifts its phase envelope to lower temperatures, and it seems that the 50% O_2 mixture or even less the 32% O_2 mixture are preferred to ensure that there is no phase change (especially phase split to liquid-vapor equilibrium) in the gas stored in the cavern.

For an overview, in Figure 6.10, the hydrate stability results of the ternary CO_2+O_2+H_2O system are plotted from pure CO_2 hydrate to pure O_2 hydrate, showing the effect of oxygen on the stability of the CO_2-rich mixed-gas hydrate. This Figure shows that at high pressure (>20 MPa) the hydrate dissociation temperature of the mixed gas CO_2+O_2 becomes higher than that of pure CO_2, therefore precautions must be taken to avoid hydrate formation at the wellhead or in the pipelines during the transport of this gas stream which is assumed to be saturated with water vapor after its withdrawal from the cavity. However, in reality the stored gas is in equilibrium with almost “pure” NaCl-brine and not pure water, which led us to study in the following section the effect of NaCl on this mixed-gas system.

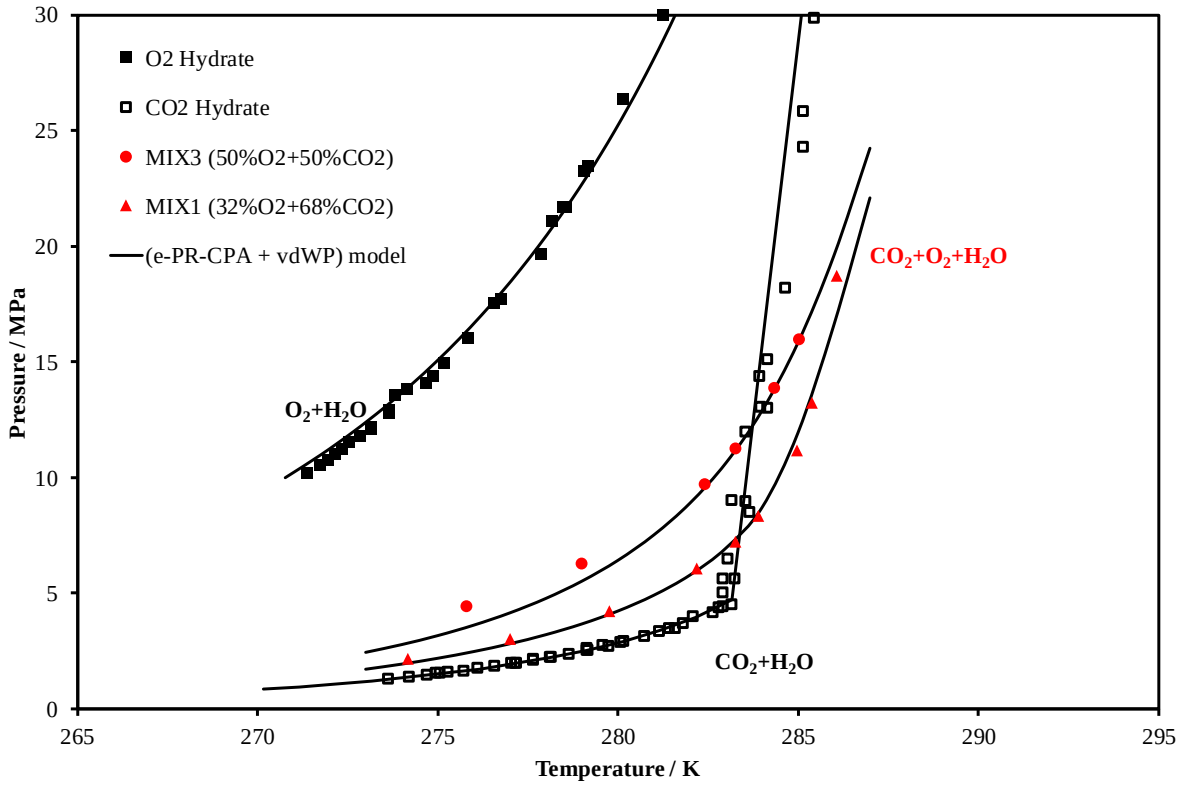

Figure 6.10: Hydrate dissociation conditions of the CO_2+O_2+H_2O ternary system from pure O_2 hydrate to pure CO_2 hydrate. Comparison of literature and measured data with predictions using the (e-PR-CPA + vdWP) model (solid lines).

6.3.4 Hydrate stability of the CO_2+O_2+H_2O+NaCl mixture

The developed model (e-PR-CPA + vdWP) has shown its predictive capabilities, in particular the transition from simple binary systems to multi-component systems (gas+water+salt and mixed-gas+water). Since all the necessary parameters are already available, in particular the interaction parameters CO_2+O_2, O_2-Na+, O_2-Cl-, O_2-H_2O, CO_2-Na+, CO_2-Cl- and CO_2-H_2O, we can model the quaternary system CO_2+O_2+H_2O+NaCl with a high degree of confidence. The study of this system involves several variables including the composition of the mixed-gas, the aqueous fraction and the salinity (NaCl molality). Taking the example of the FluidSTORY project on the combination of the Power-to-Gas (PtG) and Underground Gas Storage (UGS) technologies discussed earlier in the introduction, the quantity of O_2 in the EMO unit is relatively less than CO_2 [6. 57], that is why we choose to study the mixture with 32% O_2. The aqueous fraction was kept the same (AqFr=0.7) as that of the mixed-gas system (without salt, see Figure 6.9a) with 32% O_2, as well as two salinities were studied (1m and 4m), one was limited to 4m since the O_2 solubility data in NaCl brine on which the e-PR-CPA EoS was adjusted are limited to this salinity (4m, see Chabab et al. [6. 6]).

The modeling results obtained are shown in Figure 6.11. As expected, NaCl significantly decreases the hydrate dissociation temperature of this gas mixture. The shape of the curve remains the same with a shift to the left by adding the salt. The model also detects when there are several phases in equilibrium especially at 4m when the hydrate dissociation curve crosses the phase envelope of the gas mixture. According to the trend of the dissociation points calculated by the model in this region, we notice from the slight change in the curve that there is a phase split and that at a pressure higher than the bubble line and at the left of the gas hydrate dissociation curve, the hydrate is rather in equilibrium with a gas-rich liquid phase and not with a vapor phase.

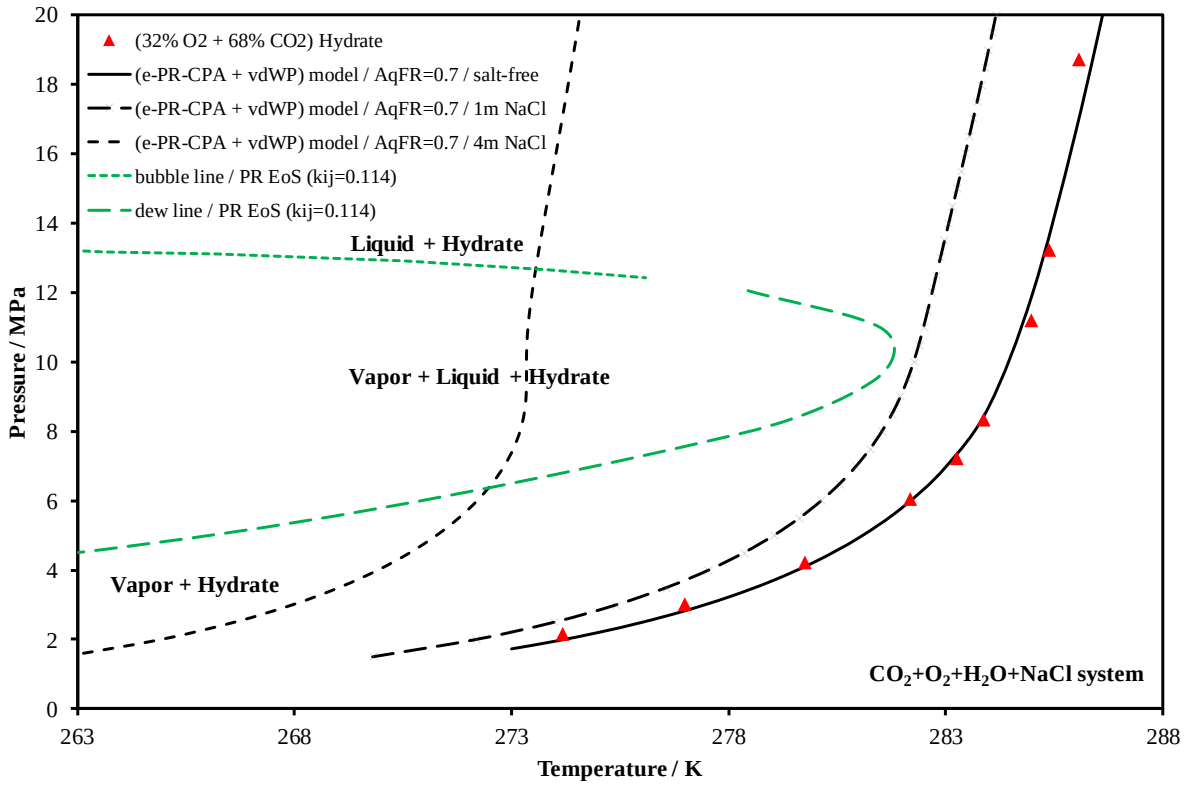

Figure 6.11: Hydrate dissociation conditions of the CO_2+O_2+H_2O+(NaCl) quaternary system: Prediction of the effect of NaCl concentration (from salt-free to 4m) on the mixed-gas hydrate system (32% O_2 , at fixed aqueous fraction AqFr=0.7) using the (e-PR-CPA + vdWP) model. The bubble and dew lines are determined by the PR EoS.

6.4 Conclusions

In this work the phase behavior of systems containing CO_2, O_2, H_2O and possibly NaCl, and in particular the gas hydrate stability conditions of CO_2, O_2 and their mixtures were studied. The isochoric pressure search method was used to overcome the lack of data for the CO_2+O_2+H_2O system by measuring new hydrate dissociation points of the CO_2+O_2 gas mixture at different global compositions. The consistency of the measured data was verified using the Clausius-Clapeyron relationship. In addition to the fact that these data were measured for a promising massive energy storage application (combination of PtG with UGS using the EMO process), these data will serve for the evaluation of predictive models, and also to help to avoid problems related to flow assurance by taking the necessary precautions when transporting gas streams composed of CO_2, O_2 and water, for instance, oxycombustion flue gas.

To predict the dissociation conditions of gas hydrates, in this work, the established hydrate theory of van der Waals and Platteeuw (vdWP) is combined with the e-PR-CPA EoS which has shown in this and previous work excellent capabilities to determine water activity in brine, gas solubility in water and brine and to predict the water content in gas-rich phase. The resulting model (e-PR-CPA + vdWP) was successfully applied to the O_2+H_2O and CO_2+H_2O+NaCl systems by comparing with literature data as well as to the CO_2+O_2+H_2O mixed-gas hydrate system by comparing predictions with the new reported measurements. The model allowed a complete study of phase equilibria (hydrate-fluids and fluid-fluids) of gas/water systems and also to accurately predict the effect of the presence of salt on the stability of gas hydrates. The excellent results obtained using this model for single-gas and mixed-gas hydrate systems without adding additional parameters for the latter are the result of an advanced equation of state (e-PR-CPA) and a theoretically solid solution for gas hydrates (vdWP).

Acknowledgments

We thank Dr. Martha Hajiw for the various useful discussions. Financial support from Agence Nationale de la Recherche (ANR) through the project FluidSTORY (n° 7747, ID ANR-15-CE06-0015) is gratefully acknowledged.

References

[6. 1] R. Habibi, An investigation into design concepts, design methods and stability criteria of salt caverns, Oil & Gas Science and Technology–Revue d'IFP Energies nouvelles, 74 (2019) 14.
[6. 2] S. Merey, Prediction of pressure and temperature changes in the salt caverns of Tuz Golu underground natural gas storage site while withdrawing or injecting natural gas by numerical simulations, Arabian Journal of Geosciences, 12 (2019) 205.
[6. 3] W. Kleinitz, E. Boehling, Underground gas storage in porous media–operating experience with bacteria on gas quality (spe94248), in: 67th EAGE Conference & Exhibition, European Association of Geoscientists & Engineers, 2005, pp. cp-1-00556.
[6. 4] S. Ahamada, A. Valtz, S. Chabab, L. Blanco-Martin, C. Coquelet, Experimental density data of three carbon dioxide and oxygen binary mixtures at temperatures from 276 to 416 K and at pressures up to 20 MPa, Journal of Chemical & Engineering Data, Submitted (2020).
[6. 5] S. Chabab, P. Théveneau, J. Corvisier, C. Coquelet, P. Paricaud, C. Houriez, E. El Ahmar, Thermodynamic study of the CO2–H2O–NaCl system: Measurements of CO2 solubility and modeling of phase equilibria using Soreide and Whitson, electrolyte CPA and SIT models, International Journal of Greenhouse Gas Control, 91 (2019) 102825.
[6. 6] S. Chabab, P. Ahmadi, P. Théveneau, C. Coquelet, A. Chapoy, J. Corvisier, P. Paricaud, Measurements and modeling of high-pressure O2 and CO2 solubility in brine (H2O+NaCl), Journal of Chemical & Engineering Data, Submitted (2020).
[6. 7] S. Chabab, P. Théveneau, C. Coquelet, J. Corvisier, P. Paricaud, Measurements and predictive models of high-pressure H2 solubility in brine (H2O+ NaCl) for underground hydrogen storage application, International Journal of Hydrogen Energy, (2020).
[6. 8] A. Chapoy, M. Nazeri, M. Kapateh, R. Burgass, C. Coquelet, B. Tohidi, Effect of impurities on thermophysical properties and phase behaviour of a CO2-rich system in CCS, International Journal of Greenhouse Gas Control, 19 (2013) 92-100.
[6. 9] S.W. Løvseth, G. Skaugen, H.J. Stang, J.P. Jakobsen, Ø. Wilhelmsen, R. Span, R. Wegge, CO2Mix Project: Experimental determination of thermo-physical properties of CO2-rich mixtures, Energy Procedia, 37 (2013) 7841-7849.
[6. 10] S.F. Westman, H.J. Stang, S.W. Løvseth, A. Austegard, I. Snustad, I.S. Ertesvåg, Vapor-liquid equilibrium data for the carbon dioxide and oxygen (CO2+ O2) system at the temperatures 218, 233, 253, 273, 288 and 298 K and pressures up to 14 MPa, Fluid Phase Equilibria, 421 (2016) 67-87.
[6. 11] A. Chapoy, C. Coquelet, R. Burgass, B. Tohidi, Final Report JIP (confidential) : Impact of Common Impurities on CO2 Capture, Transport and Storage 2011 – 2014 PROGRAMME, in, **2015**.
[6. 12] S.-P. Kang, H. Lee, C.-S. Lee, W.-M. Sung, Hydrate phase equilibria of the guest mixtures containing CO2, N2 and tetrahydrofuran, Fluid Phase Equilibria, 185 (2001) 101-109.
[6. 13] J. He, Y. Liu, Z. Ma, S. Deng, R. Zhao, L. Zhao, A literature research on the performance evaluation of hydrate-based CO2 capture and separation process, Energy Procedia, 105 (2017) 4090-4097.
[6. 14] J.I. Lunine, D.J. Stevenson, Thermodynamics of clathrate hydrate at low and high pressures with application to the outer solar system, Astrophysical Journal Supplement Series, 58 (1985) 493-531.
[6. 15] J.v.d. Waals, J. Platteeuw, Clathrate solutions, Advances in chemical physics, (1958) 1-57.
[6. 16] M. Hajiw, E. Boonaert, A. Valtz, E. El Ahmar, A. Chapoy, C. Coquelet, Impact of aromatics on acid gas injection, (2016).

[6. 17] F. Tzirakis, P. Stringari, N. von Solms, C. Coquelet, G. Kontogeorgis, Hydrate equilibrium data for the CO2+ N2 system with the use of tetra-n-butylammonium bromide (TBAB), cyclopentane (CP) and their mixture, Fluid Phase Equilibria, 408 (2016) 240-247.
[6. 18] M. Hajiw, Hydrate mitigation in sour and acid gases, in, 2014.
[6. 19] E. Sloan, F. Fleyfel, Hydrate dissociation enthalpy and guest size, Fluid Phase Equilibria, 76 (1992) 123-140.
[6. 20] M.L. Michelsen, The isothermal flash problem. Part I. Stability, Fluid phase equilibria, 9 (1982) 1-19.
[6. 21] M.L. Michelsen, The isothermal flash problem. Part II. Phase-split calculation, Fluid phase equilibria, 9 (1982) 21-40.
[6. 22] J. Munck, S. Skjold-Jørgensen, P. Rasmussen, Computations of the formation of gas hydrates, Chemical Engineering Science, 43 (1988) 2661-2672.
[6. 23] W.R. Parrish, J.M. Prausnitz, Dissociation pressures of gas hydrates formed by gas mixtures, Industrial & Engineering Chemistry Process Design and Development, 11 (1972) 26-35.
[6. 24] D.-Y. Peng, D.B. Robinson, A new two-constant equation of state, Industrial & Engineering Chemistry Fundamentals, 15 (1976) 59-64.
[6. 25] M. Wertheim, Fluids with highly directional attractive forces. I. Statistical thermodynamics, Journal of statistical physics, 35 (1984) 19-34.
[6. 26] L. Blum, Mean spherical model for asymmetric electrolytes: I. Method of solution, Molecular Physics, 30 (1975) 1529-1535.
[6. 27] M. Born, Volumen und hydratationswärme der ionen, Zeitschrift für Physik, 1 (1920) 45-48.
[6. 28] G.M. Kontogeorgis, G.K. Folas, N. Muro-Suñé, F. Roca Leon, M.L. Michelsen, Solvation Phenomena in Association Theories with Applications to Oil & Gas and Chemical Industries, Oil & Gas Science and Technology - Revue de l'IFP, 63 (2008) 305-319.
[6. 29] S. Lasala, P. Chiesa, R. Privat, J.-N. Jaubert, VLE properties of CO2–Based binary systems containing N2, O2 and Ar: Experimental measurements and modelling results with advanced cubic equations of state, Fluid Phase Equilibria, 428 (2016) 18-31.
[6. 30] T. Kihara, Determination of Intermolecular Forces from the Equation of State of Gases. II, Journal of the Physical Society of Japan, 6 (1951) 184-188.
[6. 31] V. McKoy, O. Sinanoğlu, Theory of dissociation pressures of some gas hydrates, The journal of chemical physics, 38 (1963) 2946-2956.
[6. 32] N. Hubert, Y. Gabes, J.-B. Bourdet, L. Schuffenecker, Vapor pressure measurements with a nonisothermal static method between 293.15 and 363.15 K for electrolyte solutions. Application to the H2O+ NaCl system, Journal of Chemical and Engineering Data, 40 (1995) 891-894.
[6. 33] W.J. Hamer, Y.C. Wu, Osmotic coefficients and mean activity coefficients of uni‐univalent electrolytes in water at 25° C, Journal of Physical and Chemical Reference Data, 1 (1972) 1047-1100.
[6. 34] J.A. Rard, D.G. Archer, Isopiestic Investigation of the Osmotic and Activity Coefficients of Aqueous NaBr and the Solubility of NaBr. cntdot. 2H2O (cr) at 298.15 K: Thermodynamic Properties of the NaBr+ H2O System over Wide Ranges of Temperature and Pressure, Journal of Chemical and Engineering Data, 40 (1995) 170-185.
[6. 35] J. llmari Partanen, P.O. Minkkinen, Thermodynamic Activity Quantities in Aqueous Sodium and Potassium Chloride Solutions at 298.15 K up to a Molality of 2.0 mol kg _1, Acta Chemica Scandinavica, 47 (1993) 768-776.
[6. 36] R.A. Robinson, R.H. Stokes, Tables of osmotic and activity coefficients of electrolytes in aqueous solution at 25 C, Transactions of the Faraday Society, 45 (1949) 612-624.

[6. 37] H.F. Gibbard Jr, G. Scatchard, R.A. Rousseau, J.L. Creek, Liquid-vapor equilibrium of aqueous sodium chloride, from 298 to 373. deg. K and from 1 to 6 mol kg-1, and related properties, Journal of Chemical and Engineering Data, 19 (1974) 281-288.
[6. 38] K.S. Pitzer, J.C. Peiper, R. Busey, Thermodynamic properties of aqueous sodium chloride solutions, Journal of Physical and Chemical Reference Data, 13 (1984) 1-102.
[6. 39] H. Guo, Y. Huang, Y. Chen, Q. Zhou, Quantitative Raman Spectroscopic Measurements of CO2 Solubility in NaCl Solution from (273.15 to 473.15) K at p=(10.0, 20.0, 30.0, and 40.0) MPa, Journal of Chemical & Engineering Data, 61 (2015) 466-474.
[6. 40] D. Koschel, J.-Y. Coxam, L. Rodier, V. Majer, Enthalpy and solubility data of CO 2 in water and NaCl (aq) at conditions of interest for geological sequestration, Fluid phase equilibria, 247 (2006) 107-120.
[6. 41] W. Yan, S. Huang, E.H. Stenby, Measurement and modeling of CO2 solubility in NaCl brine and CO2–saturated NaCl brine density, International Journal of Greenhouse Gas Control, 5 (2011) 1460-1477.
[6. 42] H. Messabeb, F.o. Contamine, P. Cézac, J.P. Serin, E.C. Gaucher, Experimental Measurement of CO2 Solubility in Aqueous NaCl Solution at Temperature from 323.15 to 423.15 K and Pressure of up to 20 MPa, Journal of Chemical & Engineering Data, 61 (2016) 3573-3584.
[6. 43] P. Ahmadi, A. Chapoy, CO2 solubility in formation water under sequestration conditions, Fluid Phase Equilibria, 463 (2018) 80-90.
[6. 44] A. Bamberger, G. Sieder, G. Maurer, High-pressure (vapor+ liquid) equilibrium in binary mixtures of (carbon dioxide+ water or acetic acid) at temperatures from 313 to 353 K, The Journal of Supercritical Fluids, 17 (2000) 97-110.
[6. 45] S.-X. Hou, G.C. Maitland, J.M. Trusler, Measurement and modeling of the phase behavior of the (carbon dioxide+ water) mixture at temperatures from 298.15 K to 448.15 K, The Journal of Supercritical Fluids, 73 (2013) 87-96.
[6. 46] R. Dohrn, A. Bünz, F. Devlieghere, D. Thelen, Experimental measurements of phase equilibria for ternary and quaternary systems of glucose, water, CO2 and ethanol with a novel apparatus, Fluid Phase Equilibria, 83 (1993) 149-158.
[6. 47] R. Wiebe, V. Gaddy, The solubility in water of carbon dioxide at 50, 75 and 100, at pressures to 700 atmospheres, Journal of the American Chemical Society, 61 (1939) 315-318.
[6. 48] J. Briones, J. Mullins, M. Thies, B.-U. Kim, Ternary phase equilibria for acetic acid-water mixtures with supercritical carbon dioxide, Fluid Phase Equilibria, 36 (1987) 235-246.
[6. 49] A.D. King Jr, C. Coan, Solubility of water in compressed carbon dioxide, nitrous oxide, and ethane. Evidence for hydration of carbon dioxide and nitrous oxide in the gas phase, Journal of the American Chemical Society, 93 (1971) 1857-1862.
[6. 50] K. Jackson, L.E. Bowman, J.L. Fulton, Water solubility measurements in supercritical fluids and high-pressure liquids using near-infrared spectroscopy, Analytical Chemistry, 67 (1995) 2368-2372.
[6. 51] G. Müller, E. Bender, G. Maurer, Das Dampf‐Flüssigkeitsgleichgewicht des ternären Systems Ammoniak‐Kohlendioxid‐Wasser bei hohen Wassergehalten im Bereich zwischen 373 und 473 Kelvin, Berichte der Bunsengesellschaft für physikalische Chemie, 92 (1988) 148-160.
[6. 52] R.G. Wylie, R.S. Fisher, Molecular interaction of water vapor and oxygen, Journal of Chemical & Engineering Data, 41 (1996) 175-180.
[6. 53] C.A. Koh, E.D. Sloan, A.K. Sum, D.T. Wu, Fundamentals and applications of gas hydrates, Annual review of chemical and biomolecular engineering, 2 (2011) 237-257.
[6. 54] D. Davidson, Y. Handa, C. Ratcliffe, J. Ripmeester, J. Tse, J. Dahn, F. Lee, L. Calvert, Crystallographic studies of clathrate hydrates. Part I, Molecular Crystals and Liquid Crystals, 141 (1986) 141-149.

[6. 55] J. Tse, Y. Handa, C. Ratcliffe, B. Powell, Structure of oxygen clathrate hydrate by neutron powder diffraction, Journal of inclusion phenomena, 4 (1986) 235-240.
[6. 56] A.H. Mohammadi, B. Tohidi, R.W. Burgass, Equilibrium data and thermodynamic modeling of nitrogen, oxygen, and air clathrate hydrates, Journal of Chemical & Engineering Data, 48 (2003) 612-616.
[6. 57] N. Kezibri, C. Bouallou, Conceptual design and modelling of an industrial scale power to gas-oxy-combustion power plant, International Journal of Hydrogen Energy, 42 (2017) 19411-19419.

French summary / Chapitre 7 - Principales conclusions et perspectives

L'étude thermodynamique (expérimentation et modélisation) des systèmes Gaz+Eau+Sels est d'une grande importance, que ce soit dans un contexte environnemental comme le Captage et le Stockage du dioxyde de Carbone (CSC) ou dans un contexte économique comme la récupération assistée du pétrole par injection de CO_2, ou le Stockage Souterrain réversible massif de Gaz (SSG) à usage industriel (« Power-to-Gas » (PtG) et « Gas-to-Power » (GtP), industries chimiques, pétrochimiques et pharmaceutiques...). Dans ce travail, pour pallier le manque de données expérimentales à haute pression de la solubilité des gaz (CO_2, O_2 et H_2) dans la saumure, un dispositif expérimental basé sur la méthode "statique-analytique" a été adapté et utilisé pour mesurer la solubilité des gaz dans l'eau pure et la saumure. Pour comparer/valider les nouvelles mesures, un deuxième dispositif basé sur une technique dite "volumétrique" a également été utilisé. Une équation d'état pour les électrolytes (e-PR-CPA) a été développée en prenant en compte toutes les interactions entre espèces chimiques (molécules et ions). Les résultats de ce modèle ont été comparés avec des modèles existants tels que ceux utilisés par les géochimistes et en génie des procédés. Pour une meilleure évaluation des performances de notre modèle, les paramètres des modèles précédemment cités ont été réoptimisés en incluant les nouvelles données acquises. Compte tenu de ses très bonnes performances, le modèle e-PR-CPA a ensuite été étendu à l'étude de la stabilité des hydrates de gaz en le combinant avec la théorie bien établie des hydrates de van der Waals et Platteeuw (vdWP). Le modèle résultant (e-PR-CPA + vdWP) a été appliqué avec succès pour prédire les conditions de stabilité des hydrates de gaz (purs ou mélangés) ainsi que l'effet inhibiteur du sel (NaCl). Les mesures des points de stabilité des hydrates du mélange gazeux CO_2+O_2 effectuées dans le cadre du projet ANR-FluidSTORY ont été reproduites (prédites) à l'aide de ce modèle avec une grande précision. Les différents résultats (expérimentaux et de modélisation) issus de ces travaux serviront à la bonne compréhension et au contrôle des installations de stockage souterrain d'un point de vue thermodynamique, tels que la simulation de scénarios de stockage, la surveillance de la température, de la pression et de la quantité de gaz, les calculs de spéciation chimique (notamment pour les composés réactifs tels que O_2, H_2 et CO_2)

pour l'évaluation des risques (interaction avec la roche, production de H_2S, etc.) et le contrôle de la qualité du gaz à la sortie du puits (évaluation des risques liés à la teneur en eau et à la stabilité des hydrates de gaz).

Ce travail ouvre une perspective vers l'étude de la solubilité dans les mélanges de gaz, sachant que le modèle développé n'est paramétré que sur des systèmes binaires, et donc totalement prédictif pour les mélanges multi-constituants. En effet, une des applications intéressantes est le stockage souterrain de mélanges gazeux comme le stockage de CO_2+O_2 pour le procédé EMO, le stockage de H_2+CO_2 pour le concept de bio-méthanation souterraine ou encore le stockage du mélange H_2+CH_4 (Hythane) qui est un vecteur énergétique très prometteur du point de vue de « l'éco-efficacité » par rapport au gaz naturel. Par ailleurs, il sera intéressant d'étudier l'effet d'impuretés telles que l'H_2S (qui peut être produit par la réduction de la pyrite en présence de micro-organismes réducteurs de sulfate, notamment pour le stockage en milieu poreux) sur le diagramme de phase du système complet (mélange gaz + eau + sel + impuretés), ce qui est facilement réalisable par le modèle e-PR-CPA en utilisant les règles de mélange pour le terme cubique et les règles de combinaison pour l'association (liaison hydrogène) entre les molécules, et cela ne nécessite que des paramètres d'interaction de systèmes binaires. Cependant, certaines mesures expérimentales sont nécessaires pour valider ou pour montrer les limitations du modèle. À cette fin, la méthode statique-analytique est plus adaptée à ce type de mesures (systèmes multi-constituants) puisque les différents composés sont quantifiés par chromatographie en phase gazeuse après échantillonnage de la phase aqueuse (mesure directe) ou de la phase riche en gaz (mesure indirecte, par bilan matière). Une deuxième perspective pour ce travail est l'extension de l'étude aux systèmes contenant des mélanges de sels, ce qui est très intéressant surtout pour le stockage dans les aquifères salins profonds sachant que plusieurs sels sont dissous (avec des compositions différentes selon la formation géologique) dans l'eau de formation. Une solution à tester est de relier la solubilité des gaz dans les solutions de mélanges de sels à leur solubilité dans la saumure d'NaCl, ce qui est très courant dans l'industrie pétrolière et gazière. La connaissance de la salinité des solutions de sels mixtes en termes de Solides Dissous Totaux (SDT) ainsi que de la solubilité des gaz dans la saumure de NaCl permettra d'estimer la solubilité des gaz dans une saumure réelle. Il est donc intéressant d'effectuer des mesures et de modéliser la solubilité des gaz dans différentes solutions de sels purs afin de pouvoir développer des relations permettant d'avoir l'équivalent d'une eau de formation en termes de salinité de la saumure d'NaCl.

Chapter 7: Major findings and perspectives

The thermodynamic study (experimental and modeling) of Gas+Water+Salt systems is of great importance for scientific understanding (in many disciplines, e.g. geochemistry, and oceanography, etc.) and engineering applications such as Carbon dioxide Capture and Storage (CCS), Enhanced Oil Recovery (EOR) by CO_2 injection, gas hydrate stability, and massive reversible Underground Gas Storage (UGS) for industrial use. Combining Power-to-Gas (PtG) technology with UGS and oxy-fuel combustion represents a complete solution for the massive storage of surplus electricity in the form of gaseous energy carriers such as Methane (CH_4, used in Oxy-fuel combustion units), Carbon dioxide (CO_2, used in methanation units), Oxygen (O_2, used in Oxy-fuel combustion units) and Hydrogen (H_2, used directly or to feed methanation units).

The underground storage of gas is mainly carried out in salt caverns (man-made reservoirs) and porous media (deep saline aquifers and depleted fields). The presence of brine in these geological formations completely changes the thermodynamic behavior of the stored gas (salting-out effect and geochemical reactions) due to the existence of electrolytes (NaCl, KCl, $MgCl_2$, etc.) dissolved in the residual or formation water of the reservoir, so studying these systems becomes very complicated. The solubility and water content of stored gases as well as the gas hydrate stability conditions of systems containing gas, water and salt are extremely important information to be known for the monitoring and control of the storage facilities as well as for the assessment of the various possible risks.

In this work, as part of three major industrial projects (ANR FluidSTORY, GIS Géodénergies Rostock H, and Carnot M.I.N.E.S HyTrend), the thermodynamic study of the salting-out effect on gas solubility is carried out in two parts: Experimental and modeling. A review of phase equilibrium data available in the literature, in particular the gas solubility in brine, was carried out and showed the lack of certain data, especially in the geological storage conditions (high pressure and temperature). The storage of CH_4 (or natural gas) has been carried out for a long time and is very well understood, that is why this study focuses on the measurements of the solubility of CO_2, O_2 and H_2 in brine. Na^+ and Cl^- are the main species found in the salts of most geological formations. Sodium chloride (NaCl) is therefore considered to be a representative model of salt. The solubility of CO_2 and O_2 in brine (H_2O+NaCl) was measured using two different techniques:

1) static-analytic apparatus (in *CTP Mines ParisTech, PSL University*); 2) volumetric apparatus (in *Institute for GeoEnergy Engineering, Heriot Watt University*). Experimental measurements of CO_2 solubility in H_2O+NaCl were carried out at molalities between 1 and 6 mol/kgw, temperatures between 303 and 373 K and pressures up to 395 bar. The new data of CO_2 solubility in brine were used to verify the predictions of models that are parameterized on literature data and to validate the experimental protocols by comparing with data measured by other authors. Given the unavailability of high-pressure data on the solubility of O_2 in brine, the new data carried out at molalities between 0.5 and 4 mol/kgw, at temperatures between 303 and 373 K and at pressures up to 360 bar served to provide the first high pressure measurements performed for this system, to evaluate the existing and developed (in this work) models, and to reparametrize them to improve the calculations. Measurements of H_2 solubilities in H_2O+NaCl were also carried out with the static-analytic apparatus at molalities between 0 and 5 mol/kgw, temperatures between 323 and 373 K and pressures up to 230 bar. These new data allow to overcome the great lack of experimental data at high pressure (not available to date) for this very important system since the only technology applicable for the massive storage of hydrogen is underground storage.

Equations of State (EoS) developed (e-PR-CPA) or improved (Soreide and Whitson (SW)) in this work were used to calculate phase equilibria of gas-water-salt systems. They were also used to process the measured experimental data by optimizing the model parameters. These models can be used either in "predictive" mode by fitting parameters on a very limited number of experimental data (e.g. atmospheric pressure data and/or gas solubility data in pure water) far from the application domain or in "correlative" mode for more accuracy. The performances of both EoS were compared with that of a geochemical model using the asymmetric (gamma-phi) approach.

These three models (SW, e-PR-CPA, and geochemical) describe very well the literature and measured data of solubility of CO_2, O_2, and H_2 in brine under different operating conditions (temperature, pressure, and salinity) with an absolute average deviation less than 5% comparing with the experimental data. The water content in the gas (CO_2, O_2 and H_2)-rich phases was also successfully predicted. Each of these models can be used for solubility and water content estimation. Criteria such as accuracy, simplicity and speed of calculation can be considered in selecting the appropriate model and approach. In general, the best results of gas solubility and water content estimation were obtained by the e-PR-CPA model. This model was parameterized on

equilibrium (H_2O+NaCl vapor pressure and H_2O saturation densities) and excess (osmotic coefficient) properties. Binary interaction parameters (BIPs) were optimized only on solubility data since its predictions of water content are not very sensitive to the variation of BIPs which is a very good advantage when using CPA-type model. This model has also been applied to other gases (CH_4 and N_2, etc.).

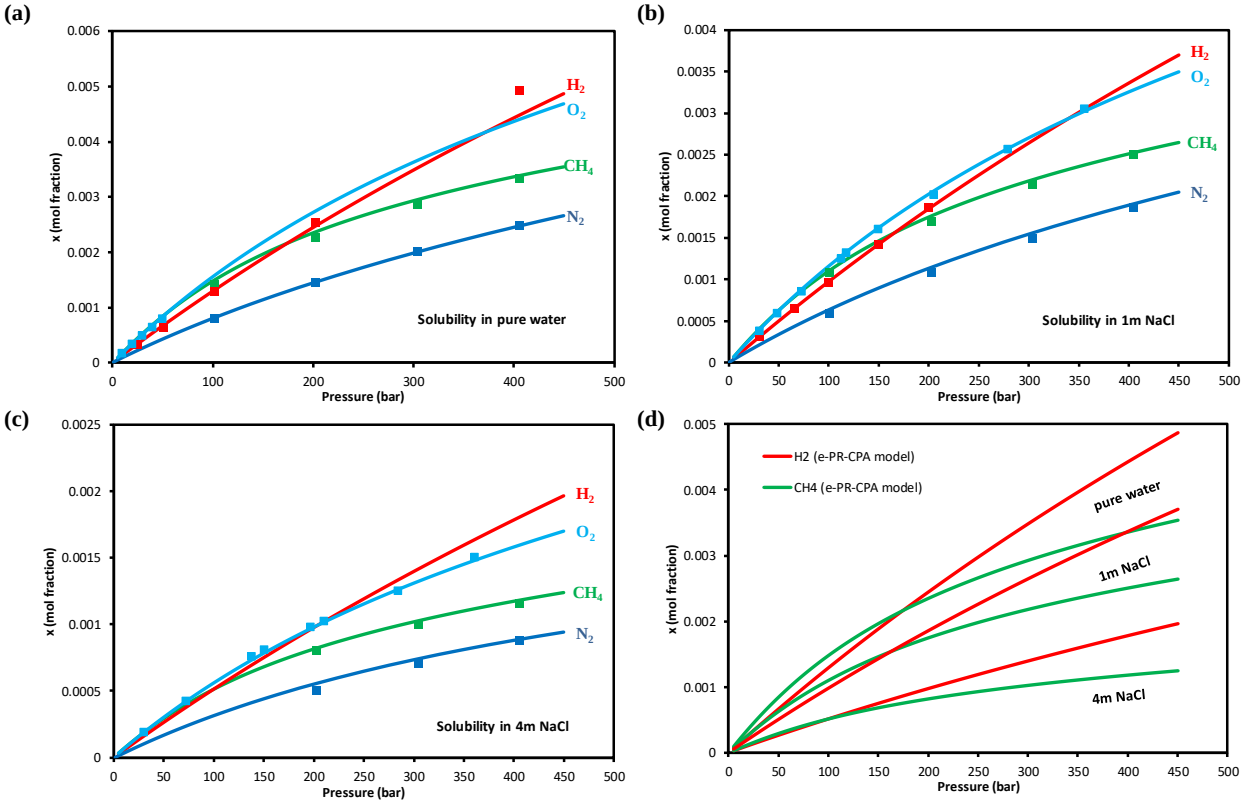

Figure 7.1: Gas (H_2, O_2, CH_4, and N_2) solubility in water and brine at 323 K: Comparison of literature and measured data (symbols) with predictions (solid lines) by e-PR-CPA EoS.

To conclude the work on gas solubility, in Figure 7.1, the predictions by the e-PR-CPA model of the solubility of O_2, H_2, N_2 and CH_4 in pure water and brine at different salinities are illustrated. CO_2 was not included in this comparison due to its high solubility compared to other gases. These predictions which have been verified against experimental data (from this work and from the literature) show that hydrogen at high pressure becomes more soluble than methane and even more soluble than oxygen (at higher pressures). Moreover, the evolution of hydrogen solubility with respect to pressure is flatter than the other gases (O_2, N_2 and CH_4) solubility. This work opens a perspective towards the study of solubility in gas mixtures, knowing that the developed model is

parameterized only on binary systems, so it is totally predictive for multi-constituent mixtures. Indeed, one of the interesting applications is the underground storage of gas mixtures such as the storage of CO_2+O_2 for the EMO process, the storage of H_2+CO_2 for the underground bio-methanation concept or even the storage of the H_2+CH_4 (Hythane) mixture which is a very promising energy vector from an eco-efficiency point of view when compared with natural gas. The effect of impurities such as H_2S (which can be produced by reduction of pyrite in the presence of sulfate-reducing microorganisms especially for storage in porous media) on the phase diagram of the complete system (mixed-gas + water + salt + impurities) will be interesting to investigate, which is easily achievable by the e-PR-CPA model using the mixing rules for the cubic term and the combining rules for the association (hydrogen bonding) between molecules, and this requires only interaction parameters of binary systems. However, some experimental measurements are necessary for validation or to show the limitations of the model. For this purpose, the static-analytic method is more suitable for this type of measurements in multi-constituent systems since the different constituents are quantified using gas chromatography after sampling the aqueous (direct measurement) or gas-rich (indirect measurement, by material balance) phase. In relation to this perspective, the influence of H_2S on the solubility of CO_2 in a low salinity mixed-salt brine was recently studied at CTP (Zaidin et al. [2]) and this study should be extended to high salinity brine and other gas mixtures depending on the applications (storage in salt caverns or porous media).

A second perspective for this work is the extension of the study to systems containing salt mixtures which is very interesting especially for storage in deep saline aquifers knowing that several salts are dissolved (with different composition according to the geological formation) in the formation water. One solution to be tested is to relate the gas solubility in mixed-salt solutions to their solubility in NaCl brine, which is very common in the oil and gas industry. The knowledge of the salinity of the mixed salts solution in terms of Total Dissolved Solids (TDS) as well as the gas solubility in the NaCl brine will allow to estimate the gas solubility in a real brine. Therefore, it is interesting to carry out measurements and modeling of gas solubility in different single-salt solutions in order to be able to develop relationships allowing to have the equivalent of a formation

[2] M.F. Zaidin, A. Chapoy, C. Coquelet, A. Valtz, M.R. A Raub, B.P. Kantaatmadja, Impact of H2S in Predicting the Storage Efficiency of CO2 Injection in a High Pressure High Temperature (HPHT) Carbonate Aquifer-A Case Study in a Sarawak Offshore High CO2 Gas Field, Malaysia, in: 14th Greenhouse Gas Control Technologies Conference Melbourne, 2018, pp. 21-26.

water in terms of NaCl-brine salinity. A typical example is shown in Figure 7.2 on the solubility of CO_2 in different salts with respect to NaCl as a reference, as well as a chart given by Schlumberger to calculate the NaCl equivalent of a brine with known TDS.

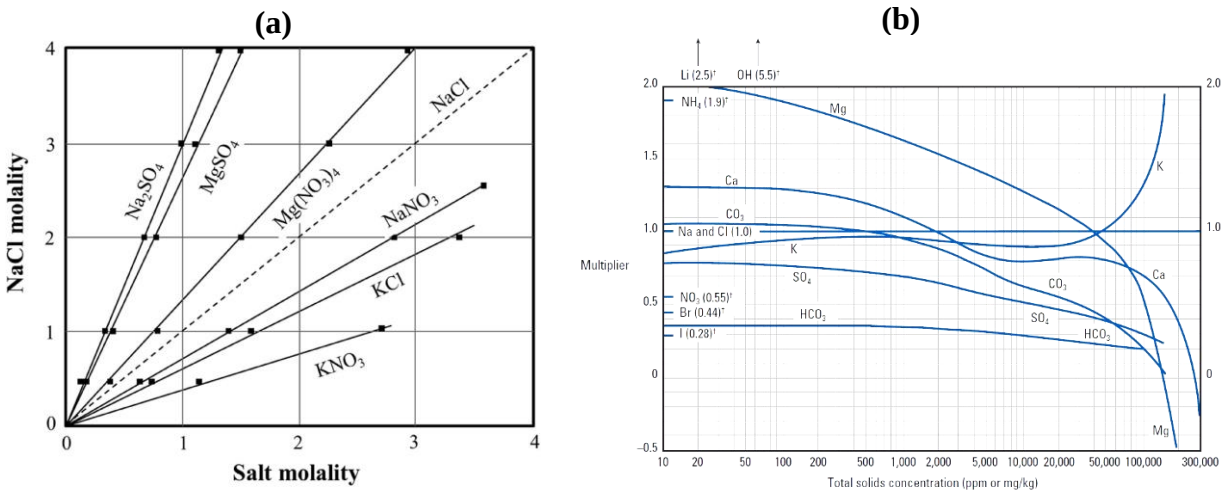

Figure 7.2: (a): Lines of equal solubilities in different salts of CO_2 with respect to NaCl (as salt reference), taken from Ratnakar et al. 2020. (b): Equivalent NaCl salinity of different salts, taken from Schlumberger (Log Interpretation Charts, 2009).

Given its very good performance, the e-PR-CPA model was then extended to study gas hydrate stability by combining it with the well-established hydrate theory of van der Waals and Platteeuw (vdWP). The resulting model (e-PR-CPA + vdWP) was successfully applied to predict gas hydrate stability conditions of single-gas and mixed-gas systems as well as the inhibitory effect of salt (NaCl). Measurements of hydrate stability points of the CO_2+O_2 gas mixture performed in the framework of the ANR FluidSTORY project have been reproduced (predicted) using this model with high accuracy. In addition, within the framework of the same project, we also carried out an experimental and modelling study of the density of the CO_2+O_2 gas mixture. The results obtained have been published and can be found in Appendix D. The different results (experimental and modeling) arising from this work will serve for the good understanding and control of underground storage facilities from a thermodynamic point of view, such as the simulation of storage scenarios, monitoring of temperature, pressure and gas quantity, chemical speciation calculations (especially for reactive compounds such as O_2, H_2 and CO_2) for risk assessment (interaction with the rock, H_2S production, etc.) and controlling the quality of the gas at the outlet of the well (water content and gas hydrate stability risk assessment).

Finally, in order to valorize the developed codes, a user-friendly graphical interface (Appendix B) for the calculation of thermophysical properties of complex systems (electrolytes, hydrates, etc.) has been developed. The models used and developed in this work (SW and e-PR-CPA) as well as other equations of state (PR, SRK, GERG) have been implemented and are accessible via the developed interface. This software package (ThermoReservoir®) is intended for industrial and academic research labs.

Appendix A: PT-Flash calculation

Under certain conditions, a mixture of overall composition z_i and flow rate F may split into several phases. If we take the example of a separation into two phases (Figure A.1), a liquid phase of flow rate L and a vapor phase of flow rate V, according to their volatilities, the different compounds are distributed by number of moles in the two phases. One can thus consider their molar fractions x_i in the liquid phase and y_i in the vapor phase. This process called flash distillation based on phase equilibria is the basic process of separation by volatility difference.

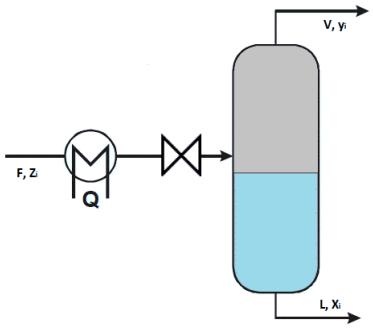

Figure A.1: Flash distillation

The partial material balance is written as follows:

$$Fz_i = Vy_i + Lx_i = Vy_i + (F - V)x_i \quad \textbf{(A-1)}$$

By defining the vaporized fraction $\beta = \frac{V}{F}$ and the partition coefficient $K_i = \frac{y_i}{x_i}$, from Equation A-1, we obtain:

$$z_i = \beta y_i + (1 - \beta)x_i \quad \textbf{(A-2)}$$

$$x_i = \frac{z_i}{\beta(K_i - 1) + 1} \quad \textbf{(A-3)}$$

$$y_i = K_i x_i = \frac{K_i z_i}{\beta(K_i - 1) + 1} \quad \textbf{(A-4)}$$

For a feed of known composition z_i, temperature T and pressure P, the vaporized fraction β can be obtained by solving numerically the so-called Rachford-Rice Equation A-7, then the compositions x_i and y_i can be calculated using Equations A-3 and A-4.

$$\sum y_i - \sum x_i = 0 \qquad \textbf{(A-5)}$$

$$\sum \frac{K_i x_i}{\beta(K_i - 1) + 1} - \sum \frac{z_i}{\beta(K_i - 1) + 1} = 0 \qquad \textbf{(A-6)}$$

$$F = \sum \frac{(K_i - 1) z_i}{\beta(K_i - 1) + 1} = 0 \qquad \textbf{(A-7)}$$

Equation A-7 is solved by the Newton-Raphson method, the derivative of the function F with respect to β is as follows:

$$F' = \frac{dF}{d\beta} = -\sum \frac{(K_i - 1)^2 z_i}{(\beta(K_i - 1) + 1)^2} \qquad \textbf{(A-8)}$$

The following calculation procedure is used to calculate the compositions of the constituents in each phase using the phi-phi approach:

1) Specify T, P, and z_i
   Iteration $j = 0 \qquad j' = 0$
2) Estimate $K_i^{(j)}$ using Michelsen's stability test, or by correlations:
   - For gases, the Wilson correlation can be used:

$$K_i^{(j)} = \frac{P_{c,i}}{P} \exp\left[5{,}37(1 + \omega_i)(1 - \frac{T_{c,i}}{T})\right] \qquad \textbf{(A-9)}$$

   - For water, this correlation can be used:

$$K_i^{(j)} = 10^6 \left(\frac{P\, T_{c,i}}{P_{c,i}\, T}\right) \qquad \textbf{(A-10)}$$

3) Initialize β : $(\beta^{(j')} = 0.5)$
4) Calculate x_i and y_i using Equations A-3 and A-4.
5) Normalize x_i and y_i : $x_i = \frac{x_i}{\sum_i x_i} \qquad y_i = \frac{y_i}{\sum_i y_i}$
6) Solving the equation of state (calculation of the volume of the two phases): use the Cardano's method for cubic equations of state, and Newton's method for non-cubic equations of state.
7) Calculate the fugacity coefficients φ_i^L and φ_i^V using Equation 2.18 (see Chapter 2).
8) Recalculate K_i : $K_i^{(j+1)} = \frac{\varphi_i^L}{\varphi_i^V} \qquad j = j + 1$

9) If $\frac{K_i^{(j)} - K_i^{(j+1)}}{K_i^{(j)}} > 10^{-8}$ return to step 4, otherwise :

   Calculate F and F' using Equations A-7 and A-8

   $\beta^{(j'+1)} = \beta^{(j')} - \frac{F}{F'} \qquad j' = j' + 1$

10) If $\left|\beta^{(j'+1)} - \beta^{(j')}\right| > 10^{-6}$ return to step 4, otherwise :

    Recalculate x_i and y_i using Equations A-3 and A-4

11) End of calculation: β, x_i, and y_i obtained

The same procedure can be used for the gamma-phi approach. The only difference is in the update (recalculation) of the k-values (step 8). This one is recalculated by activity coefficient and fugacity coefficient. From Equations 2.12-2.15 (see Chapter 2), K_i is obtained by: $K_i^{(j+1)} = \frac{\gamma_i^L \mathrm{K}_i^{henry} Poy}{P\varphi_i^V}$.

Appendix B: ThermoReservoir® software

The different codes developed in this work have been implemented in an intuitive Graphical User Interface (GUI). This will allow students/researchers to easily use the developed models to predict phase equilibria of complex systems (gas, water, salt, hydrates, etc.). The codes and the interface have been developed in Fortran which is an excellent programming language known for its speed and its adaptation to scientific problems requiring intensive calculations. The user selects the system of interest (Figure B.1) and the equation of state (SW or e-PR-CPA) and specifies the temperature, pressure and molality of the salt (NaCl) and then gets the result instantly after launching the calculation. The results can be listed in table form and/or illustrated as a phase diagram (Figure B.2). Other well-known equations of state (PR, SRK, and GERG-2008) with the main compounds found in the oil and gas field (Figure B.3) have also been implemented in the software package. Calculations of the main types of phase envelopes (Pxy, Txy, PT) are available.

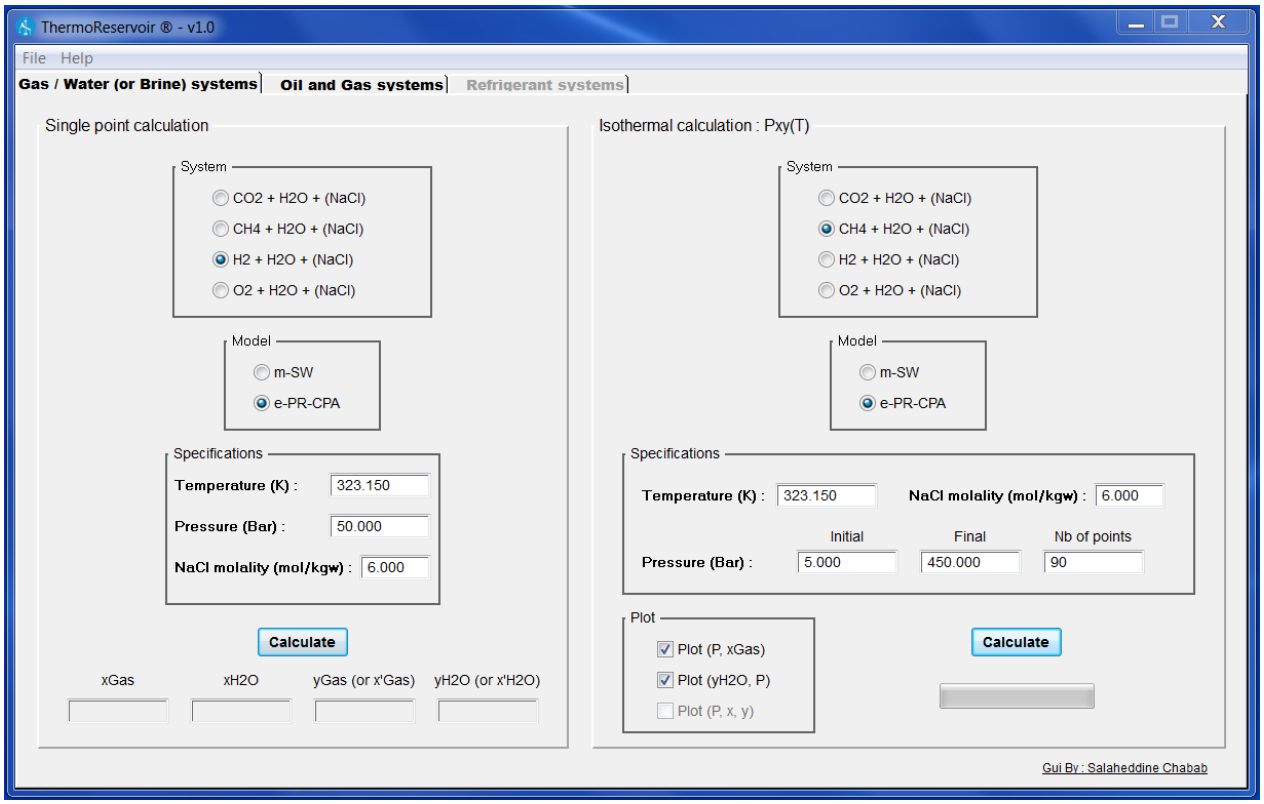

Figure B.1: ThermoReservoir® software: model and system selection and specs setting (temperature, pressure, and molality).

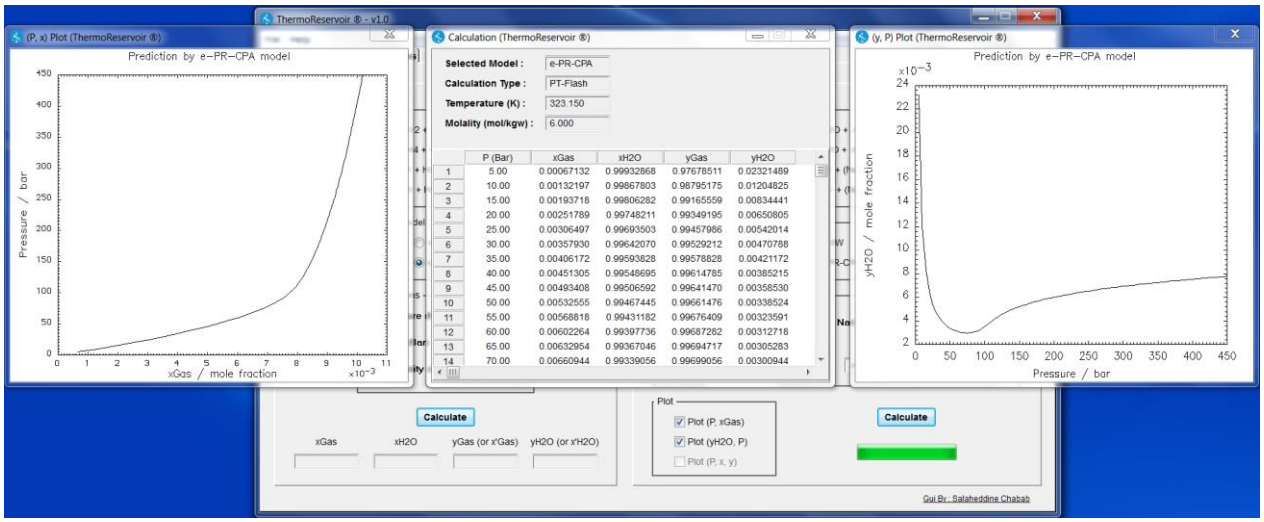

Figure B.2: ThermoReservoir® software: calculation results.

The incorporation of the e-PR-CPA + vdWP model for calculating the conditions of single-gas and mixed-gas hydrate stability as well as advanced models adapted to other types of systems (notably refrigerants) are in progress. The codes of all these models are already validated on a few systems, and we are currently working to extend them to several varieties of compounds by adding a database containing several constituents.

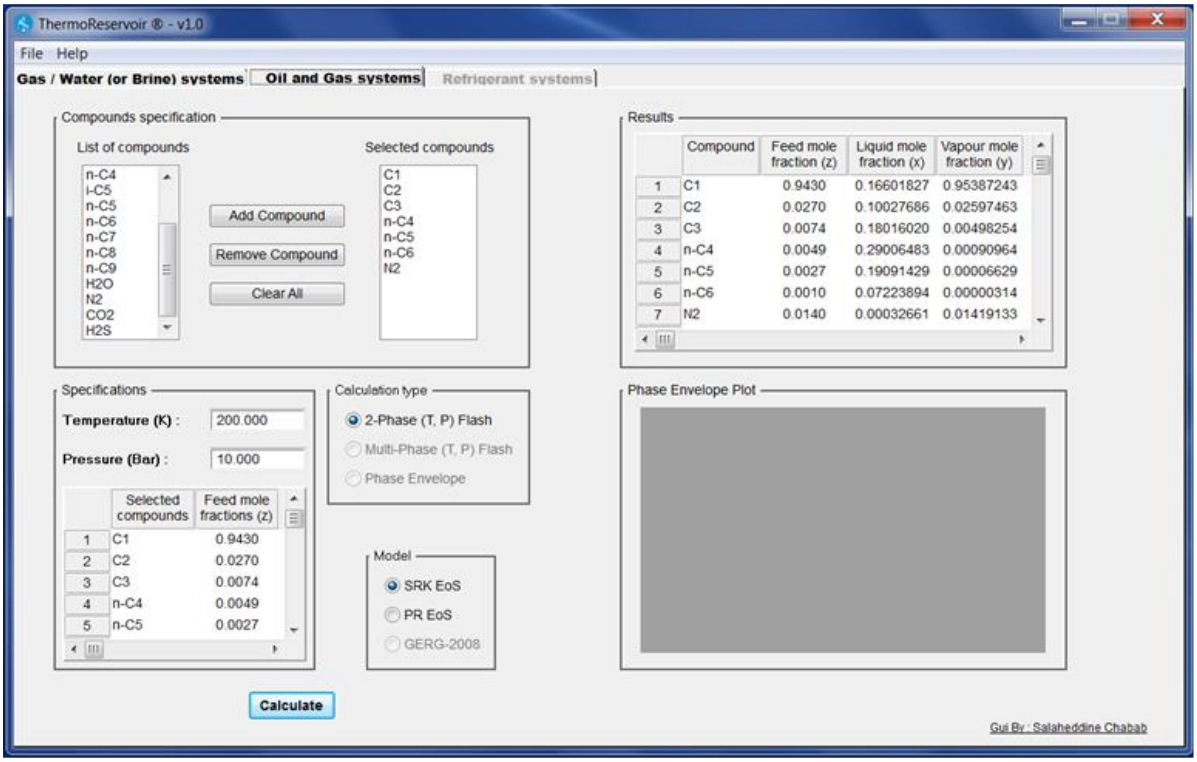

Figure B.3: ThermoReservoir® software: Phase equilibria in oil and gas systems.

Appendix C: List of publications

C.1. Papers

C.1.1. Journal articles

i. **Salaheddine Chabab**, Pascal Théveneau, Jérôme Corvisier, Christophe Coquelet, Patrice Paricaud, Céline Houriez, Elise El Ahmar, "*Thermodynamic study of the CO2–H2O–NaCl system: Measurements of CO2 solubility and modeling of phase equilibria using Soreide and Whitson, electrolyte CPA and SIT models*", International Journal of Greenhouse Gas Control, 91 (2019) 102825.

(**Author's contribution:** Under the supervision of Christophe coquelet, Patrice Paricaud, Céline Houriez and Elise El Ahmar, the author carried out the measurements with the help of Pascal Théveneau. The author coded and parametrized the equations of state (SW and e-PR-CPA) and the procedures for calculating phase equilibria, and processed the experimental data. Jerome Corvisier also processed the collected and measured data by his model using an asymmetric approach. Finally, the author prepared the results in the form of tables and figures and wrote the manuscript which was then reviewed by Christophe Coquelet and the other co-authors.)

ii. **Salaheddine Chabab**, Pascal Théveneau, Christophe Coquelet, Jérôme Corvisier, Patrice Paricaud, "*Measurements and predictive models of high-pressure H2 solubility in brine (H2O+ NaCl) for underground hydrogen storage application*", International Journal of Hydrogen Energy, 45 (2020) 32206-32220.

(**Author's contribution:** The author carried out the measurements with the help of Pascal Théveneau. The author has parameterized the previously developed equations of state (SW and e-PR-CPA), developed a new correlation to calculate accurately the solubility of hydrogen in water and brine, and processed the experimental data. Jerome Corvisier also processed the collected and measured data by his model using an asymmetric approach. Finally, the author prepared the results in the form of tables and figures and wrote the manuscript which was then reviewed by Christophe Coquelet and the other co-authors.)

iii. **Salaheddine Chabab**, Pezhman Ahmadi, Pascal Théveneau, Christophe Coquelet, Antonin Chapoy, Jérôme Corvisier, Patrice Paricaud, "*Measurements and Modeling of High-Pressure O2 and CO2 Solubility in Brine (H2O + NaCl) between 303 and 373 K and Pressures up to 36 MPa*", Journal of Chemical & Engineering Data, 66 (2021) 609-620.

(**Author's contribution:** The author carried out the measurements with the help of Pascal Théveneau, Pezhman Ahmadi and Antonin Chapoy. The author has parameterized the previously developed equations of state (SW and e-PR-CPA), and processed the experimental data. Jerome Corvisier also processed the collected and measured data by his model using an asymmetric approach. Finally, the author prepared the results in the form of tables and figures and wrote the manuscript which was then reviewed by Christophe Coquelet and the other co-authors.)

iv. **Salaheddine Chabab**, Alain Valtz, Snaïde Ahamada, Christophe Coquelet, "*Hydrate Stability of carbon dioxide + oxygen binary mixture (CO2 + O2) in pure water: Measurements and modeling*", Journal of Chemical & Engineering Data, 66 (2021) 767-779.

(**Author's contribution:** Alain Valtz and Snaïde Ahamada carried out the measurements. The author has developed and parameterized the model (e-PR-CPA + vdWP) for the prediction of gas hydrate stability conditions, and processed the experimental data using this model. Finally, the author prepared the results in the form of tables and figures and wrote the manuscript which was then reviewed by Christophe Coquelet.)

v. Snaïde Ahamada, Alain Valtz, **Salaheddine Chabab**, Laura Blanco-Martin, Christophe Coquelet, "*Experimental density data of three carbon dioxide and oxygen binary mixtures at temperatures from 276 to 416 K and at pressures up to 20 MPa*", Journal of Chemical & Engineering Data, 65 (2020) 5313-5327.

(**Author's contribution:** The author validated the models and reviewed the manuscript.)

C.1.2. Other papers

vi. **Salaheddine Chabab**, Patrice Paricaud, Christophe Coquelet, "*Détermination des propriétés thermodynamiques des fluides - Fluides purs*", Techniques de l'ingénieur, Thermodynamique et énergétique, base documentaire : TIB216DUO (2020).

(**Author's contribution:** The author co-authored the manuscript.)

vii. **Salaheddine Chabab,** Patrice Paricaud, Christophe Coquelet, "*Détermination des propriétés thermodynamiques des fluides - Mélanges*", Techniques de l'ingénieur, Thermodynamique et énergétique, base documentaire : TIB216DUO (2020).
(**Author's contribution:** The author co-authored the manuscript.)

C.2. Oral communications

C.2.1. International Conference/Symposium

i. **Salaheddine Chabab**, Pezhman Ahmadi, Pascal Théveneau, Christophe Coquelet, Antonin Chapoy, Jérôme Corvisier, Patrice Paricaud, Rod Burgass, Céline Houriez, Elise El Ahmar, "*Solubility of Gases in Brine for Underground Gas Storage Application: Experimental Measurements and Modeling*", in: **AIChE Annual Meeting**, November 10-15, 2019.

ii. **Salaheddine Chabab**, Pascal Théveneau, Jérôme Corvisier, Christophe Coquelet, "*Thermodynamic and geochemical behavior of salt caverns*", in: **European Workshop on Underground Energy Storage**, November 7-8, 2019.

iii. **Salaheddine Chabab**, Alain Valtz, Antonin Chapoy, Christophe Coquelet, "*Thermodynamic study of the hydrate phase equilibria in the gas-water-(NaCl) systems using electrolyte CPA EoS*". **GdR2026 "Hydrates de gaz" - Gas Hydrate Days**, September 9-11, 2019.

C.2.2. Scientific seminar and project meetings

The author participated in several project meetings (ANR - FluidSTORY and Géodénergies - Rostock H) and internal and external scientific seminars where the different results obtained in this work were presented. The author also wrote the progress reports and deliverables for these projects.

C.3. Poster

Salaheddine Chabab, "*Effet des électrolytes sur les équilibres de phase et sur la zone de stabilité des hydrates de gaz*". PhD Students Workshop (ED ISMME), 11th - 12th June, 2019, Paris, France.

Appendix

Effet des électrolytes sur les équilibres de phase et sur la zone de stabilité des hydrates de gaz

Salaheddine CHABAB

* Mines ParisTech, PSL University, CTP - Centre Thermodynamique des Procédés, 35 rue St Honoré, 77305 Fontainebleau Cedex, France

Introduction

Les électrolytes aqueux sont très répandus dans l'industrie et sont présents dans de nombreuses applications. Nous les rencontrons lors du stockage géologique du gaz et de l'énergie, lors de l'inhibition de formation d'hydrate dans les canalisations pétrolières avec des solutions salines ou lors de la transformation de la biomasse par des techniques de fermentation.

Dans le cadre du stockage souterrain, le dimensionnement et l'optimisation des installations de stockage, ainsi que le suivi de la température, la pression et la quantité du gaz dans les réservoirs (cavités salines et aquifères profonds), nécessitent la connaissance des diagrammes de phase (conditions opératoires principalement avec CO_2). Pour ce faire il est primordial de développer un modèle thermodynamique suffisamment précis dans les conditions opératoires du stockage et du transport (risque de formation d'hydrate dans le cas du CH_4 et CO_2). Ce modèle doit pouvoir être transféré vers l'industrie.

Le développement des modèles thermodynamiques de tels systèmes (Gaz-H_2O-Sel) exige la disponibilité de données expérimentales fiables. Pour compléter les données existantes pour ces systèmes, un nouveau dispositif expérimental a été utilisé pour mesurer la solubilité des gaz dans la saumure. Ces données ont permis de développer une équation d'état original dont toutes les interactions moléculaires et électrolytes sont prises en compte.

Le modèle électrolyte e-PR-CPA [1]

$$\frac{A^{res}_{e-PR-CPA}}{RT} = \frac{A^{PR}}{RT} + \frac{A^{Association}}{RT} + \frac{A^{MSA}}{RT} + \frac{A^{Born}}{RT}$$

Interactions attractives et dispersives [2] — Interactions associatives [3] — Interactions longue portée [4] — Interactions courte portée (solvatation) [5]

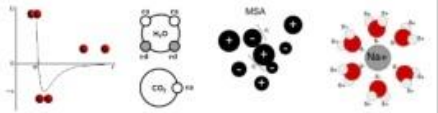

Paramétrage du modèle e-PR-CPA

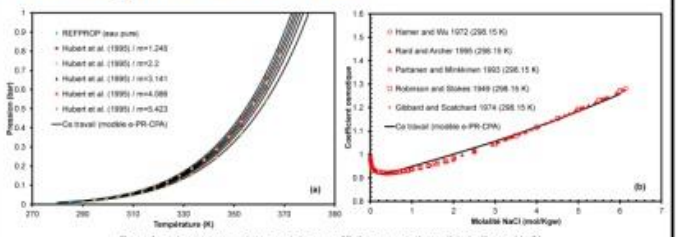

Pression de vapeur saturante (a) et coefficient osmotique (b) de l'eau+NaCl

Résultats expérimentaux et modélisation

Solubilité et teneur en eau

Validation du dispositif expérimental

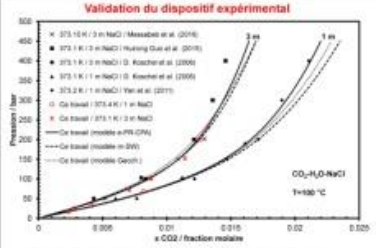

Solubilité du CO_2 dans l'eau+NaCl (effet « salting-out »)

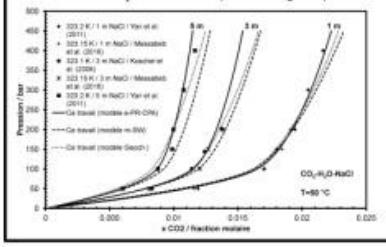

Solubilité du CH_4 dans l'eau+NaCl (effet « salting-out »)

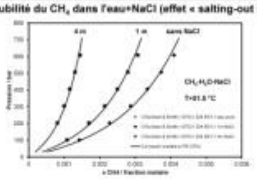

Teneur en eau du CH_4 et du CO2

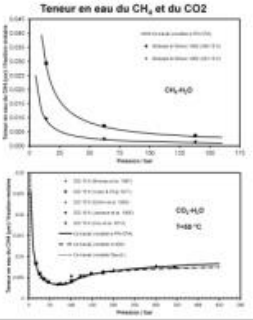

Hydrates de gaz

Effet de l'NaCl sur la zone de stabilité des hydrates de gaz

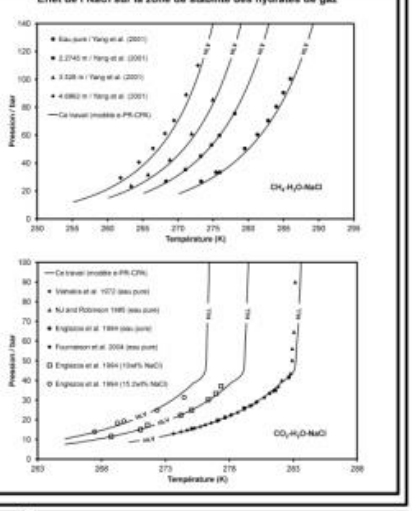

Conclusions et Perspectives

- ✓ Validation du dispositif expérimental en mesurant la solubilité du CO_2 dans l'eau + NaCl
- ✓ Développement d'un nouveau modèle électrolyte (e-PR-CPA) pour la prédiction des équilibres de phases des systèmes complexes (électrolytes, hydrates)
- ✓ Optimisation des paramètres du modèle Soreide et Whitson (m-SW).
- ❑ Mesure de la solubilité de l'O_2 et de l'H_2 dans l'eau + NaCl
- ❑ Traitement des données mesurées et modélisation des autres systèmes Gaz-H_2O-Sel par les modèles développés

Références

[1] Chabab et al., International Journal of Greenhouse Gas Control, in press 2019.

[2] Peng and Robinson, Industrial & Engineering Chemistry Fundamentals, 1976. 15(1), 59-64.

[3] Wertheim, Journal of statistical physics, 1984. 35(1-2), 19-34.

[4] Blum, Molecular Physics, 1975. 30(5): 1529-1535.

[5] Born, Zeitschrift für Physik, 1920. 1(1): 45-48.

Journées des doctorants de 2ème année (J2A) de l'ED ISMME

contact : salaheddine.chabab@mines-paristech.fr

11 et 12 juin 2019

Appendix D: Article 5: Experimental Density Data of Three Carbon Dioxide and Oxygen Binary Mixtures at Temperatures from 276 to 416 K and at Pressures up to 20 MPa

French summary / Article 5 : Données expérimentales de la densité de trois mélanges binaires de dioxyde de carbone et d'oxygène à des températures de 276 à 416 K et à des pressions allant jusqu'à 20 MPa

Dans le contexte des technologies "Power-to-Gas", y compris le Power-to-Gas-Oxycombustion, le stockage éventuel d'un mélange de CO_2 et d'O_2 nécessite des informations sur les données de densité et l'évaluation des équations d'état. Les densités de trois systèmes binaires de CO_2-O_2 ont été mesurées à l'aide d'un densitomètre à tube vibrant (VTD), et de la méthode d'étalonnage mécanique à trajet forcé (FPMC) dans les régions gazeuses, liquides et supercritiques entre 276 et 416 K et à des pressions allant jusqu'à 20 MPa (incertitudes maximales étendues U(p)= 0,0005 MPa, U(T)= 0,3 K et U(ρ)= 15 kg.m^{-3}). Les fractions molaires des mélanges de CO_2/O_2 préparés sont de 0,726/0,274, 0,517/0,483 et 0,872/0,128. L'équation d'état cubique de Peng-Robinson (PR EoS) et l'EoS-CG, basées sur le GERG-2008 (et mises en œuvre dans Refprop v10.0), ont été prises en compte pour l'analyse des données. Des comparaisons ont été faites avec les données de la littérature. Il apparaît que les données sont globalement mieux prédites par l'EoS-CG que par le PR EoS.

Experimental density data of three carbon dioxide and oxygen binary mixtures at temperatures from 276 to 416 K and at pressures up to 20 MPa

Snaide Ahamada[a], Alain Valtz[a], Salaheddine Chabab[a], Laura Blanco-Martín[b], Christophe Coquelet[a]

a MINES ParisTech PSL University, CTP-Centre of Thermodynamics of Processes, 35, Rue Saint Honoré, 77305 Fontainebleau, France

b MINES ParisTech PSL University, Department of Geosciences, 35, Rue Saint Honoré, 77305 Fontainebleau, France

** Corresponding Author: Christophe Coquelet (Christophe.coquelet@mines-paristech.fr)*

Tel: +33164694962 Fax: +33164694968

ABSTRACT

In the context of Power-to-Gas systems, including Power-to-Gas–Oxyfuel, possible storage of a mixture of CO_2 and O_2 requires density data information and evaluation of equations of state. Densities of three CO_2-O_2 binary system were measured using a vibrating tube densitometer (VTD), and the forced path mechanical calibration (FPMC) method in the gas, liquid and supercritical regions between 276 and 416 K and at pressures up to 20 MPa (maximum expanded uncertainties $U(p)$= 0.0005 MPa, $U(T)$= 0.3 K and $U(\rho)$= 15 kg.m^{-3}). The mole fractions of the prepared CO_2/O_2 mixtures are 0.726/0.274, 0.517/0.483 and 0.872/0.128. The Peng-Robinson cubic equation of state (PR EoS) and the EoS-CG, based on GERG-2008 (and implemented in Refprop v10.0), were considered for the analysis of the data. Comparisons were done with literature data. It appears that the data are overall better predicted by the EoS-CG than the PR EoS.

List of symbols

a	Parameter of the Peng-Robinson equation of state (attractive parameter) [Pa.m^6.mol^{-2}]
b	Parameter of the Peng-Robinson equation of state (co volume parameter) [m^3.mol^{-1}]
C_{ij}	NRTL model binary interaction parameter (Eq. 6) [J.mol^{-1}]
g	molar Gibbs free energy [J.mol^{-1}]
$Fobj$	Objective function
p	Pressure [MPa]
R	Gas constant [J.mol^{-1} K^{-1}]
T	Temperature [K]
Z	Compressibility factor
x	Liquid mole fraction
y	Vapor mole fraction
N	Number of components

Greek letters

α	Peng-Robinson equation of state alpha function

α_{ij}	NRTL model parameter (Eq. 6)
ω	Acentric factor
Δ	Deviation

Superscript

E	Excess property

Subscripts

C	Critical property
cal	Calculated property
exp	Experimental property
i,j	Molecular species
v	Vapor phase
l	liquid phase

1. Introduction

In the context of energy transition from fossil to low-carbon energy, the Power-to-Gas concept seems to be a very promising solution[1]. It consists of a transformation of CO_2 with H_2, produced by water electrolysis using renewable electricity, into methane, CH_4 (methanation: Sabatier reaction). Methane can be used as a fuel or can be transformed into electricity (oxyfuel combustion for example[2]). Due to the intermittent nature of renewable sources of energy like solar or wind, it is important to develop solutions for massive energy storage. Massive energy storage is necessary to succeed in the energy transition and a solution consists of storage in salt caverns. The design of salt caverns requires thermodynamic properties such as gas solubility in brine and also volumetric properties of the stored products. In Power-to-Gas–Oxyfuel, storage of CO_2, O_2 and CH_4 is required. In general, products are stored in single-phase conditions in salt caverns, but in the case of CO_2, phase changes are possible as its critical pressure and temperature are in the range of typical storage conditions. In order to overcome the problem, one solution would be to mix CO_2 and O_2 in the same salt cavern [3]. As O_2 is a cryogenic fluid, a mixture of CO_2 with O_2 will lead to a lower value of critical temperature. This way the mixture will stay in single-phase conditions.

It exists several sets of data in the open literature concerning the density of mixtures of CO_2 and O_2. Li et al.[4] have published in 2019 a very complete review concerning the available thermo-physical properties of CO_2 mixtures.in the context of CO_2 capture and storage (CCS). They have mentioned in their paper all the available references concerning the VLE and density properties of the CO_2+O_2 binary system. We can also cite the works of Lozano–Martín et al.[5], Commodore et al.[6] and Mantovani et al.[7]. In these investigations, the composition in O_2 is lower than 0.2.

In this work, the densities of three CO_2-O_2 mixtures were measured using Vibrating Tube Densitometer (VTD) in the gas, liquid and supercritical regions. A wide range of O_2 molar fractions was investigated. The measurements were carried out at eight isotherms between 276 and 416 K at pressures up to 20 MPa. The measured densities were also employed to evaluate the capability of a cubic Equation of State (EoS) to predict the density of the binary mixtures. The cubic EoS is composed of the Peng-Robinson (PR-EoS) associated with a g^E mixing rule. Additionally, a recent EoS based on GERG-2008, EOS-CG[8], was evaluated using

the measured density data and derived thermodynamic properties (compressibility factor). The experimental data obtained successfully compares to available density data in the literature.

2. Experimental part

2.1. Materials

CO_2 and O_2 were purchased from Air Liquide with a purity higher than 99.995 vol.% and 99.999 vol.% (Table 1). Table 2 presents the exact composition of the three mixtures. The mixtures were prepared in a gas reservoir considering the difference of total pressure. CO_2 was first introduced into the gas reservoir under vacuum. Pressure was recorded (*P1*). Afterwards, O_2 is introduced and pressure is recorded (*P2*). The temperature of the gas reservoir is selected in order to have a monophasic phase inside. Approximate composition is estimated using $x_{O2}=(P2-P1)/P2$.

For more accuracy, the compositions were determined by means of a Gas Chromatograph analysis (Varian, model CP 3800), using a thermal conductivity detector (TCD). WINILAB III software (Perichrom, France) is used for peaks integration and their analysis. The calibration of the GC detector is made by introducing known pure component volumes with appropriate syringes. The packed column used in the gas chromatograph is a PORAPAK R (80/100 mesh, 1.2 m X 1/8" Silcosteel) column. A calibration curve between moles number introduced and GC peak surface is determined and considered to estimate the accuracies. The resulting relative accuracies concerning the mole numbers are 1.1% for CO_2 and 1.2 % for O_2 for mixture 2 and 0.7% for CO_2 and 1.6 % for O_2 for mixtures 1 and 3. The uncertainty of molar fractions (x_1) is determined by Eq. (1):

$$u(x_1) = x_1(1-x_1)\sqrt{\left(\frac{u(n_1)}{n_1}\right)^2 + \left(\frac{u(n_2)}{n_2}\right)^2} \quad (1)$$

with $u(x_1)$ the uncertainty on mole fraction for component 1 and $\frac{u(n_i)}{n_i}$ the relative uncertainty on mole number calculated from GC calibration. It should be noticed that type B uncertainty should be considered to calculate relative uncertainties on mole numbers from calibration curves.

Table 1: Chemical samples used for experimental work.

Chemicals	CAS number	Supplier	Purity (mol %)	Analysis method[a]
Carbon dioxide	124-38-9	Air Liquide	99.995	GC
Oxygen	7782-44-7	Air Liquide	99.999	GC

[a] GC: Gas Chromatography

Table 2: Expected composition and real composition mole fractions.

Mixture number	Expected composition mole fractions		Real composition mole fractions		Standard uncertainties
	CO_2	O_2	CO_2	O_2	$u(x_1)$
1	0.7	0.3	0.726	0.274	0.003
2	0.5	0.5	0.517	0.483	0.004
3	0.9	0.1	0.872	0.128	0.002

2.2. Apparatus

The Vibrating Tube Densitometer (VTD), Anton Paar DMA 512P was used to measure the densities. This equipment is similar to that described in previous work by Rivollet et al.[9], Coquelet et al.[10] or Nazeri et al.[11]. Figure 1, from Rivollet et al., presents a schematic diagram of the apparatus.

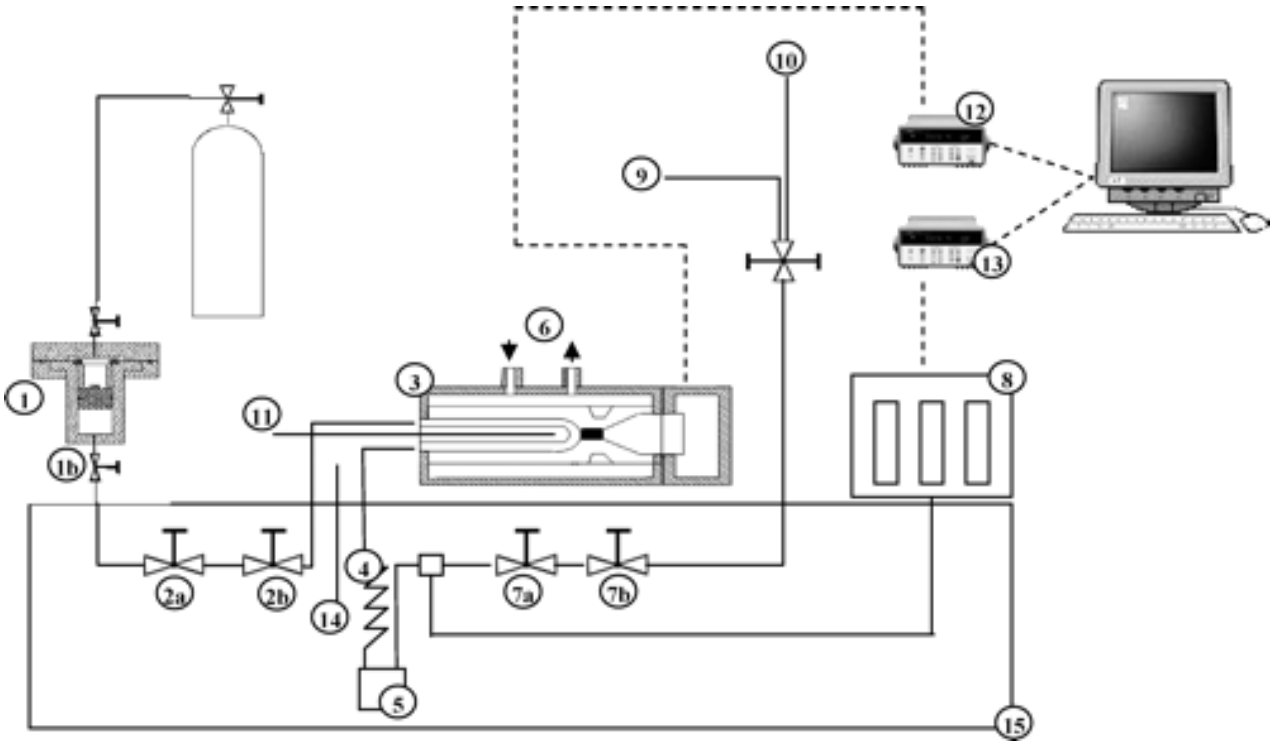

Figure 1: Flow diagram of the equipment, from Rivollet et al.[9]: 1, loading cell; 2a and 2b, regulating and shut-off valves; 3, DMA 512 P densitometer (Anton Paar); 4, heat exchanger; 5, bursting disk; 6, inlet and outlet of the temperature regulating fluid; 7a and 7b, regulating and shut-off valves; 8, pressure sensors maintained at constant temperature (373 K); 9, to vacuum pump; 10, vent; 11, vibrating cell temperature sensor; 12, HP 53131A unit; 13, HP 34970A unit; 14, bath temperature sensor; 15, liquid bath.

The main part of the setup is the U-shaped vibrating tube densitometer provided by Anton Paar. The specifications of the equipment are: pressure up to 140 MPa and temperature between 263 – 473 K. The tube material is made of Hastelloy. The temperature is controlled by fluid (silicon oil Kryo 20 from Lauda, Germany) that circulates in a jacket (small liquid bath) around the densitometer. The temperature stability is ±0.02 K.

The sample fluid is introduced from the gas reservoir into the densitometer through the tube with the diameter of 1.6 mm (1/16 inches) and valves 2. The whole connection tubes are fully immersed in the temperature controlled liquid bath model West P6100. Four-wire 100-Ω platinum resistance probes (Pt100) (PP) measure the temperature at each part of the equipment. The PP were calibrated against the 25-Ω reference thermometer (model: Tinsley Precision Instrument with an uncertainty $u(T)$=0.02 K). The standard uncertainty of the temperature probes was estimated to be $u(T)$ = 0.03 K after calibration. There are two thermostated pressure transducers (PT) of type Druck UNIK 5000 to measure different levels of pressure. PT1 can measure pressures up to 5 MPa, and PT2 can measure pressures up to 40 MPa. The transducers were calibrated using a dead weight tester (model: Desgranges & Huot 5202S) for pressures up to 30 MPa.

The pressure transducers can measure the pressure with the standard uncertainties of $u(p)$ = 0.0003 MPa and $u(p)$ = 0.0005 MPa in the ranges of 0-5 MPa and 5-20 MPa, respectively. The pressure and the temperature were recorded using Agilent HP34970A data acquisition unit and the vibration period, τ, also was recorded using a HP53131A data acquisition unit.

2.3. VTD Calibration and Experimental procedure

The calibration is performed using a reference fluid, CO_2. The forced path mechanical calibration (FPMC) model[12, 13] and the density data predicted by Span and Wagner EoS with measured values of temperature and pressure, implemented in REFPROP 10.0 software[10], were used to tune the unknown parameters in this model at full ranges of pressure for each measured isotherm. The measurement procedure is well described in previous publications (Coquelet et al.[10], Nazeri et al.[11]). Figure 2 shows calibration results with CO_2 at 276.6 and 395.19 K. The FPMC method links period of vibration, density, temperature and pressure.

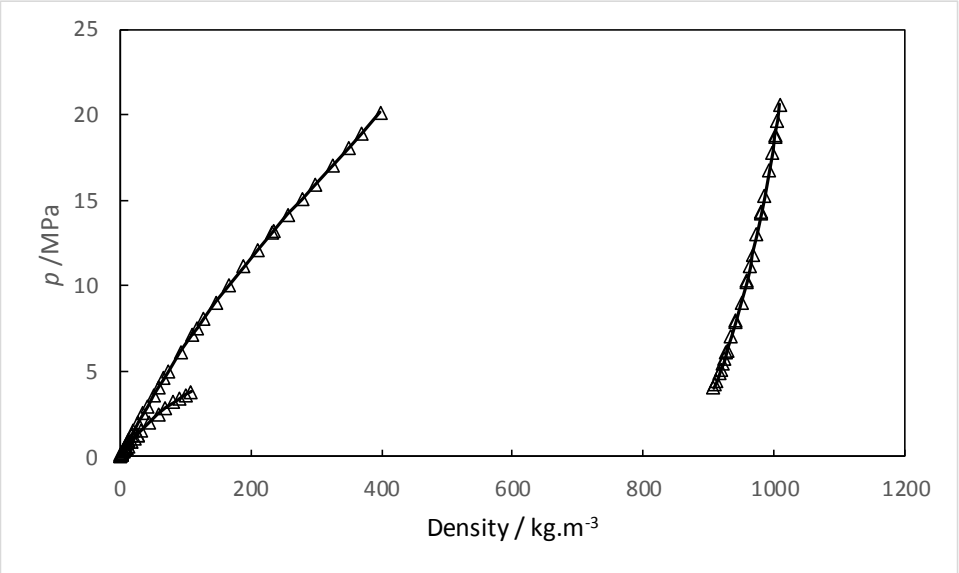

Figure 2: Calibration results with CO_2 at 276.60 and 395.19K. (Δ): density data calculated using Span and Wagner[15] model. Solid line: FPMC[12,13] model.

The experimental procedure is the following. Briefly, vacuum is made in the tube. The fluid mixture is introduced as its gas phase and densities of vapor phase are measured. More fluid mixture is added in order to increase the pressure until the dew pressure. For the liquid density, fluid mixture is added until the maximum pressure (20 MPa). Density measurements are obtained by removing mixture from the VTD (decreasing pressure) until the bubble pressure. In case there is no dew or bubble pressures, starting from vacuum, the fluid mixture is added until the maximum pressure.

It is important to remind that before the appearance of dew point, the temperature of liquid bath is fixed at a value slightly higher than that of the jacket (around the vibrating tube) (difference about 0.2-0.3 °C). It is to be sure that the first drop of fluid mixture appears exactly in the densitometer. In the same manner, before the appearance of bubble point, the temperature of liquid bath is fixed at a value slightly lower than that of the jacket. It is to be sure that the first bubble of fluid mixture appears exactly in the densitometer.

The uncertainties of densities are calculated using Eq. (2) taking into account the calibration with the reference fluid (type B) and repeatability of the measurements (acquisition of the period of vibration). Measurements are made at constant temperature and constant pressure.

$$u(\rho) = \sqrt{\left(\left(\frac{\partial \rho}{\partial p}\right)_{T,x} u(p)\right)^2 + \left(\left(\frac{\partial \rho}{\partial T}\right)_{p,x} u(T)\right)^2 + \left(\sum_i \left(\frac{\partial \rho}{\partial x_i}\right)_{T,p,x_j \neq x_i} u(x_i)\right)^2 + \left(\frac{\alpha}{\sqrt{3}}\right)^2 + u_{rep}^2} \quad (2)$$

where α represents the maximum of $|\rho_{cal} - \rho_{exp}|$, the difference between the experimental reference fluid (CO_2) density and that calculated by the calibration curve (FPMC method) at the conditions of *T* and *p* and using the reference equation of state from Span and Wagner[15]. u_{rep} is the repeatability of density measurements. Temperature and pressure contributions to density uncertainty are calculated using density derivatives with respect to temperature and pressure of calibration fluid (CO_2) with the Span and Wagner[15] equation of state.

2.4. Experimental Results

The experimental data are presented in Tables 3 to 5.

Table 3: Experimental isothermal density data for CO_2 +O_2 binary system (Mixture 1: 0.726/0.274) and expanded uncertainties (k=2): $U(p)$=0.0003 MPa if P<5 MPa and $U(p)$=0.0005 MPa if P>5 MPa. Italic grey –shaded values correspond to possible metastable states.

T=276.59 K		T= 293.18 K		T=313.18 K		T=334.78 K		T= 353.78 K		T=373.46 K		T=395.18 K		T= 416.38 K	
$U(T)$= 0.06K		$U(T)$= 0.06K		$U(T)$= 0.03K		$U(T)$= 0.04K		$U(T)$= 0.04K		$U(T)$= 0.01K		$U(T)$= 0.02K		$U(T)$= 0.03K	
$U_{min}(\rho)$= 0.2 kg.m^{-3} $U_{max}(\rho)$= 8 kg.m^{-3}		$U_{min}(\rho)$= 0.5 kg.m^{-3} $U_{max}(\rho)$= 15 kg.m^{-3}		$U_{min}(\rho)$= 0.4 kg.m^{-3} $U_{max}(\rho)$= 13 kg.m^{-3}		$U_{min}(\rho)$= 0.1 kg.m^{-3} $U_{max}(\rho)$= 3 kg.m^{-3}		$U_{min}(\rho)$= 0.1 kg.m^{-3} $U_{max}(\rho)$= 3 kg.m^{-3}		$U_{min}(\rho)$= 0.1 kg.m^{-3} $U_{max}(\rho)$= 2 kg.m^{-3}		$U_{min}(\rho)$= 0.2 kg.m^{-3} $U_{max}(\rho)$= 5 kg.m^{-3}		$U_{min}(\rho)$= 0.1kg.m^{-3} $U_{max}(\rho)$= 2.5 kg.m^{-3}	
p/MPa	ρ/kg.m^{-3}	p/MPa	ρ/kg.m^{-3}	p/MPa	ρ/kg.m^{-3}	p/MPa	ρ/kg.m^{-3}	p/MPa	ρ/kg.m^{-3}	p/MPa	ρ/kg.m^{-3}	p/MPa	ρ/kg.m^{-3}	p/MPa	ρ/kg.m^{-3}
Vapor phase		1.0261	17.9	1.0370	16.6	1.0254	15.4	1.0148	14.2	1.0219	13.6	1.0606	8.4	1.0645	12.6
0.9987	18.6	1.2667	22.4	1.2480	20.1	1.3693	20.6	1.2659	17.9	1.0250	13.6	1.5114	13.0	1.2566	15.0
1.2970	24.4	1.5059	26.8	1.5210	24.7	1.5113	22.8	1.5263	21.6	1.3410	17.9	2.0356	18.7	1.5084	18.0
1.5079	29.0	2.0296	36.9	2.0296	33.4	2.0228	31.0	1.9712	28.1	1.3688	18.3	2.4969	25.5	2.0063	24.0
2.0233	40.3	2.4379	45.1	2.5489	42.7	2.5291	39.1	2.4979	36.1	1.6226	21.7	3.0690	39.3	2.4614	29.6
2.5375	51.2	3.0468	57.9	3.0567	52.0	3.1154	48.9	3.0511	44.3	1.9322	26.0	3.5236	45.3	2.9955	36.2
3.0077	61.6	3.5789	69.7	3.4973	60.5	3.4998	55.4	3.6661	54.1	2.5360	34.5	4.0275	52.2	3.5505	43.1
3.0136	61.7	4.2899	86.5	4.0055	70.5	4.0317	64.9	4.0456	60.1	3.1352	43.0	4.5200	58.8	4.0714	49.7
3.5122	74.9	4.6668	96.0	4.4811	80.2	4.6096	75.3	4.4690	67.1	3.5451	48.9	5.1207	67.2	4.0949	50.0

3.5278	75.4	5.0075	104.9	5.1405	94.3	5.0500	83.4	5.0535	76.8	3.5736	49.4	5.5301	72.8	4.4386	54.3
4.0151	87.7	5.6455	122.5	5.5938	103.8	5.5832	93.6	5.6069	86.1	4.1283	57.4	5.5619	73.3	5.0657	62.4
4.5495	103.9	6.1151	136.8	6.1023	115.6	6.0711	103.0	6.1721	95.8	4.5213	63.2	6.255	81.3	5.6212	69.7
4.5577	104.1	6.6290	153.2	6.5735	127.0	6.5882	113.5	6.6370	103.8	4.9626	70.1	6.5614	87.5	6.1438	76.3
5.0174	118.2	7.1301	170.3	7.0527	139.1	7.0710	123.3	7.1640	113.4	5.6150	79.9	7.0629	94.8	6.5506	81.6
5.6142	140.2	7.6969	191.3	7.6326	154.4	7.5738	133.8	7.6479	122.3	6.1171	87.8	7.5466	101.8	7.1854	90.0
5.6170	140.3	8.0761	206.6	8.1030	167.4	8.0426	143.8	8.2358	133.6	6.5974	95.4	8.0372	109.0	7.6051	95.6
6.0855	159.3	8.5532	227.7	8.5405	180.1	8.5347	154.2	8.5141	139.0	6.9887	101.7	8.6102	117.8	8.1481	103.0
6.5617	*180.2*	9.0386	251.3	9.0941	196.8	9.1248	168.4	9.1170	150.6	7.5485	110.7	9.0850	124.5	8.6379	109.6
7.0648	*212.1*	9.5283	275.9	9.5589	211.0	9.5279	178.0	9.8112	164.2	8.0059	118.3	9.5294	131.3	9.1100	115.9
7.5345	*237.6*	10.0108	301.3	10.0306	225.6	10.1171	192.3	10.4826	177.8	8.5713	127.7	10.0365	139.0	9.4628	120.7
7.5454	*239.8*	10.4985	329.8	10.4962	240.7	10.5476	203.9	11.1379	191.1	8.5873	128.0	10.5693	147.2	10.1724	130.6
8.762	*276.9*	11.0112	359.2	10.4996	240.9	10.5513	204.0	11.5980	200.6	9.0714	136.2	10.5939	147.6	10.9012	140.6
10.7845	*552.3*	11.4862	387.6	10.9917	257.9	11.0054	214.9	12.1985	213.3	9.0863	136.4	10.9452	153.0	12.0581	156.7
11.0870	*574.2*	11.9968	416.8	10.9961	258.2	11.5894	229.4	12.5279	220.3	9.5341	144.1	11.7240	165.1	13.1753	172.4
11.6098	*586.4*	12.5082	444.7	11.4993	276.8	12.0057	239.9	12.9138	228.9	11.0376	170.5	12.7256	181.0	14.0531	184.8
Liquid phase		13.0310	471.3	11.9899	295.7	12.5677	254.2	13.5977	244.4	12.2323	192.0	13.6496	195.6	14.9349	197.3
12.5564	632.5	13.0168	472.3	12.4999	315.7	12.9861	265.2	14.0973	254.8	12.2374	192.1	14.1742	204.0	16.6896	221.9
13.5475	667.3	13.3725	489.3	12.9650	334.1	13.5110	279.1	14.1058	254.8	13.0519	207.0	14.2085	204.5	17.9826	240.2
14.5748	694.3	14.6538	538.5	13.5010	354.7	14.0864	296.3	14.8020	270.2	14.0469	225.4	15.3271	222.5	18.9390	253.8
15.6302	719.2	14.6416	542.8	14.0319	374.8	14.0934	296.7	15.9300	294.4	14.9435	242.0	16.1060	235.3	20.2738	272.8
16.7981	741.7	14.9744	557.7	14.3690	387.6	14.5085	306.8	16.9908	318.8	15.3993	261.7	16.2034	236.9		
17.7179	755.6	16.0189	589.4	14.9869	408.8	14.9433	321.5	16.9956	318.9	17.0421	281.6	17.2424	253.8		
18.4966	767.6	17.0775	618.3	15.3925	425.7	15.5007	334.6	17.4785	331.1	17.9468	298.4	18.1893	269.1		
20.2495	789.5	17.0630	619.1	15.6194	432.4	15.9823	348.6	18.3694	348.7	18.9235	316.3	19.2014	285.3		
		18.0731	643.4	15.9551	443.5	16.4904	362.1	19.3581	369.9	20.1421	338.8	19.2265	285.7		
		18.9935	662.1	16.4724	459.7	17.0442	376.6	20.4754	394.1	20.1378	338.8	20.2283	301.6		
		20.2968	688.1	16.9899	476.0	17.4992	388.6								
				17.5065	491.2	18.0409	402.6								
				17.5148	491.1	18.5295	414.8								
				17.9399	503.6	18.9942	426.1								

18.4855	517.8	19.5023	438.6
19.0051	531.2	19.9399	449.1
19.4521	543.1	20.3140	457.3
19.4581	543.0		
20.2928	562.5		

Table 4: Experimental isothermal density data for CO_2 +O_2 binary system (mixture 2:0.517/0.483) and expanded uncertainties (k=2):.$U(p)$=0.0003 MPa if P<5 MPa and $U(p)$=0.0005 MPa if P>5 MPa

T=280.63 K		T= 293.92 K		T=313.63 K		T=333.21 K		T= 353.46 K		T=373.60 K		T=395.72 K		T= 412.85 K	
$U(T)$= 0.3K		$U(T)$= 0.2K		$U(T)$= 0.07K		$U(T)$= 0.09K		$U(T)$= 0.06K		$U(T)$= 0.1K		$U(T)$= 0.05K		$U(T)$= 0.1K	
$U_{min}(\rho)$= 0.3 kg.m^{-3}		$U_{min}(\rho)$= 0.1 kg.m^{-3}		$U_{min}(\rho)$= 0.1 kg.m^{-3}		$U_{min}(\rho)$= 0.1 kg.m^{-3}		$U_{min}(\rho)$= 0.1 kg.m^{-3}		$U_{min}(\rho)$= 0.1 kg.m^{-3}		$U_{min}(\rho)$= 0.5 kg.m^{-3}		$U_{min}(\rho)$= 0.2kg.m^{-3}	
$U_{max}(\rho)$= 9 kg.m^{-3}		$U_{max}(\rho)$= 3 kg.m^{-3}		$U_{max}(\rho)$= 2.7 kg.m^{-3}		$U_{max}(\rho)$= 2.5 kg.m^{-3}		$U_{max}(\rho)$= 2 kg.m^{-3}		$U_{max}(\rho)$= 2 kg.m^{-3}		$U_{max}(\rho)$= 7 kg.m^{-3}		$U_{max}(\rho)$= 4 kg.m^{-3}	
p/MPa	ρ/kg.m^{-3}	p/MPa	ρ/kg.m^{-3}	p/MPa	ρ/kg.m^{-3}	p/MPa	ρ/kg.m^{-3}	p/MPa	ρ/kg.m^{-3}	p/MPa	ρ/kg.m^{-3}	p/MPa	ρ/kg.m^{-3}	p/MPa	ρ/kg.m^{-3}
1.0219	17.2	1.0246	16.3	1.0472	15.3	1.0155	14.3	1.0444	13.6	1.0241	12.6	1.0653	12.8	1.0441	11.7
1.3394	22.9	1.2331	19.7	1.2643	18.7	1.2265	17.3	1.2764	16.8	1.2614	15.6	1.2743	15.3	1.2864	14.5
1.6537	28.7	1.5047	24.3	1.5056	22.4	1.5333	21.6	1.5315	20.2	1.5458	19.2	1.5488	18.6	1.5657	17.4
2.0153	35.2	2.0222	33.0	2.0467	30.8	2.0282	28.9	2.0277	26.9	2.0885	26.0	2.0313	24.5	2.0840	23.4
2.5069	44.6	2.5310	41.9	2.6601	40.5	2.5609	36.6	2.5469	34.0	2.5646	32.0	2.5585	31.0	2.5089	28.1
3.0256	54.6	3.0318	50.9	2.6690	40.6	3.0575	43.9	3.0411	40.8	3.5445	44.8	3.0501	37.0	3.0522	34.3
3.5492	64.9	3.5266	60.0	3.0530	46.8	3.5308	51.1	3.5362	47.7	4.0720	51.8	3.5160	42.8	3.5102	39.7
4.0264	75.1	4.1454	71.7	3.5421	54.9	4.0576	59.4	4.0019	54.3	4.5326	57.8	4.0235	49.1	3.5129	39.7
4.5352	86.3	4.7065	82.7	4.0055	62.7	4.5343	67.0	4.5310	61.9	5.0571	64.8	4.5348	55.6	4.0658	46.1
5.0437	97.6	5.2948	94.6	4.5119	71.3	5.0226	75.5	5.0639	69.6	5.6110	72.2	5.0142	61.5	4.5342	51.5
5.5936	110.5	6.1200	112.1	5.0869	81.4	5.6148	85.6	5.6206	77.7	6.5922	85.5	5.6212	69.4	5.0091	57.1
6.0780	122.1	6.8166	127.4	5.5060	88.9	6.1091	93.1	6.0908	84.7	7.0975	92.4	6.1170	75.7	5.5898	63.9
6.5663	134.3	7.2607	137.5	6.1028	99.8	6.5675	100.4	6.6584	93.2	7.5801	99.0	6.5478	81.2	6.1112	70.1
6.9954	145.9	8.0523	156.1	6.1485	100.6	7.1151	109.5	7.1090	100.1	8.0887	106.1	7.1777	89.4	6.1177	70.2
7.5527	161.2	8.5833	169.2	6.1635	100.9	7.5868	117.5	7.6165	107.9	8.5637	112.8	7.5727	94.5	6.5145	74.8
8.0253	174.1	9.4241	190.6	6.5114	107.3	8.0747	126.1	8.1279	115.6	9.0477	119.6	8.0988	101.3	6.5351	75.1

8.6304	192.0	10.1205	208.9	7.1026	118.6	8.5662	134.7	8.5896	122.8	9.5688	126.9	8.5463	107.2	7.0876	81.6
8.6246	192.2	11.5615	248.2	7.1133	118.8	9.0788	143.9	9.1311	131.4	10.0544	133.9	9.0976	114.3	7.5998	87.8
9.0663	205.8	11.5565	248.4	7.6008	128.2	9.5489	152.3	10.0255	145.6	11.0624	148.2	9.5775	120.7	8.0564	93.3
9.6689	224.2	12.0924	263.5	8.1760	139.8	10.0527	161.3	11.0868	162.4	12.0623	162.5	10.1030	127.6	8.5614	99.3
10.0351	235.6	12.0880	263.5	8.2646	141.6	10.5497	170.4	12.0187	177.5	13.0453	176.6	11.0325	140.0	8.5748	99.4
11.0633	269.8	13.2030	295.6	9.5421	167.7	11.0536	179.6	13.0730	194.8	13.9880	190.2	12.1180	154.3	9.0691	105.4
11.0517	270.4	13.1990	295.9	10.0591	178.4	11.5643	189.0	13.0725	194.8	14.8730	202.6	13.0650	167.0	9.5479	111.2
11.9929	303.1	14.0458	319.4	11.0860	200.7	12.0412	198.5	14.0107	210.2	16.0800	220.5	14.0217	179.8	10.0528	117.3
13.0339	340.0	14.0378	319.5	12.1605	224.4	12.5159	207.7	15.0277	226.9	16.0822	220.6	15.1979	195.4	10.8987	127.6
14.0656	376.6	15.0380	348.4	13.0074	243.4	13.0458	217.8	15.9847	243.0	17.0522	235.1	16.2579	209.6	12.1664	142.7
15.0294	410.6	15.0341	348.7	14.316	271.7	13.5555	227.5	17.0015	259.8	17.0555	235.1	17.0434	220.2	13.0663	153.5
16.2689	449.0	16.6414	392.3	14.9472	288.2	13.9996	236.0	18.0245	276.5	17.8714	247.1	18.1289	234.7	14.1484	166.9
16.2619	449.5	16.6354	392.7	15.9882	311.6	14.5189	245.6	18.9421	291.1	19.0095	263.6	19.3526	250.7	16.4731	195.5
16.9518	468.7	17.9488	426.4	16.1772	315.8	15.0036	254.7	20.3158	312.6	19.0090	263.6	20.2032	261.7	17.0456	202.3
16.9476	468.9	17.9420	426.8	17.4641	344.8	15.9818	273.4			20.0154	277.9			18.4366	218.7
18.5980	510.7	19.1108	456.3	18.8837	375.4	16.9748	292.6							20.0959	238.3
18.5864	511.2	20.1976	480.4	20.1692	401.9	18.0141	312.7								
20.3276	553.1			20.1674	401.9	19.0085	331.1								
						19.9326	348.1								
						20.2304	353.8								

Table 5: **Experimental isothermal density data for CO_2 +O_2 binary system (mixture 3: 0.872/0.128) and expanded uncertainties (k=2): $U(p)$=0.0003 MPa if P<5 MPa and $U(p)$=0.0005 MPa if P>5 MPa. Italic grey –shaded values correspond to possible metastable states.**

T=279.05 K		T= 293.31 K		T=315.06 K		T=333.25 K		T= 353.62 K		T=374.23 K		T=394.15 K		T= 414.31 K	
$U(T)$= 0.1 K		$U(T)$= 0.09K		$U(T)$= 0.07K		$U(T)$= 0.04K		$U(T)$= 0.03K		$U(T)$= 0.07K		$U(T)$= 0.03K		$U(T)$= 0.02K	
Umin(ρ)= 0.3 kg.m^{-3} *Umax(ρ)= 13 kg.m^{-3}*		*Umin (ρ)= 0.2 kg.m^{-3}* *Umax(ρ)= 9 kg.m-$^{-3}$*		*Umin (ρ)= 0.1 kg.m^{-3}* *Umax (ρ)= 4 kg.m^{-3}*		*Umin (ρ)= 0.1 kg.m^{-3}* *Umax (ρ)= 4 kg.m^{-3}*		*Umin (ρ)= 0.1 kg.m^{-3}* *Umax (ρ)= 3 kg.m^{-3}*		*Umin (ρ)= 0.4 kg.m^{-3}* *Umax (ρ)= 4 kg.m^{-3}*		*Umin (ρ)= 0.1 kg.m^{-3}* *Umax (ρ)= 2.5 kg.m^{-3}*		*Umin (ρ)= 0.1kg.m^{-3}* *Umax (ρ)= 2.5 kg.m^{-3}*	
p/MPa	ρ/kg.m^{-3}	p/MPa	ρ/kg.m^{-3}	p/MPa	ρ/kg.m^{-3}	p/MPa	ρ/kg.m^{-3}	p/MPa	ρ/kg.m^{-3}	p/MPa	ρ/kg.m^{-3}	p/MPa	ρ/kg.m^{-3}	p/MPa	ρ/kg.m^{-3}
Vapor phase		**Vapor phase**		1.0407	17.5	1.0219	16.2	1.0073	14.9	1.0273	14.5	1.0665	14.1	1.0140	12.7
1.0416	20.4	1.0043	18.6	1.2437	21.0	1.2800	20.4	1.5203	22.9	1.5180	21.6	1.2007	15.8	1.5137	19.1
1.2633	25.1	1.2769	24.0	1.5758	27.0	1.5362	24.7	2.0373	31.1	2.0810	29.9	1.4843	19.7	2.0358	25.9
1.5048	30.5	1.5412	29.3	1.9996	34.9	2.0297	33.1	2.5328	39.1	2.5194	36.5	2.0318	27.1	2.5355	32.4
2.0163	42.2	2.0404	40.0	2.5358	45.3	2.5422	42.2	3.1299	49.2	2.9868	43.8	2.4654	33.2	3.0494	39.3
2.5130	53.7	2.5863	52.2	3.0392	55.4	3.0561	51.7	3.5407	56.2	3.5699	53.1	3.0207	41.0	3.5748	46.3
3.0151	68.2	3.0629	63.6	3.5599	66.4	3.5237	60.6	4.0393	65.0	4.0447	61.9	3.5575	48.8	4.0597	52.9
3.2625	76.1	3.5193	75.2	4.0532	77.6	4.0380	70.8	4.5088	73.5	4.5060	71.0	3.9505	54.6	4.0584	52.9
3.5074	84.8	4.0205	89.6	4.5274	88.9	4.6668	83.8	5.0562	83.8	5.0295	78.5	4.5499	63.5	4.5645	60.0
3.7587	92.8	4.5284	104.9	5.1645	105.1	5.0349	91.7	5.7330	97.0	5.5493	86.4	5.0643	71.3	5.0419	66.6
4.1541	106.1	5.0349	122.0	5.5868	116.7	5.5930	104.3	6.0705	103.1	6.1195	96.4	6.0782	87.1	5.6518	75.3
4.2843	110.7	5.6098	144.6	6.1369	132.4	6.1099	116.4	6.6522	115.1	6.1232	96.4	6.5320	94.3	6.0878	81.6
4.4095	115.6	6.0892	166.3	6.6193	147.5	6.6518	129.8	7.0612	124.4	6.6065	105.2	7.0752	103.1	6.7675	91.3

4.5645	122.5	6.6721	198.5	7.0621	162.4	6.6534	129.8	7.5756	136.4	7.0261	112.9	7.5136	110.4	8.1022	111.2
4.6561	127.0	6.9584	217.6	7.5584	180.4	7.0752	140.7	7.9620	145.4	7.5889	123.3	8.0078	118.6	8.4669	116.9
4.7489	131.5	7.2267	240.7	8.0728	200.8	7.0789	140.8	8.5421	157.1	8.0379	131.8	8.0843	119.9	9.2081	128.4
4.9287	143.3	7.3480	253.3	8.0775	200.9	7.5828	154.5	9.0142	166.6	8.5729	142.1	8.4884	126.8	10.2145	143.4
5.0117	*148.8*	*7.4496*	*267.7*	8.5480	221.5	8.0965	168.9	9.5589	179.7	9.0370	151.4	8.5278	127.4	11.2972	161.0
5.1070	*157.2*	*7.5519*	*288.0*	9.0717	247.1	8.5662	183.1	10.0558	192.0	10.0876	173.0	8.9956	135.5	11.9586	171.9
5.2149	*167.2*	*7.6842*	*316.2*	9.5412	272.3	8.5678	183.2	10.7222	210.8	10.4917	181.5	9.0607	136.6	12.9289	189.1
5.3002	*172.7*	*7.8201*	*322.8*	9.9982	298.6	9.0560	198.4	11.4360	232.6	11.0366	193.1	9.4928	144.2	13.8057	203.8
5.3906	*177.8*	*7.9261*	*335.4*	10.2212	315.2	9.2307	203.9	12.0510	252.9	11.9161	212.7	9.5248	145.1	14.7433	219.5
5.4920	*186.0*	*8.0564*	*347.0*	10.6028	335.6	9.5275	214.1	12.7049	273.9	12.9049	235.1	10.0376	154.1	16.1194	242.5
5.5824	*200.7*	*8.2371*	*389.9*	10.6898	347.8	9.5288	214.2	13.5401	294.5	14.0828	262.8	10.5522	163.4	17.5173	266.3
5.7402	*223.4*	*8.3445*	*407.1*	11.1620	372.0	9.7922	223.3	13.9400	304.6	14.9868	284.5	11.0513	172.6	18.9761	290.9
5.8086	*225.2*	*8.4536*	*419.9*	11.7107	412.0	9.7998	223.5	13.9358	304.8	16.0138	309.0	11.6063	182.9	20.0204	308.6
5.9850	*591.8*	*8.5411*	*438.2*	12.0508	435.8	10.0180	231.2	14.9049	330.9	16.9216	330.6	12.1181	192.6		
6.1056	*613.0*	*8.6407*	*465.0*	12.4275	465.9	10.2597	239.7	16.1022	367.7	16.9188	330.8	12.5181	200.2		
6.5946	*698.3*	*8.7582*	*506.2*	12.8458	491.0	10.5548	250.6	16.9052	393.3	18.0110	356.3	12.9645	208.8		
7.1041	*712.4*	*8.9342*	*527.1*	13.5490	532.0	11.0228	268.2	18.2172	432.5	18.8901	376.3	14.1039	231.0		
7.9046	*760.2*	*9.5655*	*9.1884*	553.1	558.4	11.4899	287.1	18.1943	433.4	18.8743	376.5	15.0024	248.1		
7.9152	*760.7*	*9.5655*	*590.2*	15.1136	593.3	12.0560	309.8	18.9987	458.0	20.0624	403.0	15.0023	248.1		
Liquid phase		**Liquid phase**		16.0609	625.0	12.3828	326.2	20.1842	490.7			15.9709	267.1		
8.9179	785.7	10.0875	634.7	17.0546	651.5	12.9982	349.8					17.1688	290.7		
8.9302	786.0	11.0317	680.8	18.1689	677.6	13.4962	375.2					18.6716	320.1		
9.5588	798.3	12.0270	716.9	19.2425	697.4	13.9740	391.5					20.2201	350.2		
9.9407	807.3	12.8227	737.6	20.4052	716.7	14.4890	418.9					20.2215	350.4		
10.9404	823.2	13.8256	758.5			15.2235	444.0								
12.1374	838.5	15.0309	779.0			15.6111	459.6								
12.6650	843.9	15.0396	779.0			16.1478	480.1								
13.0291	850.0	16.0513	794.6			16.8926	505.5								
14.5011	864.8	16.7640	803.4			17.9419	539.0								
15.4452	873.2	18.0263	818.7			18.9661	569.3								
16.8885	885.7	18.4149	822.9			20.2278	600.3								

17.9250	894.2	19.4981	833.5
17.9341	894.4	20.1334	838.0
19.0671	902.2	20.1539	837.1
19.8930	906.4		
20.3845	910.7		

3. Correlation and discussions

3.1. Development of PR EoS

We have used a cubic equation of state to compare its density predictions with the experimental data. Cubic equations of state are often used for the design of underground gas reservoirs as they are very easy to solve. The critical temperatures (T_c) and pressures (P_c) and acentric factors (ω) for pure CO_2 and O_2, which are collected from Simulis thermodynamic software (from Prosim, Toulouse, France), are provided in Table 6.

Table 6. Critical properties and acentric factors for Carbone dioxide and Oxygen pure components (Source Simulis thermodynamic software)

Component	T_c/K	P_c/bar	Acentric factor ω
CO_2	304.21	73.83	0.223621
O_2	154.58	50.43	0.0221798

In order to have the best representation of the phase diagrams, we have considered the Peng-Robinson Equation of State[16] (Eq. 3) with the Wong Sandler Mixing rules[17] (Eqs. 4 and 5) involving the NRTL activity coefficient model[18] (Eq. 6). Indeed, as O_2 is a cryogenic component, the phase diagram has the particularity to have a mixture critical point. Cubic EoS have some difficulties to represent accurately the equilibrium properties close to the mixture critical point.

$$\left(P+\frac{a\alpha(T)}{v^2+2vb-b^2}\right)(v-b)=RT \tag{3}$$

$$b=\frac{\sum_i\sum_j\left(b-\frac{a}{RT}\right)_{ij}}{1-\left(\frac{\sum_i x_i\frac{a_i}{b_i}}{RT}+\frac{g_\gamma^E}{CRT}\right)} \tag{4}$$

with C=ln(1/2)

$$b-\frac{a}{RT}=\sum_i\sum_j x_i x_j\left(b-\frac{a}{RT}\right)_{ij} \quad \text{with} \quad \left(b-\frac{a}{RT}\right)_{ij}=\frac{1}{2}\left[\left(b-\frac{a}{RT}\right)_i+\left(b-\frac{a}{RT}\right)_j\right]\left(1-k_{ij}\right) \quad (5)$$

$$g_\gamma^E=\sum_i x_i\sum_j\frac{x_j exp\left(-\alpha_{ij}\frac{C_{ji}}{RT}\right)}{\sum_k exp\left(-\alpha_{ik}\frac{C_{ki}}{RT}\right)}C_{ji} \quad (6)$$

with C_{ii}=0. The value of the non-randomness parameters, α_{ij}, is equal to 0.1. Note that α_{ij} is different from $\alpha(T)$ which is the alpha function of the PR EoS.

In order to adjust the binary interaction parameters (C_{ij} and k_{ij}), we have considered a database of six references presented in Table 7. As all the systems present a mixture critical point, we have just considered an objective function of the bubble pressure (Eq. 7).

$$Fobj=\sum_i^{Ndata}\left(\frac{p_{exp}-p_{cal}}{p_{exp}}\right)^2 \quad (7)$$

All the data were used to fit the binary interaction parameters. We did not consider any temperature dependency of each binary interaction parameter. The obtained values are $C_{12}=479$ J.mol^{-1}, $C_{21}=-216$ J.mol^{-1} and $k_{12}=0.2078$. The performance of the model was assessed by means of the following relative deviations, *AAD U* and *BIAS U*, which are expressed as:

$$AAD\ U=\frac{1}{N}\sum_{i=1}^{N}\frac{|U_{i,exp}-U_{i,cal}|}{U_{i,exp}} \quad (8)$$

$$BIAS\ U=\frac{1}{N}\sum_{i=1}^{N}\frac{(U_{i,exp}-U_{i,cal})}{U_{i,exp}} \quad (9)$$

where U is the pressure (p) or the vapor composition (y_1) and N is the number of experimental measurements. Results are presented in Table 8 and Figure 3. As can be seen, when the temperature approaches the critical temperature of CO_2, the model has some difficulties to represent the equilibrium properties. In order to improve the prediction of the phase diagram, we can consider temperature dependent binary interaction parameters, but it is not judicious for density prediction at temperatures higher than the critical temperature of CO_2.

Table 7 : Summary of vapor liquid equilibrium data of the binary system CO_2 + O_2.

Reference	Type of Data	Temperatures
Fredenslund and Sather 1970[19]	*pTxy*	263.15, 273.15 and 283.15
Kaminishi and Toriumi 1966[20]	*pTxy*	253.15, 273.15, 288.15 and 298.15
Muirbrook and Prausnitz 1965[21]	*pTxy*	273.15
Zenner and Dana 1963[22]	*pTxy*	273.15
Lasala et al. 2016[23]	*pTxy*	273.15, 288.15 and 298.15
Westman et al. 2016[24]	*pTxy*	273.09 and 293.08

Table 8: Values of *BIAS*, and *AAD* of pressure and vapor compositions for the different sets of data.

Reference	*T*/K	*BIAS p*/%	*BIAS y*/%	*AAD p*/%	*AAD y*/%
Fredenslund and Sather 1970[19]	263.15	6.1	-1.6	6.1	2.5
	273.15	4.8	-1.7	4.8	2.3
	283.15	8.5	-3.7	8.5	3.7
Kaminishi and Toriumi 1966[20]	253.15	6.9	-7.6	7.8	7.6
	273.15	6.3	-4.4	6.3	4.4
	288.15	5.6	-4.2	5.6	4.2
	298.15	3.5	-2.0	3.5	2.0
Muirbrook and Prausnitz 1965[21]	273.15	5.7	-1.8	5.7	3.4
Zenner and Dana 1963[22]	273.15	4.6	-4.5	5.8	4.7
Lasala et al. 2016[23]	273.15	12.6	-3.8	12.6	3.8
	288.15	6.4	-2.8	6.4	2.8
	298.15	Calculation failed close to mixture critical point			
Westman et al. 2016[24]	273.09	9.8	-3.3	9.8	3.9
	293.08	2.1	-1.2	2.1	1.2

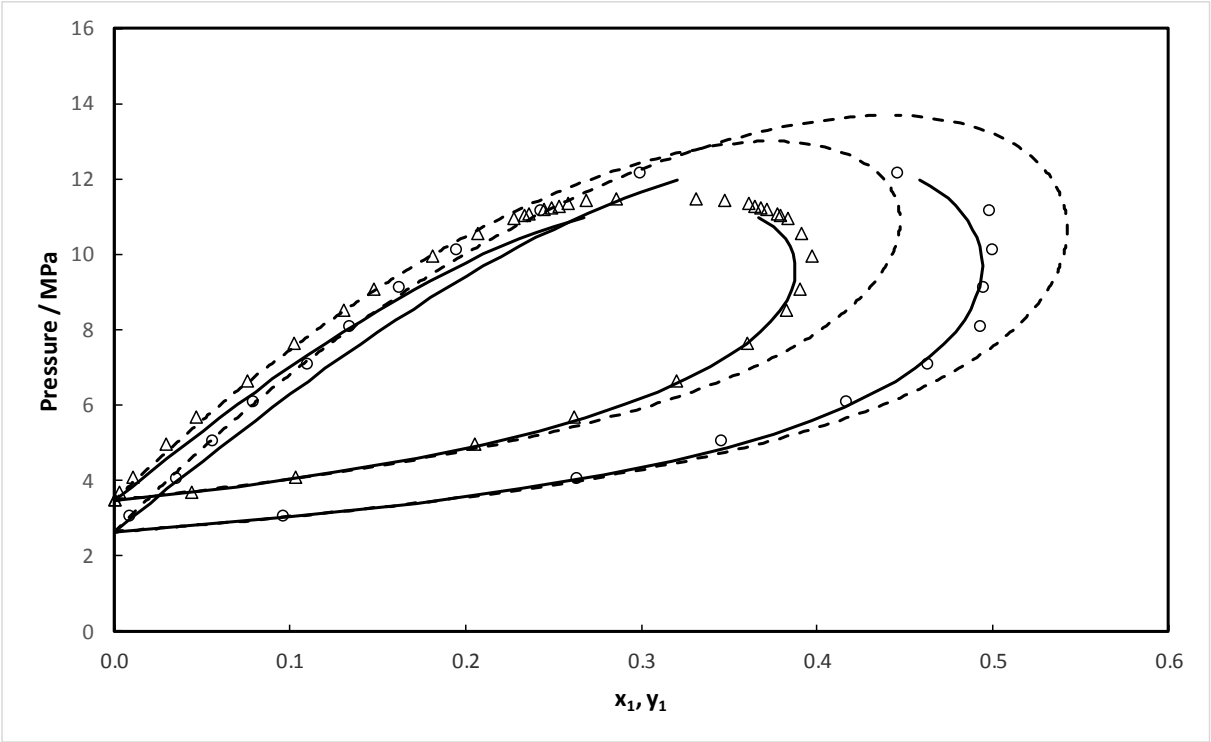

Figure 3 : Vapor – Liquid equilibrium isotherms for O_2 (1) + CO_2 (2) binary system: (Δ): 273.09 K from Westman et al.[24], (o), 263.15 K from Fredenslund and Sather[19]. Solid line: Peng Robinson EoS model, Dashed line: EoS-CG (Gernert and Span[8]) EoS model.

PT envelopes of the three mixtures (see Table 2) are predicted using our thermodynamic model and plotted in Figure 4. In this figure, we have also plotted the *PT* data of each system corresponding to the measured densities. According to Figure 4, we can observe that few density data were determined in the vapor-liquid region. Probably for these data, we are in a metastable state (mixture 3, *T*=279.05 and 293.31 K, mixture 1, *T*=276.59 K). These data are mentioned in Tables 3 and 5.

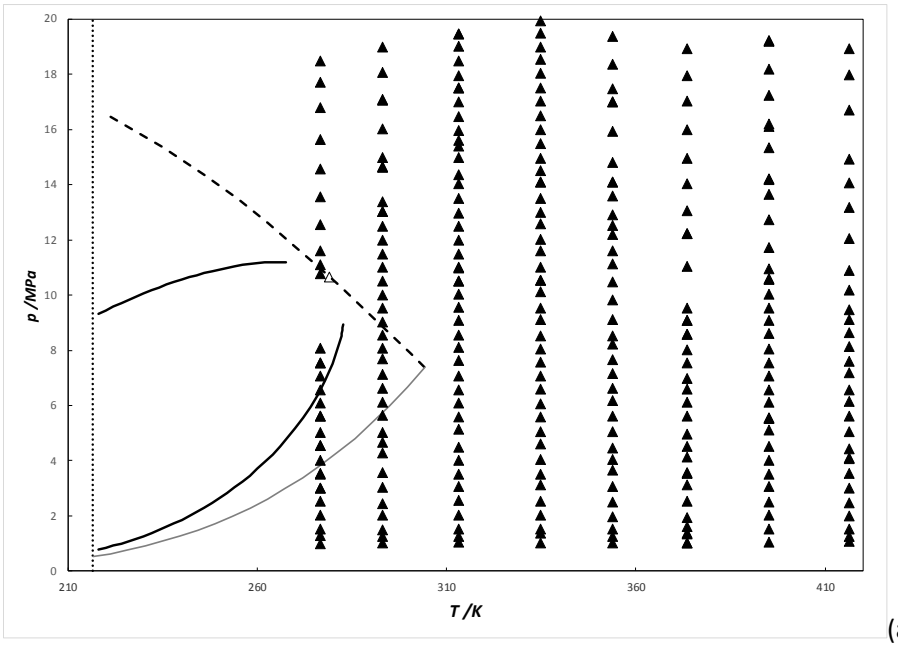
p /MPa
T /K
0
2
4
6
8
10
12
14
16
18
20
210
260
310
360
410

(a)

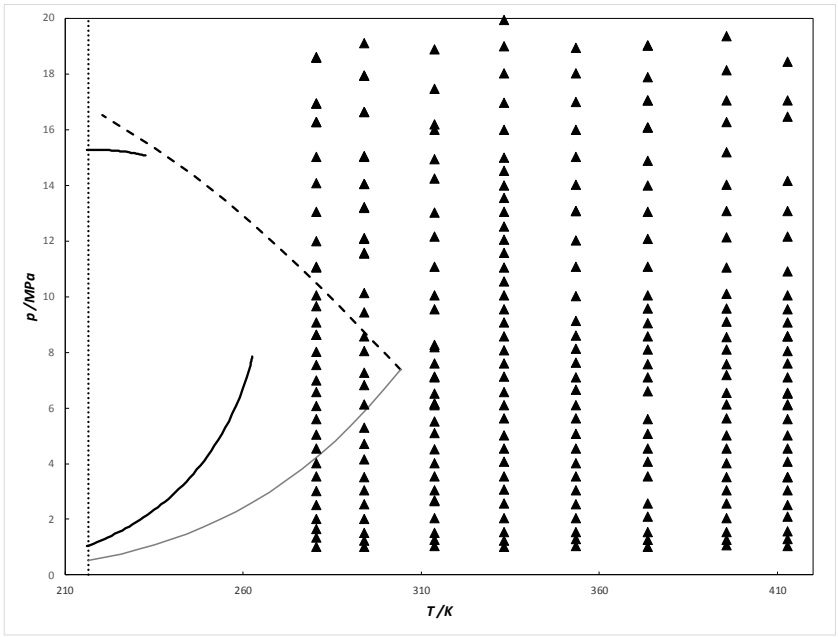
p /MPa
T /K
0
2
4
6
8
10
12
14
16
18
20
210
260
310
360
410

(b)

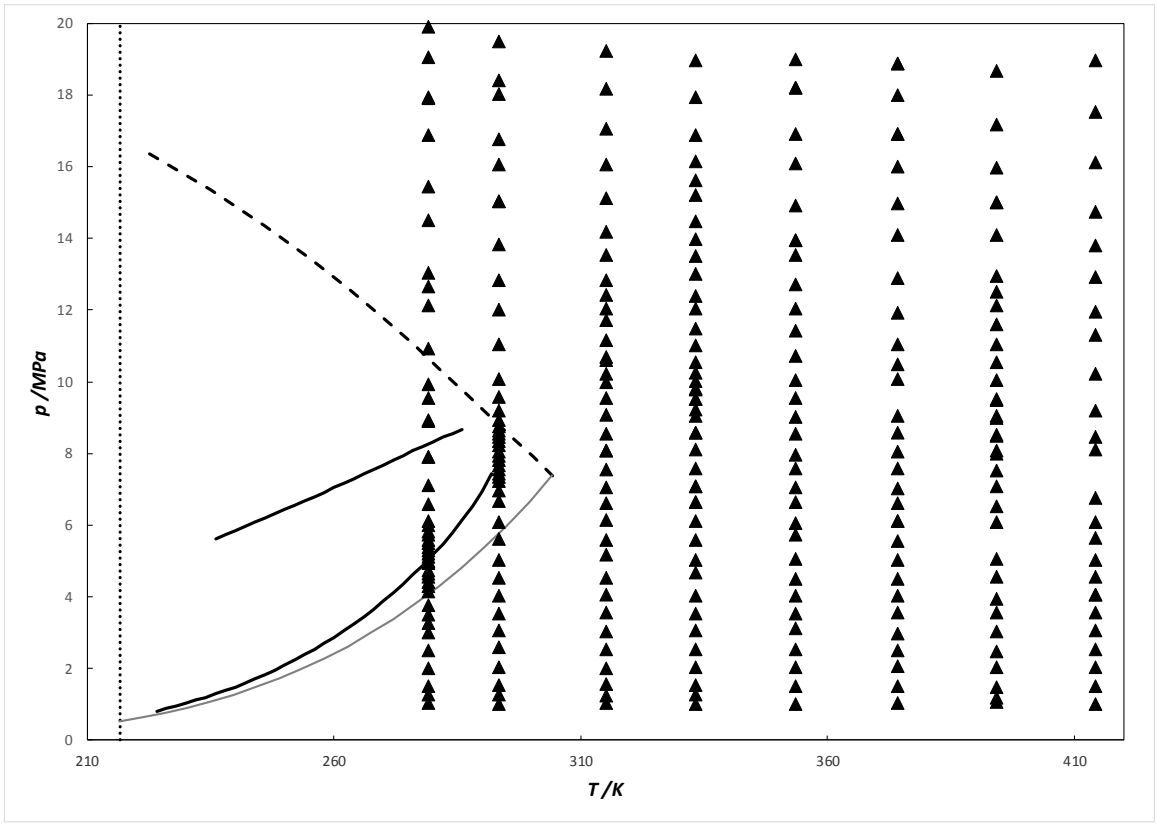

(c)

Figure 4: Pressure Temperature envelope of the CO_2-O_2 binary system calculated using Peng Robinson EoS (compositions listed in Table 2) showing the experimental points measured (▲). (a): Mixture 1, (b): mixture 2, (c): Mixture 3. Grey solid line: Pure CO_2 vapor pressure. Bold dashed line: mixture critical points line.

3.2. Comparison with experimental density data

The PR EoS previously developed is used to predict the experimental data. Table 9 summarizes the *AAD* (Eq. 10) and Maximum Absolute Deviation (*MAD*) in the gas, liquid and supercritical regions. The results (pressure *vs.* molar volume and compressibility factor) for the different mixtures are presented in Figures 5 to 7.

$$AAD\ (\%) = N^{-1} \sum_{i=1}^{N} \left(\left| \rho_{Exp.} - \rho_{Model} \right| / \rho_{Exp.} \right) \times 100 \qquad (10)$$

As it can be seen, the cubic EoS represents the experimental data with satisfactory deviations. As the compressibility factor tends to 1 when the pressure tends to 0 (ideal gas law), it is possible to evaluate the second virial coefficient of the CO_2 – O_2 binary mixture from the measured compressibility factor. Indeed, $Z = 1 + \frac{BP}{RT}$ for low to moderate pressure. It is also a good test to evaluate the consistency of the data at low pressure. In addition, we can observe that the maximum of deviation occurs for the low-pressure measurements (p < 1.5 MPa due to VTD precision) and close to bubble or dew points (possible metastable states). As the compressibility depends on the temperature, the density and the pressure, the uncertainties of the compressibility are therefore expressed using Eq. (11). It can be observed that the compressibility factor "concentrates" all the uncertainties of the measurements. The average value of *u(Z)/Z* is around 5%.

$$u(Z) = Z \sqrt{\left(\frac{u(\rho)}{\rho}\right)^2 + \left(\frac{u(T)}{T}\right)^2 + \left(\frac{u(P)}{P}\right)^2} \qquad (11)$$

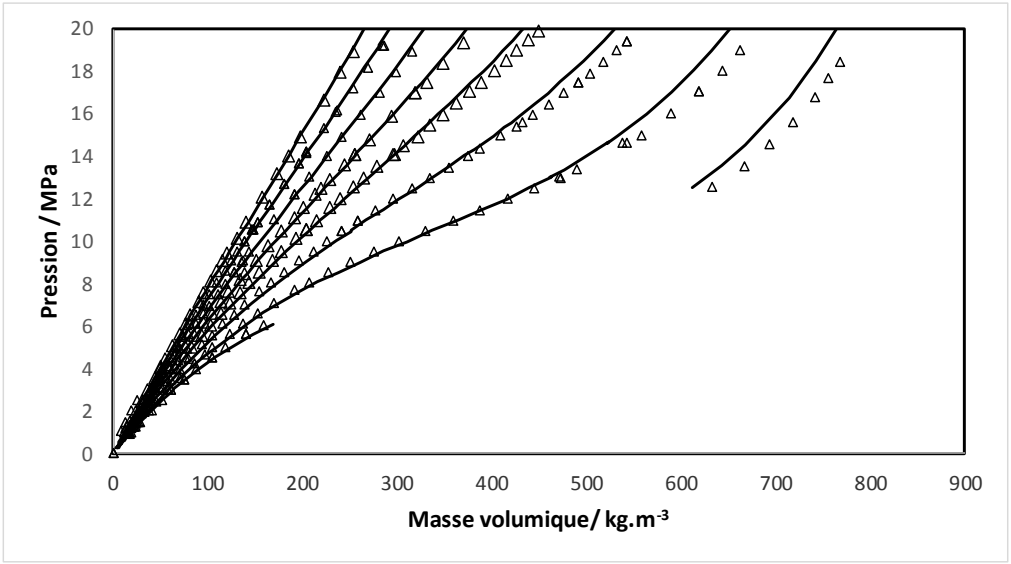

A

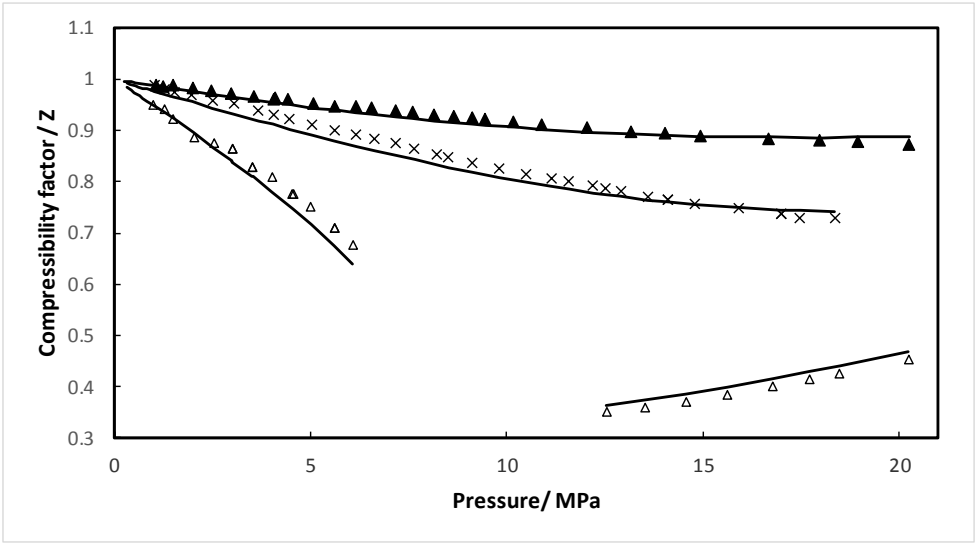

B

Figure 5: A: Pressure as a function of molar density for the O_2 + CO_2 (mixture 1: 0.274/0.726) binary system. B: Compressibility factor as a function of pressure (Δ): 276.59 K, (×): 353.78 K, (▲):416.38 K. Solid line: Peng Robinson EoS with Wong Sandler mixing rules and NRTL Activity coefficient model.

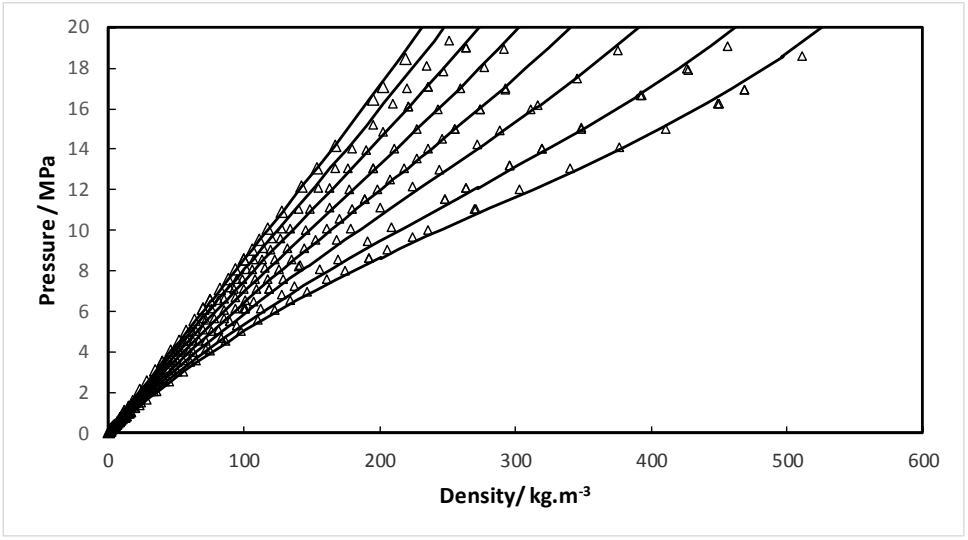

A

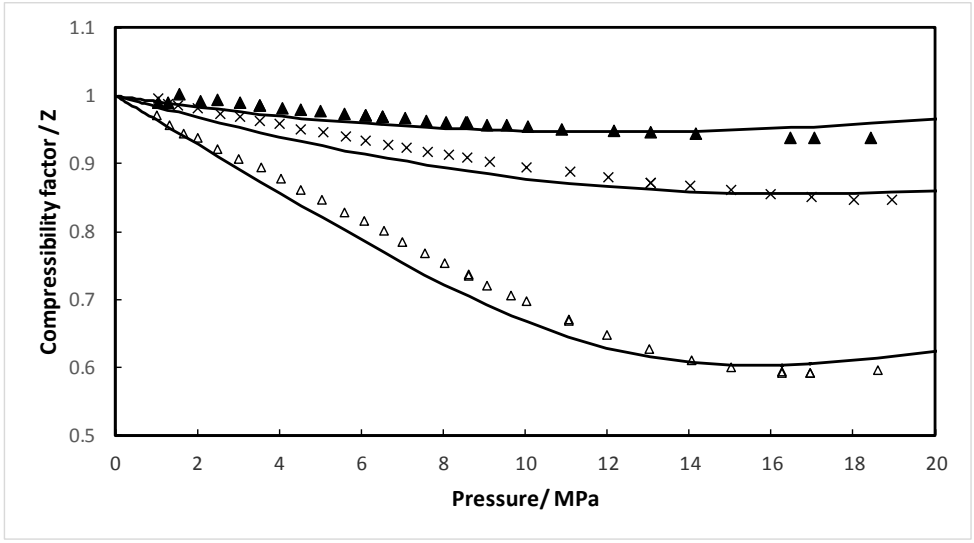

B

Figure 6: A: Pressure as a function of molar density for the O_2 + CO_2 (mixture 2: 0.483/0.517) binary system. B: Compressibility factor as a function of pressure (Δ): 280.63 K, (×): 353.46 K, (▲):412.85 K. Solid line: Peng Robinson EoS with Wong Sandler mixing rules and NRTL Activity coefficient model.

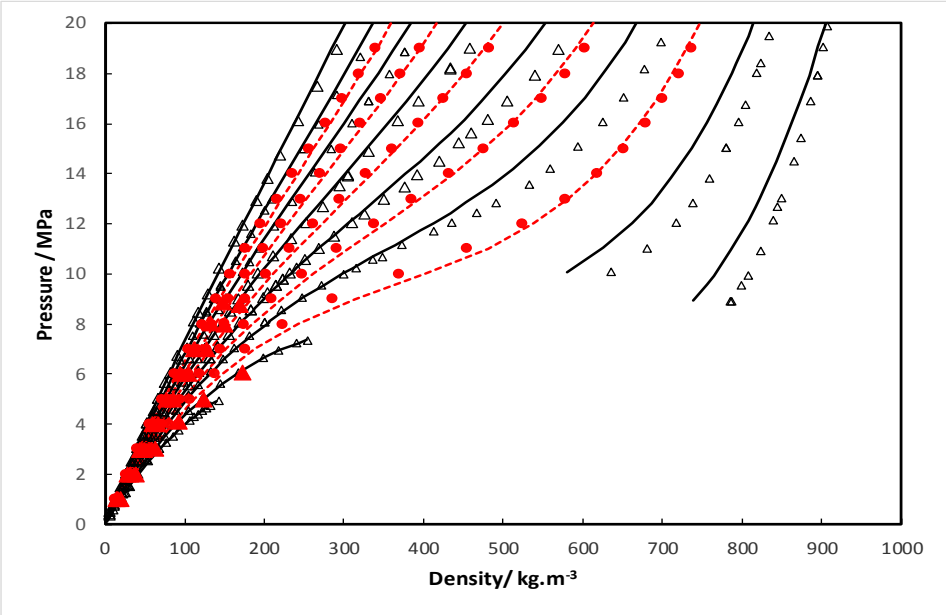
Pressure / MPa
Density/ kg.m-3
0
2
4
6
8
10
12
14
16
18
20
0
100
200
300
400
500
600
700
800
900
1000

A

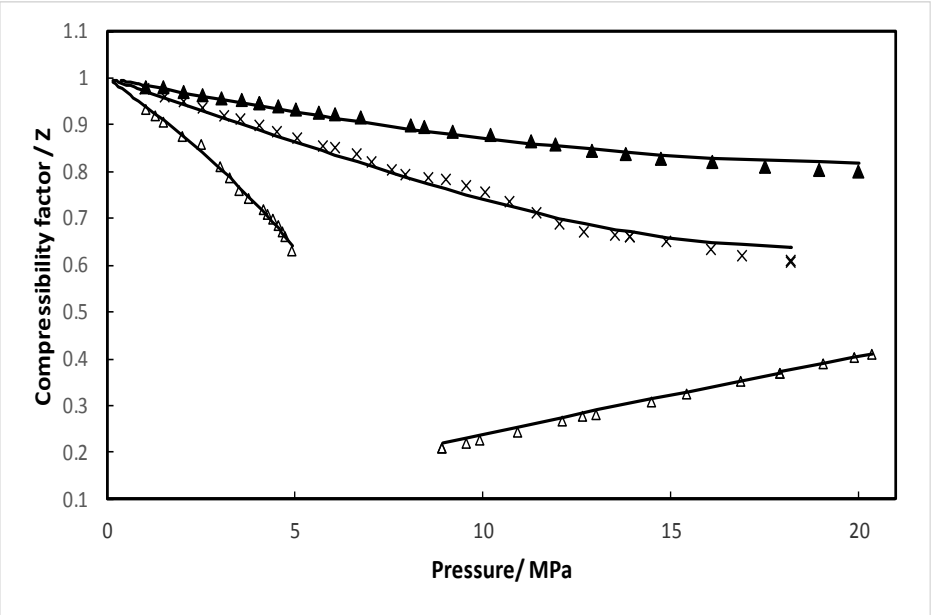
Compressibility factor / Z
Pressure/ MPa
0.1
0.2
0.3
0.4
0.5
0.6
0.7
0.8
0.9
1
1.1
0
5
10
15
20

B

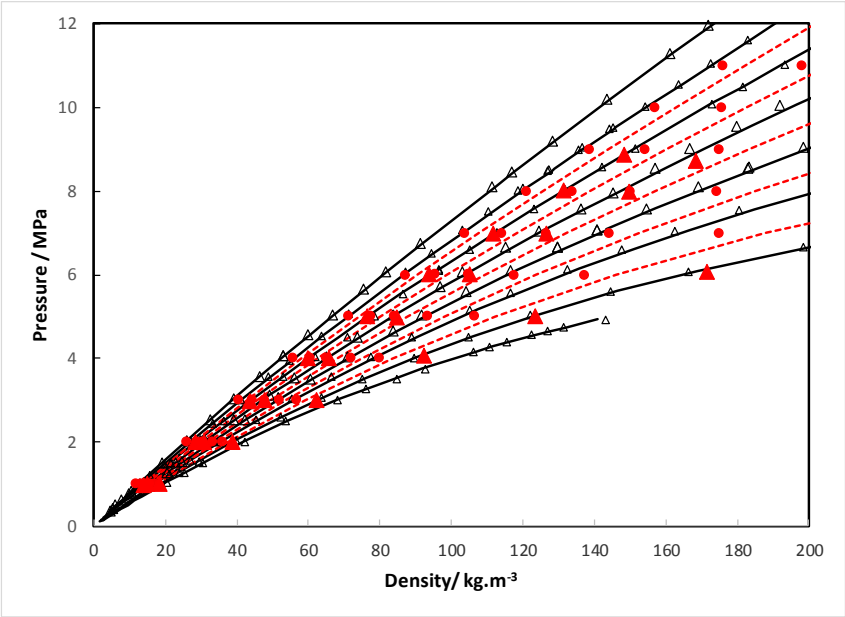

C

Figure 7: A: Pressure as a function of molar density for the O_2 + CO_2 (mixture 3: 0.128/0.872) binary system (C: zoom in the low pressure region). (Δ): this work. (●): Mantovani et al.[7], (▲): Lozano-Martin et al.[5] B: Compressibility factor as a function of pressure (Δ): 279.05 K, (×): 353.62 K, (▲):414.31 K. Solid and dashed line: Peng Robinson EoS with Wong Sandler mixing rules and NRTL Activity coefficient model.

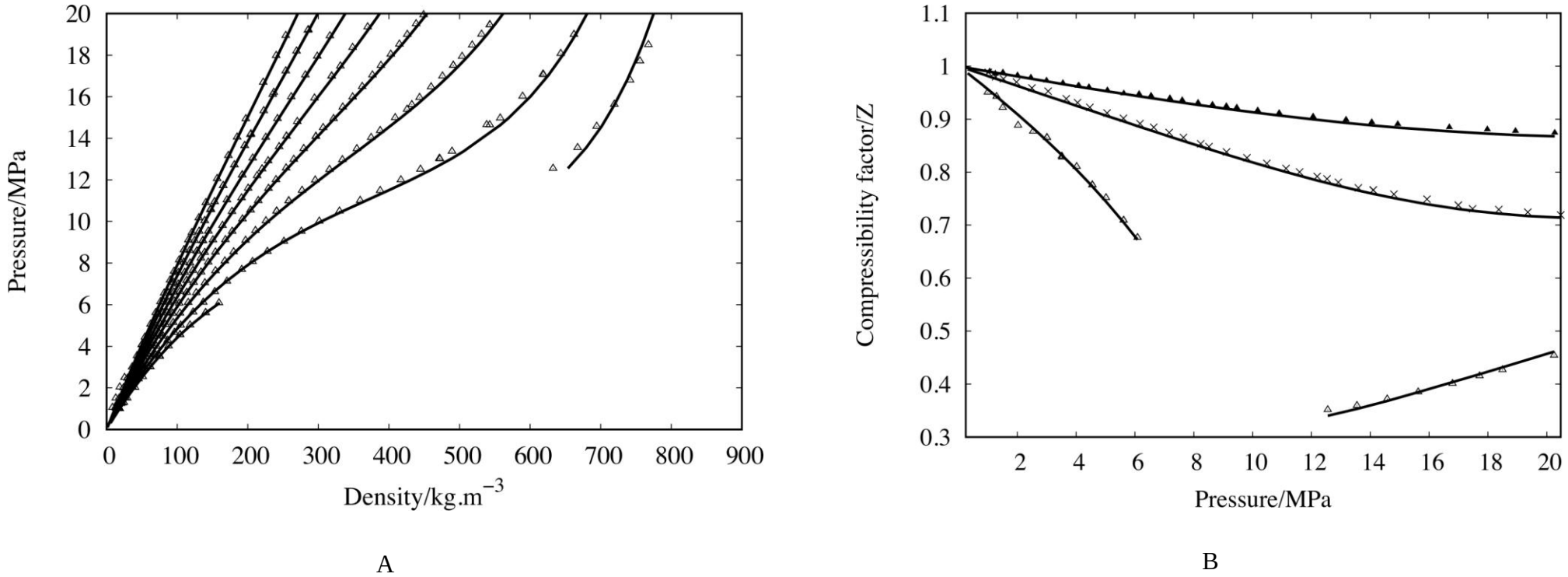

A B

Figure 8: A: Pressure as a function of density for the CO_2 + O_2 (mixture 1: 0.726/0.274) binary system. B: Compressibility factor as a function of pressure (Δ): 276. 50 K, (×): 353.78 K, (▲): 416.38 K. Solid line: EOS-CG.

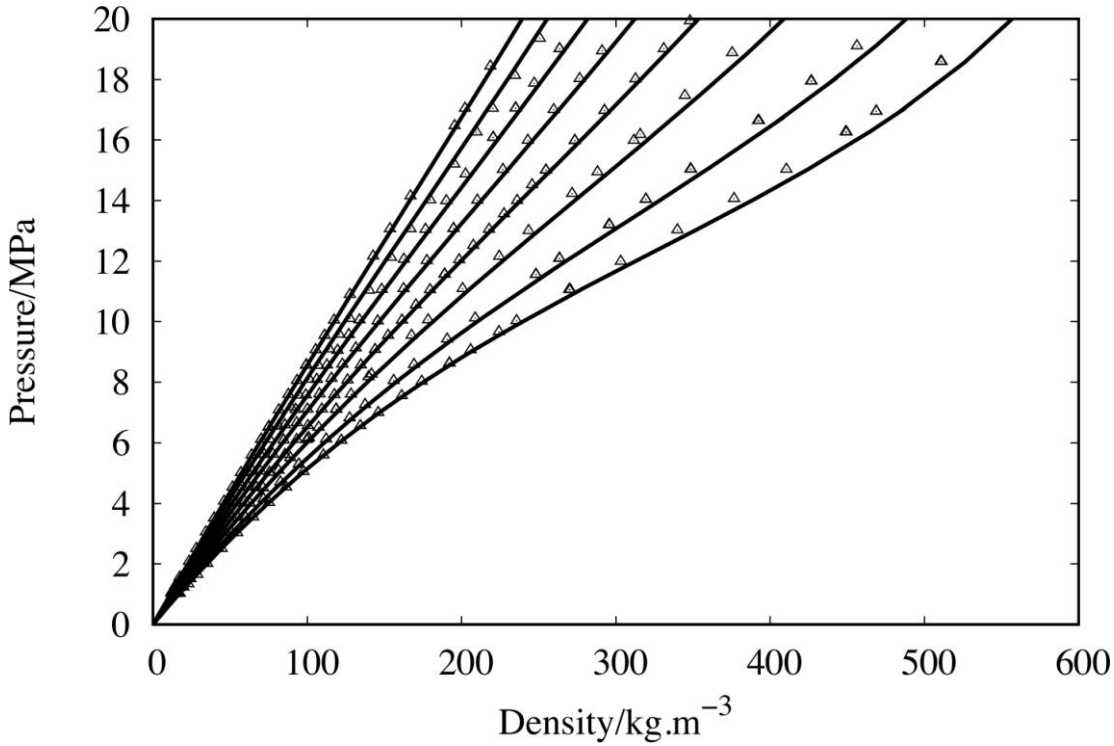

A

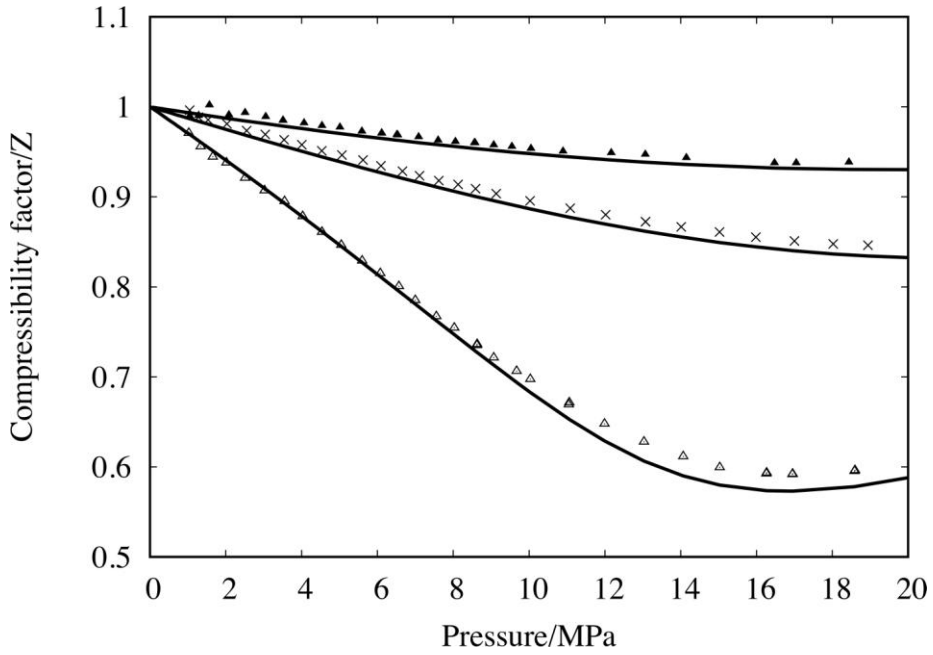

B

Figure 9: A: Pressure as a function of density for the CO_2 + O_2 (mixture 2: 0.517/0.483) binary system. B: Compressibility factor as a function of pressure (Δ): 280.63 K, (×): 353.46 K, (▲): 412.85 K. Solid line: EOS-CG.

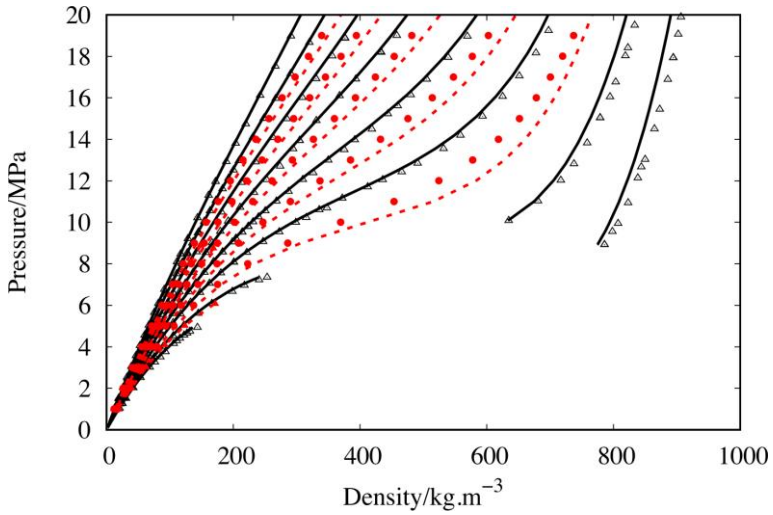
Pressure/MPa
Density/kg.m^{-3}
0
2
4
6
8
10
12
14
16
18
20
0
200
400
600
800
1000

A

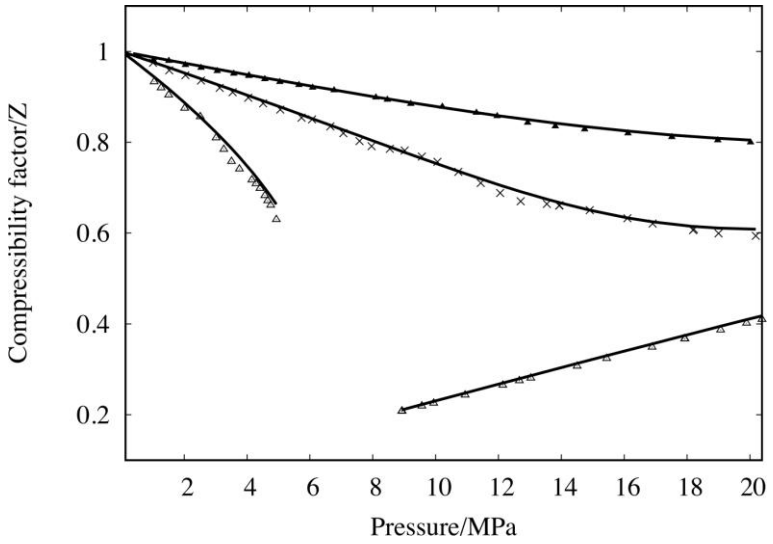
Compressibility factor/Z
Pressure/MPa
0.2
0.4
0.6
0.8
1
2
4
6
8
10
12
14
16
18
20

B

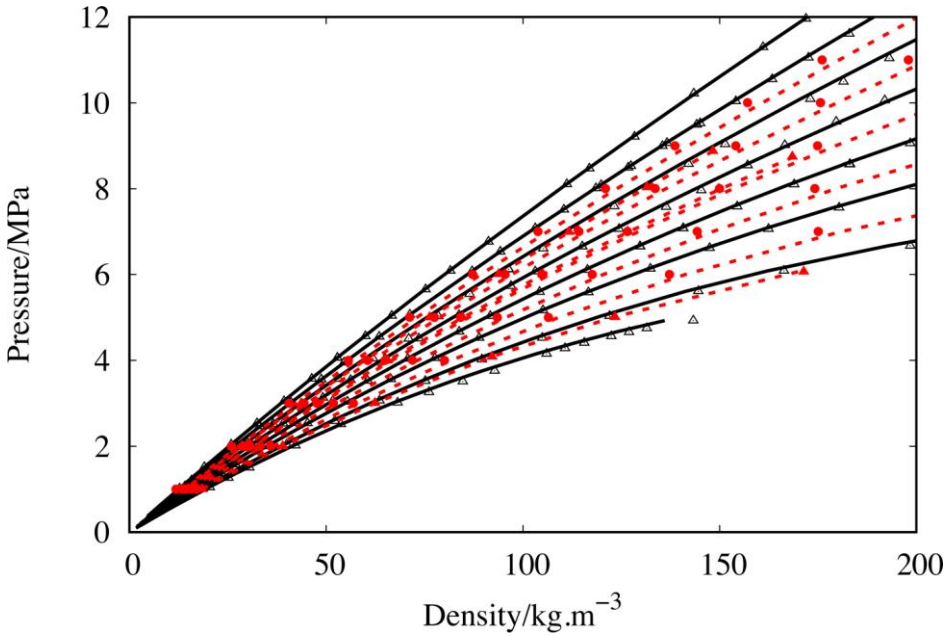

C

Figure 10: A: Pressure as a function of density for the CO_2 + O_2 (mixture 3: 0.872/0.128) binary system (C: zoom in the low pressure region). (Δ): this work. (•): Mantovani et al.[7], (▲): Lozano-Martin et al.[5] B. B: Compressibility factor as a function of pressure (Δ): 279.05 K, (×): 353.62 K, (▲): 414.31 K. Solid line: EOS-CG.

Experimental density data were also compared to a recent EoS, EOS-CG, based on GERG-2008[4, 15]. Parameters for the reduced mixture density and inverse reduced mixture temperature are provided by Gernert and Span[8], but the weighting factor F_{ij} is set to 0 for the binary system CO_2-O_2. As a result, the residual mixture behavior only includes the residual behavior of the pure components, weighted by their molar fraction. The reducing functions for density and temperature are presented in Eqs. (11) and (12), where N is the number of components, $T_{C,i}$ is the critical temperature of component i and $\rho_{C,i}$ is the critical density of component i.

$$\frac{1}{\rho_r(\bar{x})} = \sum_{i=1}^{N} x_i^2 \frac{1}{\rho_{c,i}} + \sum_{i=1}^{N-1} \sum_{j=i+1}^{N} 2x_i x_j \beta_{v,ij} \gamma_{v,ij} \frac{x_i + x_j}{\beta_{v,ij}^2 x_i + x_j} \cdot \frac{1}{8} \left(\frac{1}{\rho_{c,i}^{\frac{1}{3}}} + \frac{1}{\rho_{c,j}^{\frac{1}{3}}} \right)^3 \quad (11)$$

$$T_r(\overline{x}) = \sum_{i=1}^{N} x_i^2 T_{c,i} + \sum_{i=1}^{N-1} \sum_{j=i+1}^{N} 2\beta_{T,ij} \gamma_{T,ij} \cdot (T_{c,i} \cdot T_{c,j})^{0.5} x_i x_j \frac{x_i + x_j}{\beta_{T,ij}^2 x_i + x_j} \quad (12)$$

$\beta_{v,ij}$, $\gamma_{v,ij}$, $\beta_{T,ij}$ and $\gamma_{T,ij}$ are binary interaction parameters from GERG-2008[4, 15] and presented in Table 10 for the system CO_2-O_2.

As shown in Table 9, EoS-CG predicts the densities more accurately than the PR EoS developed in this work. It should be noted that EOS-CG is based on multi-fluid approximations and that different types of data ($P\rho T$, VLE, speed of sound, etc.) are used for the development of binary model parameters. Figures 8 - 10 compare experimental and predicted densities and compressibility factors. Due to the use of different data types, rather than only VLE as PR EoS, the phase equilibrium prediction is less accurate for EOS-CG than for PR EoS (see Figure 3). This is also influenced by the presence of a mixture critical point.

Finally, we have compared our experimental results with literature data for compositions similar to ours, i.e. mixture 3. We have plotted the literature data in Figures 7 and 10 (we have also included a zoom to better visualize the low-pressure region). Deviations between these data and PR EoS and EOS-CG are presented in Table 9. As can seen, the order of magnitude of the deviations between our models and experimental data (and our data and literature data) are very close. We can observe a good agreement between the different sets of data.

Table 9: Deviations between experimental and calculated data using Peng Robinson EoS with the Wong Sandler mixing rules involving NRTL activity coefficient model, and using EoS-CG. Vap: vapor phase, Liq: liquid phase and SC: supercritical region.

	Peng Robinson EoS						EoS-CG					
***T*/K**	***AAD*/%**	***AAD*/%**	***AAD*/%**	***MAD*%**	***MAD*%**	***MAD*%**	***AAD*/%**	***AAD*/%**	***AAD*/%**	***MAD*%**	***MAD*%**	***MAD*%**
	Vap	**Liq**	**SC**	**Vap**	**Liq**	**SC**	**Vap**	**Liq**	**SC**	**Vap**	**Liq**	**SC**
Mixture 1												
276.59	4.2	3.2		10.1	3.8		0.7	1.3		2.2	3.3	
293.18			3.2			4.5			1.3			3.8
313.18			2.0			3.9			1.5			2.2
334.78			2.2			3.9			0.6			1.3
353.78			1.5			3.1			0.8			1.3
373.46			1.4			2.4			0.5			0.7
395.18			1.3			2.1			0.6			0.7
416.38			0.9			1.4			0.4			0.9
Mixture 2												
280.63			2.8			4.6			1.6			3.7
293.92			2.7			4.7			2.1			3.4
313.63			3.1			4.4			2.1			2.8
333.21			1.4			2.4			0.8			1.4
353.46			1.6			2.4			1.0			1.6
373.60			1.5			2.2			1.3			1.9
395.72			1.9			4.7			1.7			2.3
412.85			1.1			2.8			0.7			1.2
Mixture 3												
279.05	3.0	3.7		12.6	8.2		2.3	1.8		5.1	2.0	
293.31			3.7			8.9	2.2	1.7		5.0	2.1	
315.06			3.5			8.6			1.1			3.1
333.25			2.3			7.1			0.9			2.3
353.62			1.6			6.8			0.9			3.1

374.23	1.4	4.5	1.7	5.1
394.15	1.0	3.0	0.3	0.8
414.31	0.8	2.4	0.4	0.8
Lozano-Martín et al.[5], x_{O2}=0.099856 – Maximum pressure: 9 MPa				
293.07	1.94	3.1	0.3	0.8
349.92	1.78	2.5	0.2	0.3
374.91	1.28	1.7	0.07	0.2
Mantovani et al.[7], x_{O2}=0.1291 – Maximum pressure: 20 MPa				
303.22	3.86	9.96	5.1	13.6
323.18	3.57	6.29	4.0	6.5
343.15	3.34	7.55	3.4	7.1
363.15	3.02	8.20	3.0	7.8
383.14	3.76	15.18	3.6	14.8

Table 10: Values of EoS-CG[4] binary interaction parameters.

System	β_T	γ_T	β_v	γ_v
$CO_2 + O_2$	1.0	1.032	1.0	1.0845

4. Conclusion

The densities of three CO_2-O_2 binary mixtures were measured using VTD densitometer, Anton Paar DMA 512, in the gas, liquid and supercritical regions. The densitometer was first calibrated using pure CO_2 and the FPMC calibration technique. The maximum expanded uncertainties on temperature, pressure and densities are $U(p)$= 0.0005 MPa, $U(T)$= 0.3 K and $U(\rho)$= 15 kg.m^{-3}, respectively. The highest uncertainties were observed at very low pressure conditions in the gas phase or in the vicinity of the bubble point curve in the liquid phase. The measured densities were employed to evaluate the classical Peng-Robinson cubic EoS with parameters adjusted on VLE data from the literature. The model gives satisfactory results in the prediction of the volumetric properties in the typical conditions of storage in salt caverns. However, the GERG-2008-based EoS-CG was more accurate with AAD of only 1.1% and MAD of 5.1%. The main advantage of EOS based on a thermodynamic potential is that all thermodynamic properties of a mixture or pure substance can be consistently derived from the potential; these properties are needed in the assessment of cavern stability.

5. Acknowledgments

Financial support from Agence Nationale de la Recherche (ANR) through the project FluidSTORY (n° 7747, ID ANR-15-CE06-0015) is gratefully acknowledged.

6. References

1. Götz, M.; Lefebvre, J.; Mörs, F.; Koch, A. M.; Graf, F.; Bajohr, S.; Reimert, R.; Kolb, T., Renewable Power-to-Gas: A technological and economic review. *Renewable energy* **2016,** 85, 1371-1390.

2. Kezibri, N.; Bouallou, C., Conceptual design and modelling of an industrial scale power to gas-oxy-combustion power plant. *Int. J. Hydrogen Energy* **2017,** 42, (30), 19411-19419.

3. Blanco-Martín, L.; Rouabhi, A.; Hadj-Hassen, F., Use of salt cavern in the energy transition context: application to the Power-to-Gas– Oxyfuel process. SN *Appl. Sci.* **2020,** submitted.

4. Li, H.; Dong, B.; Yu, Z.; Yan, J.; Zhu, K., Thermo-physical properties of CO_2 mixtures and their impacts on CO2 capture, transport and storage: progress since 2011. *Appl. Energy* **2019**, 255, 113789.

5. Lozano-Martin, D.; Akubue, G.U.; Moreau, A.; Tuma, D.; Chamorro, C.R., Accurate experipmental (p, ρ, T) data of the (CO2+O2) binary system for the development of models for CCs processes. *J. Chem. Thermodyn*. **2020**, 150, 106210.

6. Commodore, J.A.; Deering, C.E.; Marriott, R.A., Volumetric properties and phase behavior of sulfur dioxide, carbon disulfide and oxygen in high-pressure carbon dioxide fluid. *Fluid Phase Equilib*. **2018**, 477, 30-39.

7. Mantovani, M.; Chiesa, P.; Valenti, G.; Gatti, M.; Consonni, S., Supercritical pressure-density-temperature measurements on CO2-N2, CO2-O2 and CO2-Ar binary mixtures. *J. Supercrit. Fluids* **2012,** 61-34-43.

8. Gernert, J.; Span, R., EOS–CG: A Helmholtz energy mixture model for humid gases and CCS mixtures. *J. Chem. Thermodyn.* **2016,** 93, 274-293.

9. Rivollet, F.; Jarne, C.; Richon, D., PρT and VLE for Ethane+ Hydrogen Sulfide from (254.05 to 363.21) K at Pressures up to 20 MPa. *J Chem. Eng. Data* **2005,** 50, (6), 1883-1890.

10. Coquelet, C.; Ramjugernath, D.; Madani, H.; Valtz, A.; Naidoo, P.; Meniai, A. H., Experimental measurement of vapor pressures and densities of pure hexafluoropropylene. *J Chem. Eng. Data* **2010,** 55, (6), 2093-2099.

11. Nazeri, M.; Chapoy, A.; Valtz, A.; Coquelet, C.; Tohidi, B., Densities and derived thermophysical properties of the 0.9505 CO2+ 0.0495 H2S mixture from 273 K to 353 K and pressures up to 41 MPa. *Fluid Phase Equilib.* **2016,** 423, 156-171.

12. Bouchot, C.; Richon, D., An enhanced method to calibrate vibrating tube densimeters. *Fluid phase Equilib.* **2001,** 191, (1-2), 189-208.

13. Khalil, W.; Coquelet, C.; Richon, D., High-pressure Vapor− Liquid equilibria, liquid densities, and excess molar volumes for the carbon dioxide+ 2-propanol system from (308.10 to 348.00) K. *J. Chem. Eng. Data* **2007,** 52, (5), 2032-2040.

14. Lemmon, E.; Bell, I. H.; Huber, M.; McLinden, M., NIST Standard Reference Database 23: Reference Fluid Thermodynamic and Transport Properties-REFPROP, Version 10.0, National Institute of Standards and Technology. **2018**. *URL http://www.nist. gov/srd/nist23. cfm*.

15. Span, R.; Wagner, W., A new equation of state for carbon dioxide covering the fluid region from the triple-point temperature to 1100 K at pressures up to 800 MPa. *J. Phys. Chem. Ref. Data* **1996,** 25, (6), 1509-1596.

16. Peng, D.-Y.; Robinson, D. B., A new two-constant equation of state. *IEC Fund.* **1976,** 15, (1), 59-64.

17. Wong, D. S. H.; Sandler, S. I., A theoretically correct mixing rule for cubic equations of state. *AIChE J.* **1992,** 38, (5), 671-680.

18. Renon, H.; Prausnitz, J. M., Local compositions in thermodynamic excess functions for liquid mixtures. *AIChE J.* **1968,** 14, (1), 135-144.

19. Fredenslund, A.; Sather, G., Gas-liquid equilibrium of the oxygen-carbon dioxide system. *J. Chem. Eng. Data* **1970,** 15, (1), 17-22.

20. Kaminishi, G.-i.; Toriumi, T., Gas-liquid equilibrium under high pressures. VI. Vapor-liquid phase equilibrium in the CO2-H2, CO2-N2, and CO2-O2 systems. *Kogyo Kagaku Zasshi* **1966,** 69, (2), 175-178.

21. Muirbrook, N.; Prausnitz, J., Multicomponent vapor-liquid equilibria at high pressures: Part I. Experimental study of the nitrogen—oxygen—carbon dioxide system at 0° C. *AIChE J.* **1965,** 11, (6), 1092-1096.

22. Zenner, G.H.; Dana, L.I Liquid-vapor equilibrium compositions of carbon dioxide-oxygen-nitrogen mixtures, Chemical engineering progress symposium series, 1963, 36-41.

23. Lasala, S.; Chiesa, P.; Privat, R.; Jaubert, J.-N., VLE properties of CO2–Based binary systems containing N2, O2 and Ar: Experimental measurements and modelling results with advanced cubic equations of state. *Fluid Phase Equilib.* **2016,** 428, 18-31.

24. Westman, S. F.; Stang, H. J.; Løvseth, S. W.; Austegard, A.; Snustad, I.; Ertesvåg, I. S., Vapor-liquid equilibrium data for the carbon dioxide and oxygen (CO2+ O2) system at the temperatures 218, 233, 253, 273, 288 and 298 K and pressures up to 14 MPa. *Fluid Phase Equilib.* **2016,** 421, 67-87.

TOC GRAPHIC

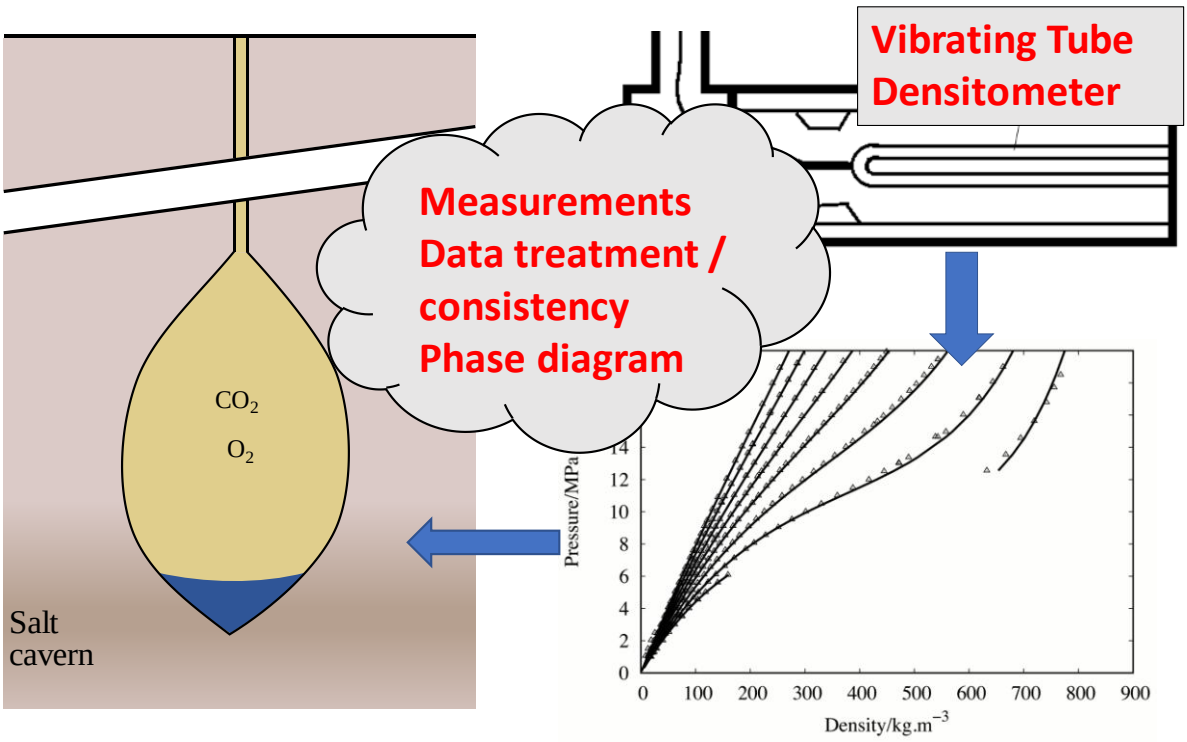
Vibrating Tube Densitometer
Measurements
Data treatment / consistency
Phase diagram
CO_2
O_2
Salt cavern
Pressure/MPa
Density/kg.m^{-3}
0
2
4
6
8
10
12
14
0
100
200
300
400
500
600
700
800
900

RÉSUMÉ

L'étude thermodynamique (expérimentation et modélisation) des systèmes Gaz+Eau+Sels est d'une grande importance, que ce soit dans un contexte environnemental comme le Captage et le Stockage du dioxyde de Carbone (CSC) ou dans un contexte économique comme la récupération assistée du pétrole par injection de CO2, ou le Stockage Souterrain réversible massif de Gaz (SSG) à usage industriel (« Power-to-Gas » (PtG) et « Gas-to-Power » (GtP), industries chimiques, pétrochimiques et pharmaceutiques, etc.). Dans le cadre du SSG, l'industrie de l'énergie s'intéresse aux vecteurs énergétiques gazeux les plus demandés dans le secteur, tels que le méthane (ou le gaz naturel (GN)), le dioxyde de carbone (pur à destination des unités de méthanation ou mélangé avec le méthane pour le stockage du GN), l'oxygène (pour les unités d'oxycombustion) et l'hydrogène (utilisé directement ou pour alimenter les unités de méthanation). La conception et l'optimisation des installations de stockage, ainsi que la surveillance de la température, de la pression, de la quantité du gaz stocké dans les réservoirs géologiques (cavités salines, aquifères salins profonds et gisements de GN épuisés) et leurs pilotages selon différents scénarii (stockage journalier, hebdomadaire, mensuel ou annuel), nécessitent la connaissance des diagrammes de phases et plus spécifiquement la solubilité des gaz dans les saumures, les teneurs en eau et aussi les conditions de stabilité des hydrates de gaz dans le cadre de l'exploitation de gaz. Pour ce faire, il est essentiel de disposer d'un modèle thermodynamique qui repose sur des fondements théoriques et qui soit peu dépendant de l'acquisition de données expérimentales. L'objectif est de pouvoir extrapoler le modèle en dehors de la gamme d'ajustement des paramètres (température, pression et composition de la saumure) et également le transposer à d'autres applications. Pour pallier le manque de données expérimentales à haute pression de la solubilité des gaz (CO2, O2 et H2) dans la saumure, un dispositif expérimental basé sur la méthode "statique-analytique" a été adapté et utilisé pour mesurer la solubilité des gaz dans l'eau pure et la saumure. Pour comparer/valider les nouvelles mesures, un deuxième dispositif basé sur une technique dite "volumétrique" a également été utilisé. Une équation d'état pour les électrolytes (e-PR-CPA) a été développée en prenant en compte toutes les interactions entre espèces chimiques (molécules et ions). Les résultats de ce modèle ont été comparés avec des modèles existants tels que ceux utilisés par les géochimistes et en génie des procédés. Pour une meilleure évaluation des performances de notre modèle, les paramètres des modèles précédemment cités ont été réoptimisés en incluant les nouvelles données acquises.

MOTS CLÉS

Stockage Souterrain de Gaz, Solubilité des gaz, Teneur en eau, Hydrates de gaz, e-PR-CPA, Stockage de l'Hydrogène

ABSTRACT

The thermodynamic study (experimental and modeling) of Gas+Water+Salt systems is of great importance, whether in an environmental context such as Carbon Dioxide Capture and Storage (CCS) or in an economic context such as Enhanced Oil Recovery (EOR) by CO2 injection, or massive reversible Underground Gas Storage (UGS) for industrial use ("Power-to-Gas" (PtG) and "Gas-to-Power" (GtP), chemical, petrochemical and pharmaceutical industries, etc.). In the context of UGS, the energy industry is interested in the gaseous energy carriers that are most in demand in the sector, such as methane (or natural gas (NG)), carbon dioxide (pure for methanation units or mixed with methane for NG storage), oxygen (for Oxy-fuel combustion units) and hydrogen (used directly or to feed methanation units). The design and optimization of storage facilities, as well as the monitoring of the temperature, pressure and quantity of gas stored in geological reservoirs (salt caverns, deep saline aquifers and depleted NG fields) and their control according to different scenarios (daily, weekly, monthly or annual storage), require knowledge of phase diagrams and more specifically gas solubility in brine, water content and also gas hydrate stability conditions during gas exploitation. For this purpose, it is essential to develop a thermodynamic model based on theoretical foundations and with a low dependence on experimental data. The objective is to be able to extrapolate the model outside the adjustment range of the parameters (temperature, pressure and brine composition) and also to transpose it to other applications. To overcome the lack of experimental data of high pressure gas (CO2, O2 and H2) solubility in brine, an experimental apparatus based on the "static-analytic" method has been adapted and used to measure gas solubility in pure water and brine. To compare/validate the new measurements, a second apparatus based on a "volumetric" technique was also used. An electrolyte equation of state (e-PR-CPA) was developed taking into account all interactions between chemical species (molecules and ions). The results of this model were compared with existing models such as those used by geochemists and in process engineering. For a better evaluation of the performance of our model, the parameters of the previously mentioned models were re-optimized by including the newly acquired data.

KEYWORDS

Underground Gas Storage, Gas solubility, water content, Gas hydrates, e-PR-CPA, Hydrogen storage